Densification and refreezing in the percolation zone of the Greenland Ice Sheet: implications for mass balance measurements

Victoria Parry

PhD

The University of Edinburgh

2008

Declaration of originality

All of the work included in this thesis is original and my own, unless indicated otherwise. The work presented in this thesis has not been submitted for any other degree or professional qualification.

Signed…….. Date…….

Abstract

In order to increase coverage, mass balance changes of the world's ice sheets are increasingly derived from surface elevation changes measured via satellite. Across the percolation zone of the Greenland Ice Sheet, meltwater, percolation and refreezing cause a re-distribution of mass through densification which may result in elevation change with no associated mass loss. Therefore, densification processes need to be quantified, spatially and temporally, and accounted for in mass balance measurements. This thesis investigates the relationships between patterns of elevation change and temporally and spatially variable accumulation and densification processes. In doing so, it provides an important contribution to the validation of the European Space Agency's CryoSat-2 mission by placing error bars on the accuracy to which changes in satellite-measured ice-mass surface elevation represent *real* changes in ice mass.

Temporal variability in near-surface (<10 m) snowpack and firn density and structure was measured in snowpits, shallow cores and using a neutron probe in the spring and autumn of 2004 at ~1945 m elevation (T05, 69^{o} 51N, 47^{o} 15W) in the percolation zone of the Greenland Ice Sheet. Results show that average snowpack density increased by 26% from spring to autumn, with a 5% (7.6 cm) increase in elevation, and a corresponding 32% increase in mass. Spatial variability was investigated at 11 sites along two transects at spatial scales of 1 m – 10 km. Whilst there was little variability in small scale (1 - 100 m) density changes, 'seasonal densification' increased at lower elevations, rising to 47% 10 km closer to the ice sheet margin at 1860 m a.s.l. The spatial variability in seasonal densification was further investigated in spring 2006 at seven sites located at ~10 km intervals along a 57 km transect spanning a 350 m elevation range. Snowpits and shallow cores reveal no significant variation in spring (prior to melt) snowpack density but following

summer melt and refreezing cycles, seasonal densification decreased with increasing elevation at 32 kg m^{-3} per 100 m. Measurements at three sites ranging in elevation from 1860 – 2015 m and spanning three melt-seasons show inter-annual variation in the seasonal densification gradient.

In order to obtain a longer time series of mass balance, a 17 m core retrieved in spring 2004 was analysed for stratigraphy, density and ionic and isotopic concentrations to identify annual layers. Unfortunately, the seasonal melt cycle (whereby on average 10% of the snowpack undergoes melt), results in a complex stratigraphy and density and ionic concentrations that cannot be resolved into a seasonal signature. However, the $\delta^{18}O$ and δ D isotopes show clear sinusoidal fluctuations, which have been used to derive annual mass balance from 1986 to 2003. These show a mean annual accumulation of 53.7 cm w.e. (s.d. 12.9 cm w.e.) although the accuracy of these measurements is compromised by the percolation of meltwater through more than more year's snowpack.

These findings confirm that estimates of mass balance cannot be calculated solely from observed changes in surface elevation. However, predicting spatial and temporal variations in densification is not straightforward because of the complex inter-annual variations in the processes of accumulation, melt, percolation and refreezing.

Acknowledgements

I am indebted to the following people for help with field work. For data collection in the field I extend my thanks to Veit Helm, Sebastian Chastin, Carl Bøggild, Julian Scott and the Ben and Jerry's 'Climate Change College' – with a special thanks to Ben Richards for his exceptional sketching skills. For logistical support in the field I would like to thank the following people: Kristian Keller, Rene Forsberg, Malcolm Davidson, Robin Abbot, Basse Vaengtoft, Mark Begnaud, Jens Larsen and Kate Bar Friis. Thank you also to Liz Morris for help with logistics, and the neutron probe.

For exceptional help in the laboraties (LOWTEX), analysing ion concentrations, thank you to Jenny Mills, who had incredible patience with the samples (and me)! For help at SUERC I would like to thank Terry Donnelly and Tony Fallick. For help in retrieving my samples off the M8, thank you to the Lothian and Borders Police.

Thank you also to my supervisors, Pete Nienow, Doug Mair, Jemma Wadham and Bryn Hubbard. I am also grateful to Duncan Wingham for securing NERC funding (grant NER/O/S/2003/00620), Koni Steffen for access to GC-Net data, and his continued support.

I have been lucky enough to have a lot of support from friends and family, and so thank you to: Dad, for proof reading; Mum, for constant support; Stew and Ian for IT help; Tim and Janette for being great flat mates; Simon for easing the strain and Nick for always being able to help me, especially with perspective.

Table of Contents

Figures

Tables

Equations

Chapter 1: Introduction

The Greenland Ice Sheet is the largest store of freshwater in the northern hemisphere. Recent satellite observations indicate an increase in the melt extent around the margins of the ice sheet (Steffen & others, 2004; Mote, 2007) and any future warming will affect mass balance through surface melting and runoff, and through ice dynamics (Zwally & others 2002; Joughin & others, 2008). Any changes in mass balance will affect global sea levels and increased runoff may affect the strength of the ocean thermohaline circulation (Rahmstorf & Ganopolski, 1999). This can affect the expanse of sea ice cover, which has potential consequences for albedo and insulation feedback (Fichefet & others, 2003). With warming in the Arctic estimated to be twice that of the global average (Trenberth & others, 2007) there is a growing need to understand the likely response of the ice sheet to future climate change.

Current estimates of the balance of the Greenland Ice Sheet vary between -227 ±33 Gt yr^{-1} (Velicogna & Wahr, 2006b) and +11 ±3 Gt yr^{-1} (Zwally & others 2005). In order to model the effect of future warming on the ice sheet, current mass balance measurements need to be constrained. Accurate elevation changes over large areas of the polar ice sheets can be measured using satellite radar altimetry from which mass balance can be derived (Zwally & others 2005). However, in the percolation zone seasonal changes in snow pack density ensure that changes in surface elevation cannot be directly correlated with changes in mass. Melt water generated at the surface refreezes at depth in the snowpack/firn causing a redistribution of mass through densification. There may be a measured decrease in elevation caused by surface melt, percolation and refreezing, but with no mass loss (Braithwaite & others, 1994). Similarly, there may be positive summer accumulation in the form of rain or solid precipitation which melts and refreezes, thus causing an increase in

snow pack density and mass, but little change in surface elevation. Determining the influences of summer densification on accurate geodetic mass balance measurements is limited in the percolation zone of ice masses by inadequate data to constrain the extent, intensity and processes of melt water refreezing (Pfeffer & others, 1991).

In order to gauge whether changes in annual accumulation are as a response to current climate change, or part of the natural cyclicity of the ice sheet, it is important to take measurements over a longer time series. Accumulation records over a long time series can be derived from identifying annual layers in firn and ice cores (Alley, 1988). Melt water percolation may distort indices which typically have an annual fluctuation, such as density, stratigraphy, ion and isotope concentrations. It is important to identify limitations with accumulation record measurements, which may be used at higher, cooler elevations (e.g. firn cores), but may be redundant in areas of high melt, such as the percolation zone.

While estimates of meltwater production from ice in the ablation zone are relatively well predicted by positive degree day models (Braithwaite & Ølesen, 1989), estimates of net runoff from the accumulation zone are very poor (Pfeffer & others, 1991). The upper boundary of effective melt is known as the 'runoff limit'; above this altitude any meltwater produced during the summer subsequently refreezes in the snowpack/firn. However, while the position of the runoff limit corresponds approximately to the boundary of the percolation/wet snow facies identified by Benson (1962), the actual position of the runoff limit remains a "source of substantial uncertainty" (Pfeffer & others, 1991). Furthermore, the proportion of meltwater which actually runs off rather than refreezes in the wet snow zone is also highly uncertain. These uncertainties compromise estimates of current and future runoff from the Greenland Ice Sheet. Projected warming in the Arctic is expected to be between 2 °C and 4 °C by 2040 (ACIA, 2005); this increase in temperature will result in increased melt, and a change in the position of the runoff limit. It is important to

develop an understanding of the interaction between melt water percolation and internal refreezing, and the effect changes in climate will have on the location of the runoff limit.

1.2 CryoSat

As part of The European Space Agency's (ESA) Living Planet Programme there are a series of research missions dedicated to specific aspects of the Earth's environment (ESA, 2007). CryoSat was selected for the Earth Explorer Opportunity mission in June 1999 with the intention of making accurate elevation measurements of the variations in the thickness of the Earth's continental ice sheets and marine ice cover, thereby determining the contribution that the Greenland and Antarctic ice masses are making to mean global sea level rise (Drinkwater & others, 2004).

By making high-resolution radar altimeter measurements over the Greenland and Antarctic ice sheets, ice thickness trends can be interpreted as variations in ice mass. Density fluctuations and surface mass accumulations make the uncertainties in converting elevation change to mass change considerably larger than those associated with measuring the elevation change itself (Wingham & others, 1998). In areas of high surface temperatures, for example the percolation zone, surface melting and subsequent internal refreezing results in a volume change with no associated mass loss or gain. To improve the accuracy of these measurements, and the mass balances derived from them, ground measurements of elevation; snow, ice and density profiles are needed, which can be used to constrain estimates of uncertainty. This requirement, and in particular, the need to calibrate the new satellite resulted in the establishment of the CryoSat Validation Experiment (CryoVEX).

A key component of the ground calibration and validation activity was designated to work in the percolation zone of the Greenland Ice Sheet. The objectives of this field team were to provide ground measurements of snowpack density and structure prior to summer melt in the spring, and following the processes of melt and refreezing in the autumn. In order to constrain errors within the observation window of CryoSat (60 x 250 m) a detailed investigation across a 1 km^2 area was undertaken to investigate covariance of density and accumulation changes over short (1 m – 1 km) spatial scales. The field validation programme was designed to undertake field campaigns in spring and autumn 2004, pre-launch, and spring and autumn 2006, post launch.

Following the unsuccessful launch of CryoSat in autumn 2005, the final (autumn 2006) field season was cancelled. In spring 2006 the investigation was widened across the percolation zone, aiming to provide further data to constrain seasonal densification on a larger spatial scale. All the data collected to date will be used in the planning of future field work as part of the CryoSat 2 mission, due for launch in 2009. The work presented in this thesis comprises an integral field based component of the CryoSat calibration and validation experiment working in the percolation zone of the Greenland Ice Sheet.

1.3 Aims and objectives

Overall, this thesis aims to investigate the effects of summer melt, percolation and refreezing on the snowpack in the percolation zone of the Greenland Ice Sheet. It will address the problems associated with deriving annual accumulations in areas of melt from ground measurements, and also the problems the internal refreezing of meltwater may have on deriving mass balance inferred from elevation change as measured from remote sensing platforms. The effect seasonal densification will

have on elevation changes is constrained in order to provide error bars on the accuracy to which changes in satellite-measured ice mass surface elevation changes represent real changes in ice mass gain or loss. More specifically this thesis will address the following objectives:

1. To measure inter-annual variability in accumulation.
2. To investigate the reliability of using long cores to measure inter-annual accumulation in the percolation zone of the Greenland Ice Sheet.
3. To develop an understanding of spatial and temporal changes in snowpack properties, including ice layer concentration and location, and firn grain size, at small length scales (1 m to 1 km) and longer length scales (>10 km).
4. To quantify seasonal changes in density and accumulation of the snowpack.
5. To determine densification gradients across longer scale (>10 km) transects of the percolation zone.
6. To determine inter-annual variation of densification gradients across a >10 km transect of the percolation zone.

The results presented in this thesis are derived from data collected during three fieldwork seasons in the percolation zone of the Greenland Ice Sheet, and from a nearby Automatic Weather Station (Steffen and others, 1996). The process of snowpack densification can be modelled, however this approach has not been used in this thesis for several reasons. Firstly, the field data collected is unique as it is the first set of data from this location that allows a direct comparison of the snowpack prior to and post summer melt, percolation and refreezing. Due to the remote field site location and the rarity of this data, it was imperative this data was fully investigated. Additionally, following the unsuccessful launch of CrysoSat, and the go ahead to CrysoSat 2, the full analysis of this field data is essential as the results can be used for the planning of future field work for the calibration of CryoSat 2.

1.4 Thesis structure

Much work has already been undertaken to measure the mass balance of Greenland, and the development of different methods have been trialled throughout the Arctic and Antarctic environments. Chapter 2 provides a summary of the research that has been carried out across Greenland to put the current research programme in context. With the increasing concern surrounding rising global temperatures (Trenberth & others, 2007), Chapter 2 also discusses the possible implications of climate change for Greenland.

Chapter 3 provides a description of the field site, the timing of the fieldwork and the suite of measurement techniques that were used for data collection in the field and in the laboratory.

Chapter 4 investigates the possibility of using long (>15 m) firn cores to find annual accumulation over an extended time series in the percolation zone, thus addressing objective 2. Results from a 17 m core retrieved in spring 2004 are presented and a variety of standard techniques are used to try and determine annual layers (and thus mass balance) throughout the full length of the core.

Chapter 5 aims to quantify seasonal changes in densification and accumulation (objectives 3 and 4), in a small scale investigation over 1 km^2. The variation in accumulation, snowpack thickness, density and stratigraphy in a spring (pre summer melt) snowpack, and in an end-of-summer (post melt) snowpack are presented and discussed in conjunction with the subsequent implications for mass balance measurements. Objective 1 is addressed by comparing the accumulation for the 2003 to 2004 mass balance year to accumulation results derived from the 17 m core and from records obtained by previous researchers (Benson, 1962). The effect of ice layers on radar return signals is discussed and the location of ice layers within the snowpack is examined over both the 1 km^2 area and along a 57 km transect

across the percolation zone (objective 3). The percentage of the annual accumulation that is present in the form of ice is compared between the end-of-summer 2004 snowpack and the amount of ice found within each annual layer in the 17 m long core retrieved.

Chapter 6 focuses on objectives 5 and 6, investigating densification gradients along transects within the percolation zone, and inter-annual variations in these densification gradients. The change in average snowpack density with elevation is calculated for the 2004-2005 balance year along a 57 km transect spanning a 370 m change in elevation, and along a 20 km transect for three balance years spanning a 155 m change in elevation. The implications of the gradient of snowpack densification with elevation are discussed and placed in the context of mass balance estimates derived from remotely sensed elevation changes. The potential errors that may arise in mass balance estimates derived from elevation changes, if the densification gradient or annual change in this gradient are not accounted for, are calculated, and a basic model of the impact warming climates may have on firn densification is included.

In Chapter 7 the main conclusions from this thesis are summarised and placed in the context of the original aims and objectives. Further investigations that this work has proven would be scientifically worthwhile are discussed, alongside the necessary limitations of this body of research.

Chapter 2: An overview of the Greenland Ice Sheet, research methods and results

The most recent estimates suggest the Greenland Ice Sheet is currently losing about 100 Gt yr^{-1} (Shepherd & Wingham, 2007), equivalent to 0.28 mm yr^{-1} sea level rise. This represents less than 10% of the total sea level rise of 3 mm yr^{-1} (IPCC, 2007). There is however, still uncertainty in the magnitude of mass change that the Greenland Ice Sheet is experiencing. Current estimates of Greenland's mass balance for periods between 1992-2005 vary between -227 ±33 Gt yr^{-1} (Velicogna & Wahr, 2006b), -75 ± 21 Gt yr^{-1} (Velicogna & Wahr, 2005) and +11 ± 3 Gt yr^{-1} (Zwally & others 2005). These variations are mainly related to the method of measurement, as discussed later in this Chapter, and the associated limitations. More details on estimates, and methods are available in e.g. Lemke & others (2007) and Shepherd & Wingham (2007). The highest estimates of the aerial extent of the Greenland Ice Sheet that experienced melt from 2000 to 2004, vary between 44% and 79% (Wang & others, 2007). A warmer climate will clearly increase this melt extent, as witnessed in the summer of 2002 (Wang & others, 2007).

The Greenland Ice Sheet mainly comprises of ice formed in the Holocene, although older ice formed in the Wisconsin (75ka – 10 ka yr b.p.) can be found in deep cores retrieved from the centre (Wingham, 1995). It is the second largest ice sheet on Earth covering 1.7 x 10^6 km^2 or 80% of Greenland's land mass with ice (Comiso & Parkinson, 2004). With ice thicknesses reaching 3400 m it contains 2.85 x 10^{18} km^3 of ice, enough to raise sea levels by 7 m if the whole ice sheet were to melt (Bamber & Payne, 2004).

2.1 An overview of the Greenland Ice Sheet and snowpack densification

The Greenland Ice Sheet comprises of four main supraglacial zones (Figure 1), distinguished by their snow facies as represented by snowpack density and resulting from spatial patterns of melt and accumulation (Benson, 1962; Fahnestock & others, 1993).

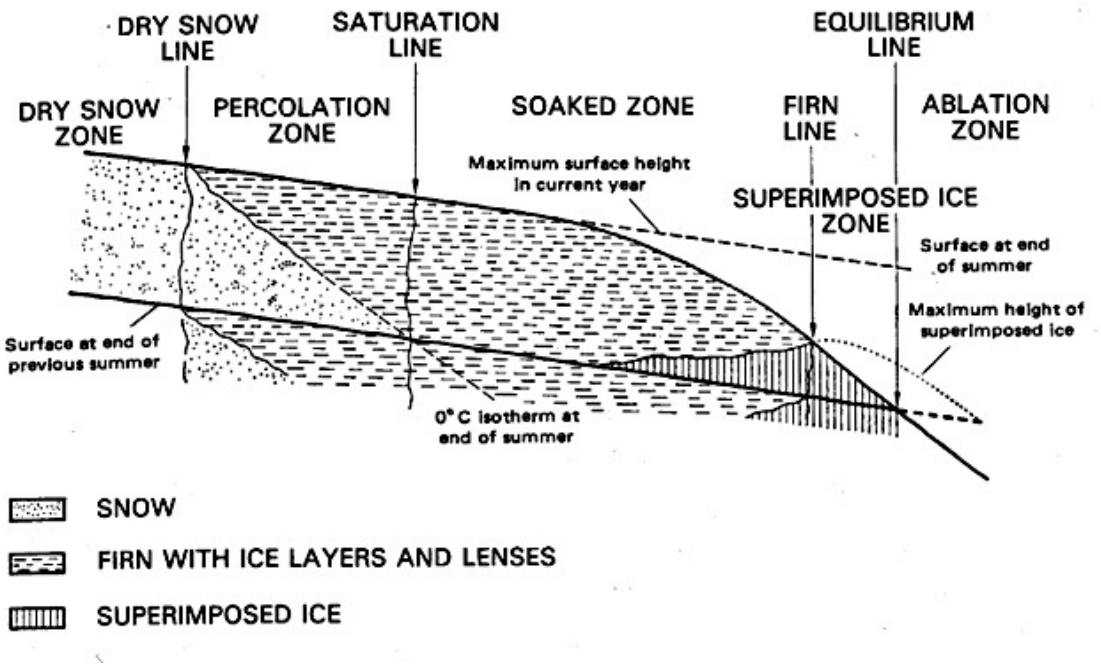

Figure 1: Ice sheet snow facies, from Benson (1962).

The ice sheet interior is higher and colder and consequently experiences little or no melt during the summer, referred to as the dry snow zone (Benson, 1962). Typically the snow is of low density and relatively small grain size (Wang & others, 2007). At lower elevations temperatures are warmer, which results in summer melt. This meltwater then percolates into the snowpack and refreezes in the colder snowpack forming ice lenses and pipes (Jezek & others, 1994), this area is the percolation zone. In the saturation zone the entire snowpack melts in the summer, due to latent heat release from re-freezing of melt water (Benson, 1962). At the lowest elevations

summer melt is extensive enough that all the annual snow accumulation is melted and removed exposing glacier ice, this is the zone of ablation (Benson, 1962).

The extent of these zones varies annually (Wang & others, 2007), with clear implications for the annual mass balance. The Equilibrium line defines the altitude (ELA), above which there is mass gain (dry snow, percolation and saturation zones) and below which there is mass loss (ablation zone). The approximate extent of the zone are shown in Figure 2, as determined using remote sensing by Jezek and others, (1994).

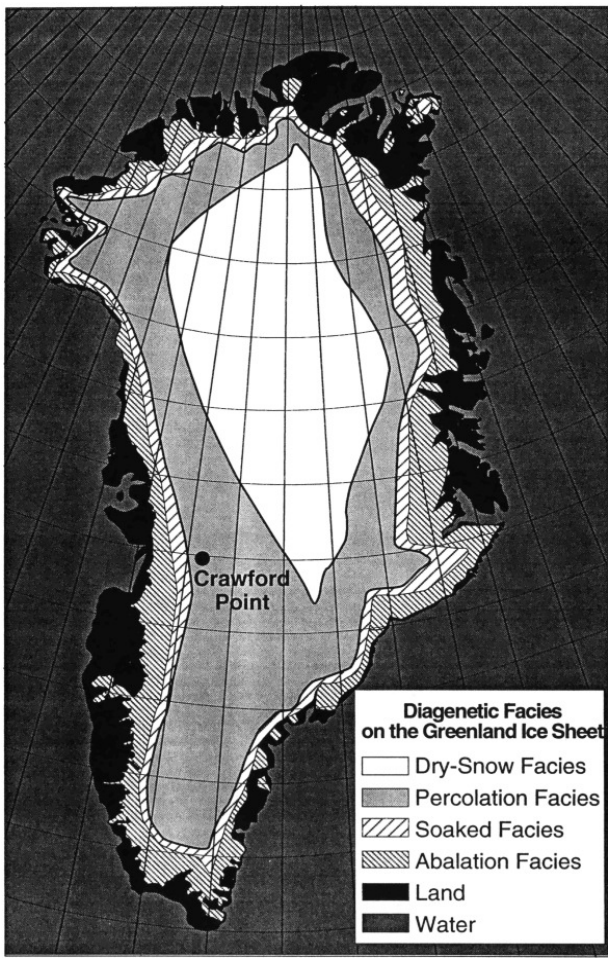

Figure 2: Snow facies of the Greenland Ice Sheet, based on Benson (1962), with Crawford Point AWS marked, from (Jezek and others, 1994).

Across the ice sheet snow is slowly transformed to glacier ice through densification processes, which vary spatially. Fundamentally, the increased compaction of the

snowpack reduces the volume of air between grains results in an increase in density. Once all interconnected are passages are closed off, and the air is separated in individual bubbles, the snow has undergone a full transition to glacier ice (Benn and Evans, 1998).

The volume of air between snow grains is reduced via changes in crystal size and shape. For example, freshly fallen snow may have intricate complex shapes, however when a snow grain is blown along the ground, or compressed beneath other snow grains, the extremities will be broken off, and the grain will become rounded in shape (Benn and Evans, 1998). This allows the crystals to move relative to each other, and find a more stable and compact packing lattice. As burial is deeper, the overlying pressure increases, causing a compression of the air between grains (Ben and Evans, 1998) and an increase in overall material density.

In areas where there is melt, such as the percolation zone, the transformation from snow to ice is accelerated. At the surface the cycle of freezing and thawing results in the joining of grains as the surface tension of the water films tends to pull the grains together (Paterson, 1994). When meltwater percolates into the colder snowpack it refreezes creating superimposed ice features, such as ice lenses, layers and pipes (Paterson, 1994). This rapid transition from snow to ice increases the overall density of the snowpack. Additionally, the latent heat produced on refreezing warms the surrounding snowpack, making it easier for further melting to occur (Benn and Evans, 1998). Due to the fluidity of the meltwater, pore spaces can be filled prior to refreezing. The meltwater also accelerates packing as it acts as a lubricant between the grains, allowing very close packing, and consequently an increase in density (Paterson, 1994).

2.2 Measuring ice sheets mass balance

The mass balance of an ice sheet is the sum of the total accumulation and ablation; it is therefore necessary to measure both these processes across the ice sheet to accurately monitor changes in mass. The scale of an ice sheet ensures that determining mass balance is a difficult problem. In situ measurements can be both detailed and accurate; however, they are typically limited spatially. Remote measurement techniques, using planes and satellites allow greater spatial and potentially temporal coverage, but they are limited in their resolution.

Geodetic mass balance measurements are derived from elevation changes which are interpreted in terms of change in mass. This does not take account of any natural fluctuations in the densification of the snowpack and firn. Changes in temperature and accumulation rate affect the density of recently deposited snow; if these factors vary, so does the rate of snow densification (Arthern and Wingham, 1998). Natural fluctuations in density result in elevation changes which are significant compared to the natural fluctuations in elevation as a result of mass input (Braithwaite, 1994). If the effects of density fluctuations on elevation changes are not accounted for, the accuracy over which a secular trend in ice sheet mass can be found, using the geodetic method, is limited (Van de Veen, 1993).

2.2.1 In situ mass balance measurements

Measurements made in the field allow detailed investigations of high accuracy and great detail. Mass balance measurements at a point are derived from the annual snow depth and the snowpack density, which can be measured in several ways.

In areas of accumulation, annual net balance is commonly measured from the previous year's end-of-summer surface. This occurs beneath a layer of low density depth hoar which typically forms in the autumn (Alley, 1988) and can be identified in the winter snowpack (Williams, 1964; Work & others, 1965). The accumulation can be found by measuring the thickness and density of the annual layer, and noting any ice features and estimating their volume. These can be used to calculate an accumulation as a 'water equivalent' (w.e.) (Østrem & Brugman, 1991). This is easily done in a snowpit, where the face that is sampled provides a larger area to be measured than point measurements, for example, in a core (Paterson, 1994). Overall, snowpits provide an accurate way of measuring accumulation, and investigating snowpack stratigraphy. However, digging and logging snowpits is time consuming and labour intensive, especially on the scale of an ice sheet, making wide scale use of them impractical.

In areas where there is a lot of ice in the snowpack, or areas of very high accumulation, digging snowpits may not be practical, and so cores can be used instead (Østrem & Brugman, 1991). Cylindrical cores are extracted, but are prone to breaking and crumbling (Figure 3) depending on the degree of packing, crystal size and the density (Østrem & Brugman, 1991). Successfully extracted sections can be measured to obtain volume and density to determine the accumulation as a water equivalent. Cores provide a point measurement of accumulation and so are subject to spatial noise from surface features (Van der Veen & Bolzan, 1999), such as sastrugi and other topographic undulations (Mosley-Thompson & others, 2001).

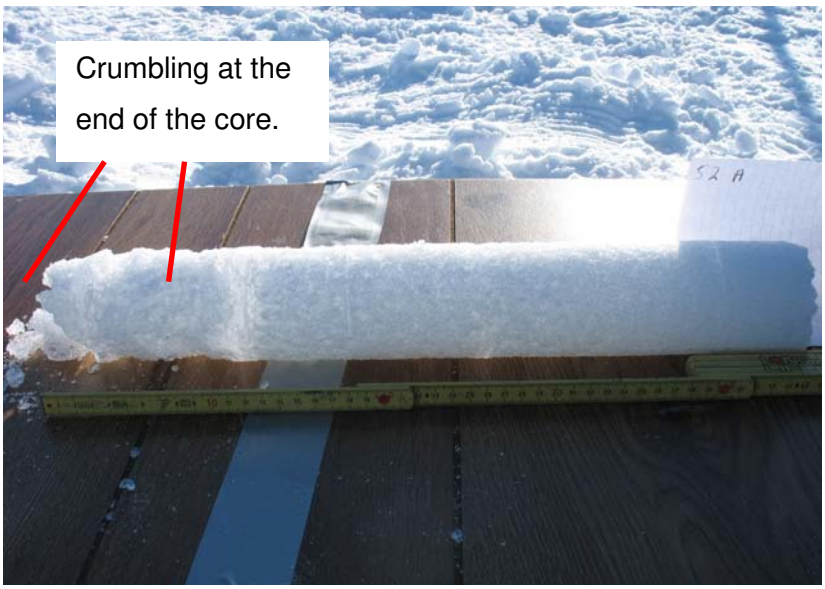

Figure 3: Picture of core extracted with SIPRE corer; crumbling and loss of core can be seen on the left (the deepest section of the core).

Surface roughness and the effects of wind redistribution of mass can cause large spatial variability in snow accumulation over short distances (Thomas & others, 2001). For example variations in local topography and surface windflow can result in microrelief (less than a few kilometres), such as wind drifts, sastrugi and macrorelief, with surface undulations over wavelengths of tens of kilometres (Van der Veen & Bolzan, 1999). This spatial variation in accumulation is at scales of centimetres to kilometres, thus reducing the accuracy of a single measurement location representing regional accumulation (McConnell & others, 2000a). Microrelief occurs as random noise, whereas macrorelief can persist over years changing spatial accumulation distributions (Van der Veen & Bolzan, 1999). As part of the Greenland Ice Sheet Project 2 (GISP2), in 1987 nine cores of 17 m length were retrieved from central Greenland (Figure 4), providing a 24-year accumulation record (Van der Veen & Bolzan, 1999). The cores were retrieved over a 150 km^2 area where the average annual accumulation is 250 mm w.e. and the standard deviation due to spatial variability was found to be 25 mm w.e. per year (Van der Veen & Bolzan, 1999), providing information on spatial variability, due to macrorelief in the area.

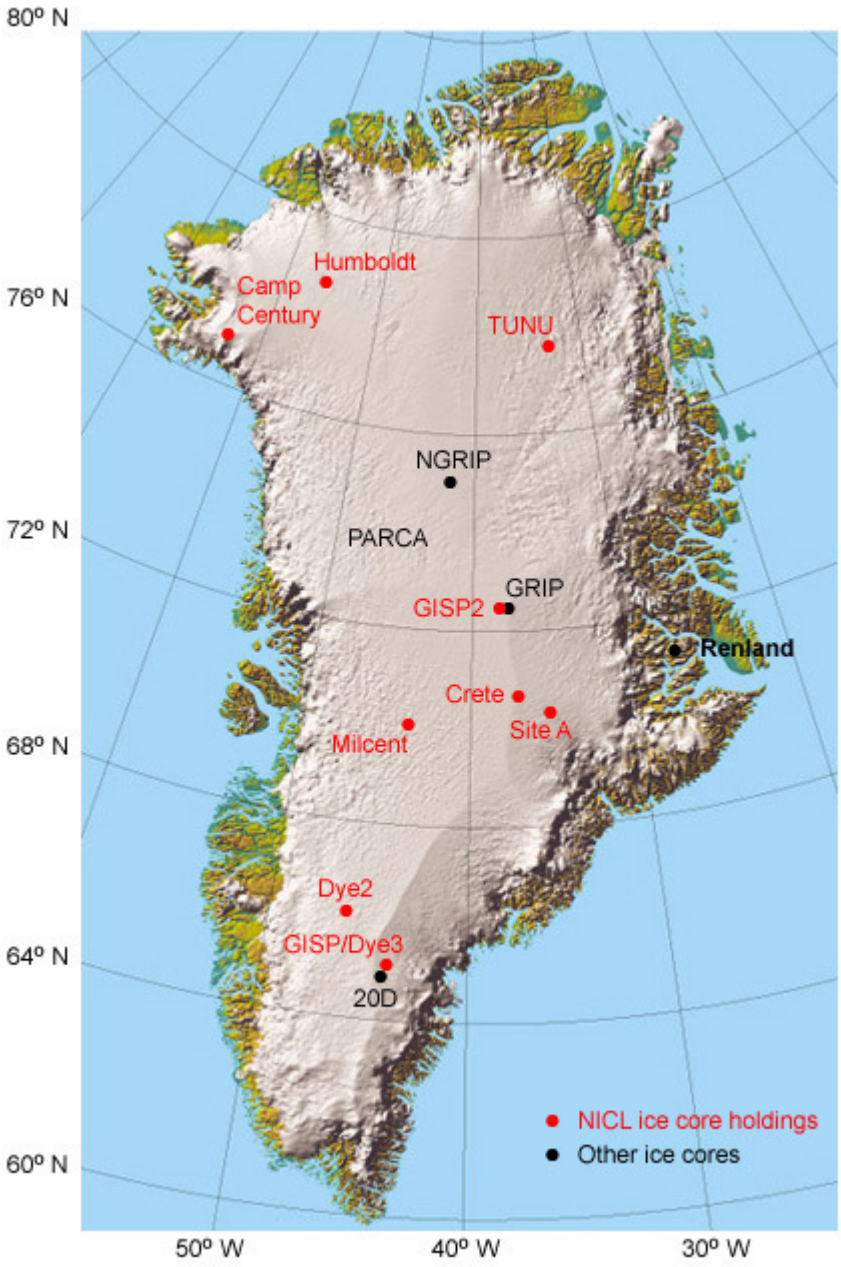

Figure 4: Map of core sites across Greenland (NICL, 2008a).

To reduce the effects of spatial variability on measured annual accumulation rates, the Program for Arctic Regional Climate Assessment (PARCA), in Greenland, found that for a single core in an area of high accumulation (>250 mm w.e. yr^{-1}) it was necessary to find the average annual accumulation over 10 years, and in areas of low accumulation (<205 mm w.e. yr^{-1}) an average over 20 years was required (Thomas & others, 2001). Alternatively spatial variability can be accounted for if the

average annual accumulation was derived from many cores retrieved from one area (Warrick & others, 1996). This temporal variability is impossible to quantify in ice cores, without drilling many within a close area (Thomas & others, 2001).

Cores can also be dated in a variety of ways, and in doing so can provide an historical record of accumulation and temperature. If the atmospheric chemistry changes throughout the year, seasonal variations in the solute deposits may be preserved in the ice sheet stratigraphy. If the variations in solute concentrations can be measured, layers can be dated relative to each other and thus provide a means for annual accumulation to be determined (Sharp & others, 2002).

The effectiveness of different dating techniques can vary between cores, and some techniques are only reliable for part of a core. Nitrate concentrations were suitable for dating for part of the Humbolt core in north-west Greenland (Figure 4) but in recent decades anthropogenic factors have masked its signal (Anklin, 1998).

When an appropriate dating technique has been identified for a core, and the errors can be constrained, cores can provide accumulation and temperature records back throughout the Holocene. The GISP2 (Figure 4) core (3053 m long) was drilled from the surface of the Greenland Ice Sheet, to bedrock, and provides a paleoclimate history for the last 200 000 years, and an accumulation record for the last 11 000 years (Meese & others, 1994).

In order to determine recent accumulation records across the ice sheet, the PARCA program has retrieved cores from 60 sites (Figure 5), and used multiple chemical species, alongside seasonal variations in dust, and $\delta^{18}O$ to increase the precision of their dating to the extent where in some cases there is no dating error (Thomas & others, 2001).

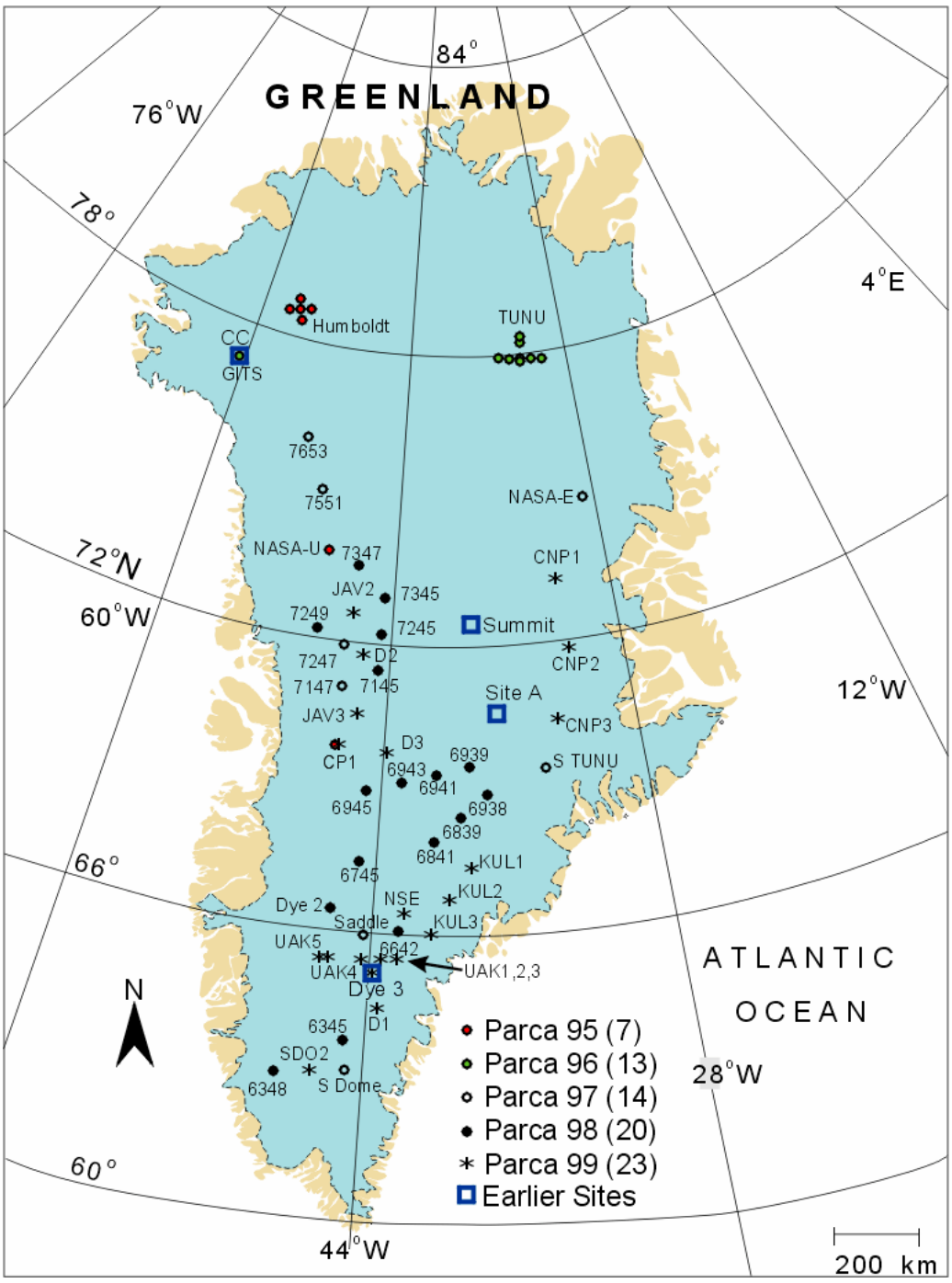

Figure 5: Location of sites where cores were retrieved as part of PARCA (NICL, 2008a).

Seasonal temperature changes throughout the year can result in distinctive stratigraphy within a snowpack. For example, the end-of-summer surface is typically a distinctive hard layer and often has a crumbly layer of large autumn hoar crystals overlying it (Alley, 1988). Visual identification of seasonally varying

stratigraphy can sometimes be used to identify annual layers, and provide a basis on which dating of the core can be done (Alley, & others, 1990). This method allowed successful dating of the GISP2 (Figure 4) core to 50 000 yrs b.p. (Meese & others, 1994).

Once annual layers have been successfully identified in core records, the length between the layers and the average density can be used to calculate the annual accumulation.

Accumulation can also be measured using 'mass-balance' stakes drilled into place and left for a period of time. The change in the distance between the top of the stake and the snowpack can be used to measure accumulation or ablation (Paterson, 1994). This is a relatively quick method to find the mass loss/gain, although to be accurate the density of the snowpack needs to be incorporated into the measurements. Stakes can also be used to mark reference horizons (Paterson, 1994), such as the previous year's end-of-summer surface.

Changes in the stratigraphy due to seasonal temperature variations can result in distinctive changes in density, for example the end-of-summer surface and autumn hoar couplet. Density measurements can be made in a snowpit, but to extend measurements to a greater depth requires either a firn/core or neutron probe. The neutron probe has been used for measuring soil moisture content, and can also be used to derive the density and stratigraphy of snow and ice (Morris & Cooper, 2003; Hawley & Morris, 2006), and has been successfully used to identify higher density winter layers in the dry snow zone on the Greenland Ice Sheet, and an example of this is shown in Figure 6.

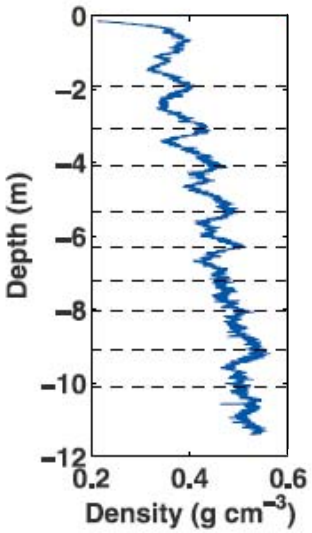

Figure 6: Density profile derived from a neutron-probe. The high density peaks indicate the winter layer (Hawley & others, 2006).

2.2.2 Remote measurements of elevation and mass balance

Satellite altimetry was first developed for oceanographers to measure mean sea levels. The first satellite radar altimeter, flown aboard Skylab proved that oceanographic and geodetic data could be collected from space (McGoogan & others, 1974). With orbits reaching latitudes of 72.1 ^{0}N and S, it was proposed to use satellite altimetry to survey ice sheets (Robin, 1966). Subsequently Geos-3, Seasat and Geosat were the first satellites that were used to study ice sheets (Brooks & others, 1978; Zwally & others, 1983; Bindschadler & others, 1989).

Satellite radar altimetry measurements can cover large areas of the ice sheet, and measurements are potentially accurate to a few centimeters per year when elevations are compared at crossover points in the satellite ground track (Zwally & others, 1989). However, errors are introduced through changes in the shape of the radar echo. Commonly the expected echo shape is approximated to that returned from the ocean surface (Brown, 1977). Ice sheets are more undulating than the ocean surface, with topography and penetration into the snowpack playing an important

role in the shape of the return echo's shape (Wingham, 1995; Legresy & Remy 1997) which means the approximation to the Gaussian convolution (as used over oceans) is insufficient for accurate measurements.

Radar altimeters are primarily used to measure ice sheet elevation although the shape of the altimeter-return wave is influenced by volume scattering (Ridley & Partington, 1988; Davis & Moore, 1993), which can give important geophysical information concerning the near-surface properties of the ice sheet (Davis & Moore, 1993). By looking at individual return wave forms, seasonal and spatial variations of facies across the ice sheet can be determined by using a surface and volume scattering model. The greater the penetration of the wave into the snowpack, the higher the volume scattering, indicating a decrease in surface melting. In areas of no melt the extinction coefficient can reveal information about the temperature of the region. The colder the region, the smaller the grain sizes and the coefficient decreases (Davis & Moore, 1993). Where surface melt, percolation and refreezing results in the formation of ice layers, lenses and pipes, these features intensify the backscatter, making it one of the brightest radar targets on earth (Jezek & others, 1994). These results indicate that satellite based altimeters can be used to measure the aerial extent of melt across ice sheets.

Microwave backscatter is sensitive to the physical characteristics of the snow and firn in the top few metres. This is characterized by the duration and intensity of summer melting and the seasonal metamorphosis of the firn. The occurrence of summer melt will also result in stratification of the snowpack and firn; the presence of ice pipes, lenses and layers can result in a more intense backscatter (Thomas & others, 2001). Isolation of these factors which determine the shape of the echo return is important to reduce measured elevation errors (Scott & others, 2006a).

In order to measure the mass balance of an ice sheet from space, accurate measurements of elevation change are needed. This is done by comparing elevation

measurements at satellite cross-over points (Zwally & others, 1989). However, the changes in the shape of the return wave, attributed to glaciological features such as ice layers and pipes (Jezek & others, 1994), can cause errors in estimates of the elevation. It is important to investigate the cause and magnitude of these errors, as well as their spatial and temporal variability, before elevation changes can be accurately measured from satellite altimeters (Arthern & others, 2001). It is also important to distinguish reflections from topography and penetration (Jezek & Gogineni, 1992). The assumption previously made that ice sheet topography would distort echoes in the same way as ocean waves has lead to errors in estimates of surface elevation, extinction coefficient, surface backscatter and volume backscatter. Gaussian convolution models are used to remove the effects of wave undulations, but using similar algorithms across ice sheets will result in errors in all but the flattest regions (Arthern & others, 2001).

Aircraft laser altimeter measurements are now possible due to recent improvements in the accuracy of aircraft trajectories using Global Positioning Systems (Krabill & Martin, 1987). Airborne laser altimetry works by collecting dense accurate measurements of topography made through a combination of GPS, internal navigation and laser ranging (Krabill & others, 1995). Vectors are worked out from laser ranging from the aircraft to the surface, providing a swath of data, 140-250 m wide. Elevation change can be estimated by comparing the elevations of the footprints from different flights, which lie within 1 m horizontally of each other (Thomas and others, 2001). An example of this is the NASA Airborne Topographic Mapper (ATM), which consists of a conically scanning laser altimeter, which can estimate elevation of the 1 m footprints with a 140-210 m swath when flying at 400 m above the surface (Krabill & others, 1995) thus providing a high resolution of measurements, however, with limited coverage for each mission.

2.3 Current state of the Greenland Ice Sheet

2.3.1 Accumulation

Long term records of mass accumulation are derived on an annual basis are a key input to ice sheet mass balance calculations (Mosely-Thompson & others, 2001). Accumulation primarily depends on precipitation (Hanna & others, 2001) and a changing climate could clearly change circulation and precipitation patterns over Greenland and so affect the accumulation patterns (Houghton & others, 1996).

Re-analysis of European Centre for Medium Range Weather Forecast (ECMWF) model (ERA-40) data, validated against 58 ice cores retrieved as part of the PARCA programme (Figure 5), found mean accumulation across the ice sheet to be 0.28 m yr^{-1} between 1958 and 2003, with no significant trends apparent (Hanna & others, 2006).

Accumulation shows little variation over the past 100 years, as recorded in cores extending back 350 years in northwest Greenland at NASA-U (Figure 5), and 852 years at the Humbolt Glacier (Figure 4) site. NASA-U had a mean annual accumulation of 0.34 m yr^{-1} w.e., Humboldt of 0.14 m yr^{-1} w.e. and the Humboldt core shows a tend of increasing accumulation of 1.3 ± 0.4% per century (Anklin & others 1998).

The PARCA cores (Figure 5) have enabled time specific maps of spatial variability in annual accumulation to be developed (Figure 7). However, there is a lack of core based measurements in the southeast, where accumulation rates are very high. The maps do show that temporal variability in net snow accumulation at annual to multi-annual scales is large. Such variability can produce short term changes in ice

sheet elevation, and mask longer term changes in elevation associated with ice sheet balance. Accumulation in the south is highly spatially variable, so there is still a lot of uncertainty. Comparisons between the PARCA accumulation maps and maps derived from meteorological model simulations show good correlation for temporal variability, but large differences in magnitude (McConnell & others, 2001).

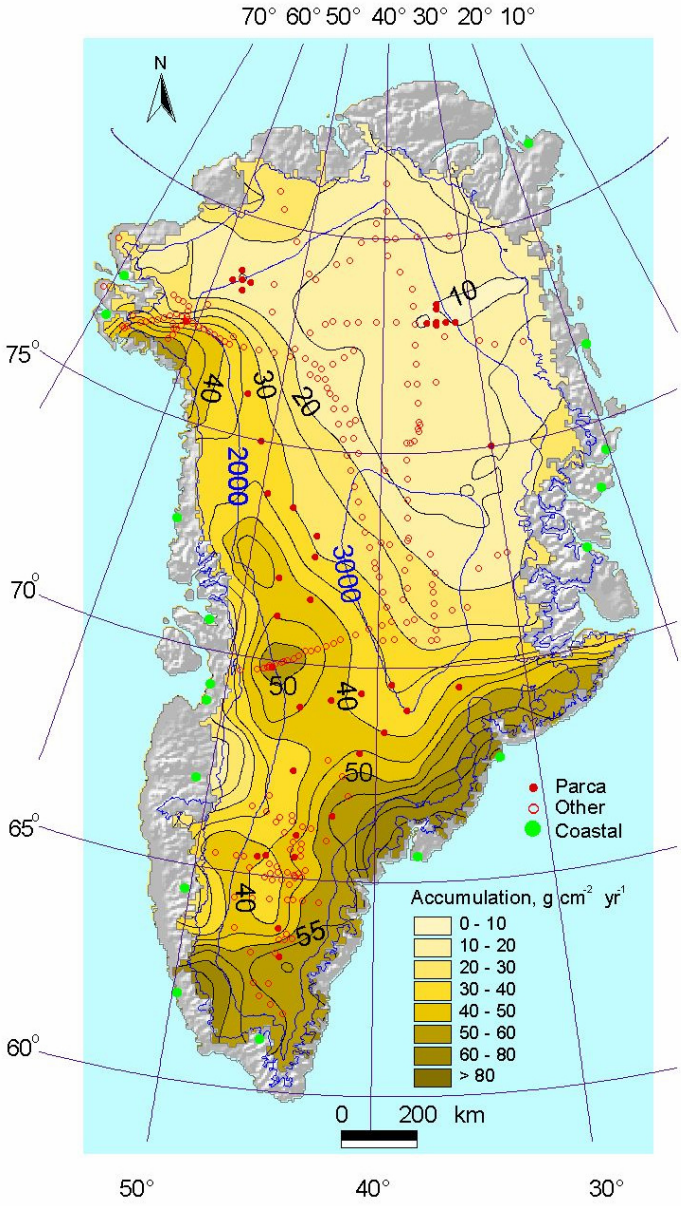

Figure 7: Accumulation map derived from PARCA cores (Bales & others, 2001b).

ECMWF operational analyses and re-analyses show significant increases in accumulation from 1958 – 2006 of 90 $km^3\ yr^{-1}$ (Hanna & others, 2008). Models and observations indicate high snow accumulation in the winter 2004/2005, concentrated in west Greenland (Nghiem & others, 2007), and winter-spring 2002/2003 in southeast Greenland (Hanna & others, 2006).

2.3.2 Melt

Overall, the area and length of time over which melt occurs each summer across the Greenland Ice Sheet has been seen to increase since 1979, reaching a maximum in 2005, as shown in Figure 8 (Abdalati & Steffen, 2001; Steffen & others, 2004; Mote, 2007; Hall & others, 2008; Hanna & others, 2008). The increase in summer temperatures and melt since 1990 can be attributed to global warming (Hanna & others, 2008).

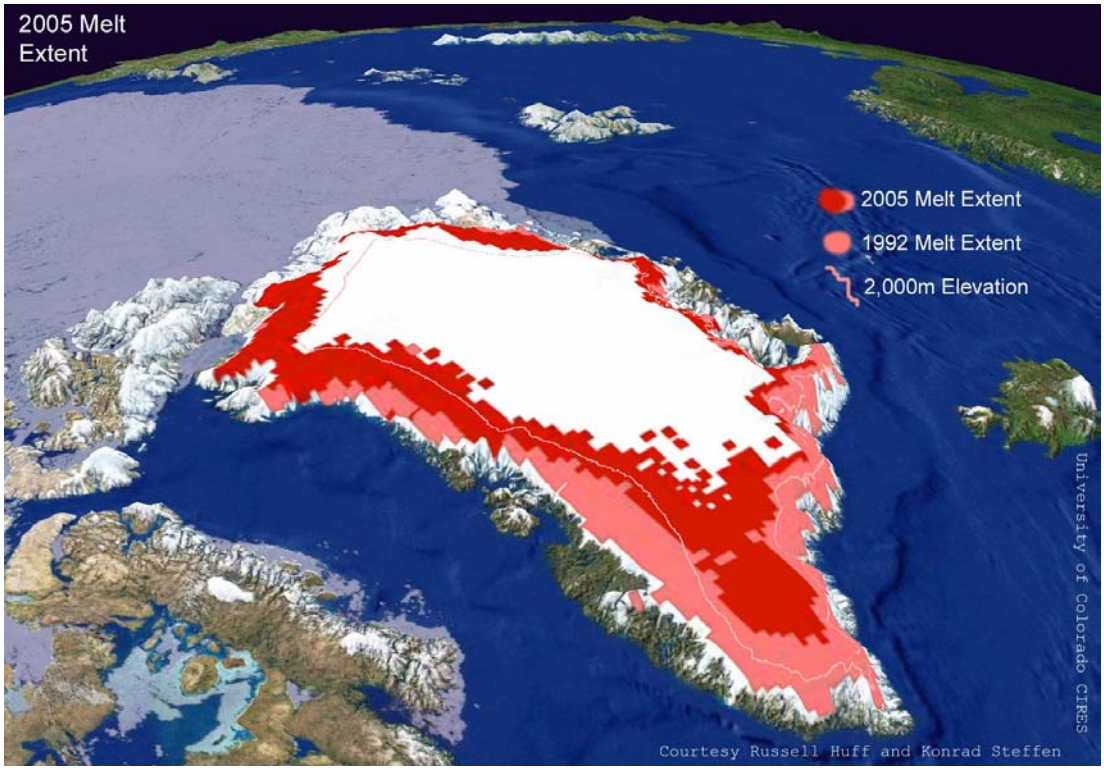

Figure 8: Greenland melt extent in 2005 (Steffen & Huff, 2008).

Between 1979 and 2003 the average area of melt across the Greenland Ice Sheet was 455 000 km^2, measured from passive satellite microwave data (Steffen & others, 2004); over this 24 year time period there has been a positive trend in melt area of 1% per year (Abdalati & Steffen, 2001), this is shown in Figure 9 and Figure 10.

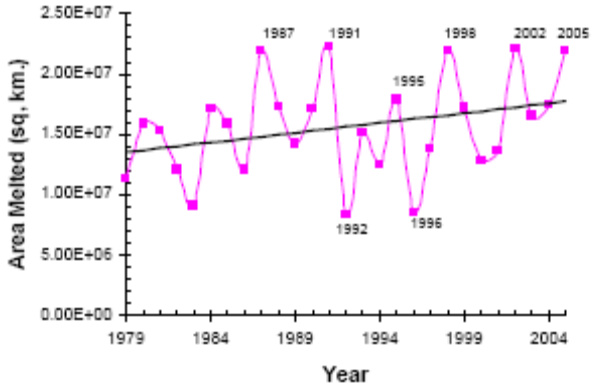

Figure 9: Total melt extent (Steffen & Huff, 2008).

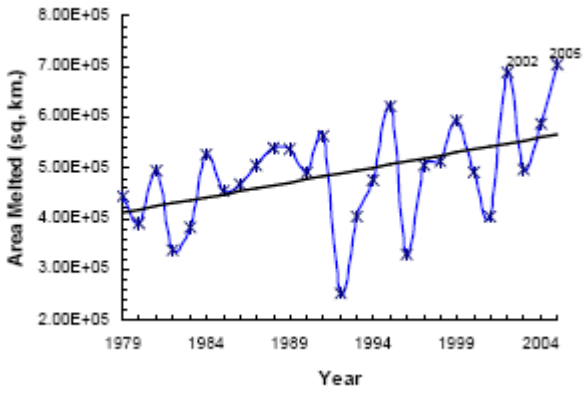

Figure 10: Area of melt experiencing at least one day's melt between April and September (Steffen & Huff, 2008).

Satellite and airborne altimetry measurements suggest the volume of melt between 1993 and 1998 increased at a rate of 60 km^3 yr^{-1} and between 1997 and 2003 this rate increased to 80 km^3 yr^{-1} (Krabill & others, 2000; Krabill & others, 2004; Thomas & others, 2006). In 2002 the melt extent reached 690 000 km^2, with an additional 3000 km^2 of the ice sheet experiencing melt (Mote, 2007).

The maximum melt extent increased again in 2005 to 731 000 km^2, 43% of the total ice sheet (Hanna & others, 2008). These measurements contrast to those reported by Wang & others (2007), where analyses of QuikSCAT images between 2000 and 2004 found the proportion of the ice sheet experiencing melt for at least one day was between 44.2% and 79.2% (Figure 11).

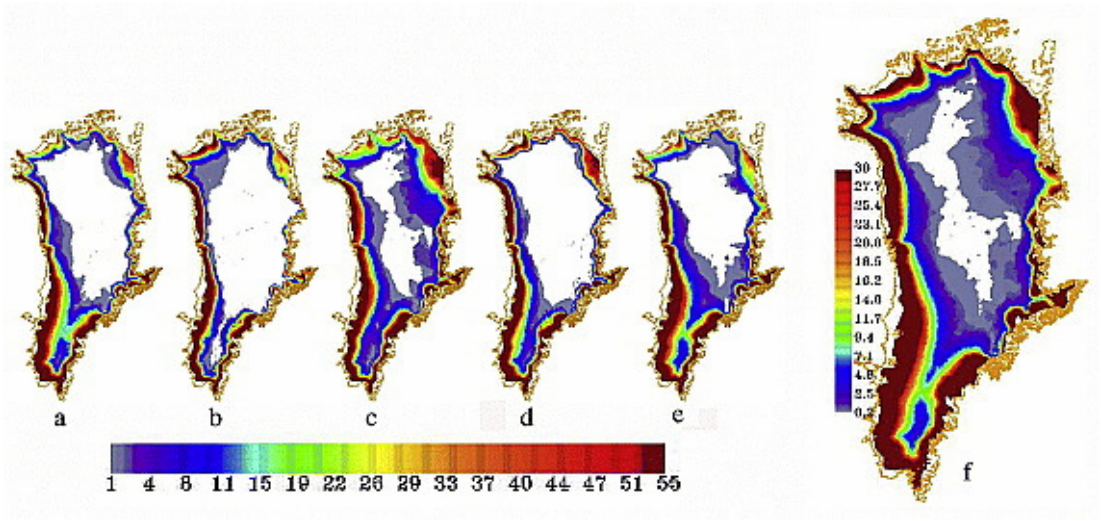

Figure 11: Area of Greenland experiencing at least one day's melt, as measured by QuikSCAT images between 2000 (a) and 2004 (e). The average is shown in (f) (Wang & others, 2007).

Looking at the sum of all daily departures of the areal extent of melt from the daily mean (Seasonal Melt Departure, SMD) for 1973, 1974, 1979-1987 and 1987-2007 the rate of increase in the melt area is 2980 km^2 yr^{-1} (Mote, 2007). During this time period 2007 had the greatest melt extent and covered an area 60% greater than in 1998 (Mote, 2007). The areas where the greatest increase in melt extent have been observed are south of 70° N between 2000 and 2400 m a.s.l. (Mote, 2007).

Between 2003 and 2006 land surface temperatures on Greenland increased by 0.26 °C yr^{-1} (Hall & others, 2008), 2003 was the warmest year since 1958, 2005 the second warmest and 2006 the 3rd warmest, with the 3rd highest melt runoff (Hanna & others, 2008). Five of the nine years with highest runoff have occurred since 2000 (Hanna & others, 2008). However, 2005 was only the 8th highest runoff year,

indicating warmer air masses are reaching higher elevation (Hanna & others, 2008), where meltwater is not contributing to runoff.

Mote and others (2007) also find the onset of melt is occurring earlier in addition to the overall increase in melt area. In 2007 the onset of melt was found to be as much as 30 days earlier than the average previously measured start of melt and in the south of Greenland the average melt duration was up to 50 days longer than previously measured melt duration. These findings were replicated in the south west of Greenland, where the melt season was found to start 18 to 22 days earlier than in 2000 (Hall & others, 2008).

Surface melt has a direct and important relationship with mass loss from the ice sheet. In 2004 and 2005 mass loss started after <1% of the ice sheet had experienced melt and mass loss typically occured <15 days after the onset of surface melt (Hall & others, 2008). There are two main explanations as to why surface melt can enhance mass loss in addition to normal melt-runoff relationships: 1) that evaporation may increase when surface melt begins (Hall & others, 2008) or 2) surface melt flows to the base of the ice sheet causing faster movement of outlet glaciers (Zwally & others, 2002).

2.3.3 Overall mass balance

Between 1978 and 1988 satellite radar altimetry measurements in south Greenland (to 72 °N) were made by Geosat and Seasat (Zwally & others, 1989). Initial interpretation of the results comparing the intersections between Geosat and Seasat show thickening (above 2000 m) of 0.2 ±0.06 m yr^{-1} between 1978 and 1985, and 0.28 ±0.02 m yr^{-1} above the ELA between 1985 and 1986 (Zwally & others, 1989). Re-examination of this data, with improved processing accounting for orbit errors and

re-tracking errors (Douglas & others, 1990; Van de Veen, 1993), shows slight thickening above 2000 m elevation, of 1.5 ± 0.5 cm yr^{-1}. The variability across the region was recorded as -15 to +18 cm yr^{-1}, with seasonal fluctuations of ±15 cm yr^{-1}, and inter-annual fluctuations of ±18 cm yr^{-1}. A physically based model of firn densification combined with patterns of snow accumulation from 12 cores show the rate of elevation change across the ice sheet can vary by ±24 cm yr^{-1} over distances as small as 200 km due to changes in accumulation (McConnell & others, 2000b).

The discharge and thinning of Greenland's outlet glaciers is a major source of mass loss from the ice sheet (Rignot & Thomas, 2002). In east Greenland the negative mass balance of -17 ±4 km^3 yr^{-1}, measured in 1996, is a consequence of high ice discharge from the glaciers (46 ±3 km^3 yr^{-1}) (Rignot & others, 2004), which is not balanced by the mass input of only 29 ±3 km^3 yr^{-1} (Rignot & others, 2004). These findings are not restricted to the east coast, and are seen across the ice sheet, as found by Krabill and others (2004) where laser altimeter surveys by ATM, and modelled snowpack melt, showed a loss of 60 km^3 yr^{-1} for the whole ice sheet between 1993 to 1999. This loss of mass due to ice discharge and peripheral thinning is also seen to be increasing, between 1997 and 2003 ATM measurements showed a mass loss of 80 ±12 km^3 yr^{-1} (Krabill & others, 2004). Half of this loss is due to increased melting, however the other half is a result of the increased velocity of glaciers, exceeding that which is required to balance upstream accumulation (Krabill & others, 2004). Acceleration of Greenland's outlet glaciers is correlated with surface melting (Zwally & others, 2002). Enhanced glacial sliding is measured as a consequence of rapid migration of surface meltwater to the ice bedrock interface (Zwally & others, 2002). Widespread glacier acceleration below 66 °N has been measured by satellite interferometry, by ERS-1 & 2, and in 2005, a year of exceptionally high melt (Steffen & Huff, 2008), glacier acceleration was measured up to 70 °N. This accelerated ice discharge has resulted in a significant increase in the mass loss from the ice sheet. In the 1990's ERS 1&2 measured this to be 90 km^3 yr^{-1}, but in 2005 was measured to be 220 km^3 yr^{-1} (Steffen & Huff, 2008). These

measurements contrast with those from ATM laser altimetry, where although the net mass loss is seen to increase, from 1993 to 1999, estimates were 4 – 50 $km^3\ yr^{-1}$, and in 1998 to 2004, 57 – 105 $km^3\ yr^{-1}$ (Thomas & others, 2006). These results are summarised in Figure 12. The difference in these results is likely due to the larger footprint size of ERS (Thomas & others, 2006).

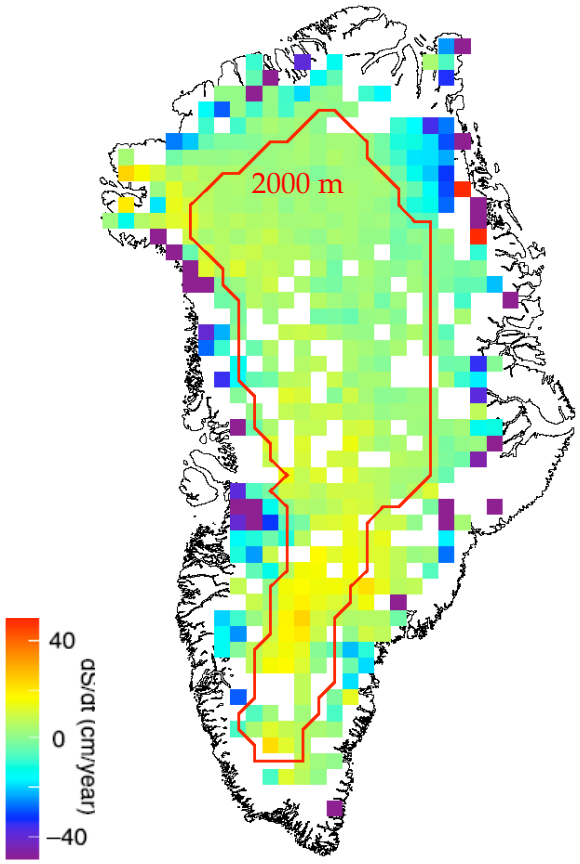

Figure 12: Rates of elevation change across Greenland (Thomas & others, 2006).

PARCA's prime objectives were to measure and understand the mass balance of the Greenland Ice Sheet, using a variety of approaches to measure ice sheet volume, including data collected in situ, and via satellite and aircraft. Analysis of the data has enabled detailed spatial understanding of volume changes across the ice sheet, as well as progressing the development of measurement techniques. As part of the PARCA programme, three measurement techniques were combined by Thomas and others (2001): satellite radar data from ERS-1 and ERS-2; aircraft laser altimeter data and a volume budget comparison were used to determine the mass balance of the

Greenland Ice Sheet above 2000 m. Above 2000 m elevation the entire region was found to be in balance to within ±1 cm yr^{-1} (Thomas & others, 2001) although with considerable variation temporally and spatially. A minimum of five years data is required to identify any thickening or thinning (Thomas & others, 2001). The northeast of Greenland showed low rates of regional thickness change compared to significant thinning in the northwest (Thomas, 2001). Below 2000 m in the southeast there has been significant thinning over the past few decades, at rates of ~1 m yr^{-1} near the coast. This is in part due to increased melt, but also as a consequence of increased ice discharged velocities (Thomas & others, 2001). The south west of the ice sheet was also found to have long term thickening rates due to increased snowfall in contrast to the thinning rates seen in the south east due to the increased ice discharge (Thomas & others, 2001).

The variability in mass balance is modelled by Box (2005) using the MM5 mesoscale atmospheric model. The model parameters are driven by data from satellite observations, weather stations, weather balloons and the ECMWF. When run from 1991 to 2003 at 24 km resolution, results show that precipitation and temperature have the same spatial pattern, and that increasing temperature contributes to the increase in ablation in terms of volume and area despite corresponding increases in precipitation (Box, 2005). The greatest variability in mass balance ± 500 cm w.e. is found along the ice sheet margin (Box & others, 2004).

Mass loss can be directly measured using satellite-based gravity measurements, and this has been applied through NASA's Gravity Recovery and Climate Experiment (GRACE) mission, launched in 2002 (Luthcke & others, 2006). A number of different interpretations have been made using the data but they all result in mass loss. Between 2002 and 2005 estimates range from -169 ± 66 Gt yr^{-1} (Ramillien & others, 2006) to -227 ± 33 Gt yr^{-1} (Velicogna & Wahr, 2005). These measurements are, however, over a short period of time, and in addition gravity measurements are

highly sensitive to glacial isostatic adjustment of the crust and mantle (Ramillien & others, 2006) which introduces errors which are hard to quantify.

Overall the consensus results from a variety of different methodologies suggest that there has been an increase in mass loss from the Greenland Ice Sheet. Thus mass gains due to increased precipitation associated with warming are exceeded by mass loss from enhanced surface melt and dynamic thinning (Alley & others, 2007). The Greenland Ice Sheet is currently losing about 100 Gt yr^{-1}, and a major component of this loss results from tidewater glacier acceleration of between 20 to 100% (Shepherd & Wingham, 2007). With projected future warming, additional loss from the ice sheet is more likely than not (Alley & others, 2007). This general trend is apparent in a summary graph (Figure 13) of mass balance estimates (Thomas & others, 2008)

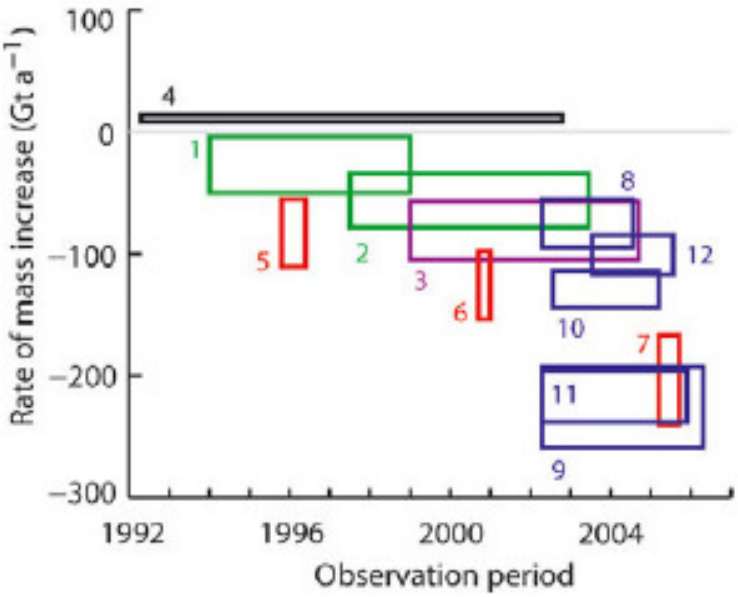

Figure 13: Estimated rates of mass balance change across the Greenland Ice Sheet Airbourne laser altimeters: (1) (Krabill & others, 2000),(2) (Krabill & others, 2004); Airbourne and satellite laser altimeters (3) (Thomas & others, 2006); ERS (4) (Zwally & others, 2005); Mass budget calculations (5 – 7) (Rignot & Kanagaratnam, 2006); Gravity measurements, (8) (Velicogna & Wahr, 2005), (9) (Velicogna & Wahr, 2006a), (10) (Ramillien & others, 2006), (11) (Chen & others, 2006), (12) (Luthcke & others, 2006). Graph from (Thomas & others, 2008).

2.4 Limitation of mass balance measurements in the percolation zone

Surface melting and refreezing complicates mass balance measurements derived from elevation change, due to the re-distribution of mass through densification. One scenario is that surface melt, percolation and re-refreezing will cause a decrease in elevation but with no associated mass loss. In this case, the lost surface snow has been redistributed as ice layers in the near-surface layer whose bulk density has correspondingly increased (Braithwaite & others, 1994). This commonly occurs throughout the percolation zone (Pfeffer & others, 1991). Therefore, refreezing processes complicate accurate mass balance assessments, where the near-surface change in density results in an elevation change, not a change in mass. Unfortunately, determining the influence of summer densification on accurate geodetic measurements of mass balance is currently severely limited in the percolation zone of ice sheets by inadequate characterisation of the extent, intensity and processes of meltwater refreezing (Pfeffer & others, 1991).

If measurements are to be made in terms of change in mass, and not volume, density changes must be accounted for (Arthern & Wingham, 1998; Zwally & Li, 2002). In the dry snow zone, firn densification may account for a few centimetres change in elevation (Arthern and Wingham, 1998), however in the percolation zone and wet snow zone there may be much larger changes (Reeh, 2005).

Temperature changes will affect the amount of surface melting and refreezing as ice lenses or superimposed ice. Clearly if temperature changes persist, the surface elevation changes due to densification will also continue to change. Reeh (2004) shows in a melting/refreezing model that a 1 °C increase in surface temperature across the Greenland Ice Sheet results in a 128 $km^3\ yr^{-1}$ volume loss, however, only

96 km^3 yr^{-1} (75%) off this mass is actually lost from the ice sheet, the remainder refreezes within the snowpack and firn, at a higher density, and so lower volume. When a firn densification model is applied across the Greenland Ice Sheet, there is a reduction in surface elevation with a mean of -1.8 cm yr^{-1} (Li & others, 2007); from this model, 20% of surface elevation changes recently measured by satellite can be attributed to densification, as opposed to mass loss (Li & others, 2007).

In the lower elevations of the ice sheet, the main control on firn density is the percentage of ice present relative to the accumulation (Braithwaite & others, 1994). Relatively small changes in annual melt or accumulation can have a significant impact on the firn density profile (Braithwaite & others, 1994). A numerical model of infiltration and refreezing and fine to coarse grain boundaries finds more ice layers will not be due to uniform warming in summer and winter, but instead due to an increased contrast between winter snow temperatures, and summer melt rate (Pfeffer & Humphrey, 1998).

An understanding of the development of ice layers in the percolation zone is also important, as it can potentially affect the location of the runoff limit, and so mass loss from the percolation zone. There are two anticipated scenarios which would results in the movement of the runoff limit to higher elevations: 1) that all pore spaces in the firn are filled with water, and 2) that ice layers that are traceable over kilometres, but discontinuous on a metre scale, coalesce and form an impermeable horizon (Pfeffer & others, 1991). The first of these scenarios would occur over long periods of time, however, the second may take only a few years of high melt (Pfeffer & others, 1991). If the near surface ice layers coalesce into a single impermeable horizon they will create a thin perched horizon, which could establish a new runoff limit within a few years (Pfeffer & others, 1991).

Since meltwater will only runoff once all accessible pore spaces are saturated, the location of the runoff limit is essential if accurate assessment of melt extent, and

mass loss are to be derived (Pfeffer & others, 1991). If melt increases more than accumulation, greater quantities of meltwater would be expected to refreeze in cold permeable firn, and the elevation of the runoff limit and therefore the total runoff will increase, although not as much as total melt (Pfeffer & others, 1991). Pfeffer and others (1991) found that not accounting for possible changes in the location of the runoff limit, and re-freezing of meltwater in the percolation zone may result in over-estimations of runoff induced sea level rise by 5 cm over 150 years.

Additional problems in satellite derived measurements of mass balance also result from the presence of ice layers, which can result in a 'lifting' of the radar reflecting horizon (Thomas & others, 2008) due to summer melt affecting the dielectric properties of the surface snow, and firn below. This effect is not only due to the formation of ice layers and lenses in the percolation zone, but short melt events in the dry snow zone may have a similar effect on snowpack properties, resulting in overestimates of rates of thickening (Thomas & others, 2008).

When satellite radar altimeter measurements from ERS-2 are compared with laser altimeter elevation measurements, it is found that above 1500 m elevation in the north, radar altimeter estimates of thickening are 9 ±1 cm yr^{-1} higher than laser, and 3 ± 1 cm yr^{-1} higher than laser estimates at elevations above 2000 m in the south. Overall this results in a volume increase of 75 ± 15 km^3 yr^{-1} higher than laser derived measurements (Thomas & others, 2008), which may only be due to the apparent 'lifting' of the reflecting horizon due to the presence of ice layers (Thomas & others, 2008).

2.5 The EGIG line

The Expedition Glaciologiques Internationales au Groenland (EGIG) line, is a ~800 km survey line that transects Greenland from west to east between 69 and 71 °N. There are 66 sites located along the line, T1 to T66, from west to east, and these are spaced at approximately 10 km intervals. Figure 14 shows the location of the EGIG line, and the individual sites along it. Site T1 is at approximately 1700 m a.s.l in the west, T41 is in the centre of the ice sheet, at an elevation of ~3100 m a.s.l and then drops down to T66 ~2100 m a.s.l. in the east. Surveys along the EGIG, or parts of the EGIG have been taking place since the 1950's (Benson, 1962; Seckel, 1977; Stober, 1986; Anklin & others, 1994).

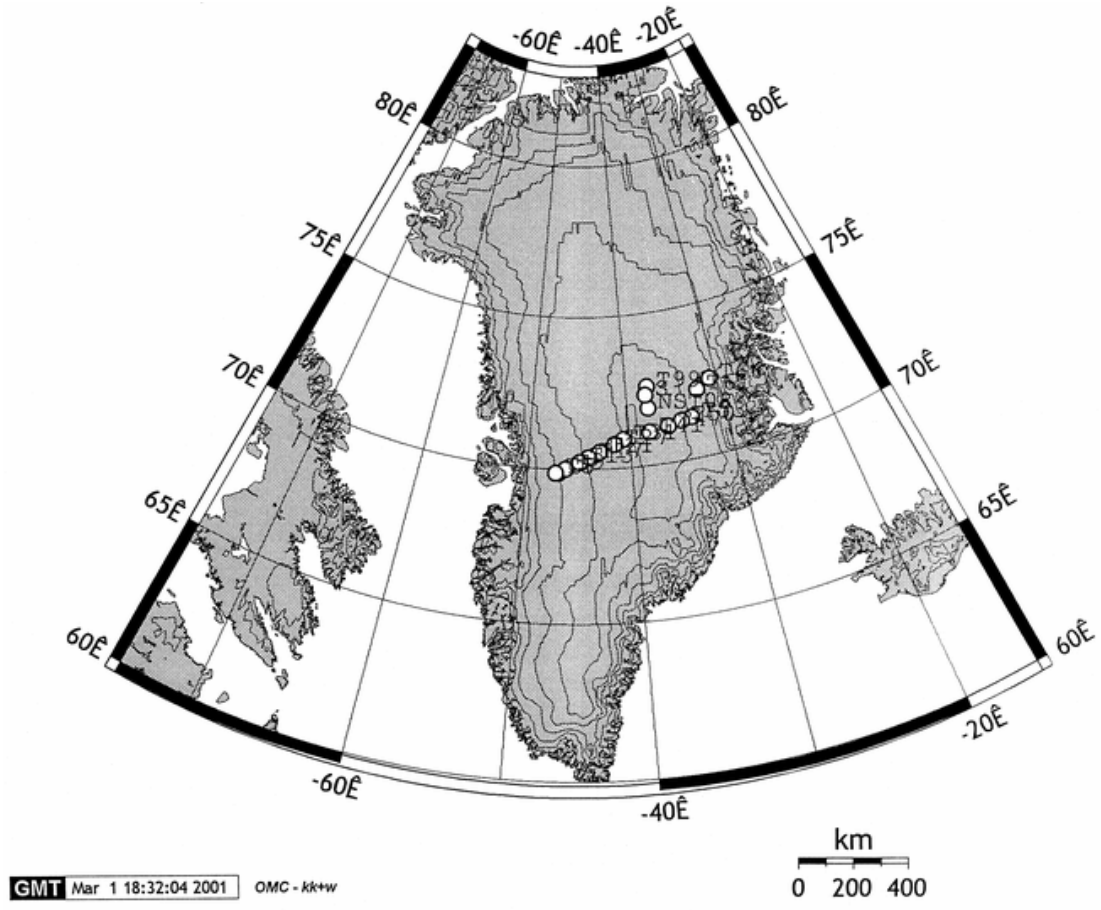

Figure 14: Location of sites along EGIG line (Hanna & others, 2001).

Taking results across a traverse of the ice sheet should in theory give a better indication of ice sheet behaviour (Thomas, 2001). The EGIG line is one such traverse, where results have been collected since 1959.

Fischer and others (1995) analysed the isotopes and chemistry of 18 shallow ice cores taken along a transect across the EGIG line collected in two field seasons in 1990 and 1992. Temperature readings were also taken at 15 m depth at each of these sites (Fischer & others, 1995). Chemistry results from 18 shallow cores retrieved along the EGIG line in 1990 and 1992 reveal that annual accumulation decreases from the west towards the ice divide at a rate of ~47 cm w.e. yr^{-1}, showing Greenland to have two climatologically different regions, either side of the ice divide (summit, T41). The main field site in this thesis, T5, falls to the west of this, in area of higher annual accumulation.

The Geodetic Institute TU Braunschweig repeated the traverse from summit (T41) to T1 re-measuring the position of the markers that were placed during the original 1959 traverse. Results from shallow cores reveal that there were large variations in the local annual accumulation rates in the 1980's, with a typical standard deviation of 10-25% (Anklin & others, 1994). This correlates to variability seen in precipitation records. The western sites, (T1 to T17), show a smaller annual accumulation rates during the last decade; the eastern sites show a higher rate, implying that the annual accumulation rates are increasing in central Greenland, and decreasing in mid and low elevation areas. Along the traverse (T1 to T41) the accumulation rates are seen to change by less than 10% for the last forty years (Anklin & others, 1994).

The accumulation at T5, the main field site in this study, was measured by Benson (1962) Anklin (1994) and varied between 60 and 45 cm w.e. yr^{-1} respectively. Accumulation rates close to Crawford Point (in the vicinity of T6) vary between 0.48 m w.e. yr^{-1} and 0.47 m w.e. yr^{-1} for 1983 – 1989 (Anklin, 1994).

2.6 Summary

Overall, the current literature demonstrates that increased global temperatures are having an effect on the mass balance of the Greenland Ice Sheet. Complications exist in determining the accuracy of the measurements, due to different measurement techniques, and the errors associated with each. In addition, it is clear that near surface processes in the percolation zone can lead to the re-distribution of mass in the form of ice layers, which has implications for mass balance measurements derived from elevations changes, and also the location of the runoff limit (Pfeffer & others, 1991). This thesis aims to constrain some of the limitations associated with mass balance measurements in the percolation zone. The research is focused at site T5, along the EGIG line, so comparisons with previous measurements can be made.

Chapter 3: Field Site and methodology

3.1 Introduction

The aim of this thesis is to investigate the extent to which surface melt water, generated during the summer in the percolation zone of the Greenland Ice Sheet, percolates into the underlying snowpack and refreezes thereby affecting the snowpack structure. More specifically, changes in firn and snowpack density and associated elevation change are investigated in conjunction with chemical analyses of distinctive snowpack/firn facies.

The process of meltwater generation, percolation and refreezing within the snowpack results in the same mass occupying a smaller volume; this investigation aims to quantify the impact changes in density (and thus volume) have on surface elevation. In addition, the movement of meltwater through the snowpack has the potential to mobilise ions and isotopes within the snowpack and firn which may affect the potential use of chemical signatures in resolving annual layers (and so mass balance) within the firn.

Data were collected over three field seasons on the Greenland Ice Sheet and from further laboratory analysis. This Chapter will describe field site locations, the meteorological conditions at the primary field site, specific measurement locations, the timing of the fieldwork, field work techniques and subsequent preparation of samples for laboratory analysis, and the methods used for ionic and isotopic analysis of samples.

3.2 Field Site

The study was located in the percolation zone on the western margin of the Greenland Ice Sheet along the EGIG line, which traverses Greenland at approximately 70°N (Figure 15). This investigation focused on seven sites at approximately 10 km intervals along a transect spanning 57 km, from T1 at 1680 m elevation to T7 at 2050 m elevation (Figure 15, a copy of this figure is also provided in a pocket in the back cover).

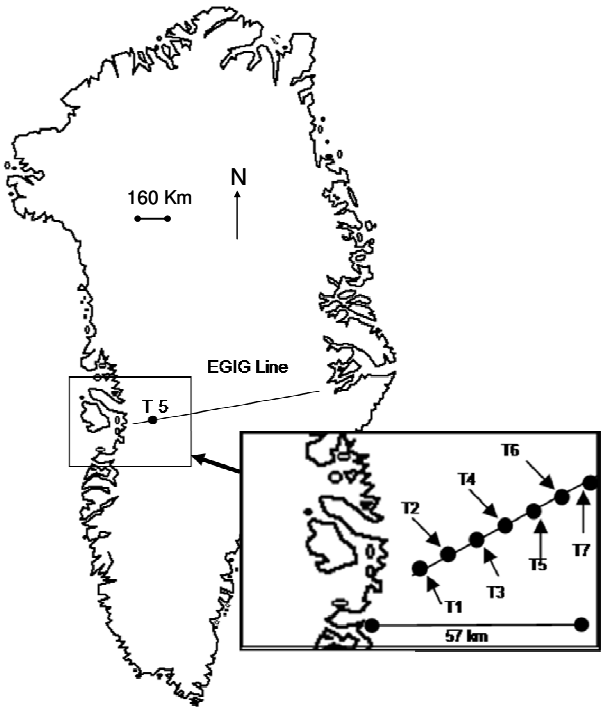

Figure **15***: The location of measurement sites along the EGIG line, a copy of this is included in a handout in the back cover.*

Additionally, a more detailed investigation was undertaken over a 1 km² area in the vicinity of T5 at ~1945m elevation (69°51'4.6"N, 47°15'11.2"W), where variability over spatial scales from 10^0 to 10^3 m are investigated (Figure 16, this figure is also included on the handout in the back cover).

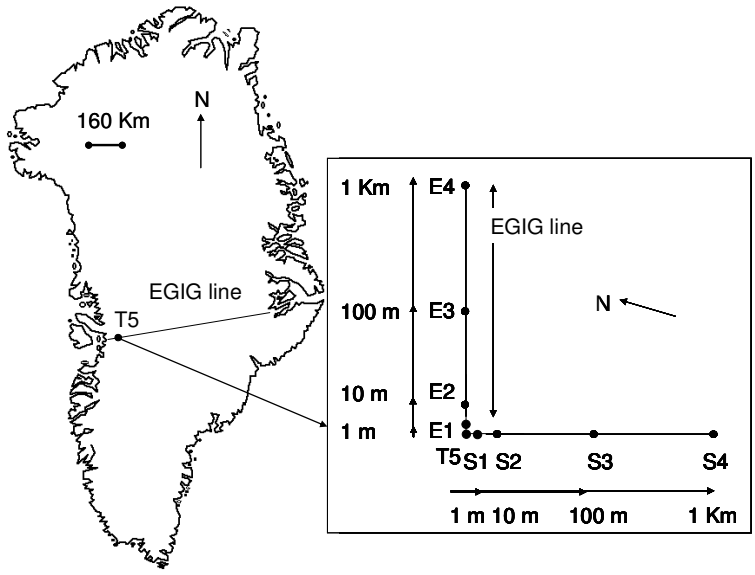

Figure **16***: Layout of detailed investigation at T5 covering 1 km² (included on the handout in the back cover).*

T5 was selected as the field site due to: i) its location within the percolation zone, ii) the availability of data from previous glaciological/meteorological studies along the EGIG line (Benson, 1962; Seckel, 1977; Stober, 1986; Anklin & others, 1994) and iii) its proximity to an Automatic Weather Station (Crawford Point). Crawford Point is operated as part of the NASA Greenland Climate Network: GC-Net (Steffen & others, 1996) located at 69°52'47"N, 46°59'12"W, approximately 10 km east-north-east of T5 in the vicinity of T6 (Figure 15, also shown in Figure 2).

The Greenland Climate Network, 'GC-Net', part of the PARCA programme consists of eighteen automatic weather stations (AWS) located across the Greenland Ice Sheet (Steffen & others, 1996). Each AWS makes hourly measurements of: wind speed and direction, net radiation, air temperature, relative humidity, air pressure, accumulation, snow temperature, and albedo. The proximity of Crawford Point AWS to T5 provides valuable meteorological data for the primary field site. Limitations exist where there has been instrument failure, creating a gap in otherwise continuous measurements, before repairs are able to be carried out.

Results from Crawford Point AWS, where air temperature measurements are taken once every hour using a thermocouple and Campbell Scientific thermometers (CS500), show that February is the coldest month and July the warmest, with average temperatures of -31.3 °C and -6.2 °C respectively (Steffen & Box, 2001). An average annual temperature profile is plotted in Figure 17 for data collected in 2002 on the CS500 thermometers at Crawford Point AWS. Temperatures above 0 °C typically occur between June and August but with significant inter-annual variability.

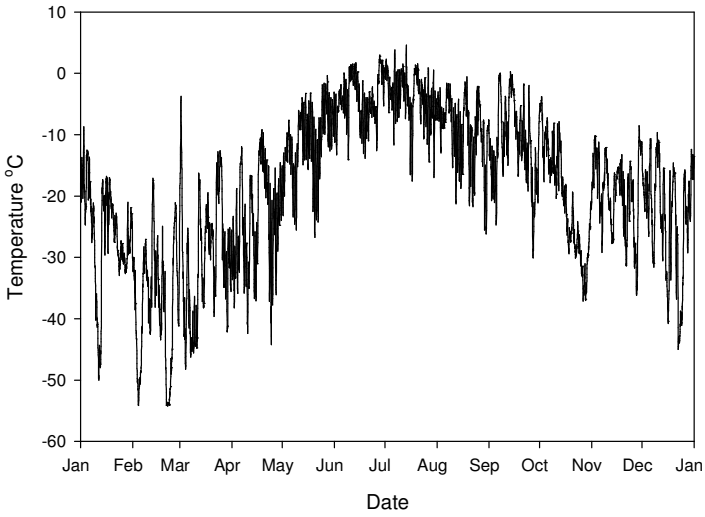

Figure 17: Annual temperature fluctuations for 2002 recorded at Crawford Pont AWS (Steffen & others, 1996).

The total number of 'Positive Degree Days' (PDDs) for each year have been calculated using data collected at Crawford Point AWS (Steffen & others, 1996) by integrating positive daily temperature with time (Figure 18).

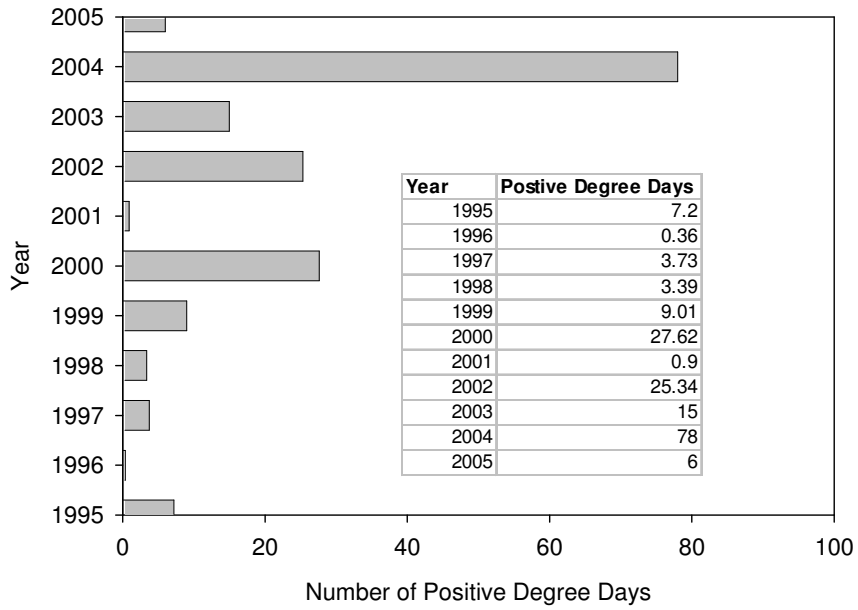

Year	Postive Degree Days
1995	7.2
1996	0.36
1997	3.73
1998	3.39
1999	9.01
2000	27.62
2001	0.9
2002	25.34
2003	15
2004	78
2005	6

*Figure **18**: Number of Positive Degree Days per year calculated from Crawford Point AWS data (Steffen & others, 1996).*

The survey area is subject to down slope katabatic acceleration (Heinemann & Klein, 2002), the dominant wind system on the ice sheet (Steffen & Box, 2001). At Crawford Point AWS the average annual wind speed is 6.5 m s^{-1} at 135°. October to March are the windiest months, with average speeds above 8 m s^{-1} (apart from February) (Steffen & Box, 2001). The wind regime has major implications for snowpack characteristics in the vicinity of T5, as blowing snow can result in the constant redistribution of surface snow and the formation of surface features such as sastrugi and ice crusts, as shown in Figure 19.

Figure **19***: Surface features typical of those seen at T5, caused by re-distribution of snow by wind action. The top picture shows sastrugi, and the bottom a scoured wind crust.*

Under certain conditions, where incoming solar radiation is in excess of 50 W m^{-2} and wind speed is <5 m s^{-1} , temperatures measured using the CS500 (non-ventilated sensor) can be up to 8 °C higher than the temperature measured with the ventilated sensor. To account for this source of error the following correction algorithm (Equation 1) has been applied to such measurements.

$$C = -\left(0.207 - 0.107 \times u + 0.014 \times s + 0.131 u^2 - 0.002 \times u \times s - 4.743 \times 10^{-6} S^2\right)$$

u = wind speed m $^{s-1}$
S = incoming solar radiation (W m^{-2})

Equation 1: Correction algorithm applied to CS500 measurements found to be too high due to solar overheating (Box, 2001).

3.3 Measurement Locations

Fieldwork was undertaken between 1680 m and 2050 m elevation in the percolation zone of the Greenland Ice Sheet, between T1 (69°43′52.7″N, 48°7′58″W) and T7 (69°56′28.1″N, 46°48′3.2″W) on the EGIG line (Figure 15). Additionally, small scale variations in snowpack properties were investigated in the region of T5 (69°51′N, 47°15′W, Figure **16**).

3.3.1 Measurement locations along the EGIG line from T1 to T7

In order to investigate variations in snowpack and firn characteristics at large (~10 km) length scales, measurements were made at approximately 10 km intervals at seven sites along a 57 km section of the EGIG line between and including T1 (69°43′52.7″N, 48°7′58″W 1680 m elevation) and T7 (69°56′28.1″N, 46°48′3.2″W, 2050 m elevation). These points were chosen as they were selected as survey sites on the original EGIG line transect in 1957, the precise positions, elevations and distance between sites are shown in Table 1.

Site location	Distance from T1 along EGIG line	Elevation above sea level m
T1	0 km	1680 m
T2	8.1 km	1750 m
T3	16.3 km	1795 m
T4	25.7 km	1860 m
T5	36.6 km	1945 m
T6	47.03 km	2015 m
T7	57 km	2050 m

Table 1: Site locations along EGIG line investigated in spring 2006, showing distance in km from T1, and elevation in m.

3.3.2 Measurement locations for small scale investigation at T5

In order to investigate snowpack and firn variations over a range of spatial scales, two 1 km long transects, entitled 'E' and 'S', centred on T5, were established with eight additional measurement locations at 1 m, 10 m, 100 m and 1 km intervals from T5. Transect E is aligned in an east-north-easterly direction along the EGIG line towards the centre of the ice sheet (measurement locations E1, E2, E3 and E4). Transect S is aligned in a south-south-easterly direction, perpendicular to the EGIG line (measurement locations S1, S2, S3 and S4) as detailed in Figure 16.

3.4 Timing of Fieldwork

The field work was timed so as to record snowpack properties prior to the onset of spring melt (Figure 17) and following the cessation of summer melt, percolation and refreezing processes; thereby enabling quantification of the seasonal changes in the snowpack. Field investigations took place in the spring (19th April – 13th May) and autumn (28th August – 21st September) of 2004, and spring (19th April – 11th May) 2006.

3.5 Field measurement techniques

In order to characterise variations in snowpack and firn properties, a suite of different measurement techniques were utilised, the data collected in each field season are listed in Appendix 6. More specifically, data were collected from snowpits, shallow firn cores, down bore-hole neutron probe density profiles, snowpit trenches and avalanche probe snow depth transects. Additionally, snow and firn samples were retrieved from snowpits for future analysis in the UK.

3.5.1 Snowpits

Spring 2004

In spring 2004, seven ~1 m^2 snowpits were excavated within 1 km^2 of T5 at sites T5, E2, E3, E4, S2, S3 and S4 (Figure 16). Sites T1, S1 and E1 are all 1 m apart, and so one snowpit was excavated, and measurements taken 1 m from each other within this snowpit, as close to the measurement location as possible (Figure 21). Additional snowpits were also dug at T4 and T6 located approximately 10 km down and up the EGIG line respectively (Figure 15).

At each location the snowpits were dug down to the end-of-summer 2003 snow surface. This distinctive layer was recognisable as a hard icy layer that was continuous across the floor of the snowpit and located directly below a layer of unconsolidated autumn hoar. The autumn hoar has distinctive large (1-3 mm) faceted crystals in a loosely consolidated, soft layer. The icy surface is distinctive due to its continuity, and also its flat, slightly 'dimpled' appearance, distinguishing it from the thinner fossilised windcrusts commonly observed higher up in the snowpack. The identification of the 2003 end-of-summer surface enables the

snowpack above it to be assigned to the autumn 2003 and winter 2003-4 accumulation. Metal 'accumulation' stakes were inserted into the snowpack and firn to mark the pit locations and to ensure the future recognition of the end-of-summer 2003 layer and subsequent accumulation. Once the snowpits had been logged, they were re-filled with the excavated snow.

Autumn 2004

In autumn 2004, snowpits were excavated within 1 m of the spring sites.
The locations varied to avoid sampling the spring snowpits where the snowpack had been artificially disturbed by excavation and subsequent re-filling (Figure 20).

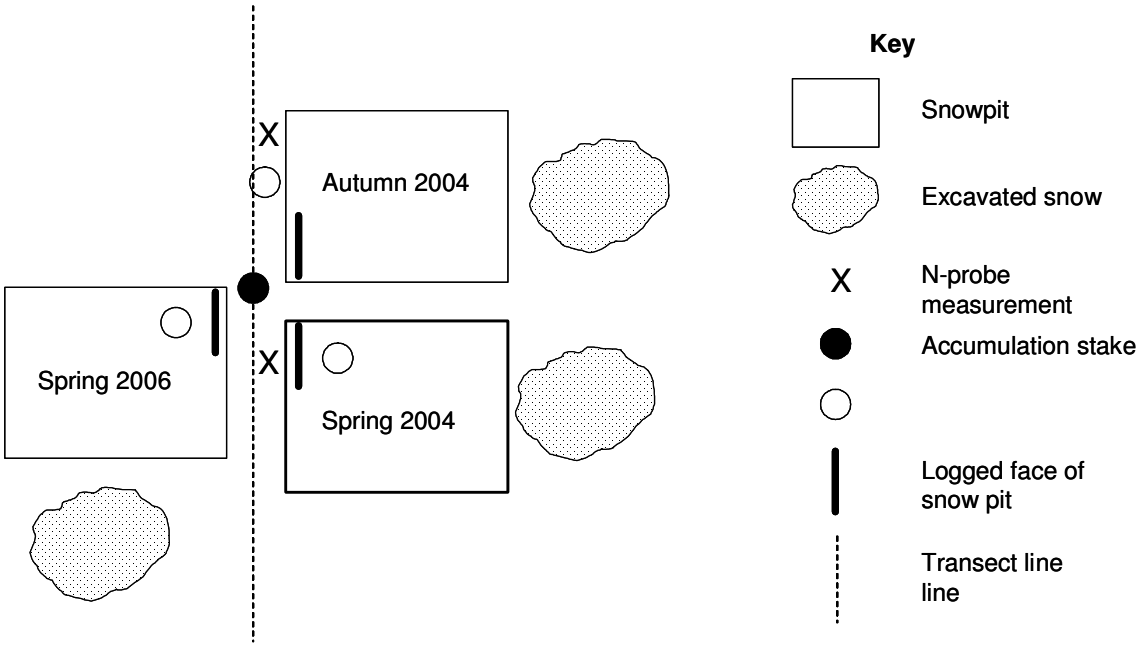

Figure 20: Example of where snowpits were dug, cores were drilled and neutron probe holes were bored for each field season at locations S2-S4, E2-E4, T4 and T6 in plan view.

The snowpits were dug to the end-of-summer 2003 surface which was identified with reference to the accumulation stake left in spring. In addition, recognition of the summer 2003 layer was generally possible due to the presence of the spatially continuous and icy end-of-summer 2003 layer located beneath the autumn hoar; its

continuity distinguishing it from other ice layers common in the autumn snowpit (Figure 22). The snowpit was once more back-filled and at the end of the autumn 2004 field season, the accumulation stakes were extended to act as a datum and locator for the following spring 2006 visit.

Spring 2006

Repeat snowpit excavations were carried out at T4, T5, T6, E1-E4 and S1-S4 as close to each of the accumulation stakes as possible, avoiding digging in an area excavated in 2004 (Figure 20). For T5, S1 and E1, the snowpit was located 3.5 m along the EGIG line, towards E2 (Figure 16) and measurements were made 1 m apart from each other, as close to the site location as possible (Figure 21).

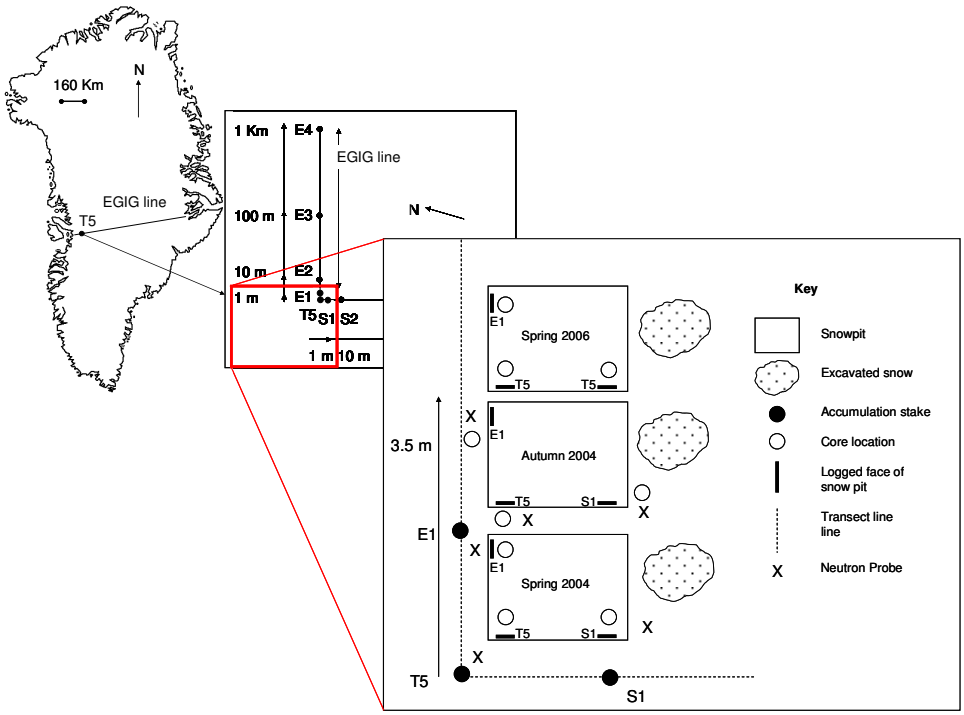

Figure 21: Location where measurements were taken at T5, S1 and E1 for each field season.

Additionally snowpits were excavated at locations T1, T2, T3 and T7 (Figure 15). The end-of-summer 2005 surface was identified in the same way as the end-of-summer 2003 layer was located at the base of the spring 2004 snowpits; namely as the first continuous icy layer which occurs beneath a layer of autumn hoar.

Logging snowpits

One part of one face of each excavated snowpit was logged following standard snowpit surveying protocol (Colbeck & others, 1990). The vertical snowpit face closest to the accumulation stake was 'levelled' with a spade. A ruler was set up against this face (Figure 22) and the probe of the digital thermometer (precise to 0.1 °C) was inserted into the snowpack every 5 cm for the first 30 cm below the surface, and then every 10 cm to the bottom of each snowpit. The probe was held in place in the snowpack until a constant temperature (±0.2 °C) was reached.

The vertical face was then cleaned with a plastic brush to aid visual determination of stratigraphic layers, without chemical contamination. Stratigraphic layers were then identified using a semi-quantitative assessment of hardness: a measure of the resistance to penetration by a material that is harder than the snow (Pielmeier & Schneebeli, 2002). This was done by attempting to push, in the following order, a fist, finger, pencil then knife into the snowpack at 10 mm intervals from the surface down each profile and recording the largest item that could be inserted (Colbeck & others, 1990). The snowpack was thus broken down into stratigraphic layers that were distinguished by this standard simple snow hardness test. Once identified, the thickness of each layer was measured using a ruler (1 mm precision).

Snow grain samples were collected from each individual stratigraphic layer, sprinkled on a snowpack scale card, observed and measured under a hand-lens

against a scale card, with 1, 2 and 3 mm grids. The crystal type for each layer was also identified using the 'Field guide to snow crystals' (LaChapelle, 1969). The location and thickness of windcrusts were recorded in both spring and autumn snowpits whilst ice features, including layers and pipes (Figure 22), present in the autumn snowpits were recorded in the same way.

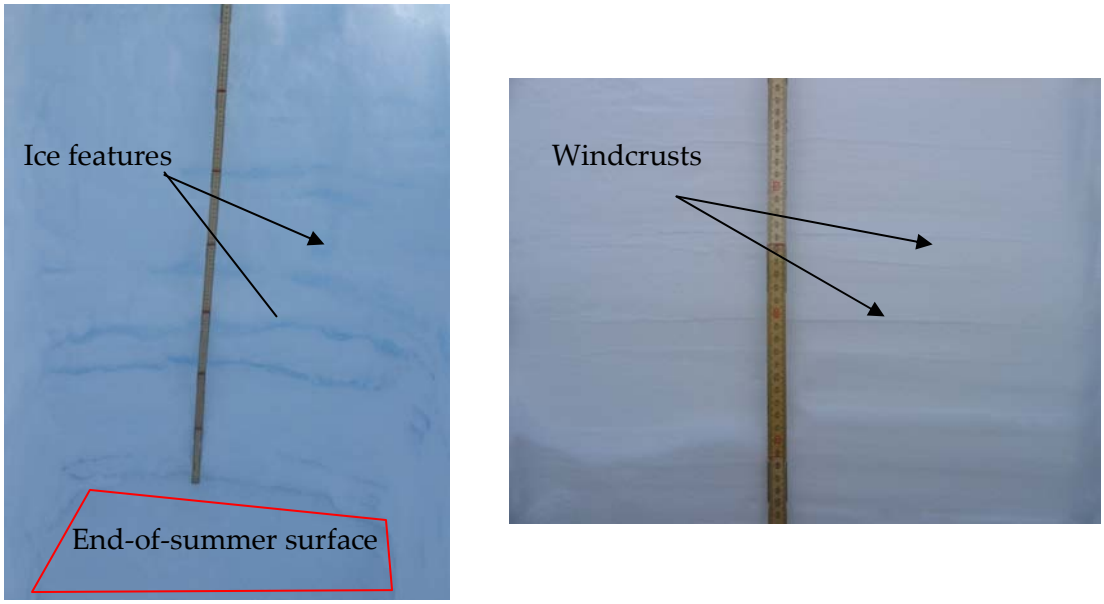

Figure 22: Two snowpits showing the ruler set against the face to be logged. On the left is an autumn snowpit, where clear ice layers are seen across the pit. On the right is a spring snowpit, where wind crusts are visible.

Density measurements were obtained from each stratigraphic layer using snow sampling tubes. The largest plastic tube (diameters of 1.9, 3.2 and 3.8 cm) that could be pushed into a given stratigraphic layer was used to extract a known volume of snow/firn (57, 161 or 227 cm^3), which was then weighed using a Newton balance, sheltered from the wind, to obtain density (Østrem & Brugman,1991). Repeat measurements from each stratigraphic layer were taken and averaged. Variability was found to be 2 – 3% for the large and medium sized tubes, and 17% for the small tube. Since it was not feasible to accurately sample the density of the thin ice layers, they were allocated a density of 0.8 g cm^{-3}, as the ice was typically observed to contain bubbles. In addition, the snowpack in autumn 2004 at T4, was too hard for

the insertion of any of the plastic tubes, hence density measurements were not taken from the snowpit.

3.5.2 Firn Cores

Shallow 2-3 m firn cores were collected close to the logged face of the snowpits in order to characterise the density and stratigraphy of the upper firn. In addition, one longer (~17 m) core was collected from E3 in spring 2004 with the intention of investigating the identification of annual layers and thus annual accumulation rates in the firn. A second 18 m core was collected from E3 in autumn 2004 to provide a comparison set of data, however this core was delayed en-route to the UK and melted.

3.5.2.1 Shallow Firn Cores

Spring cores

In spring 2004 and 2006, firn cores of 2-3 m length and 70 mm diameter, were drilled using a Kovacs corer from the end-of-summer 2003 and 2005 surfaces, respectively located at the bottom of each snowpit. Cores were retrieved as close as possible to the face that was logged in the snowpit (Figure 20 and Figure 23), to provide stratigraphy and density profiles that were as continuous as possible (Figure 20). It was not possible to drill from the surface as the winter snowpack was not sufficiently consolidated and the snowpit data already provided the requisite density and stratigraphic profiles.

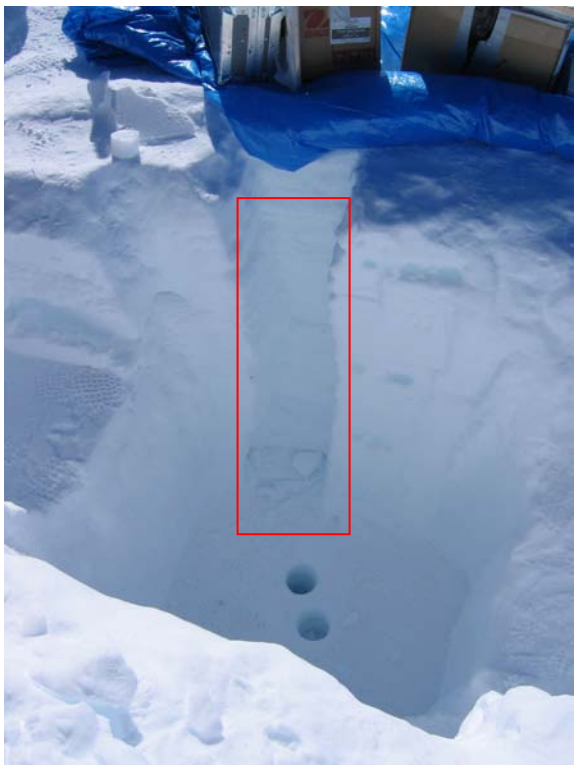

Figure 23: A spring snowpit, the face that has been logged is indicated, snow has been removed for chemical sampling. Core holes are located at the base of the snowpit, as close as possible to the logged face.

During drilling, individual sections of core of between 0.3 – 1.1 m were retrieved (Figure 24). After the total length of core was retrieved, the length of the section was measured and compared to the depth of the hole, measured using an avalanche probe, to account for any loss of firn in the drilling process. The average loss along the total length of a typical 2-3 m core was 5%.

Each section of core was logged in the field by visually identifying each stratigraphic layer, and the length and visual properties of each were recorded including the presence and location of ice features. An example of this is shown for the first section of core retrieved at E3 in autumn 2004 in Table 2.

T05-E3					
Tray mass g		32.5			
Core section		1			
section length		101			
Layers cm		**Description**	**Length**	**Diameter**	**Mass with Tray**
Top	**Bottom**		**cm**	**cm**	**g**
0	10	Snow	9.5	6.5	174
10	21	Firn	11	6.75	209
21	64	Firn - Large crystals	42	7	758
64	99	Firn - smaller crystals	33	7	660
99	101	Ice	1.8	7	80
Multiple thin ice layers at 18 cm, 21 cm Ice layers are 63.5 cm, 66.5 cm					

Table 2: An example of how firn cores were logged in the field. This is for the first section of core retrieved from E3 in autumn 2004.

Figure 24: Section of core retrieved from drilling showing one clear large ice layer, and other ice features.

Following logging, each individual stratigraphic layer was sequentially separated by cutting from the main core, and the length and diameter of the resulting cylindrical sections were measured with a ruler to 1 mm accuracy. Each section was then placed in a foil tray of known mass, and these were weighed on a triple beam balance (precise to 1 g). This was protected from the wind either on a level shelf cut into the snowpit walls and/or behind a temporary tarpaulin windbreak (Figure 25). The mass and volume were then used to calculate the density of each section.

Figure 25: Logging the core, measuring cylindrical sections, and then weighing them on a triple beam balance, protected from the wind by a tarpaulin shelter.

Autumn core

In autumn 2004, the same basic coring technique as detailed for the spring cores, was used to retrieve and log 2-3 m length cores from the snowpack surface. The cores were retrieved within 0.5 m of the logged face of each snowpit (Figure 20).

3.5.2.2 Deeper Firn Cores

In spring 2004, a 17 m core was retrieved from the bottom of the snowpit at E3. Each individual section was measured in length and wrapped in protective plastic, labelled and subsequently shipped back to the UK in cold storage for further analysis. I autumn 2004 m ~18 m core was retrieved from the surface at E3, each section was wrapped in protective plastic, labelled and subsequently shipped back to the UK. However due to logistical difficulties the core melted before analysis took place.

3.5.3 Neutron Probe

The neutron probe (n-probe) provides an automated way of measuring continuously integrated snow and firn densities down a bore-hole. The n-probe has a source of fast neutrons which lose energy by scattering when they interact with hydrogen atoms in the snow or ice. The density of the snow or ice is related to the number of slow neutrons returning to the probe detector (Morris & Cooper, 2003).

Boreholes of ~50 mm diameter were augured to depths of 6-10 m, as close as possible to where the shallow firn cores were retrieved at each site (Figure 20). The n-probe was raised to the surface at the slowest possible speed (~50 mm min^{-1}, selected to maximize vertical resolution) by an electric winch. The winch rate and data retrieval were controlled by a GeoVista Platform Logger linked to a laptop computer located at the snowpack surface (Figure 26).

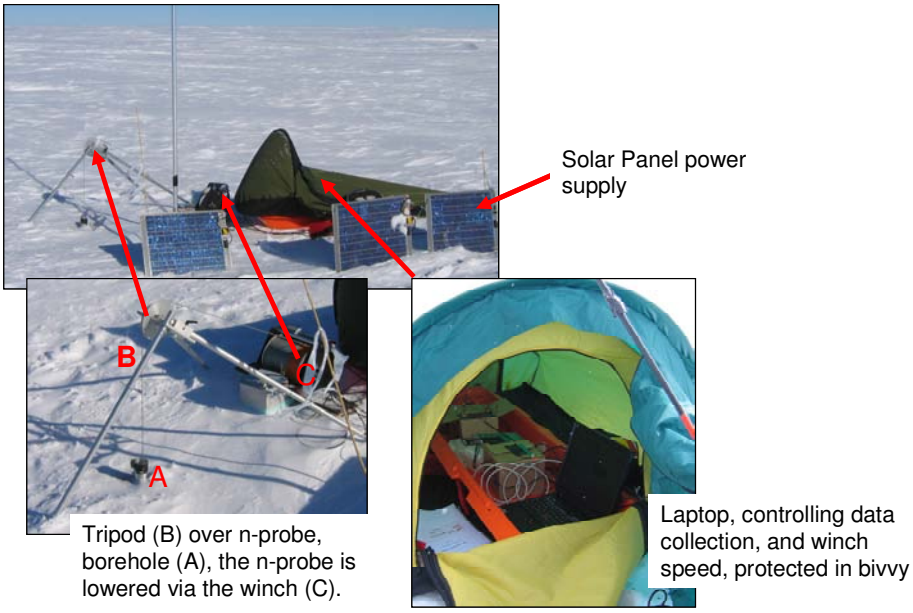

Figure 26: A picture showing how the n-probe was set up in the field, the winch cable placed over the tripod to keep the n-probes position. The laptop was protected in the bivvy.

The n-probe logs the slow neutron count rate as a function of depth below surface at 10 mm intervals. The depth/count-rate profile was subsequently converted to a density profile using a calibration equation (Morris & Cooper, 2003) to produce records of bulk density as a function of depth:

$$\rho = \frac{\left[107.88 + \frac{(1.347 \times C \times 0.9)}{1.00875} - \frac{\left(0.0003458 \times C^2 \times 0.9^2\right)}{1.008752^2}\right]}{1000}.$$

Equation 2: Calibration equation for n-probe to convert count rate (C) to density.

The n-probe measurements at 10 mm intervals average the density over a 5-10 cm sphere of snow/firn around the sonde. This results in a profile representing the running mean of the snowpack density, smoothing out short length scale variations.

In spring 2004, n-probe derived density profiles were collected from T5, E1, E2, E3, E4, S1, S2, S3 and S4. In autumn 2004, density profiles were obtained from T5, E1, E2, S1, S2, S3 and S4. A communications link malfunction prevented the collection of n-probe profiles at all sites in spring 2006 and at E3 and E4 in autumn 2004. The n-probe was also used to profile the wider 8 mm diameter hole that was present to ~18 m depth following retrieval of the long firn core at site E3 in spring 2004.

3.5.4 Trenches

In order to investigate the spatial continuity of snowpack features such as windcrusts and ice layers, a 7.5 m long, and ~2 m deep trench was excavated in spring 2006. This was located 11 m ~N of T5, parallel to the EGIG line as shown in Figure 27.

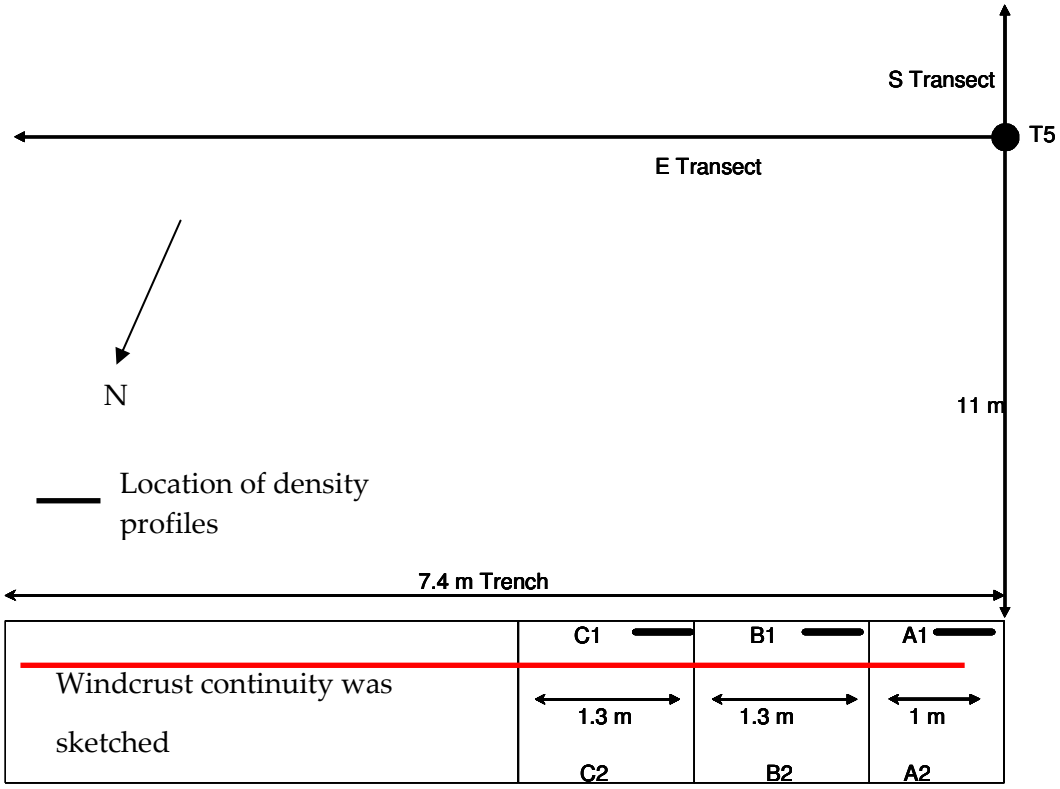

Figure 27: Diagram showing the location of the trench dug in spring 2006. The 3 faces that were sketched are marked (A1-C1, A2-C2), and the location of where the density measurements were made is also marked (this is included in a handout in the back cover).

The first ~3 m of the trench was subdivided into 3 sections (A, B and C), and both sides of the trench for each section were sketched, detailing where changes in hardness occurred, the presence of all ice and wind features and some grain size characteristics. Density profiles were taken from each section on the side closest to transect E, measurements were made in the same way as in the snowpits (section 3.5.1). Pit, A, B and C, and beyond section C (as indicated by the red line in Figure 27), windcrusts were recorded in sketches and measurements taken detailing their length, and depth within the snowpack along the side closest to transect E (the EGIG line) as indicated in Figure 27.

3.5.5 Avalanche Probe

Avalanche probe surveys were carried out over 100 m transects in order to investigate the depth to, and spatial continuity of, harder windcrust or ice features buried within the snowpack. The avalanche probe was inserted through the snowpack and the depth to each layer of greater resistance was recorded to a depth of ~2 m. This somewhat subjective technique was undertaken by the same person to ensure consistency in the results. Measurements were made at intervals of 5 m in spring 2004 and 1 m in autumn 2004 and spring 2006 between T5, S3 (Figure 16).

3.5.6 Chemistry sampling

In order to try and identify annual layers in the underlying firn from chemical signatures (Isaksson & others, 2001; Rasmussen & others, 2002; Anderson & others, 2006), snow and firn samples were retrieved in the field and analysed in laboratory conditions in the UK. Specifically, snowpit samples were retrieved from each stratigraphic layer in spring and autumn 2004, and at 10 cm intervals in spring 2006 and analysed for ionic concentrations. The whole of the 17 m core collected in spring 2004 at E3 was returned to the UK and subsequently analysed at 10 cm resolution for density, ionic concentration, and stable isotope (oxygen and hydrogen) concentration.

Spring and autumn 2004 snowpits

Plastic bags were filled with snow from each stratigraphic layer from the snowpits at T5, E1, E2, E3, E4, S1, S2, S3, S4, and T6 and at T4 (spring only). Samples were retrieved using plastic tubes to minimise contamination. An integrated sample for

the depth of each stratigraphic layer was retrieved to ensure a continuous profile down the snowpit.

In spring 2004 all samples collected were melted in a microwave in the field. The samples were then filtered through 0.4 μm filter papers using a pump. The pump was initially rinsed 3 times with the unfiltered sample, then 2-3 ml of the sample was then filtered and the filtrate was used to rinse the nalgene sample bottles 3 times. The bottles were then filled completely and sealed ensuring the exclusion of air bubbles and the samples were re-frozen, before being shipped back to the UK (where they were stored at room temperature) for further analysis. In autumn 2004 it was not possible to melt and filter the samples in the field. On completion of the field season, the samples were flown off the ice sheet, and then melted using a microwave and filtered as detailed above. These were then shipped back to the UK for further analysis, and stored in a liquid state at room temperature (Sharp & others, 2002; Wadham & others, 2004).

Spring 2006 snowpits

In spring 2006, snow samples were taken from T5, E1, E2, E4, S1 and S2, in 10 cm bands from the surface to the bottom of the snowpit, one sample was also taken from the bottom of the snowpit, the end-of-summer 2005 layer. Again by integrating the samples collected over the bands, a continuous profile was ensured. Samples remained frozen until removed from the field, when they were then melted in a microwave, and filtered immediately, and then stored in nalgene bottles at room temperature, as for the autumn 2004 samples.

3.6 Laboratory analysis

In an attempt to reveal a longer record of annual mass balance from the underlying firn at the field site, the samples were analysed for the following chemical indices; ionic content, and oxygen and hydrogen isotope concentrations: and for the 17 m core retrieved, the density profile was measured at 10 cm resolution. These methods have been used with success in numerous firn and ice core studies (Meese & others, 1994; Alley & others, 1997; Isaksson & others, 2001; Pohjola & others, 2002).

3.6.1 Sample preparation and storage

All samples had to be melted, and for ionic analysis, filtered before analysis. In the case of samples from the 17 m core, density measurements were made prior to cleaning and melting of sample.

Snowpit samples

Snowpit samples collected in spring 2004 were melted and filtered in the field (as detailed in section 3.5.6). These samples were then stored in plastic nalgene bottles at room temperature until analysis.

In autumn 2004 and spring 2006 it was not possible to melt and filter the samples in the field; these samples were melted and filtered as soon after leaving the ice sheet as possible. Techniques used were the same as detailed in section 3.5.6.

Core samples

In spring 2004, the 17 m core retrieved from the bottom of the E3 snowpit was transported to the cold room at the University of Aberystwyth wrapped in protective plastic, in a frozen state. In the cold room (set at -20 °C) each section was sliced longitudinally using a band saw. One half of the core was wrapped again in protective plastic and stored at -30 °C. The other half was cut into 10 cm lengths, the radius and length of each of the sections were measured using a slide calliper with a precision of 1 mm, and the mass measured using an electric balance with a precision of 0.1 g, in order to determine the densities. Prior to any chemical analyses and in order to remove any possible contamination, either from the outer surface of the core, or from the band saw, the outer 1-2 mm of core was removed with a clean razor blade.

These samples were then placed in plastic bags, and left to melt at room temperature. They were then filtered through 0.4 μm filter papers using a syringe. Unfiltered sample was used to rinse the syringe 3 times, before pushing a small amount of sample through the filter paper 3 times, and using this to rinse a beaker. The sample was then pushed through the filter paper into the beaker. This filtered sample was then used to rinse the nalgene bottle 3 times, before filling it with filtered sample. As this sample was to be used for isotopic analysis, the bottles were filled as completely as the volume of sample allowed, fully in approximately 70% of the cases. This was to reduce water-vapour exchange with the ambient air, ensuring no change in the isotopic content of the sample (Fischer & others, 1995).

Following some ambiguity in the initial results once compared with accumulation data from Crawford Point AWS, further isotopic measurements were made at 2.5 cm resolution between core depths 271 cm and 465 cm. These were cut using a band saw, at -20 °C, and the outer surface removed using a clean razor blade. The samples were then placed in plastic bags, which in turn were placed inside 3 other

plastic bags. This was to ensure if there was a leak from the inner bag, the outer bag would build up a separate water-vapour atmosphere with identical average isotopic contact as the samples, thereby reducing water-vapour exchange with the ambient air. This technique ensures no change in isotopic content of the sample (Fischer & others, 1995). These samples were not filtered as neither deuterium (^{2}H) or ^{18}O are affected by any chemical and biological reactions that may occur, and they were not being re-sampled for their ionic concentration (Clark & Fritz, 1997).

3.6.2 Ionic analysis

All samples were analysed at Bristol University's Low Temperature Experimental Facility (LOWTEX) using a Dionex DX500 chromatography system to measure the concentrations of anions (chloride, sulphate and nitrate) and cations (sodium, potassium, magnesium and calcium). Samples were chosen randomly and analysed twice in each run. The samples were decanted into 5 ml vials, and placed in racks on the auto-analyser ready to be injected into the Dionex.

Nitrogen gas injects the sample into the Dionex and high purity helium gas forces the eluent into the system. Contaminants in the sample are removed in the guard column, before being processed in the ion exchange column. The greater the charge on the ions in the analyte, the more strongly the ion is attracted to the exchange column. The ions can only move forward when in solution, so the speed at which an ion is carried through the column is dependent on the time the ion is in solution, which in turn is dependent on the charge of the ion, thus separating the solution into bands of different ions according to their charge (Sinniah & Piers, 2001). Details on the eluent and ion exchange columns for cation and anion analysis are in Table 3. All ions in the eluent are removed in the suppressor, leaving a solution of pure water and analyte. The conductance of the solution is measured in the detector, this

is proportional to the concentration of the ions dissolved in the solution (Sinniah & Piers, 2001). Chromeleon (Dionex standard software) version 6.4 was used for processing the results.

	Anion	Cation
Column	IonPac AS11-HC 4mm x 250 mm	IonPac CS12A 4 mmx 250 mm
Guard column	IonPac AS11-HC 4mm x 50 mm	IonPac CS12A 4 mmx 50 mm
Suppressor	Anion self regenerating suppressor - Ultra 4 mm	Cation self regenerating suppressor - Ultra 4 mm
Sample loop size	100 µl	100 µl
Eluent	30 mM NaOH (sodium hydroxide)	20 mM MSA (methanesulphonic acid)

Table 3: Details of ion exchange column, and eluent used in ionic analysis

The retention time for each ion, and so conductivity can be identified by comparison with analysis of standards of known substance and concentration (Fischer & Wagenbach, 1996). Standards of similar concentration of ions to that found in the sample are made up and run alongside the analyte to measure machine drift. Preliminary analysis identified the standard concentrations required and these are detailed in Table 4.

Standards	Chloride	Nitrate	Sulphate	Sodium	Potasium	Magnesium	Calcium
0.5	0.01775	0.03100	0.02400	0.01150	0.01950	0.00600	0.01000
1	0.03550	0.06200	0.04800	0.02300	0.03900	0.01200	0.02000
2	0.07100	0.12400	0.09600	0.04600	0.07800	0.02400	0.04000
3	0.17750	0.31000	0.24000	0.11500	0.19500	6.00000	0.10000
10	0.35500	0.62000	0.48000	0.23000	0.39000	0.12000	0.20000
20	0.71000	1.24000	0.96000	46.00000	0.78000	0.24000	0.40000

Table 4: Concentrations of standard solution in atomic dilution ppm .

All standards are measured at the start and end of each run to allow overall measurement of machine drift. Additionally the three lowest concentrations of anion and cation standard are run between each full sample set (including repeats), allowing the machine drift to be regularly measured. This is important as runs can last up to 24 hours. Samples are run in sets of five; in each set, five samples are run, then a vial of ultrapure water, followed by the same five repeated. At the end of every run Dionex standards for anions and cations are run 4 times to calibrate the machine and ensure 99% accuracy. An example of run order can be seen in Table 5.

In order to avoid contamination rubber gloves were worn when handling all samples, standards, vials and caps, and were washed with ultra-pure water and dried on paper towels between samples and standards. All vials and caps are washed in ultra-pure water using an ultrasonic bath for 30 minutes, then rinsed 6 times in ultra-pure water and heat dried.

Vial number	Sample to be analyised
1	Ultrapure water
2	Ultrapure water
3	Anion standard 0.5
4	Cation standart 0.5
5	Anion standard 1
6	Cation standard 1
7	Anion standard 2
8	Cation standard 2
9	Anion standard 3
10	Cation standard 3
11	Anion standard 10
12	Cation standard 10
13	Anion standard 20
14	Cation standard 20
15	Ultrapure water
16	Ultrapure water
17	Sample 1
18	Sample 2
19	Sample 3
20	Sample 4
21	Sample 5
22	Ultrapure water
23	Sample 1
24	Sample 2
25	Sample 3
26	Sample 4
27	Sample 5
28	Anion standard 0.5
29	Anion standard 1
30	Anion standard 2
31	Cation standard 0.5
32	Cation standard 1
33	Cation standard 2

Vial number	Sample to be analyised
34	Sample 6
35	Sample 7
36	Sample 8
37	Sample 9
38	Sample 10
39	Ultrapure water
40	Sample 6
41	Sample 7
42	Sample 8
43	Sample 9
44	Sample 10
45	Anion standard 0.5
46	Anion standard 1
47	Anion standard 2
48	Anion standard 3
49	Anion standard 10
50	Anion standard 20
51	Cation standard 0.5
52	Cation standard 1
53	Cation standard 2
54	Cation standard 3
55	Cation standard 10
56	Cation standard 20
57	Dionex Anion standard
58	Dionex Anion standard
59	Dionex Anion standard
60	Dionex Anion standard
61	Dionex Cation standard
62	Dionex Cation standard
63	Dionex Cation standard
64	Dionex Cation standard

Table 5: An example of an order run for the Dionex. These are for samples taken from the 17 m core, the samples are in blue.

3.6.3 Isotope analysis

Samples were analysed for oxygen and hydrogen stable isotope concentrations at the Scottish Universities Environmental Research Centre (SUERC) at East Kilbride.

Measuring deuterium

For analysis of δ^2H, the sample to be analysed is used to clean the syringe 3-4 times to reduce the memory in the syringe needle between samples (Donnelly & others, 2001). 1 μl of this sample is then injected into the chromium furnace at the steady running temperature of 830 °C. The oxygen in the sample reacts with the chromium to form chromium oxide, releasing the hydrogen for analysis (Equation 3). The hydrogen gas then flows into the VG optima dual inlet Stabilise Isotope Ratio Mass Spectrometer (SIRMS) and results are processed using optima DI 2.20 β. In order to avoid memory effects in the furnace, which can occur where there are large jumps in δ^2H_{RAW} between samples, the samples are run in order of their depth down the core (Donnelly & others, 2001).

$$H_2O + Cr \rightarrow CrO_2 + H_2$$

Equation 3: Separating hydrogen from the water sample for isotopic analysis.

Calibration of the sample is undertaken by running standards of known concentration close to the concentration of the field samples. The International Atomic Environmental Agency (IAEE) Greenland Ice Sheet Precipitation standard of -120‰ was used to calibrate the results, with an accuracy of 0.8‰.

Oxygen 18 preparation

Measurement of $\delta^{18}O$ is undertaken using the Epstein-Mayeda equilibration method (Epstein & Mayeda, 1953). This involves the transfer of the isotope signal of H_2O to CO_2 (Trigt, 2002), as shown in Equation 4 and then analysing the CO_2 (Clark & Fritz, 1997).

$$^{12}CO_2 + H_2{}^{18}O \longleftrightarrow HC^{16}O_2 + H^+$$

Equation 4: The Epstein-Mayeda equilibration equation (Epstein & Mayeda, 1953) used to transfer the isotope signal from the sample (H_2O) to CO_2 which can then be analysed.

1 μl of water sample is mixed with 300 ml of CO_2 of known isotopic concentration. After 24 hours, equilibrium is reached and the CO_2 is pumped into the Analytical Precision 2003 Mass Spectrometer using helium gas. The sample is calibrated by interspacing with samples of known isotopic concentration. Data output is via Analytical Precisions propriety software with accuracy of within 0.3‰ (Donnelly & others, 2001).

Mass spectrometer analysis

Once ionised the sample passes through electrostatic plates, where the ions are channelled into a beam, and then passed into a magnetic field. The ions are deflected by the Lorentz force; the deflection is dependant on the ions' mass and velocity. Since the velocities are equal, any difference in deflection is due to a difference in mass. The ions are deflected into Faraday cups in the double collector where the interaction of the ions results in a current being produced (Clark & Fritz,

1997). The signal processor measures any small variations in the current output and this can be expressed as a mass ratio (Clark & Fritz, 1997).

58 samples (from depth 149.2 cm to 973.0 cm) were measured for δO^{18} and δ^2H; these samples were found to have a very good correlation (r^2=0.9995). The remaining samples, (between depths 973.0 cm to 1891 cm, and the high resolution (2.5 cm) samples between depths 271 m and 465 m were only analysed for ^{18}O and the ^2H value calculated from this the regression equation shown in Figure 28 (significant, p<0.0001).

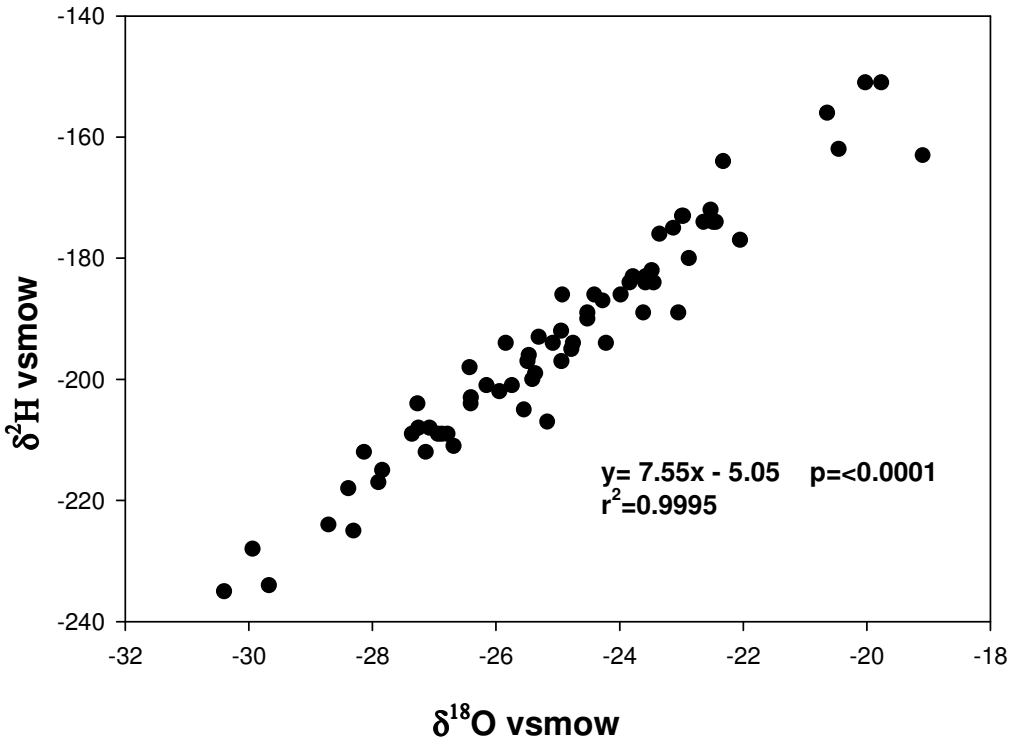

Figure 28: Plot showing the relationship between δ ^{18}O values and δ^2H values.

Chapter 4: Identifying annual layers

4.1 Introduction

Ground measurements of annual accumulations are an important tool to ascertain the impact recent changes in global temperatures (IPCC, 2007) have had on the Greenland Ice Sheet's mass balance. Changes in elevation have been measured by satellite (Wingham, 1995; Zwally & others, 2005; Shepherd & Wingham, 2007) and it is important to understand these measurement in terms of actual change in mass. Furthermore it is essential that inter-annual variability is constrained so that any changes in elevation/mass balance measured by the three year CryoSat 2 mission can be offset against natural variability. The first year of recorded accumulation in the vicinity of T5 and T6 is 1951 (Benson, 1962). Records for 1950 – 1955 (Benson, 1962), 1959 – 1974 (Stober, 1986), 1959 – 1986 (Seckel, 1977) and 1982 – 1988 (Anklin, 1994) have been measured on subsequent expeditions. Recent changes in mass balance, and inter-annual variability need to be measured for years in which field work has not been carried out.

Annual accumulation can, in principle, be calculated by identifying 'annual layers' in ice and firn cores. 'Annual layers' are the result of cyclical events which have an annual periodicity, which leave a record in the snow; for example, the sequential combination of low density autumn hoar crystals, overlying a higher-density fine grain wind slab (Alley, 1988). If this layer couplet can be identified it is then possible to divide the core into years, and in conjunction with density measurements, to determine an annual mass balance. Additionally, cores have been analysed in terms of their stratigraphy, density, ionic or isotope content in order to identify annual layers (Isaksson & others, 2001; Rasmussen & others, 2002; Anderson & others, 2006).

A variety of techniques are utilised in this thesis in an attempt to reveal annual layers and thus mass balance. Basic snow and firn facies ('stratigraphy') were recorded in all snowpits and along the 17 m core retrieved at E3 in spring 2004 (Figure 16). Density measurements were obtained from i) the snowpits; ii) the 17 m core, at 10 cm resolution; iii) n-probe profiling to depths of between 4 - 9 m below the end-of-summer 2003 surface, at nine and six sites within 1 km^2 of T5 in spring 2004 and autumn 2004, respectively. Snow samples were retrieved from stratigraphically distinct layers in all snowpits in spring and autumn 2004, and at 10 cm resolution from six snowpits in 2006. Subsequently all snow samples were analysed for ionic content. The ionic content was also measured at 10 cm resolution along the 17 m core. Oxygen 18 (^{18}O) and deuterium (^{2}H or D) concentrations were also measured at 10 cm resolution along the 17 m core. Following some ambiguity in the initial results, an additional ~2 m section of the core was re-analysed at 2.5 cm resolution. The accumulation data collected from the PARCA AWS at Crawford Point was also analysed to provide a comparative data set.

Previous studies (Pfeffer & others, 1991) have indicated summer melt may percolate through the previous year's end-of-summer surface. Consequently, the density and ion content profiles were analysed to determine if this process was occurring. Clearly, percolation between annual layers results in the movement of mass, consequently these processes must be quantified in order to reduce errors and avoid both under and over estimates of annual mass balance.

This Chapter briefly explains how the measurements have been obtained, full details on the methodologies employed are provided in Chapter 3. The analysis of the data from Crawford Point AWS is also explained. The data are analysed with the specific intent of identifying annual layers; further analysis and discussion regarding the problems associated with using the method of annual layer identification in the percolation zone and with each methodology is also included.

4.2 Methods

4.2.1 Investigating stratigraphy

Statigraphic changes in the snowpack can be associated with thermal gradients, (Alley, 1988) deposition events (Svensson & others, 2005) and wind and melt effects. Regular changes in stratigraphy associated with seasonal temperature changes that are preserved, and can be identified in the core record may be used to identify annual layers. Strong temperature gradients in the late summer result in thermal-gradient metamorphism, resulting in a layer of depth (autumn) hoar forming above the 'wind slab' hard and icy end-of-summer surface (Svensson & others, 2005). This couplet was used to identify the end-of-summer surface at the bottom of snowpits. If this couplet is preserved in the 17 m core it enables the end-of-summer and start of autumn to be identified for each year, thus providing an annual layer marker. Additional measurements of the hardness of visually distinctive stratigraphic layers, and the grain size were measured and recorded in all snowpits to determine whether just visual identification of this stratigraphy is sufficient to reveal annual layers.

4.2.2 Measuring density changes

Table 6 shows the variability in densities of different types of the snow, firn or ice. For example, depth hoar typically has a density of 0.1 – 0.3 g cm^{-3}, whereas firn and wind packed snow have densities of 0.4 – 0.83 g cm^{-3} and 0.35 – 0.4 g cm^{-3} respectively; the end-of-summer surface, although icy, is not yet glacier ice, and the density would be closer to that of firn or wind packed snow. Therefore the autumn hoar/end-of-summer surface couplet may be crucial in revealing a distinctive density profile.

Typical snow, firn and ice densities	g cm^{-3}
New snow	0.05 - 0.07
Damp new snow	0.1 - 0.2
Settled snow	0.2 - 0.3
Depth Hoar	0.1 - 0.3
Wind packed snow	0.35 - 0.4
Firn	0.4 - 0.83
Very wet snow and firn	0.7 - 0.8
Glacier ice	0.83 - 0.917

Table 6: Typical densities of snow, firn and ice (Paterson, 1994).

Density measurements were taken from each stratigraphically distinct layer in all snowpits. The density along the 17 m core was measured in 10 cm sections, the n-probe also provides density profiles from the surface to depth of between 4 and 8 m. Full details on the techniques are given in Chapter 3.

4.2.3 Measuring ion content

Changes in the ion concentrations in solid precipitation can be preserved in the snowpack upon deposition. Identification of the seasonal peaks and troughs associated with precipitation concentrations is one way to identify annual layers within a snowpack. This method has been successfully employed in cores extracted from the dry snow zones of ice sheets (Bales & others, 2001a), and also in areas of high melt in Svalbard (Pohjola, 2002). To test the effectiveness of this technique in the percolation zone of the Greenland Ice Sheet, it is important to initially establish if there is an ionic signature in a snowpack prior to melt. This was investigated by retrieving samples from the spring snowpacks. In spring 2004, samples were retrieved across each stratigraphically distinct layer, in spring 2006 samples were retrieved across 10 cm sections of the snowpack. Details on the sampling procedure are in Chapter 3. There are two distinct advantages to sampling from the spring snowpack: i) The snowpack has not been subjected to melt, and so it should be

possible to detect any ionic signature present ii) The time period over which the samples were deposited is established. The bottom of the snowpits are the 2003 and 2005 end-of-summer surfaces in the spring 2004 and 2006 snowpits, respectively; therefore any ionic signature present is a consequences of changes in ion concentration in precipitation in the winter and spring accumulation.

By comparing the ion concentration profiles from the spring snowpits, to those from the autumn snowpits, it should be possible to determine if there is an annual signature in ion concentrations, and whether this is preserved through summer melt, percolation and internal refreezing. If so, it may be possible to identify annual layers in the 17 m core by measuring ion concentrations at 10 cm resolution (details in Chapter 3).

4.2.4 Measuring Isotopic concentrations

Due to the different atomic weights of stable isotopes of oxygen (^{18}O) and hydrogen (^{2}H or D) compared to the most abundant isotopes, ^{16}O and ^{1}H, the molecules have different reactions rates, which leads to isotope fractionation (Urey, 1947). The concentrations of ^{18}O and ^{2}H are measured as a ratio to their most abundant isotopes (^{16}O and ^{1}H), fractionation modifies this ratio (Urey, 1947). This apparent ratio is compared to a known standard, in this case, Vienna Standard Mean Ocean Water (VSMOW). Changes in temperature can result in fractionation, this is commonly observed across latitudes (Dansgaard, 1964). When temperatures are cooler, clouds condense losing precipitation, preferentially fractionating ^{18}O and ^{2}H, the heavier isotopes, this is called the Rayleigh distillation (Clark & Fritz, 1997). As the water vapour moves north, and cools, it becomes progressively more depleted in ^{18}O and ^{2}H; so at more northerly latitudes, ^{18}O and ^{2}H ratios to VSMOW are more negative than southerly latitudes. The Rayleigh distillation also occurs in response to

seasonal temperature changes; cooler winter precipitation is more depleted in ^{18}O and ^{2}H than precipitation falling in warming summers (Clark & Fritz, 1997). The input variations in isotopic concentrations can be measured in isotopically distinct layers, where enriched summer layers alternate with isotopically depleted winter horizons (Clark & Fritz, 1997). This can be preserved for thousands of years, and has been used for climate reconstruction from the European Greenland Ice Core Program (GRIP), and American Greenland Ice Sheet Program (GISP) (Dansgaard & others, 1993). Eight to ten samples per year are required to observe the 'summer high and winter low' pattern (Pohjola & others, 2002b), and so the 17 m core was divided into 10 cm sections, and sampled for ^{18}O and ^{2}H. From initial results, a further 2 m section of core was re-sampled at 2.5 cm resolution, as this possibly corresponded to a year of low accumulation (as observed from AWS measurements). Full experimental details are in Chapter 3.

4.3 Results

4.3.1 Stratigraphy of snowpits and shallow cores

4.3.1.1 Snowpit stratigraphy

Snowpits were dug down to the layer demarcating the previous year's end-of-summer surface. In all snowpits, this surface is easily identified as a hard, icy and continuous layer located beneath the autumn hoar. By using this as a common reference at the bottom of all snowpits, stratigraphic features can be compared between locations as a height above this datum surface.

Snow facies in snowpits were found to vary at very short spatial scales. Figure 29 shows the profiles derived from a basic description of facies in each distinctive stratigraphic layer at T5 and S1. These profiles are typical of those observed in all snowpits (stratigraphic descriptions for all snowpits and cores are detailed in Appendix 7). Since they are taken within 1 m of each other in the same snowpit (section 3.5.1) it is also possible to observe short scale variations in snowpack facies. In the spring snowpack, some continuity is present between facies; the heights above the end-of-summer 2003 surface are the same at both locations where facetted crystals are first observed. This continuity is not present in the autumn profiles where, for example, ice layers are present at S1 but not T5. However, the autumn hoar is clearly identifiable in both spring and autumn profiles from the facetted crystals although some rounding has occurred in the autumn snowpack. The presence of facetted crystals overlying an icy layer is a distinctive couplet present in all profiles; consequently the identification of the previous year's end-of-summer surface is possible from snowpit facie observations.

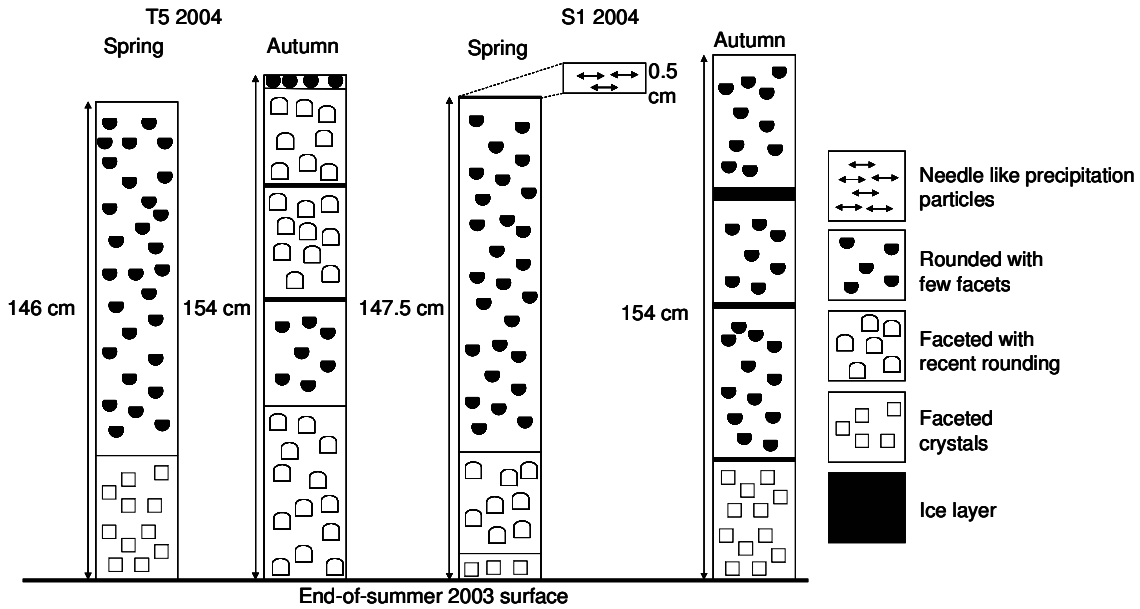

Figure 29:Stratigraphic profiles for T5 and S1 in the spring and autumn of 2004, based on Colbeck & others, (1990).

Visually, the autumn hoar layers are distinctive as they are facetted, however, as shown in Table 7, their grain size is not distinctive. Typically autumn hoar crystals are unconsolidated, which results in this layer being 'soft'. When the hardness profiles are measured the layer at the base of the snowpit is soft, indicating the autumn hoar, as seen in Figure 30.

Spring 2004								
T5			**E1**			**S1**		
Height cm		**Grain size**	**Height cm**		**Grain size**	**Height cm**		**Grain size**
Top	**Bottom**	**mm**	**Top**	**Bottom**	**mm**	**Top**	**Bottom**	**mm**
146.0	139.5	<0.5	147.0	146.0	1.0	147.5	147.0	1.0
139.5	134.0	<0.5	146.0	143.0	<0.5	147.0	142.0	<0.5
134.0	87.5	<0.5	143.0	139.0	<0.5	142.0	139.0	<0.5
87.5	78.5	0.5	139.0	89.0	<0.5	139.0	85.0	<0.5
78.5	38.0	1.0	89.0	80.0	0.5 - 1.0	85.0	39.0	0.5 - 1.0
38.0	18.0	1.0	80.0	75.0	0.5 - 1.0	39.0	19.0	1.0 - 2.0
18.0	8.0	1.0 - 2.0	75.0	74.0	0.5 - 1.0	19.0	8.0	1.0 - 2.0
8.0	0.0	1.0 - 2.0	74.0	69.0	0.5 - 1.0	8.0	0.0	2.0
			69.0	41.0	1.0			
			41.0	18.0	1.0 - 2.0			
			18.0	5.0	1.0 - 2.0			
			5.0	0.0	1.0 - 2.0			
Autumn 2004								
T5			**E1**			**S1**		
Height cm		**Grain size**	**Height cm**		**Grain size**	**Height cm**		**Grain size**
Top	**Bottom**	**mm**	**Top**	**Bottom**	**mm**	**Top**	**Bottom**	**mm**
154.0	150.0	<1.0	154.0	150.0	<1.0	160.3	153.8	<1.0
150.0	121.0	1.0 - 3.0	150.0	84.5	1.0 - 2.0	153.8	120.0	
121.0	120.0		84.5	80.5		120.0	118.5	
120.0	86.0	1.0 - 2.0	80.5	37.0	1.0 - 2.0	118.5	86.0	1.0 - 2.0
86.0	81.0		37.0	34.0		86.0	84.5	
81.0	35.0	1.0 - 2.0	34.0	0.0	1.0 - 3.0	84.5	37.5	1.0 - 2.0
35.0	0.0	1.0 - 3.0				37.5	36.0	
						36.0	0.0	1.0 - 3.0

Table 7: Grain size as measured to each stratigraphically distinct layer along 3 profiles within 1 m of each other in spring and autumn 2004. The height above the end-of-summer 2003 surface to the top and bottom of each stratigraphic layer is given. No grain size is given for ice layers.

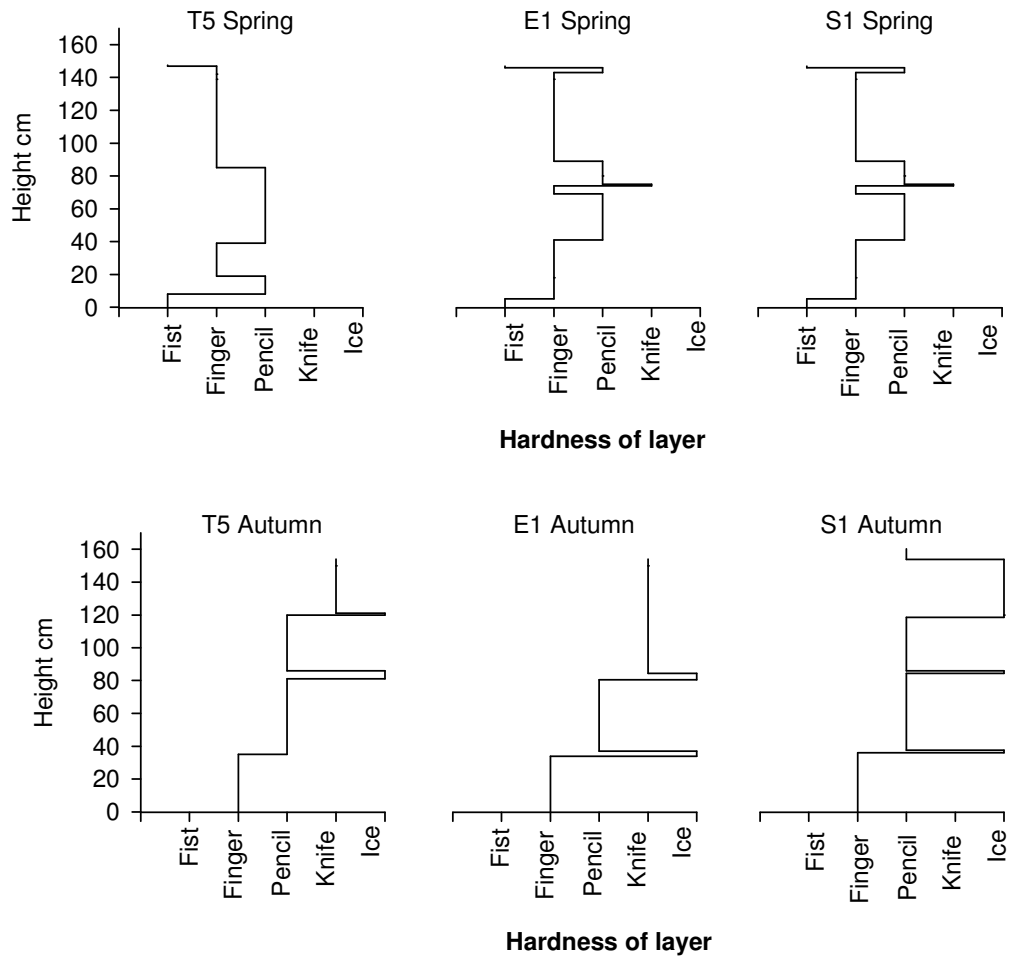

Figure 30: Graphs depicting the 'hardness' of each layer in spring and autumn profiles within 1 m of each other. At the bottom of each snowpit (height 0 cm) there is a 'soft' layer, the autumn hoar.

4.3.1.2 Stratigraphy of the 17 m core

The stratigraphy along the 17 m core (Figure 31) varies with depth. However, the visual description of the stratigraphy is not sufficient to identify the autumn hoar and end-of-summer surfaces unambiguously. Grain size for each stratigraphically distinct layer could have been measured in the laboratory. However, as is apparent in the snowpit record, this is not enough to distinguish the autumn hoar. It is not possible to measure the 'hardness' of each layer in the core, and so this means of identifying the summer layer is not possible. If the autumn hoar and end-of-summer surface couplet were visually distinctive in the stratigraphic descriptions, it would have been observed.

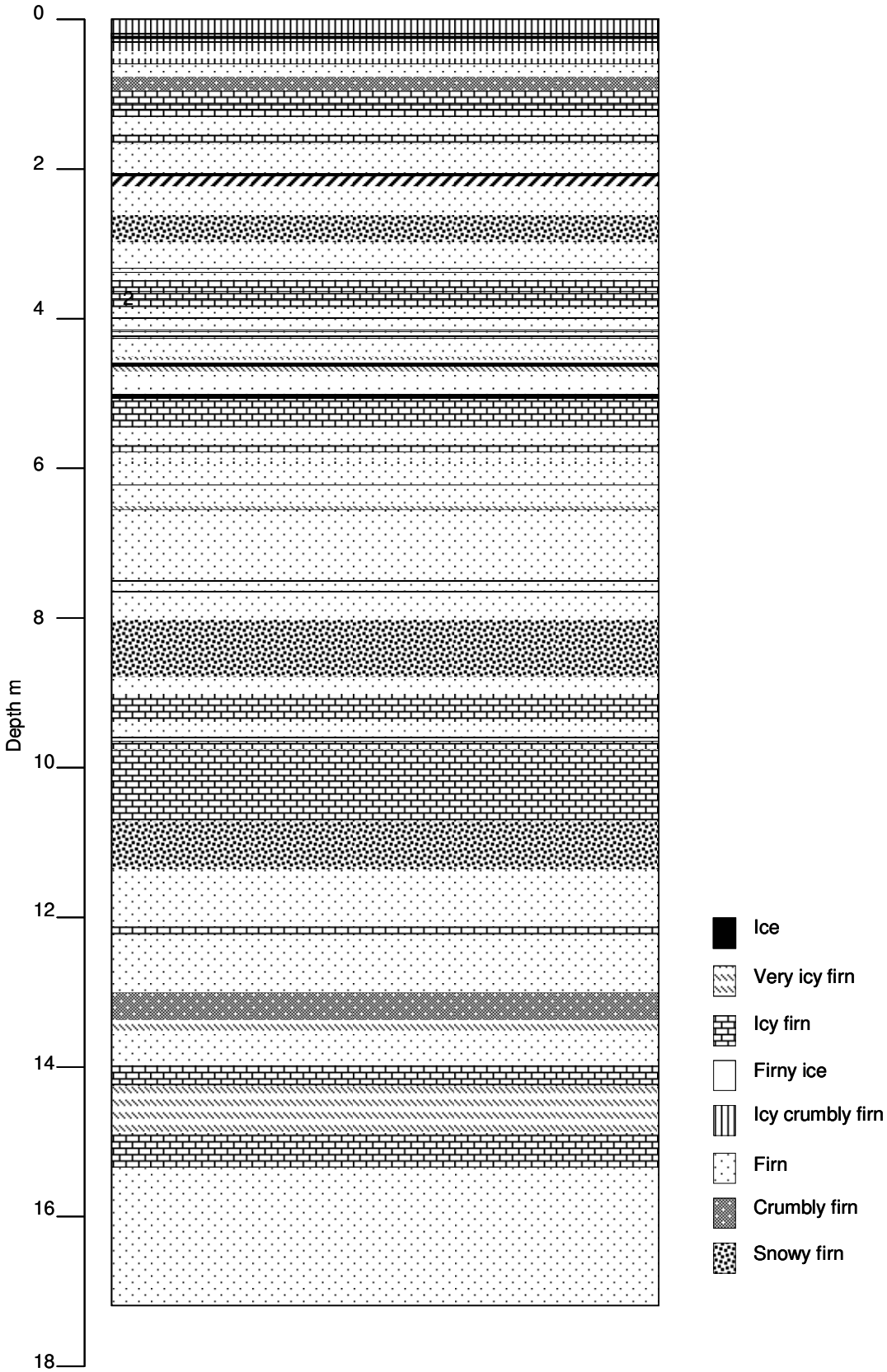

Figure 31: Stratigraphic profile for 17 m core, retrieved from the end-of-summer 2003 surface (0 m).

4.3.2 Density profiles

4.3.2.1 Neutron-probe density profiles

The n-probe was used to measure density profiles at 1 cm resolution extending to depths between 4 – 9 m at T5, E1, E2, E3, E4, S1, S2, S3 and S4 in spring 2004 and at T5, E1, E2, S1, S2, S3 and S4 in autumn 2004. Additionally the hole from which the 17 m core had been retrieved was used to obtain a density profile using the n-probe (the standard borehole for the neutron probe is 5 cm diameter, the diameter of the core hole that the 17 m core was retrieved from is 8 cm).

The neutron probe profiles recorded between spring and autumn 2004 show clear densification of surface snowpack over the summer period (Figure 32) – indicating, as expected, there are density changes associated with seasonality. All density profiles derived from the n-probe are shown in Appendix 8.

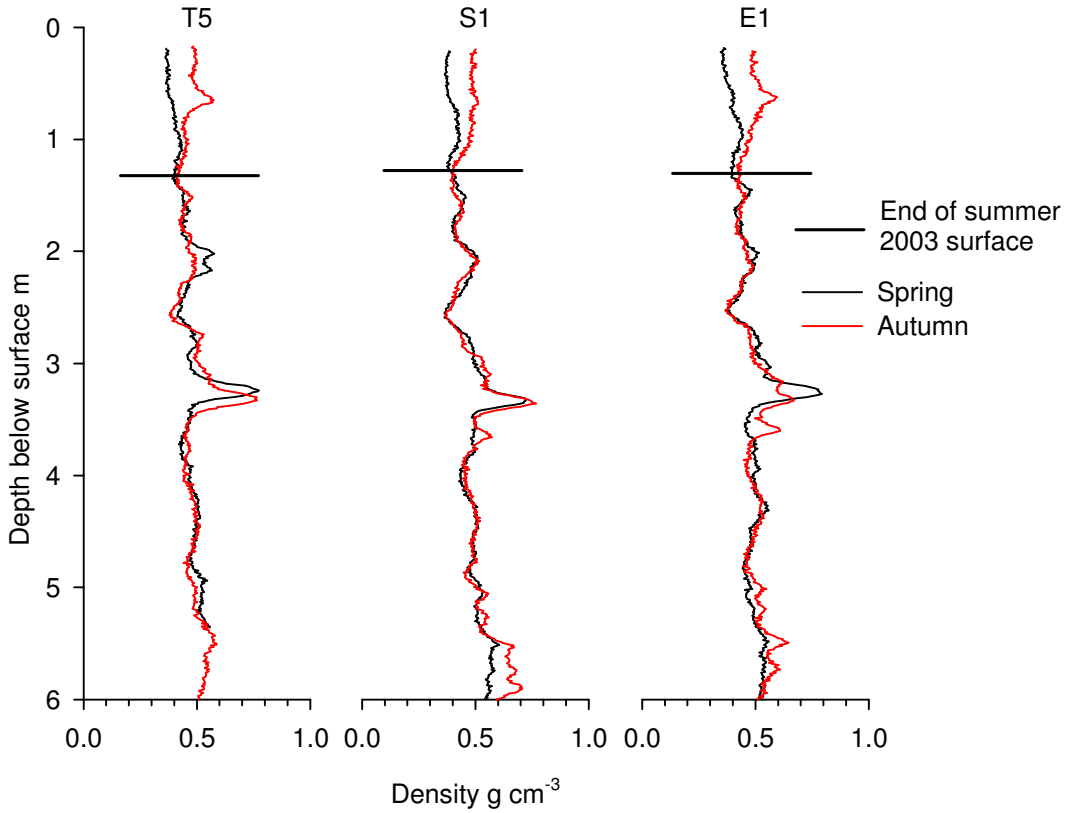

Figure 32: N-probe derived density profiles for T5, S1 and E1 in spring and autumn 2004. The autumn profile indicates higher densities than the spring above the end-of-summer 2003 surface.

There are clear fluctuations in density along each of the density profiles, and the troughs of low density may be associated with the low density autumn hoar. The density profile derived from the n-probe from the 17 m core hole (Figure 33) also shows these clear density fluctuations. In Figure 33 an attempt to correlate troughs of low density with autumn hoar has been made in order to identify annual layers. However, it becomes apparent that the identification of the low density troughs using this subjective technique is highly ambiguous. As there is no clear way of differentiating low density autumn hoar from low density firn in the n-probe derived density record, this technique is not suitable for annual layer identification in the vicinity of T5.

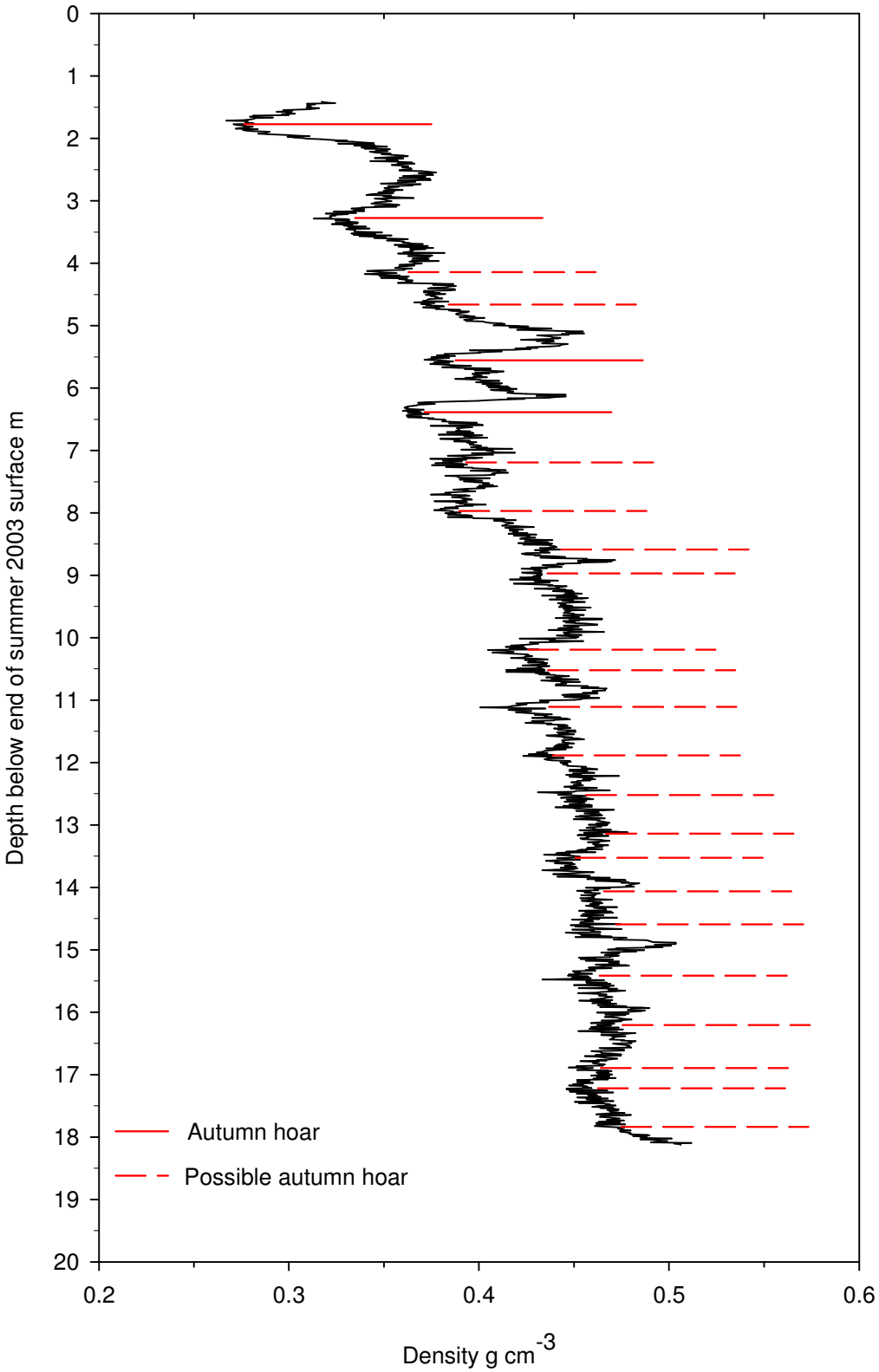

Figure 33: Density profile for E3, derived from measurements made with the n-probe from the hole that the 17 m core was extracted from.

4.3.2.2 The density of the 17 m core

The density of 10 cm sections of the 17 m core were measured in the cold room of Aberystwyth University. The density profile is shown in Figure 34. Although there are clear density fluctuations present there is no cyclicity present from which the low density autumn hoar, and high density end-of-summer surface couplet can be used to determine annual layers. This profile also shows a greater range of densities than those measured along the core hole using the neutron probe. There is also less cyclicity present in this density profile, hence it is not possible even to attempt to identify annual layers. This is likely due to the fact that the density derived from the neutron probe is averaged over a larger spherical area, as the probe is the centre point of an 8 cm diameter hole. This averaging will result in the data smoothing out high and low density features, which may dominate the section of core measured.

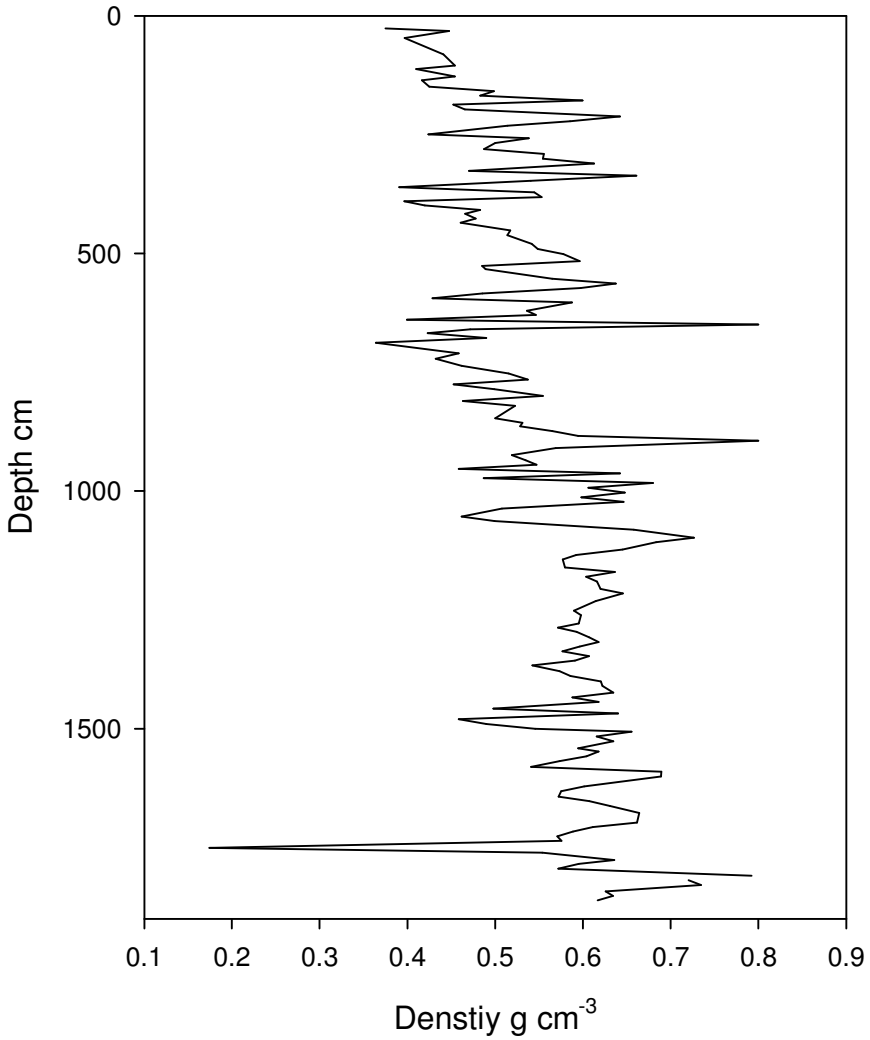

Figure 34: Density profile for E3, 10 cm resolution.

4.3.3 Snowpack ion content

Variations in the concentration of chloride (Cl^-), sulphate (SO_4^{2-}), nitrate (NO_3^-), sodium (Na^+), potassium (K^+), magnesium (Mg^{2+}) and calcium (Ca^{2+}) ions, present in solid precipitation and preserved in the snowpack throughout the year can be used to identify annual layers (Fischer & Wagenbach, 1996). Measurements of ion concentrations were made in pre melt (spring) snowpits, and post melt and refreezing (autumn) snowpits. By looking at the chemistry of the spring snowpack

over a known time period, any ion concentration fluctuations can be temporarily constrained. It is then possible to see if these fluctuations are preserved through the summer melt into the autumn snowpack. If this is the case, the variations of ion concentrations may be used to identify annual layers in the 17 m core.

4.3.3.1 Snowpit ion concentrations

Chemical samples were taken from stratigraphically distinct layers in autumn and spring snowpits in 2004, and every 10 cm in spring 2006 snowpits – both sampling techniques ensured a continuous profile.

In the winter snowpack peaks of SO_4^{2-}, NO_3^- and Cl^- are expected, with a late spring peak of Ca^{2+} (Fischer & Wagenbach, 1996; Dibb & others, 2007). The concentration of these ions should therefore peak near the top of the snowpit in spring, and mid snowpack in autumn.

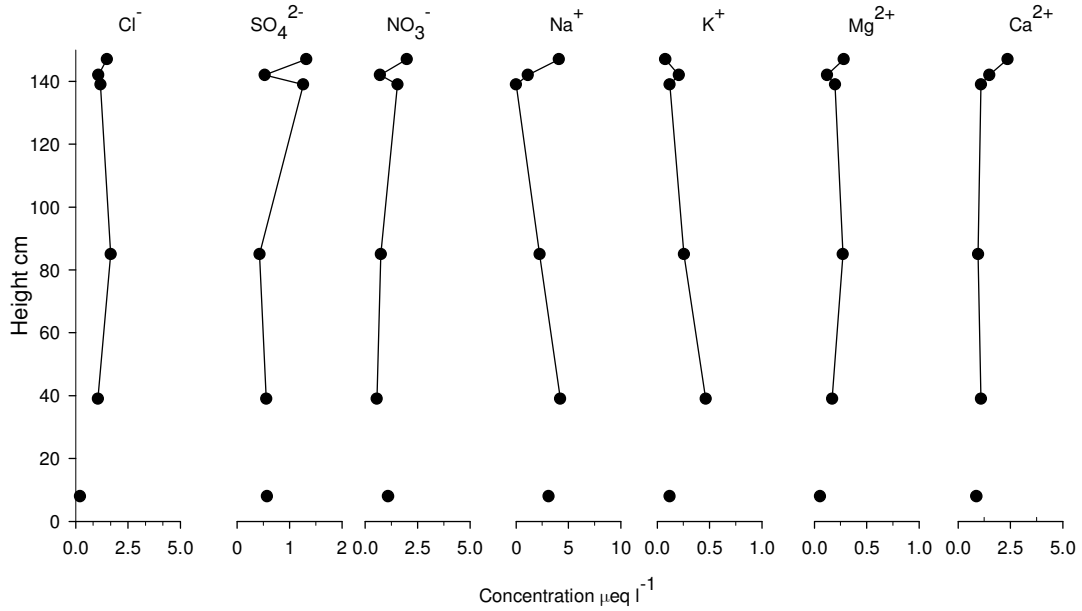

Figure 35: Ion concentrations in S1 spring 2004 snowpack.

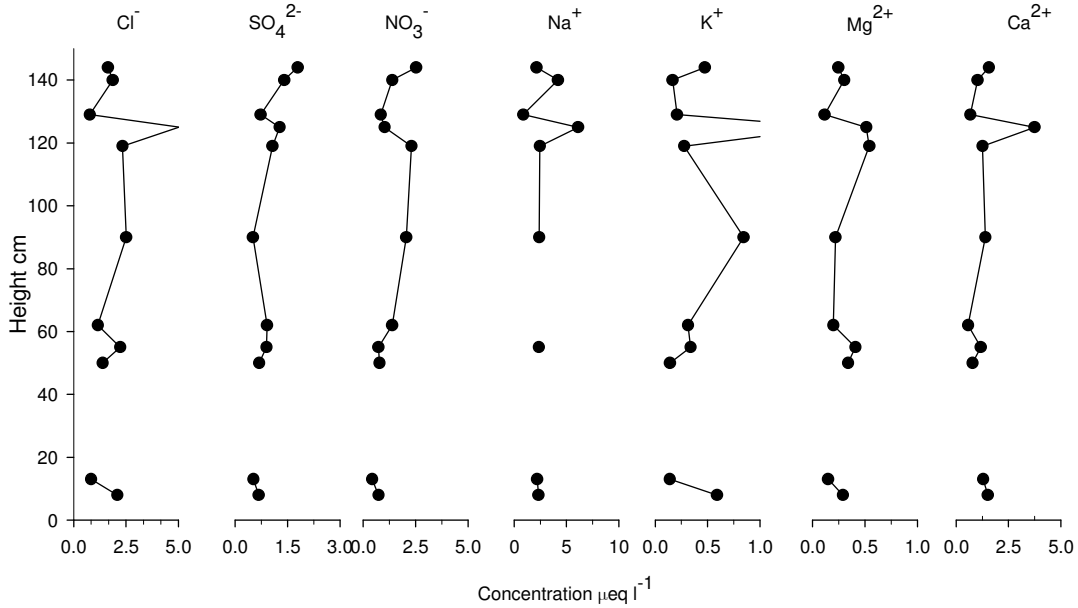

Figure 36: Ion concentration in S3 spring 2004 snowpack.

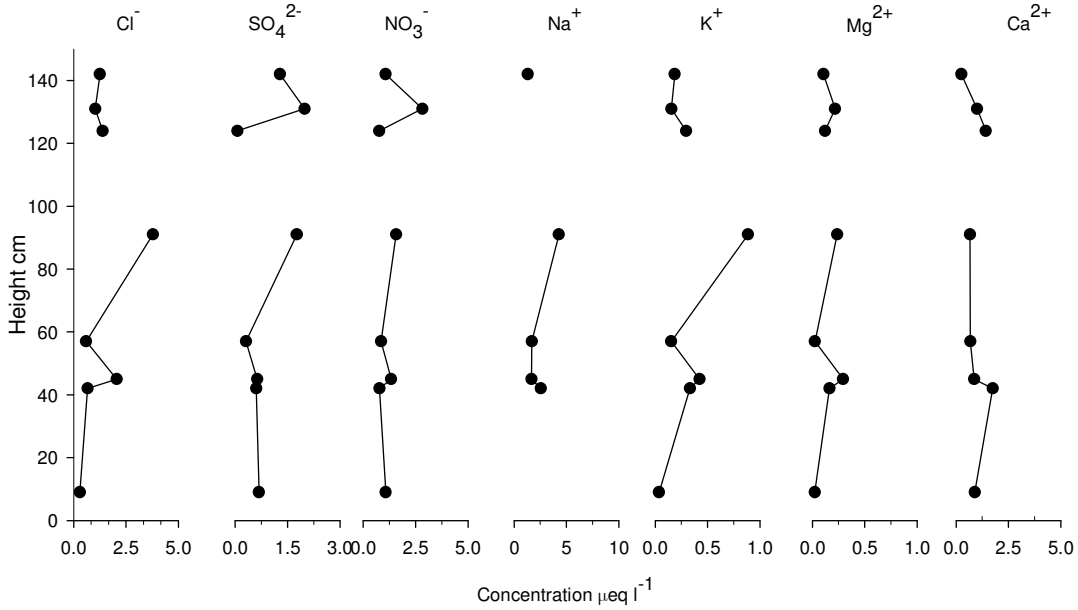

Figure 37: Ion concentration in S4 spring 2004 snowpack.

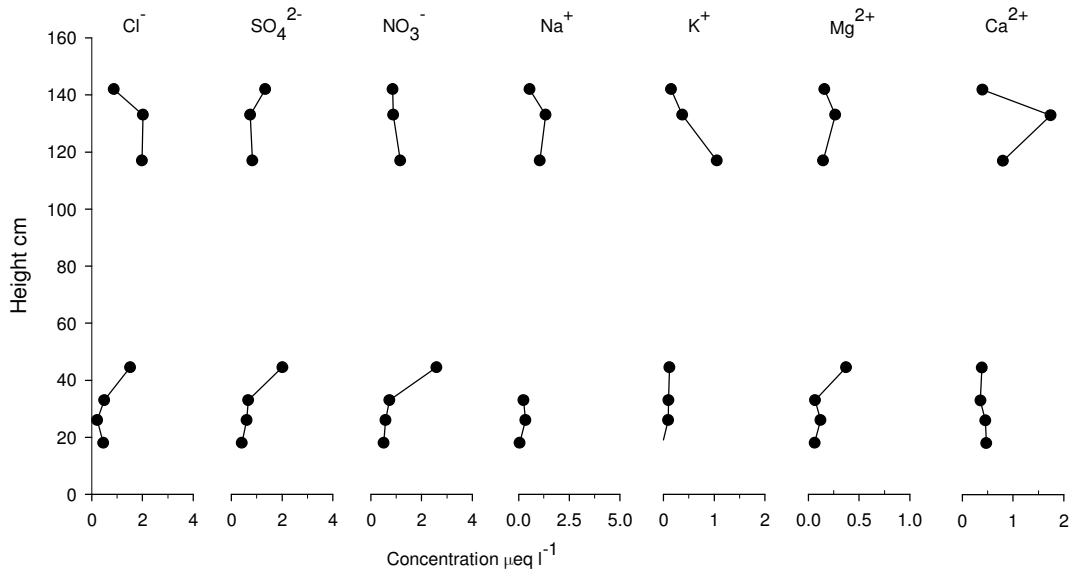

Figure 38: Ion concentration is autumn E3 2004 snowpack.

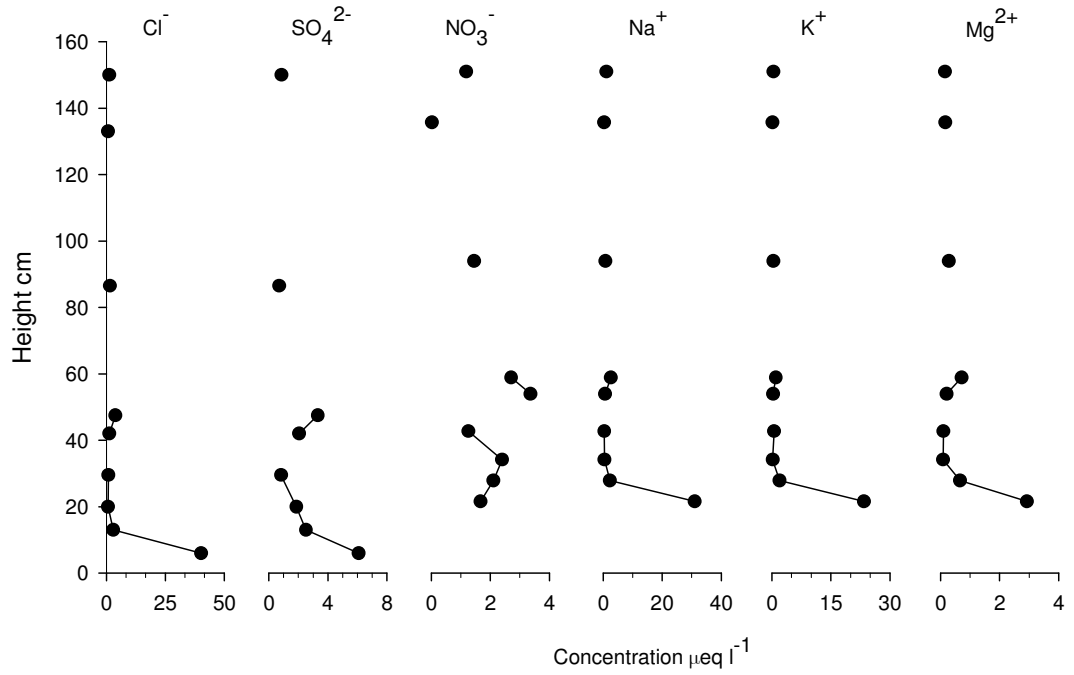

Figure 39: Ion concentration in autumn E4 2004 snowpack.

Due to a loss of samples, it was not possible to compare ion concentration profiles at the same location in spring and autumn 2004 snowpits. From the profiles shown in Figure 35, Figure 36, Figure 37, Figure 38 and Figure 39 it is apparent that the SO_4^{2-}, NO_3^- and Cl^- peaks that would be expected in the upper part of the spring snowpack (Figure 35, Figure 36 and Figure 37) and the middle third of the autumn snowpack (Figure 38 and Figure 39) are not obviously present. In spring 2006 a different

sampling procedure was used. Instead of sampling according to stratigraphy, a continuous profile was obtained from samples taken over 10 cm bands in spring 2006. Continuous ion concentration profiles at 10 cm resolution were measured for T5, E1, E2, E4, S1 and S3. No samples were lost for S2, S4 and E4, and the profiles are shown in Figure 40, Figure 41 and Figure 42.

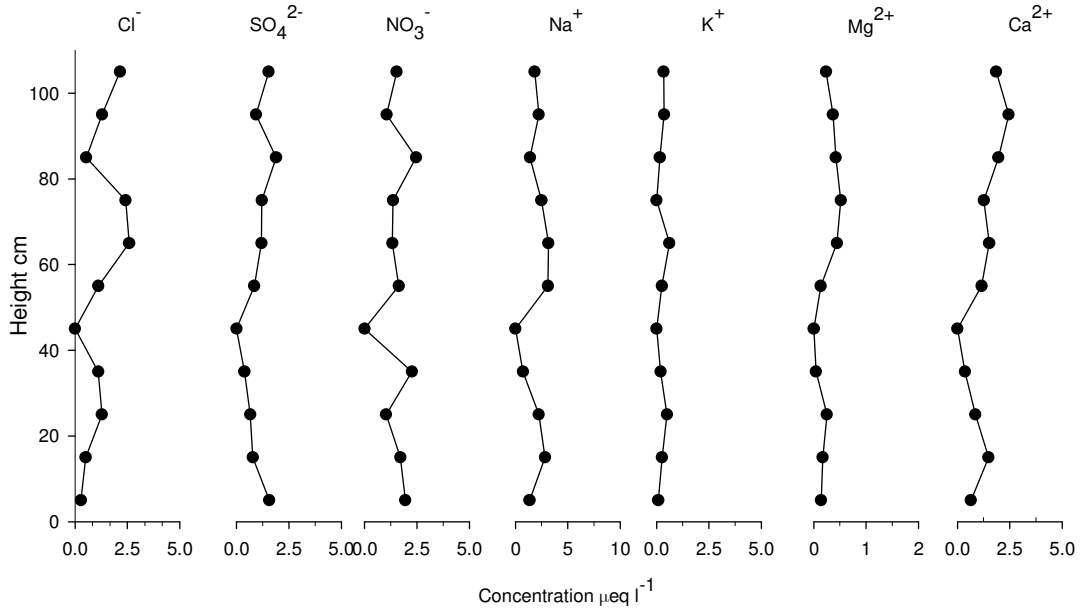

Figure 40: Ion concentration profile in spring 2006 at S2.

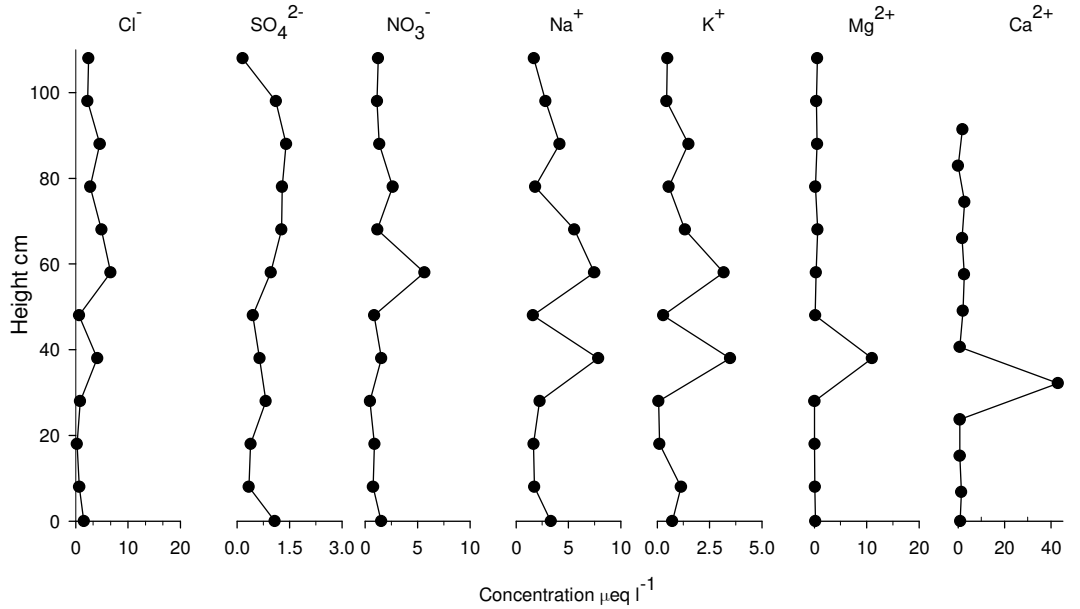

Figure 41: Ion concentration profile in spring 2006 at S4.

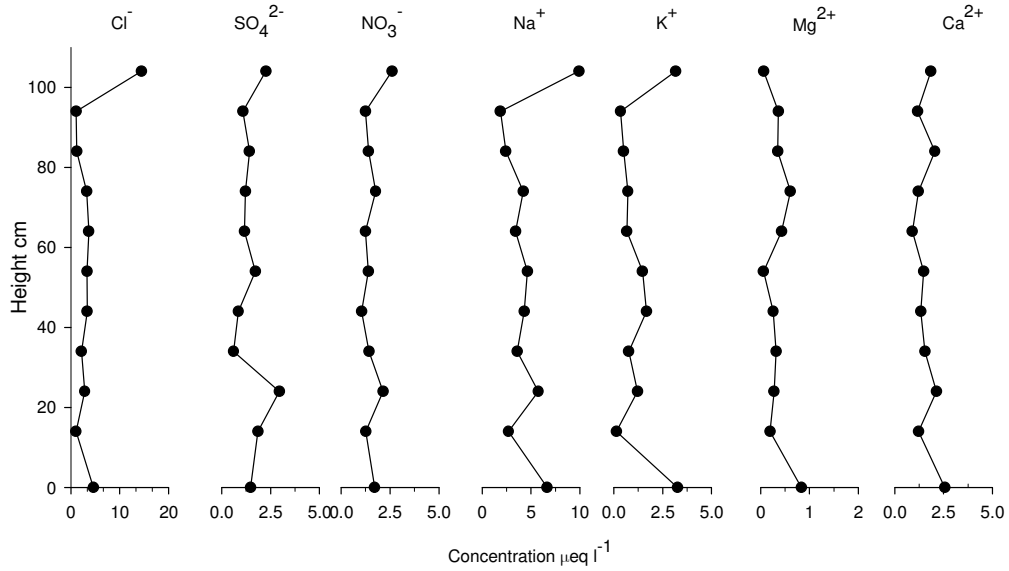

Figure 42: Ion concentration profile in spring 2006 at E4.

In the ion concentration profiles for S2 (Figure 40), S4 (Figure 41) and E4 (Figure 42) in spring 2006 peaks in the upper part of the snowpack are present in Cl^-, SO_4^{2-} and NO_3^- at E4 and S2, but not at S4 (Figure 41). Additionally, it is apparent that there is similarity between some profiles; for example, all anions (Na^+, K^+, Mg^{2+} and Ca^{2+}) have a peak at 40 cm above the end-of-summer 2005 surface in the profiles at S4. Since the ions are deposited in the snowpack at different times throughout the year, it is necessary to compare the concentrations for each ion in different snowpits.

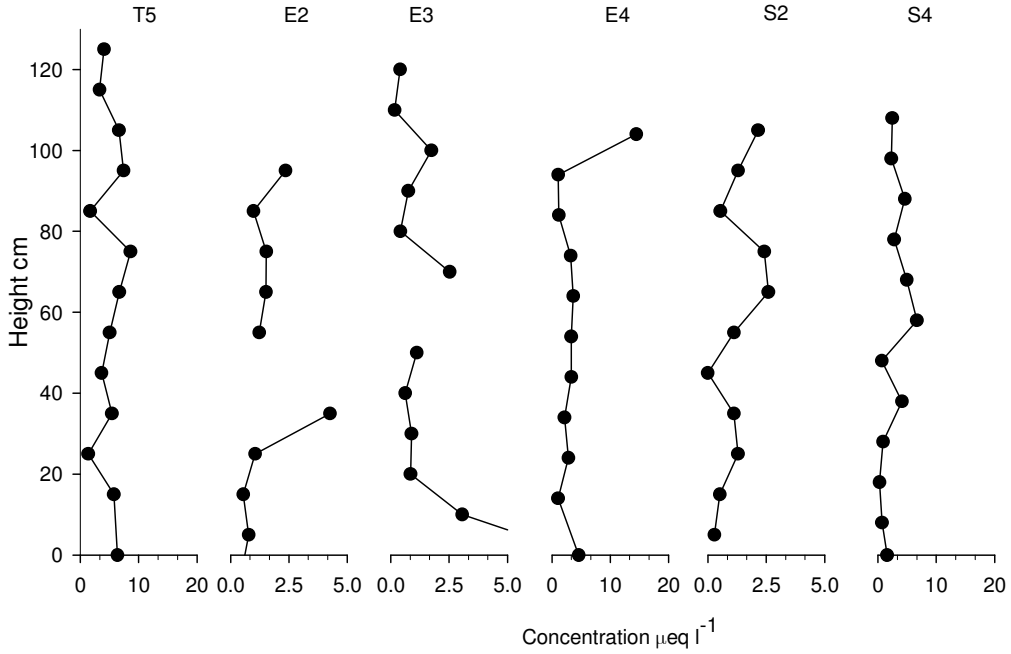

Figure 43: Cl- concentration in spring 2006

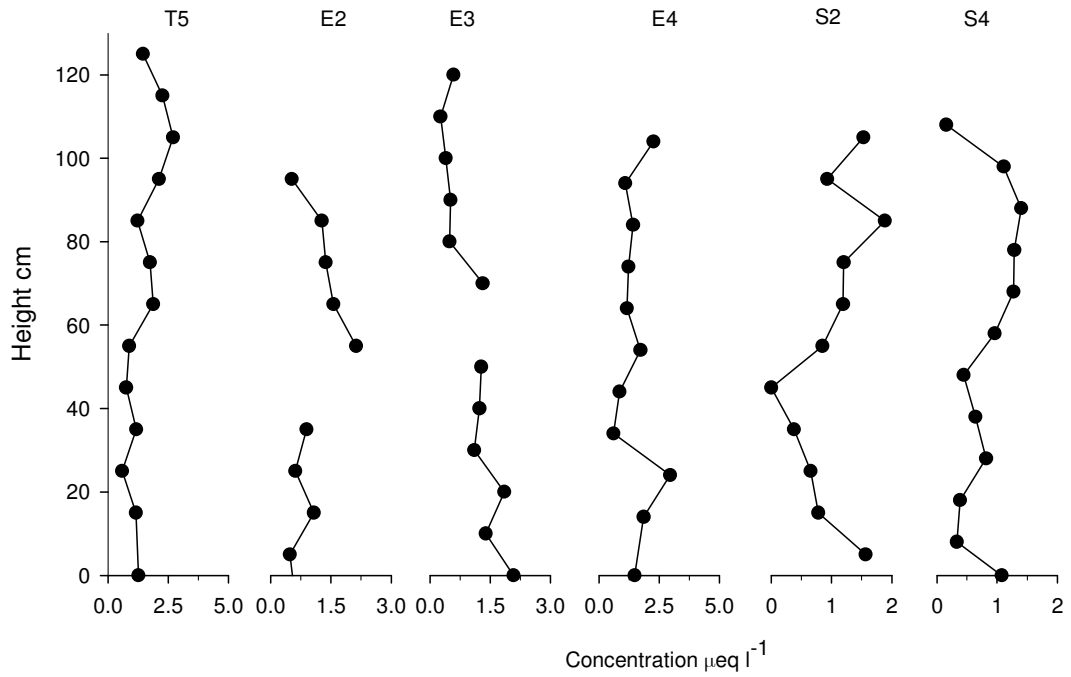

Figure 44: SO_4^{2-} concentration in spring 2006.

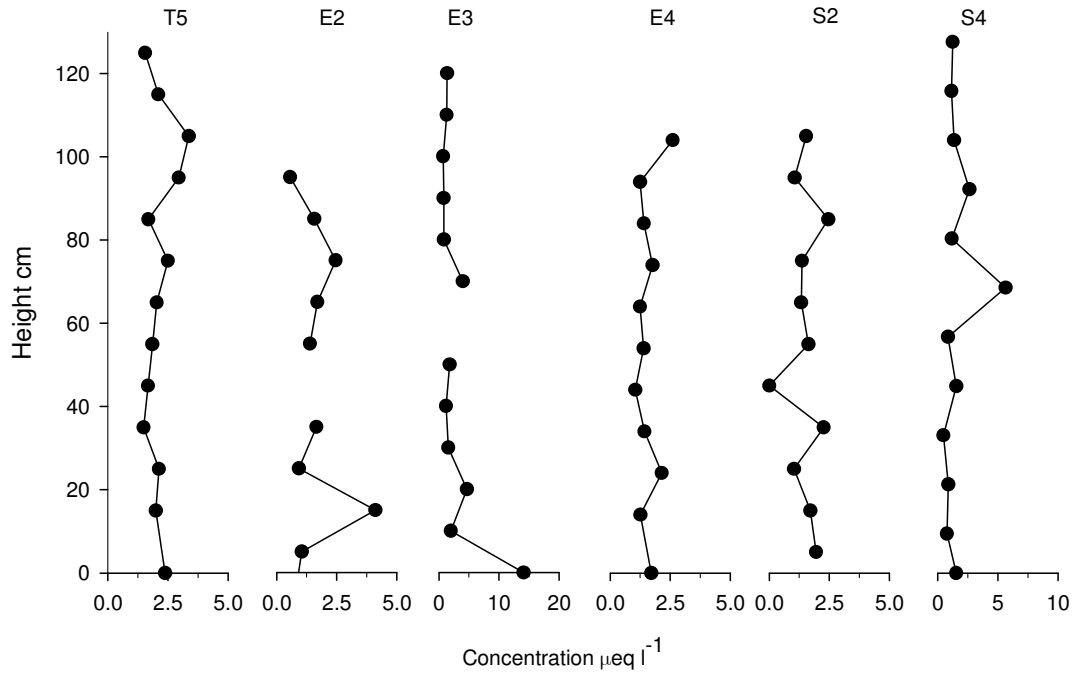

Figure 45: NO_3^- concentration in spring 2006.

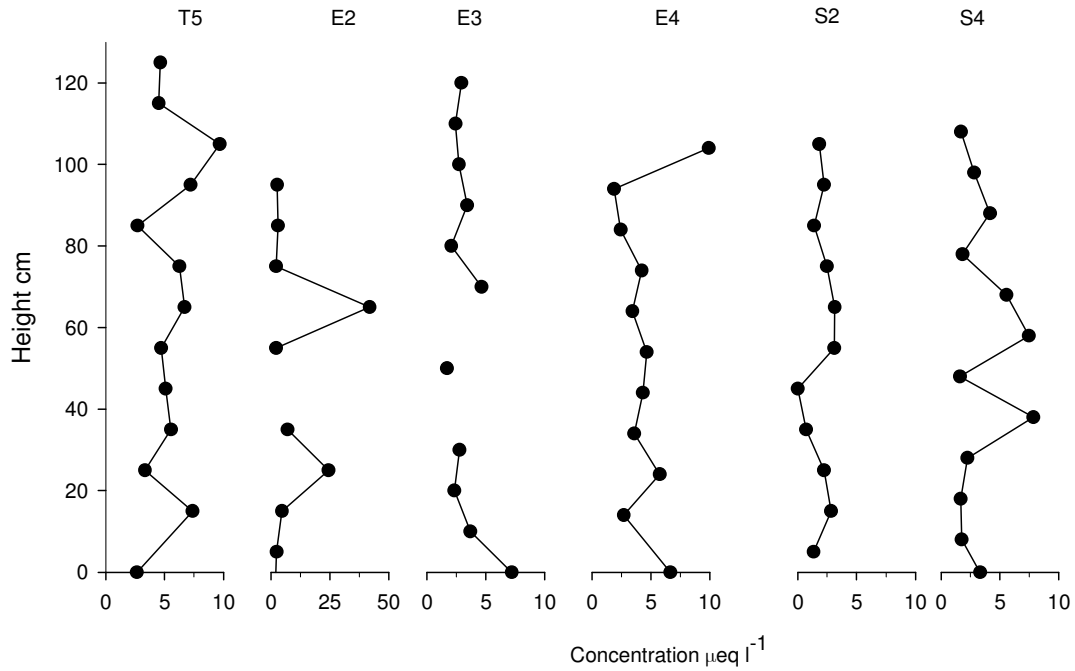

Figure 46: Na^+ concentration in spring 2006.

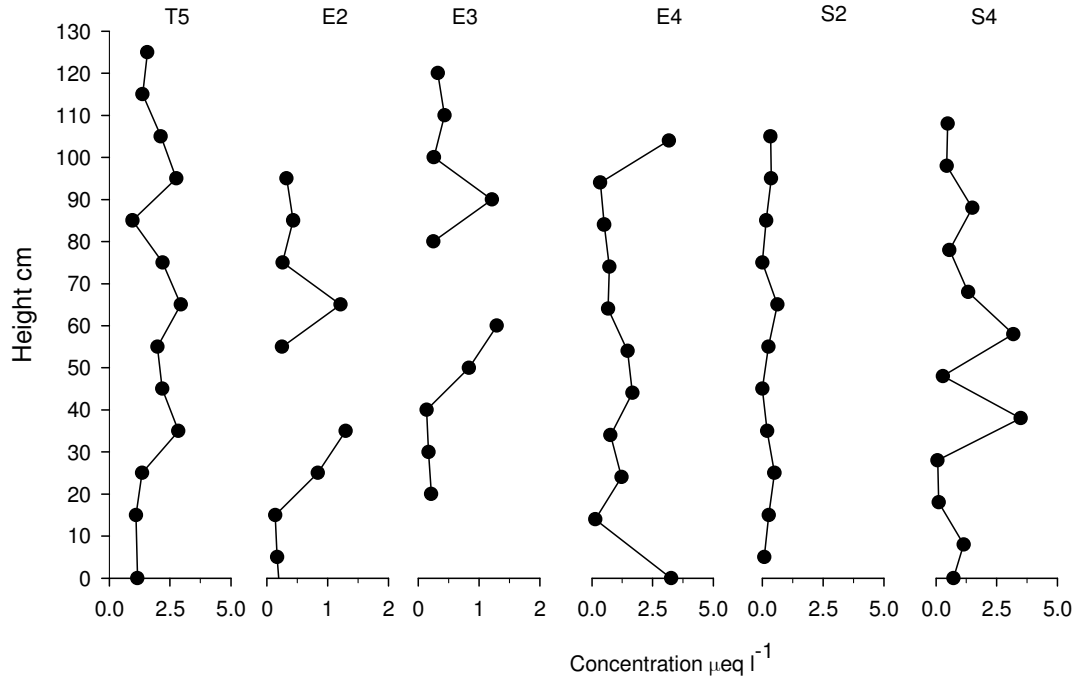

Figure 47: K^+ concentration in spring 2006.

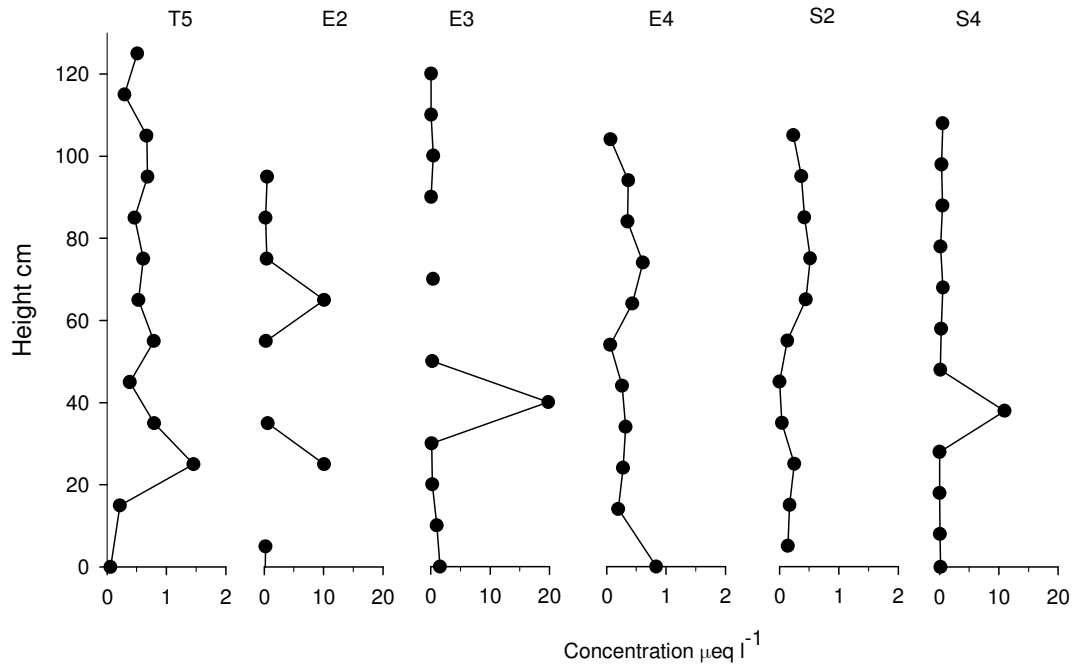

Figure 48: Mg^{2+} concentration in spring 2006.

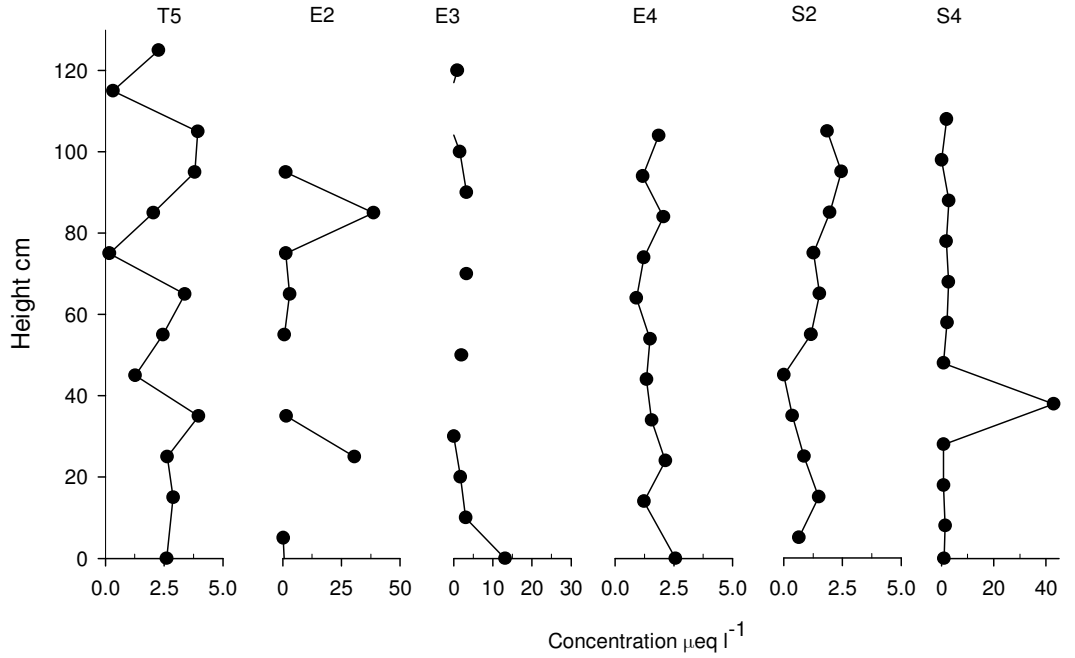

Figure 49: Ca^{2+} concentration in spring 2006.

From Figures 43-49 it is apparent that there are no obvious peaks in the concentration of any of the ions associated with position within the snowpack; this implies that the seasonality associated with ion concentration in solid precipitation is not preserved in the snowpack in the vicinity of T5.

4.3.3.2 Ion concentrations in the 17 m core

Ion concentrations were measured in 10 cm sections from the 17 m core, the profiles are shown in Figure 50 alongside the density profile. All ions show substantial variability in concentration, and there is clearly some continuity in concentrations between ions (peaks are seen across all profiles at the same depth, for example at 10 m depth there is a series of peaks, present in Cl^-, Na^+, K^+, Mg^{2+} and Ca^{2+}). However, the variations in ion concentration show no obvious cyclicity, or periodicity with depth, this indicates that fluctuation in ion concentration is not a suitable method for identifying annual layers.

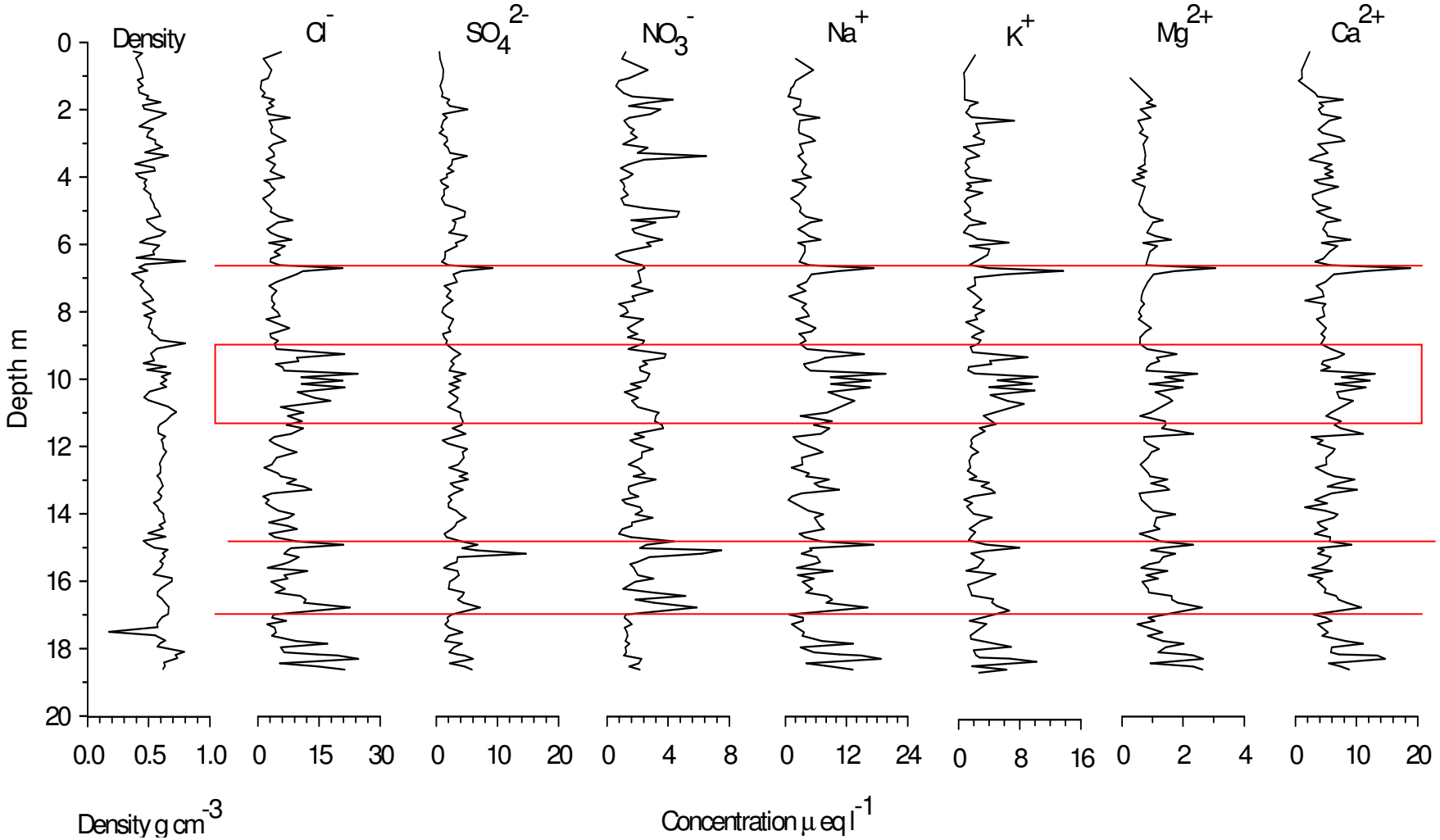

Figure 50: Density profile and ion concentration profiles from the 17 m core extracted from E4 in spring 2004.

	Concentration μeq l^{-1}						
	Cl^-	SO_4^{2-}	NO_3^-	Na^+	K^+	Mg^{2+}	Ca^{2+}
Mean	6.65	2.87	2.08	5.48	2.99	1.15	5.67
Standard Error	0.41	0.14	0.09	0.34	0.19	0.06	0.22
Standard Deviation	5.17	1.77	1.13	4.02	2.30	0.71	2.67
Minimum	0.65	0.52	0.58	0.54	0.66	0.27	0.55
Maximum	24.68	14.70	7.50	19.73	13.71	4.98	18.84

Table 8: Basic statistics of ion concentration for samples from the 17 m core.

Average ion concentrations are between 1.15 and 6.65 μeq l^{-1} (Table 8) the largest concentration peaks are seen in Cl^- (24 .7 μeq l^{-1}, which also has the highest average concentration), Na^+ (19.7 μeq l^{-1}) and Ca^{2+} (18.8 μeq l^{-1}). The lowest range of concentrations measured are in Mg^{2+} (0.27 – 5.0 μeq l^{-1}), where the average concentration is 0.15 μeq l^{-1}.

From visual inspection, peaks in ions occur at the same depth for all ions, for example at ~7 m clear peaks are seen in all ions, apart from NO_3^-. Between 9 and 11 m there are a series of peaks seem in Cl^-, Na^+, K^+, Mg^{2+} and Ca^{2+}; further peaks are seen in all ions at ~15 m and ~17 m (Figure 50).

Pearson's correlation coefficient between ion concentrations							
	Cl^-	SO_4^{2-}	NO_3^-	Na^+	K^+	Mg^{2+}	Ca^{2+}
Cl^-	-						
SO_4^{2-}	0.62***	-					
NO_3^-	0.29***	0.62***	-				
Na^+	0.93***	0.57***	0.26**	-			
K^+	0.83***	0.42***	0.21*	0.80***	-		
Mg^{2+}	0.90***	0.74***	0.34***	0.83***	0.73***	-	
Ca^{2+}	0.80***	0.53***	0.17*	0.80***	0.75***	0.78***	-
	P value						
	*	0.05					
	**	0.01					
	***	0.001					

Table 9: Pearson correlation coefficients between log transformed ion concentrations.

Table 9 shows the (Pearson) correlation coefficients between ion concentrations, with significance values. The data were log-transformed to meet assumptions of

normality. These data clearly indicate that there are significant correlations between ion concentrations. The weakest correlation is found between Ca^{2+} and NO_3^-, and the strongest between Na^+ and Cl^-. It would be expected that ion peaks associated with seasonal changes in concentration in precipitation would be deposited at different depths within the snowpack – therefore correlation between ions would not be expected.

From Figure 50 there are some peaks in the ion profiles that correspond to peaks in the corresponding density profiles, however, visually the density to ion profiles do not appear as similar as the ion profiles do to each other. The data were again log-transformed to meet normality assumptions, and Pearson's correlation coefficient values were calculated, with significance values (Table 10).

	Pearson's correlation coefficient	P value
Cl^-	0.28	0.001
SO_4^{2-}	0.3	0.0004
NO_3^-	0.22	0.012
Na^{2+}	0.23	0.007
K^+	0.13	0.13
Mg^{2+}	0.31	0.0002
Ca^{2+}	0.15	0.09

Table 10: Pearson's correlation coefficient values between ion concentration and density.

Table 10 shows there are significant correlations between all ion concentrations and densities, although the correlations are not strong (<0.31). These results indicate that peaks in all ion concentrations are correlated with each other, and with density. This indicates that the seasonal variation in ion concentration in precipitation is not preserved in the snowpack; since concentration correlates with density. This also indicates that the redistribution of mass within the snowpack due to melt water percolation may also result in the redistribution of ions.

4.3.4 Isotope concentrations

Seasonal variations in isotope concentrations in precipitation are well understood (Dansgaard, 1964). An increase in the concentration of heavier isotopes (^{18}O, ^{2}H) indicates a period of warmth (summer), (Paterson, 1994), and a trough a cooler winter period.

The 17 m core was analysed at 10 cm resolution. A minimum of eight samples per year are typically required to derive any annual signal (Pohjola, 2002a); the annual accumulation is between 35 cm w.e. and 80 cm w.e. at T5 (Benson, 1962; Seckel, 1977; Stober, 1986; Anklin, 1994). Thus, using the average density of the autumn snowpack at T5 in 2004 of 0.53 g cm^{-3}, the variability in annual accumulation as a thickness would be between 66 and 150 cm. Sampling at 10 cm resolution should therefore ensure that any annual signal, if present, is identified in all but the lowest accumulation years.

Initially samples between depths of 149.2 cm to 973 cm depth were analysed for ^{18}O and ^{2}H. These were found to be strongly positively correlated, with an r^2 value of 0.9995. For the remainder of the core, only the ^{18}O concentrations were measured and subsequent ^{2}H values were derived from linear regression ($p<0.0001$) (details in Chapter 3, Figure 28).

In order to ensure the sampling resolution is sufficient, a ~2 m section (from depth 2.42 – 4.28 m) was re-sampled at 2.5 cm resolution. This section includes accumulation from 2002, which has a very low accumulation of 30 cm (depth), as measured at Crawford Point AWS. Figure 51 shows plots of ^{18}O and ^{2}H concentrations, where ^{18}O concentrations have been multiplied by 10 for comparison to ^{2}H. The re-sampled section is shown as a separate plot to the right.

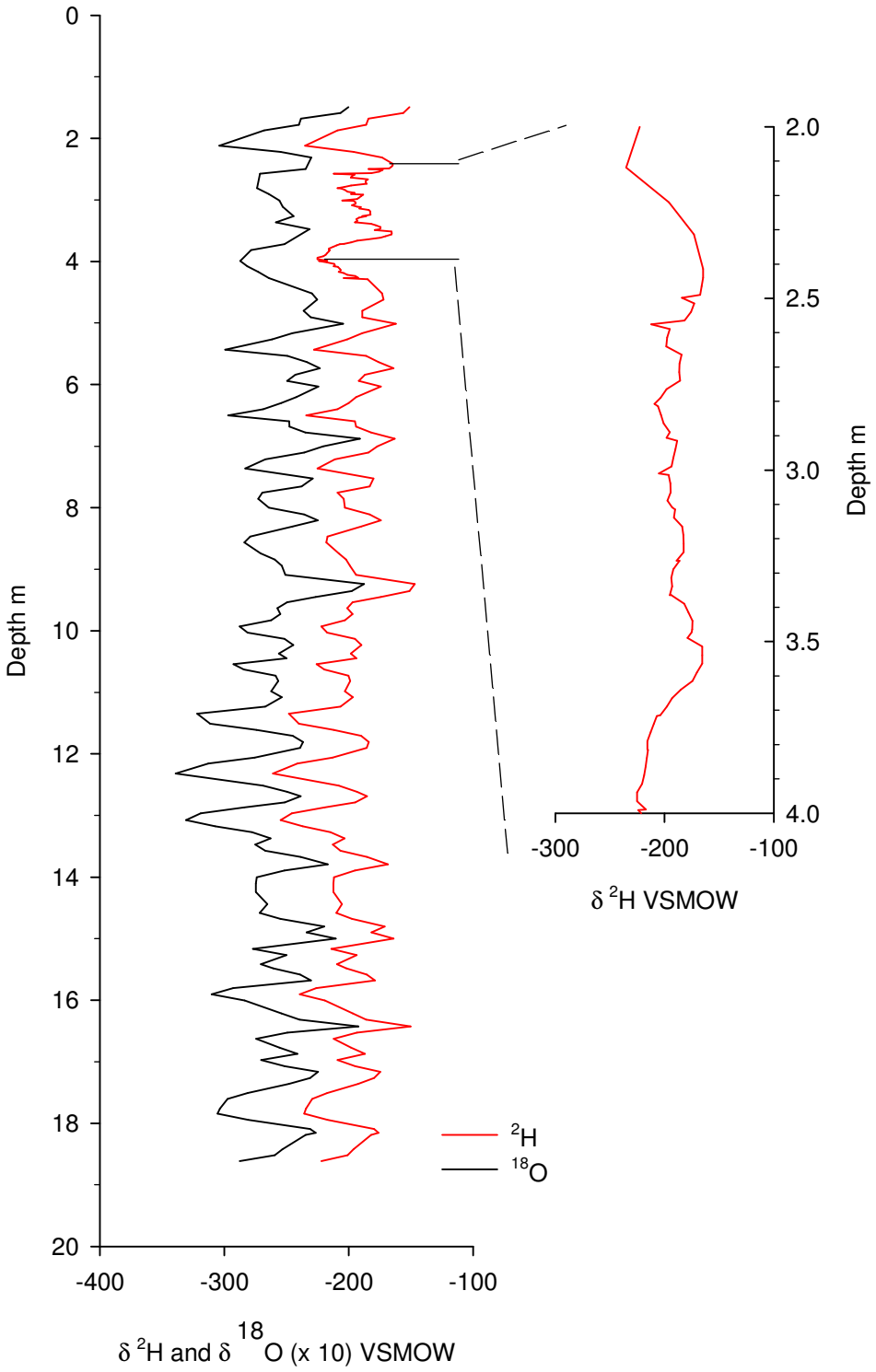

Figure 51: Graph showing $\delta^{18}O$ (x 10) and $\delta^{2}H$ values. The graph on the left shows measurements at 10 cm resolution and on the right a 2.5 cm resolution for depths between 241.5 cm and 428.9 cm.

The average concentration for ^{18}O is -25.7 ‰ VSMOW and varies between -33.9 and -18.7‰ VSMOW. The ^{2}H average concentration is -197.4 ‰ VSMOW and varies between -146.7 and -261.0 ‰ VSMOW. For the re-sampled section the average ^{2}H concentration is -194 ‰ VSMOW, varying between -225 and -164 ‰ VSMOW. The smaller range in values indicates that the maximum 'peaks' and 'troughs' are not present between these depths.

Overall the record starts at a 'peak', which represents the end-of-summer 2003 layer, at the top of the core. 'End-of-summer surface' peaks have been identified to 1985 (Figure 52) and while this is a subjective technique, the magnitude in variation between concentrations is considered in peak selection, as are the shapes of the oscillations.

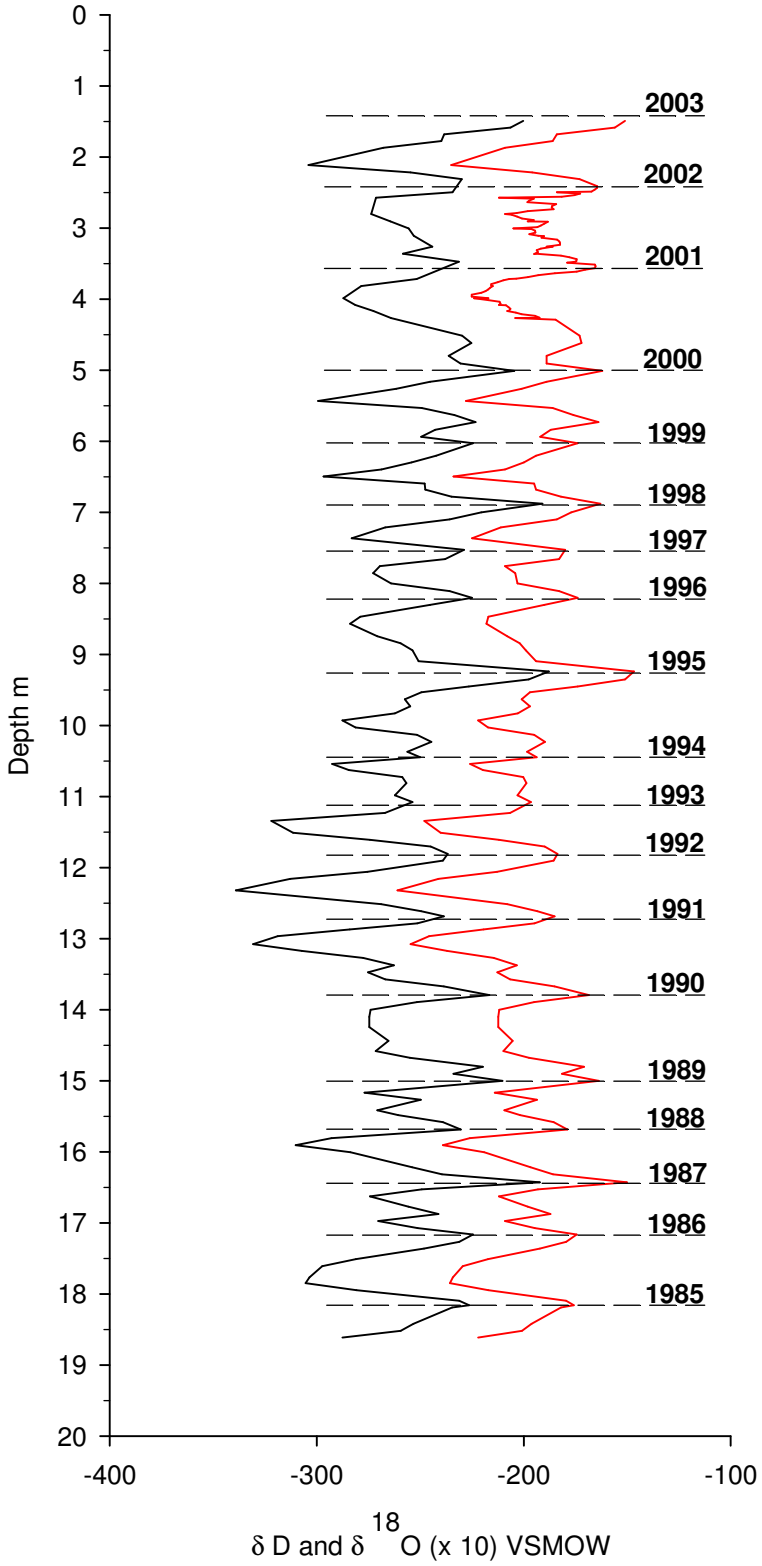

Figure 52: $\delta^{18}O$ (x 10) and ^{2}H values, with summer peaks marked. These peaks denote the end-of-summer surface for the year labelled.

4.3.5 Meteorological records

It is possible to compare accumulation derived from identifying annual layers in the 17 m core from isotope oscillations; to accumulation measurements from Crawford Point AWS (located ~10 km from T5). Crawford Point has recorded snow surface elevation using four sonic ranging sensors every hour since 1995, providing a record of accumulation. However the data are subject to gaps where there has been instrument failure, and significant time lags (typically over the winter) between repairs (Figure 53). Where gaps exist, linear regressions are performed on the data before, and after the gaps – where the regressions are comparable, the missing data is interpolated. Further complications exist when sensors are re-set to a new height, appearing as a 'jump' in the data (Figure 53). Where this occurs it is not possible to interpolate values; for this reason there are no accumulation data for 1998 and 1999.

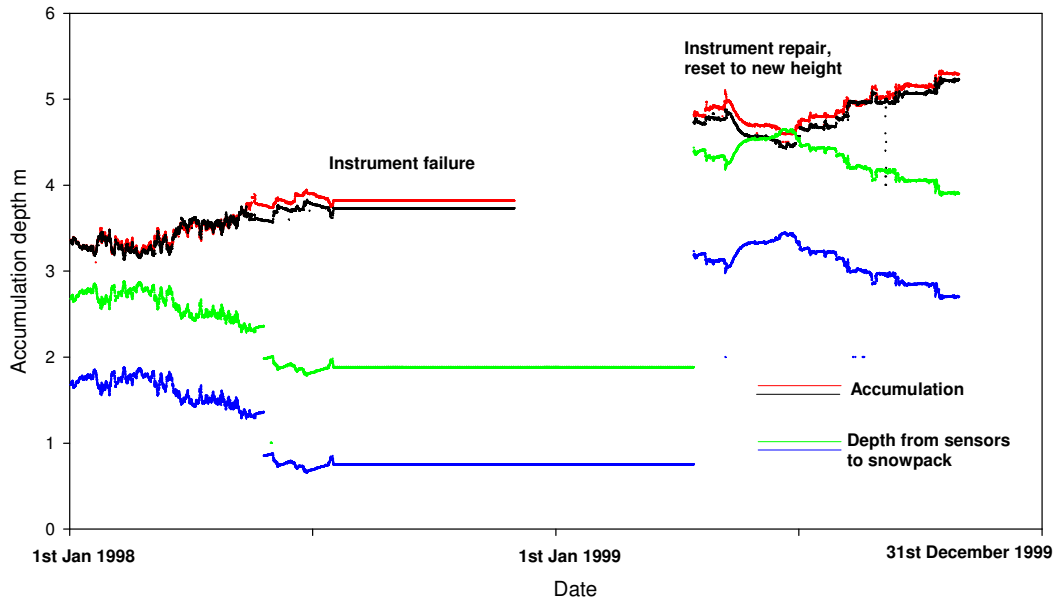

Figure 53: Elevation change data for 1999 from Crawford Point AWS, showing periods of instrument failure, jump in measurements as instrument is re-set and lowering of surface during summer melt.

The accumulation measurements at Crawford Point are changes in snow height; these have been converted to a w.e. accumulation by using the average density for

the autumn 2004 snowpit at T6. This record provides us with a guide to the accumulation for years 1996 to 2003, and so provides a comparison of accumulation as a water equivalent derived from the ice core data and AWS data as shown in Figure 54.

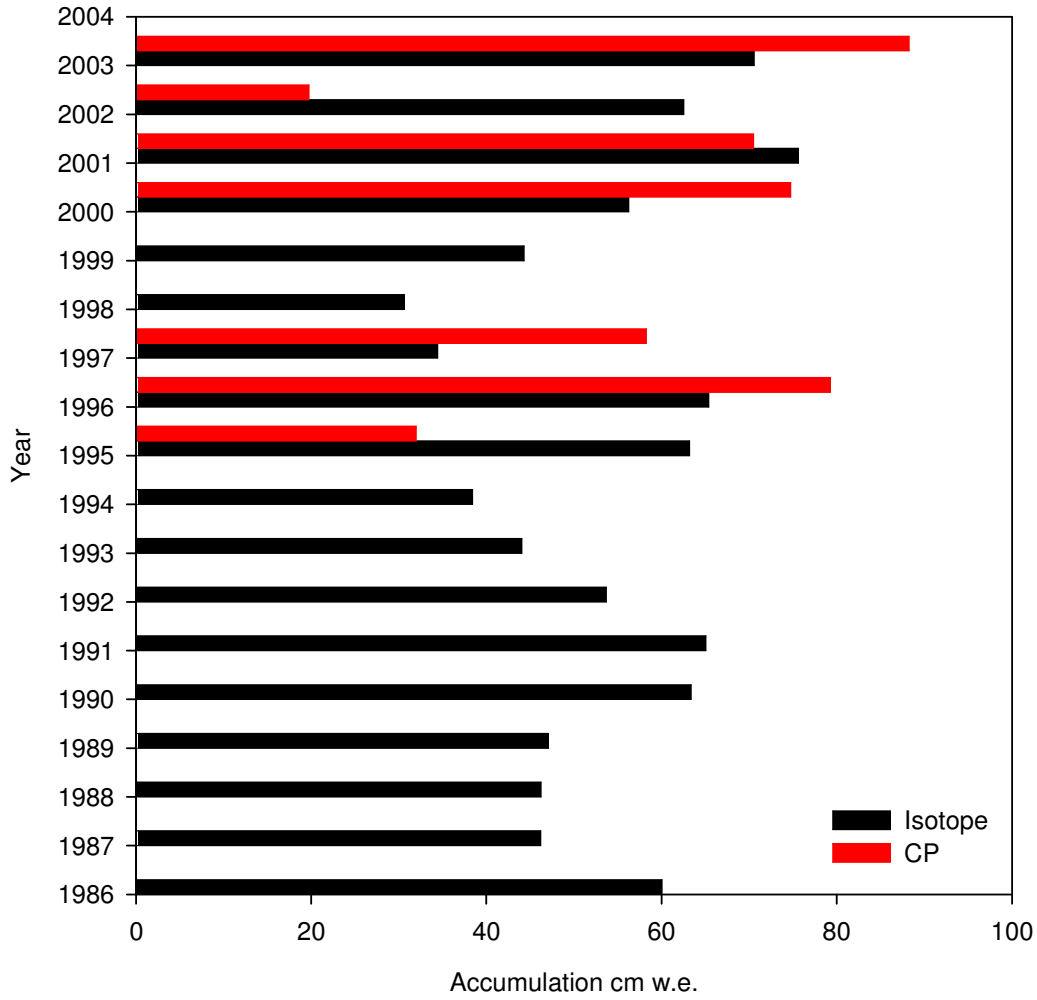

Figure 54: Comparison of summer to summer accumulation measured using the 17 m core densities, and annual layers found from the isotope profile, and elevation change at Crawford Point AWS.

There are clear differences between the accumulations calculated from identifying annual layers in the 17 m core using the isotope record, and from measurements made at Crawford Point AWS. The largest difference between accumulations is in 1996 – 1997 where accumulation measured at Crawford Point exceeds that derived

from the 17 m core by 69%, and in 2001 – 2002, where the accumulation derived from the 17 m core exceeds that measured at Crawford Point by 68%

4.4 Discussion

From the isotope results it is apparent that annual layers in the percolation zone of the Greenland Ice Sheet can in principle be identified, and annual mass balance derived. However, if meltwater percolates through the previous year's end-of-summer surface, the mass balance results will be distorted. Previous work (Pfeffer & others, 1991) indicates percolation depth may be 2 - 4 m at T5, which would clearly exceed one year's snowpack thickness and lead to mass transfer over more than one than one year's accumulation. Temperature results in autumn 2004 show the average bottom of pit temperature to be -5.3 ^{o}C. It is therefore not impossible to suggest temperatures may be high enough for liquid water to percolate through the bottom of the snowpit. No ice features (e.g. pipes) directly showing percolation through this layer, were present in the snowpits dug in autumn 2004. However, the spatial variability of ice structures (Campbell & others, 2006) ensures that visual confirmation of downward percolation is unlikely to be observed.

To further investigate the possibility of percolation and mass movement through more than one years' accumulation, the density of ~1.5 m columns of firn from below the end-of-summer 2003 surface have been compared from cores retrieved in spring and autumn 2004 to investigate: 1) if there is densification occurring in the previous year's snowpack over the summer period and 2) if this densification can be accounted for due to compaction alone.

The densification due to compaction was measured from the 17 m core at E3 (Figure 55), the density gradient was found to be:

$$y = 0.0086x + 0.47$$

Equation 5: Densification (y) due to compaction at depth (x), where depth is measured in m, and density in g cm^{-3}.

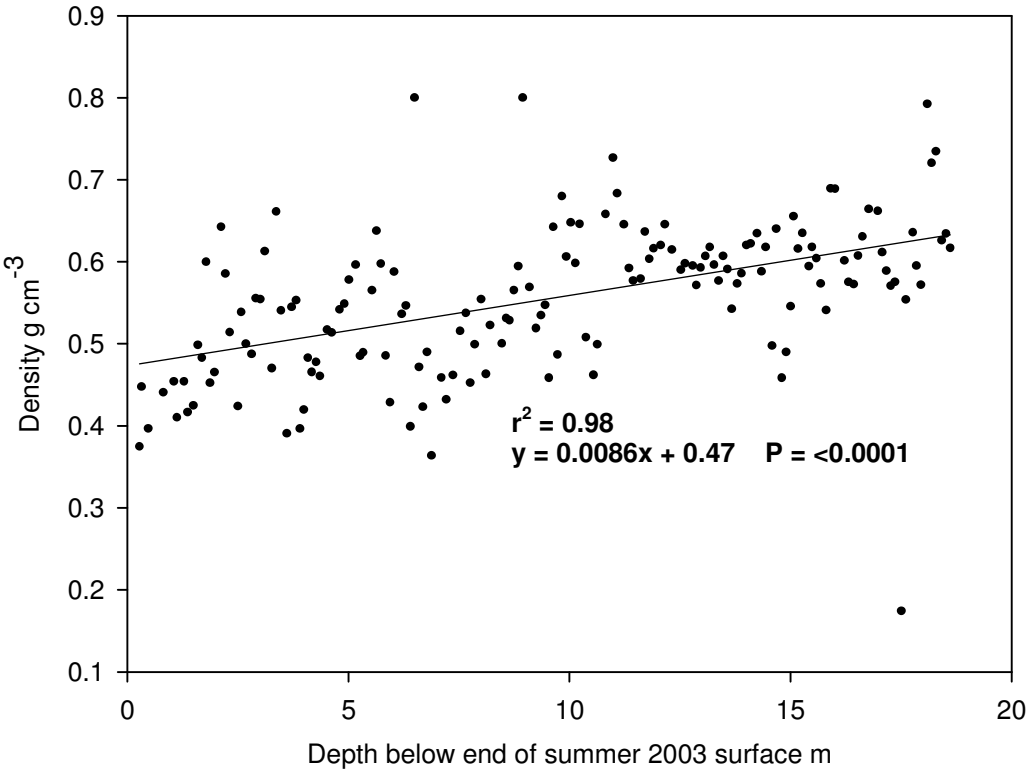

Figure 55: Overall densification gradient in 17 m core, where densification is due to compaction.

The average density measured in the spring 2004 cores is the average density for 2002 - 2003 accumulation which has undergone summer 2003 melt, percolation and refreezing processes. The comparable section retrieved in autumn 2004 will still represent the 2003 summer melt and refreezing processes, but will also have undergone compaction due to the weight of the overlying snow, and possibly have been affected by the summer 2004 melt and refreezing processes.

The average density in 1.5 m firn column below the end-of-summer 2003 surface was measured in spring and autumn cores in 2004. If there is no melt water percolation and refreezing from the 2003 – 2004 snowpack, the 1.5 m firn column would be expected to in increase in density as a result of compaction alone. Accounting for the depth of the snowpit (2003 – 2004 accumulation) and length of section of the core, the expected increase in density would be 0.026 g cm^{-3} between the cores retrieved in spring and autumn, due to compaction alone.

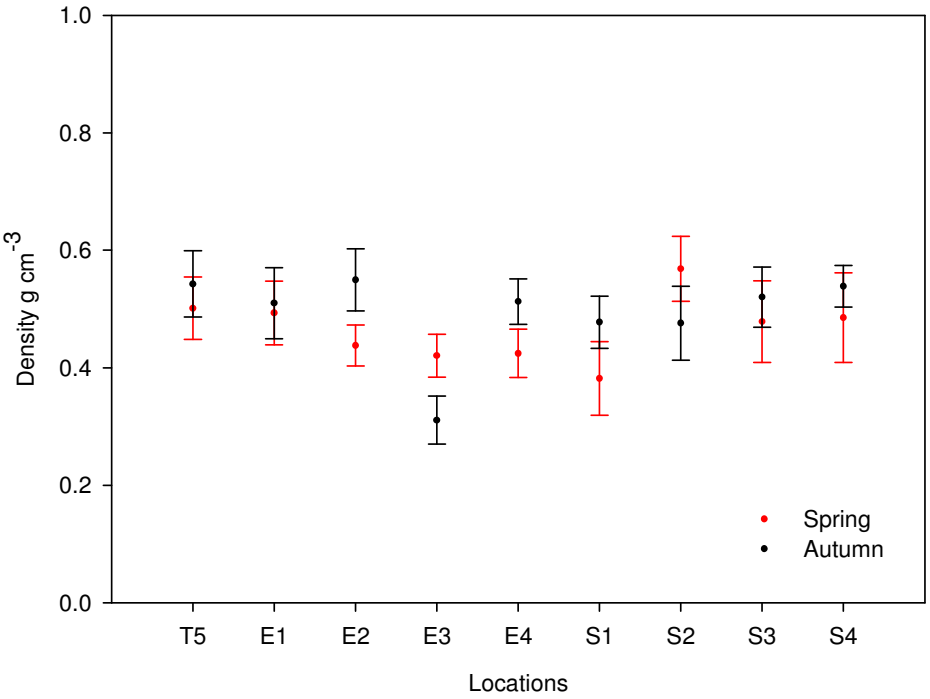

Figure 56: Average densities for 1.5 m of firn core retrieved below the summer 2003 surface in spring and autumn 2004. Error bars represent standard error of average density for each section of core.

Figure 56 shows the average densities along the 1.5 m section of the cores retrieved in spring 2004 and autumn 2004. There is a significant change in density at E2, E4, S3 and S4, and at these sites, the average increase in density between spring and autumn is 0.077 g cm^{-3}; this is an increase in density 66% higher than that expected from compaction alone. It is possible that melt water from summer 2004 has percolated through the end-of-summer 2003 surface, and may contribute to this increase in density.

There are also indications of percolation through more that one years' snowpack in the ion record. Many of the peaks which occur in the 17 m core are significantly higher than the average concentrations. Additionally, as these peaks coincide between different ions this indicates preferential elution may be moving the ions through the snowpack (Davies & others, 1982). These peaks almost certainly act as an indicator of meltwater movement. The peaks are typically several metres apart – exceeding one year's typical snowpack depth. This indicates that meltwater and associated ions may be moving through more than one year.

If the increase in density between the cores retrieved in spring and autumn 2004 is 0.077 g cm^{-3} and of this 0.026 g cm^{-3} would be expected due to compaction, then there is a 0.051 g cm^{-3} increase in density which is not accounted for by compaction. This can be multiplied by the length of the core (0.0051 g cm^{-3} x 1.5 m), to find the mass as a water equivalent of 7.65 cm w.e. this can be attributed to a mass input from the overlying snowpack (the 2003 – 2004 accumulation). The accumulation for 2003 – 2004 was found by measuring the accumulation above the end of summer 2003 surface and was 79.72 cm w.e. (see Chapter 5 for details). If 7.65 cm w.e. has percolated into the underlying snowpack, the actual accumulation for 2003 – 2004 should be 87.37 cm w.e. For mass balance measurements derived from annual layers to be accurate, any melt water percolation through more than one year needs to be quantified and accounted for. Neglecting to factor for this may result in underestimates of mass balance, in this example, by 9%.

The isotopes showed clear cyclicity and peaks in the data were identified as indicator of the end-of-summer surface (Clark & Fritz, 1997) allowing annual accumulation to be derived using corresponding density values. These data were compared to accumulation values derived from elevation changes measured at Crawford Point AWS (Figure 54).

There are several possible reasons why there is variability between these two sets of measurements. Firstly there are sources of error in the Crawford Point data since elevation records have been extrapolated where gaps exist due to instrument failure. Additionally, the AWS measures elevation change which has been converted to density using the 2004 autumn snowpit average density value at T6 rather than a direct measurement of each year's average density. Furthermore Crawford Point is ~10 km further into the ice sheet that the core location at E3, and spatial variations are seen in snowpack thickness in autumn 2004, where the annual snowpack depth at E3 was 67 cm w.e. compared with 76 cm w.e. at T6 (~2 km from Crawford Point).

Previous studies of ionic chemistry at T5 indicate that Cl^-, SO_4^{2-}, NO_3^-, Na^+ and Ca^{2+} show a distinct seasonal variation, with no geographical variation in peak timing (Fischer & Wagenbach, 1996). Sulphate peaks governed by anthropogenic emissions are traditionally high in winter/spring as there is efficient transport of SO_4^{2-} emission from mid latitudes to the arctic (Heidam, 1984). Ca^{2+} is also documented as peaking in spring as large parts of continental mineral dust source areas are enclosed by the polar front (Steffensen, 1988). Na^+ and Cl^- concentrations are also higher in the spring/winter, a secondary peak may be seen in the summer if there is cyclonic activity (Liljequist, 1970). In the summer snowpack, NO_3^- peaks are expected although the overall concentration is low compared to other species (Fischer & Wagenbach, 1996).

These results (Figures 35 – 49) show no seasonal signature in ion concentrations, even in the spring snowpack which has not undergone melt and re-freezing. However, it has been documented that snow chemistry is subject to post depositional changes such as sublimation, diffusion, wind drift (Bales & Wolff, 1995).

Peaks in ion concentrations show correlations between each other, and with density. Since ions are located on the outer surface of snow crystal (Morris & Thomas, 1985), this leaching and movement of ions through the snowpack is seen in the ionic record, but not in the isotopic record, as ice crystals are isotopically homogenous (Souchez & Lorrain, 1991), so although the signal may be smoothed (Pohjola & others, 2002b), it will not be lost from the record.

4.5 Conclusions

It is possible to identify annual layers in the 17 m core retrieved at E3, despite 10% of the snowack undergoing melt and refreezing, by measuring seasonal fluctuations in isotope concentrations. Visual identification of stratigraphy is not sufficient to depict the autumn hoar and end-of-summer 'couplet', hardness measurements, which are not able to be taken from the core, are also required. The hoar/end-of-summer couplet exhibits a density profile that is apparent in the 'smoothed' n-probe derived density profiles, but not from direct measurements from the 17 m core. Within the n-probe derived profile this technique is highly subjective, and too ambiguous for accurate annual layer identification. The concentration of ions within the 17 m core are correlated with each other, and with density, and do not show the expected seasonal signature (Fischer & Wagenbach, 1996).

Once annual layers have been identified in the 17 m core, using fluctuations in ^{18}O and ^{2}H concentrations, the annual mass balances for 1986 to 2003 were calculated, using corresponding density measurements. These vary significantly to those obtained from measurements of snowpack height (from Crawford Point AWS), and the average autumn 2004 density at T6. There are however many errors associated with determining the mass balance from the AWS measurements, including, gaps in

measurement and the distance the AWS is from E3 (where the core was retrieved from).

The core, however, is a point measurement, and to accurately determine the mass balance of an area, several cores would need to be taken to negate the effects of snow scouring and deposition. Additionally, density and ion profiles indicate, combined with previous work and snowpit temperatures, that it may be possible for melt water (~9% of the annual accumulation) to percolate into the previous year's snowpack. For mass balance measurements derived from annual layers to be accurate, any melt water percolation through more than one year needs to be quantified and accounted for. Neglecting to factor for this may result in underestimates of mass balance.

Chapter 5: Temporal and small scale variability in density and snowpack structure

In the previous Chapter it was established that it is possible to use $\delta^{18}O$ and $\delta^{2}H$ to identify the end-of-summer surfaces in firn cores retrieved from the percolation zone of the Greenland Ice Sheet. From this the annual accumulations were calculated from 2003 to 1986 – these show high inter-annual variability. It is important to have some understanding of the inter-annual variability, as the CryoSat 2 mission is only planned for three years, and any trends identified in this time will need to be offset against natural fluctuations. In this Chapter the annual accumulations, calculated from the 17 m core are compared to previous measurements to further develop the understanding of inter-annual variation.

In the percolation zone of the Greenland Ice Sheet, it is important to quantify the effect summer melt, percolation and refreezing has on the snowpack; and how these processes vary spatially. In this Chapter snowpack accumulation, density and stratigraphic measurements from two spring seasons (2004 and 2006) and autumn (2004) are presented, showing seasonal variations, and small spatial (1 km^2) variations. This Chapter is based primarily on a paper published in 2007 in the Annals of Glaciology 46 (Parry & others, 2007); this paper is included in Appendix 1.

5.1 Introduction

Interpreting changes in surface elevation in terms of change in mass is complicated by surface melting and refreezing. In the most commonly anticipated scenario, surface melt, percolation and re-refreezing will cause a decrease in elevation but

with no actual mass loss. In this case, the lost surface snow has been redistributed as ice layers in the near-surface layer whose bulk density has correspondingly increased (Braithwaite & others, 1994). Similarly, elevation may also remain constant between two periods even though mass has increased due to the addition of rain or solid summer precipitation which has subsequently melted and percolated into the underlying snowpack before refreezing (again thereby increasing snowpack density but not surface elevation). Thus, accurate assessment of mass balance may be masked by refreezing processes whose remaining signature is a near-surface density change rather than a surface elevation change. Unfortunately, determining the influence of summer densification on accurate geodetic measurements of mass balance is currently severely limited in the percolation zone of ice sheets by inadequate characterisation of the extent, intensity and processes of meltwater refreezing (Pfeffer & others, 1991).

Measurements of elevation change from satellite radar altimeters depend on accurate identification of radar reflections from the surface of the ice mass. However, the shape of the radar return wave is affected by reflections from internal structure of the near surface snow and firn, termed volume backscatter (Ridley & Partington, 1988). Summer melting and refreezing within the percolation zone of ice masses may create ice layers, lenses and pipes within the near surface snow and firn that can result in intense volume backscatter (Thomas, 2001) thereby generating ambiguous surface returns. Thus, temporal changes in the shape of the radar echo can result from seasonal variations in near surface snow and firn density (Jezek & others, 1994; Scott & others, 2006a; Scott & others, 2006b). Determining spatial variability in the extent of the seasonal metamorphism of the near surface stratigraphy caused by summer melting and refreezing is therefore an important component of efforts to discriminate between surface and volume radar returns. Thus, there is a need to isolate the factors that determine the shape of the echo return in order to reduce measured elevation errors for satellite applications.

Pfeffer and Humphrey (1998) investigated ice layer formation along a 40 km transect (1640 m to 1900 m a.s.l) in the percolation zone of the Greenland Ice Sheet, and found that ice layers were more frequent at higher, colder sites, where infiltration was more limited, than at the lower, warmer sites. This suggests that volume backscatter will not automatically scale with increasing summer melt-rate (and thus decreasing elevation) within the percolation zone. In addition, as well as ice-layer frequency, the precise position of ice layers within the snowpack is crucial to radar estimates of surface elevation since the nearer to the upper surface of the snowpack the ice layers form, the smaller the likely disparity between actual elevation and radar-derived elevation. However, predicting the precise location of a given ice layer may not be straightforward since it is governed by many factors, including local energy balance conditions driving melt and freezing processes, and the presence of hydraulic barriers inducing ponding of downward-percolating meltwaters (Wankiewicz, 1979; Pfeffer & others, 1990). Pfeffer and Humphrey (1996) in a further study of ice-layer formation in the percolation zone of the Tassersiaq ice cap, West Greenland, found the presence of fine-to-coarse grain stratigraphic boundaries provided a critical hydraulic barrier preventing downward percolation of meltwater and promoting the development of ice layers. Thus, overall snowpack stratigraphy, and spatial and temporal changes in its structure, will affect the contemporaneous and subsequent development of ice layers.

In this Chapter the field data from spring 2004 and 2006, and autumn 2004 is presented from within 1 km^2 of T5 (Figure **16**), and along a 57 km transect within the percolation zone of the Greenland Ice Sheet (Figure **15**). Density measurements from snowpits, shallow firn cores and the neutron probe are presented in conjunction with avalanche probe measurements and stratigraphic sketches of a 5 m section of spring 2006 snowpack. These data are presented in order to: (1) Quantify the effect of the seasonal densification of near surface snow and firn on annual mass balance, (2) Determine the seasonal and spatial changes in near-surface stratigraphy caused by the processes of summer melting, percolation and refreezing, and (3) Determine

the spatial variability in ice layer formation, and possible snowpack characteristics that pre-determine this.

5.2 Field sites and Methods

The effect seasonal melt, percolation and internal refreezing has on the snowpack is investigated at nine sites (T5, E1, E2, E3, E4, S1, S2, S3 and S4 –Figure **16**) over 1 km^2, prior to melt in spring 2004 and spring 2006, and post melt in autumn 2004. Full details on measurement locations and timing of field work are given in Chapter 3.

The change in density, accumulation and snowpack depth are measured at all nine sites using the snowpit methods detailed in Chapter 3. In spring and autumn 2004 the bottom of each snowpit is the end-of-summer 2003 surface; in spring 2006 the bottom of the snowpits is the end-of-summer 2005 surface. Additionally, density profiles from the n-probe records from spring and autumn 2004 are compared.

The continuity of 'hard' features within the snowpack were measured using an avalanche probe between T5 and S1 (100 m, Figure **16**) at 1 m (autumn 2004 and spring 2006) and 5 m (spring 2004) intervals. In the spring snowpack this would likely pick out windcrusts, and the autumn (post melt) snowpack, ice layers and windcrusts.

In spring 2006 a ~7 m trench was dug close to T5, parallel to the EGIG line. A 3 m section of the trench was divided into three 'pits' approximately 2 m depth, extending over half way into the 2004 to 2005 snowpack (Figure 27, Figure 57, Figure 58). These three 'pits' were sketched on both sides to record the varying stratigraphy. Additionally, the density profiles for the first 3 m (at ~1 m intervals) closest to the EGIG line were recorded above the end-of-summer 2005 surface.

The remaining ~4 m of the trench were only dug to ~90 cm depth, revealing the winter 2005 – 2006 snowpack. The continuity of windcrusts in the 2005-2006 winter snowpack were recorded along the full length of the trench.

Figure 57: The ~7 m trench looking west, i.e. the far end (furthest from the camera) is nearest to T5. The far end is divided into three 'pits' ~2 m deep. The end closest to the camera is ~ 90 cm deep.

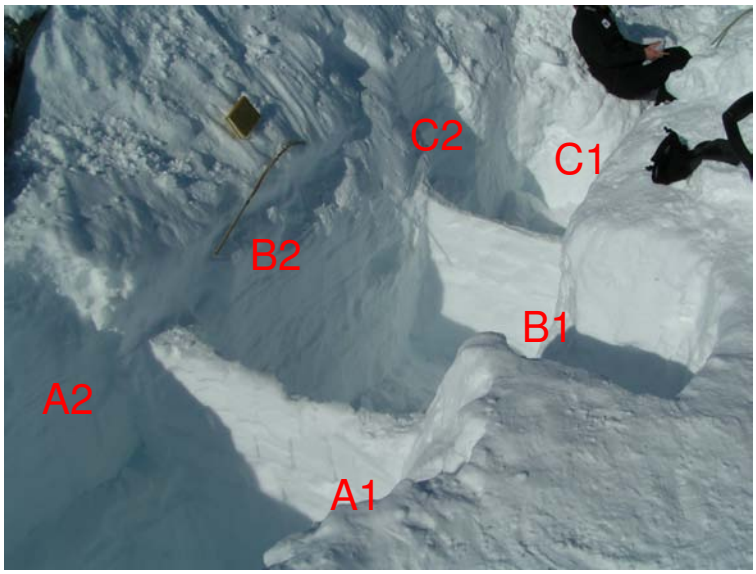

Figure 58: These are the three 'pits' within the trench, both sides were sketched, and density measurements were taken from each pit on the side closest to the camera.

The location of ice layers within the snowpack were recorded at each snowpit in autumn 2004. The w.e. accumulation for each ice layer is then calculated as a percentage of the total annual (2003 – 2004) accumulation. The depth of each ice layer is also converted to a percentage of the total depth, in order for the locations of ice layers to be readily comparable between snowpits. In spring 2006, cores were retrieved at T1 to T7 from the end-of-summer 2005 surface. Ice features within these cores have been recorded, as a depth below the end-of-summer 2005 surface, up to 2 m. The w.e. for the layer with the ice feature has then been calculated as a percentage of the total w.e. accumulation over the 2 m of the core. It was not possible to constrain this within one year, as the depth to the end-of-summer 2004 surface is not know at T1 to T3, and T7. The grain sizes above and below each ice layer were recorded in all snowpits, in order to determine potential hydraulic controls on ice layer formation.

5.3 Results

5.3.1 Seasonal changes in elevation, snowpack density and accumulation

5.3.1.1 Seasonal elevation changes

The snowpack depths at the nine sites located within 1 km^2 of T05 are presented in Figure 59. The mean snowpack depths for each of the three field seasons were 143.2 cm (standard deviation (s.d.) 4.0 cm) in spring 2004, 110.8 cm (s.d. 8.1) in spring 2006 and 150.8 cm (s.d. 11.7) in autumn 2004. The increase in snow depth between spring and autumn 2004 is 5.3% (Figure 59), this difference is found to be statistically significant using the 't-test' ($p=0.02$). The depth of the snowpits is also seen to vary inter-annually, between the spring 2004 snowpack and spring 2006

snowpack. As expected from the results in Chapter 4, where inter-annual variability in accumulation is high, the difference in snowpack depth between spring 2004 and spring 2006 is significant (p=0.01), again found using the t-test.

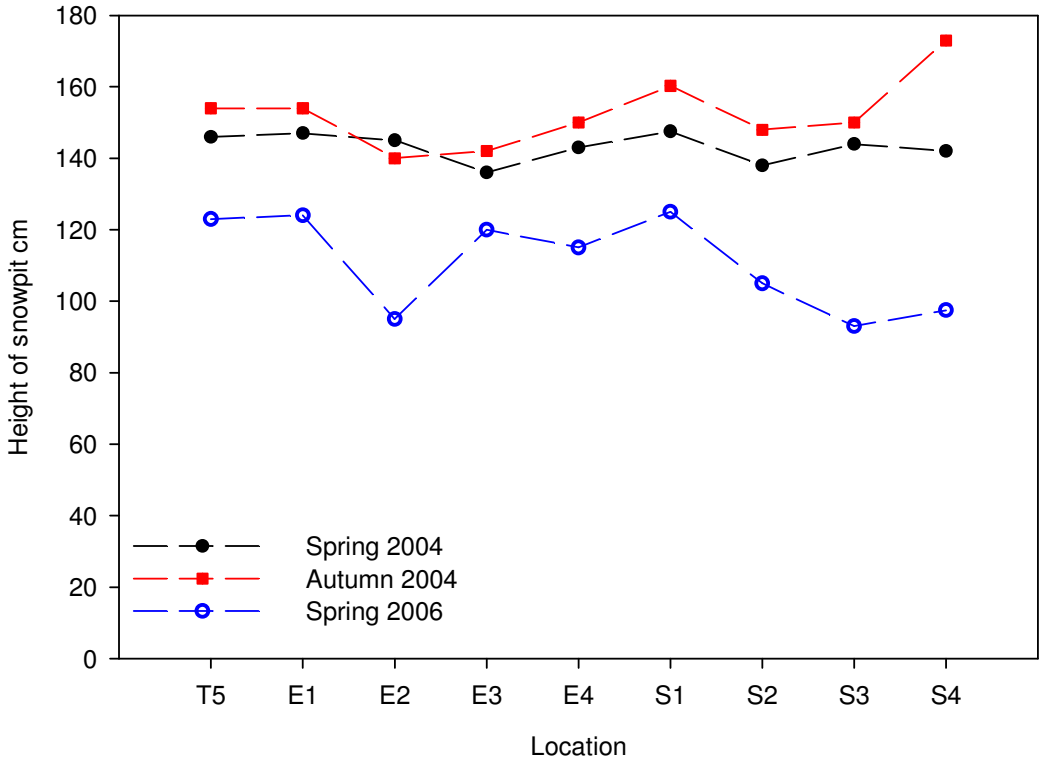

Figure 59: Graph showing height of snowpack above end-of-summer (2003/2005) layers in spring 2004 and 2006, and autumn 2004.

5.3.1.2 Seasonal density changes

Snowpack densities at the nine sample sites during the three field seasons are presented in Figure 60. The average density of the snowpack was less in spring 2004 and 2006 than in autumn 2004. Between spring and autumn 2004 the average density increased at all snowpits (Figure 60). The mean snowpack density of all sites in spring 2004 was 0.42 g cm^{-3} (s.d. 0.02), slightly higher than in spring 2006, 0.39 g cm^{-3} (s.d. 0.04), and 0.53 g cm^{-3} (s.d. 0.04) in autumn (Figure 60). The average increase in snowpack density from spring to autumn 2004 is 26.2% (p=0.01). The

difference in average density between spring 2004 and spring 2006 is not statistically significant.

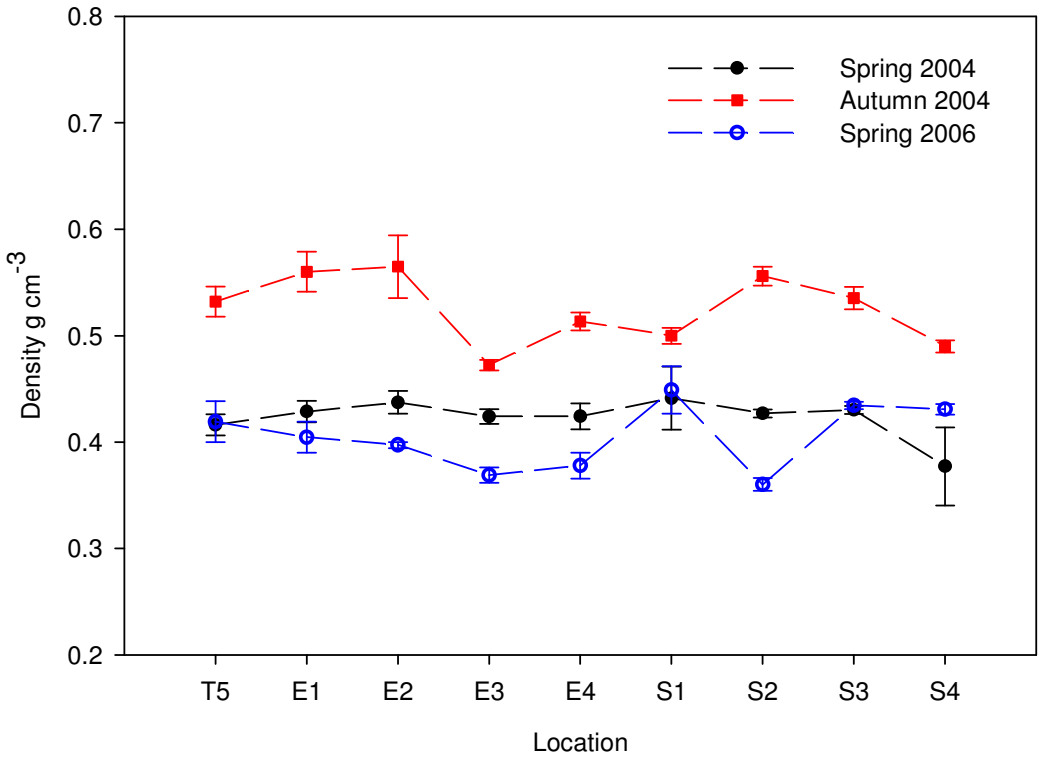

Figure 60: Graph showing average snowpack densities within 1 km² of T5 for spring 2004 and 2006 and autumn 2004. Error bars are the standard error for the average snowpit densities.

This seasonal densification was also seen in the n-probe profiles, where the upper part of the 2003-2004 snowpack is seen to increase in average density from spring 2004 (mean T5=0.40 g cm^{-3}, E1=0.40 g cm^{-3}) to autumn 2004 (mean T5=0.47 g cm^{-3}, E1=0.48 g cm^{-3}) as exemplified in the density profiles derived from the n-probe measurements at T5 and E1 in Figure 61 (all other profiles are in Appendix 8).

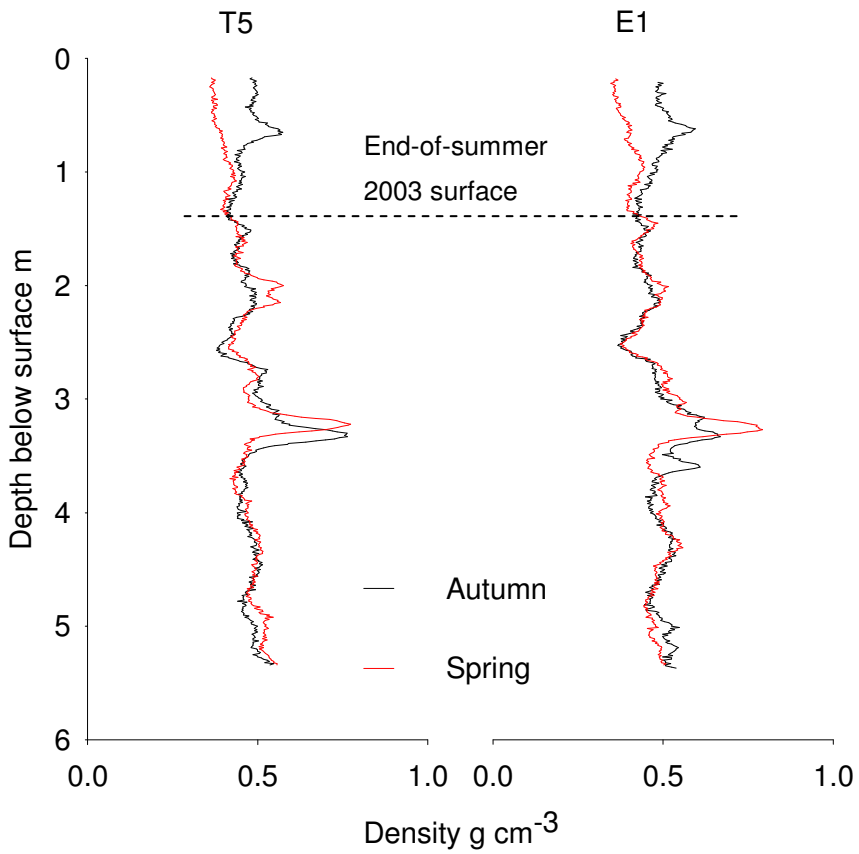

Figure 61: Graph showing density derived from n-probe measurements at T5 and E1 in spring and autumn 2004 where clear seasonal densification of the snowpack is apparent in the top 1.5 m.

5.3.1.3 Seasonal accumulation changes

The average snowpit accumulation increased from 60.5 cm w.e. (s.d. 3.4), in spring 2004 to 79.6 cm w.e. (s.d. 5.5) in the autumn 2004, an increase of 31.6% (p=0.01) (Figure 62). Accumulation was 43.5 cm w.e. (s.d. 8.1) in spring 2006, a difference in accumulation between spring 2006 and spring 2004 of 17 cm w.e. (p=0.01).

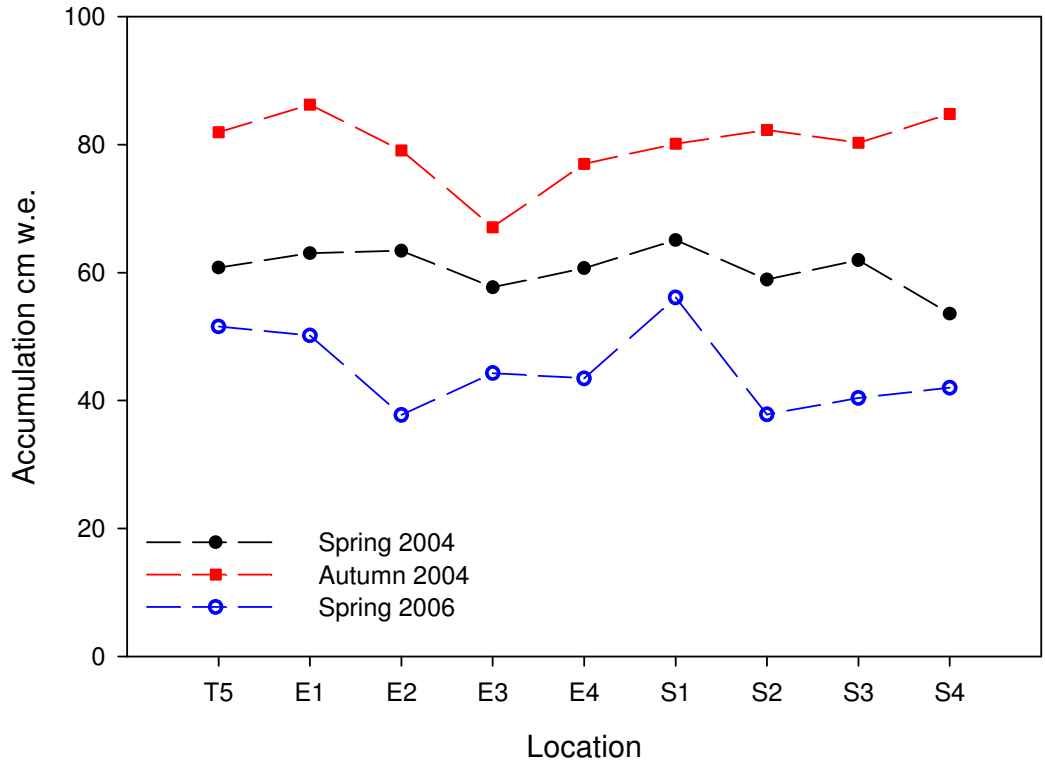

Figure 62: Graph showing accumulation as a water equivalent for spring 2006, spring 2004 and autumn 2004.

5.3.2 Spatial variability in snowpack characteristics

5.3.2.1 Spatial variability in density profiles

It is clear from Figure 60, that there are distinct variations in mean density between the spring and autumn snowpacks. Plots of density with depth at individual snowpits demonstrate this seasonal variability in more detail. Density profiles for spring 2004 and 2006 and autumn 2004 for all sites within 1 km^2 of T5 are plotted against each other in Figure 63. These plots clearly show autumn 2004 densities are invariably higher and characterised by more extreme variations in density due to the presence of ice layers relative to the spring 2004 snowpack.

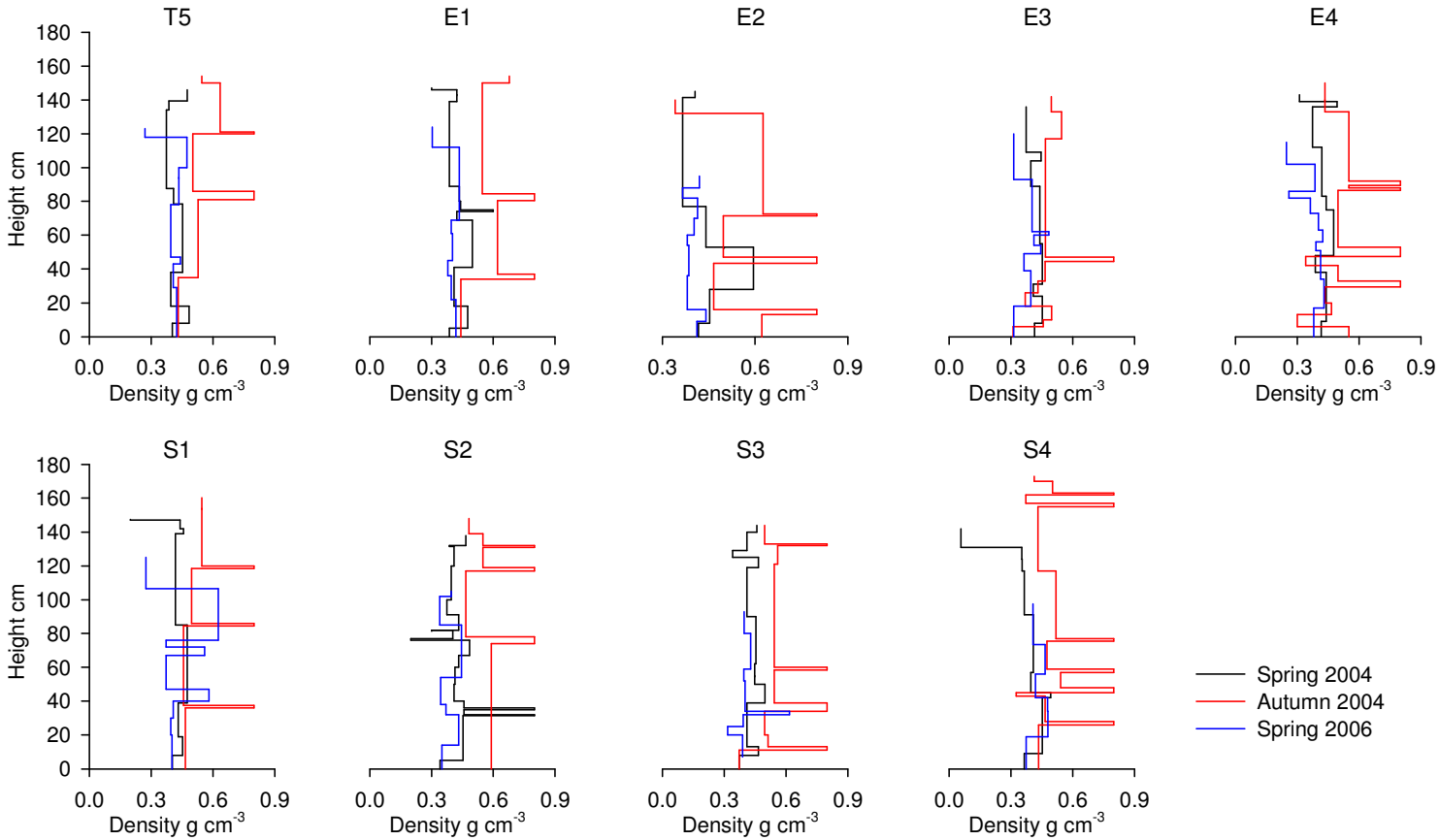

Figure 63: Snowpack density plotted again height above the previous year's end-of-summer surface for all pits within 1 km² of T5 in spring 2004 and 2006 and autumn 2004.

It is also apparent from Figure 63 that the snowpack density structure varies on small length scales. The measurements at T5, E1 and S1 (Figure 63) are made within 1 m of each other on opposite walls of the same snowpit, yet the profiles are quite different, with areas of low and high density often not correlating with each other. In the autumn profile, a continuous ice layer is measured at ~80 cm in T5, E1 and S1. However this is not seen to continue 10 m to the next pit at S2, although an ice layer is present at ~60 cm at E2, which may be a continuation of this. At E1 and S1 an ice layer is present at ~40 cm, but this is not seen at T5. This short scale variability is echoed in the density profiles from the trench excavated in spring 2006 (Figure 27), sampled at ~1 m intervals along a ~3 m section (Figure 64). Here there is no continuity in the density profiles, apart from at the base (between 0 and 10 cm above the end-of-summer 2005 surface) where all three profiles have low density (~0.33 – 0.37 g cm^{-3}).

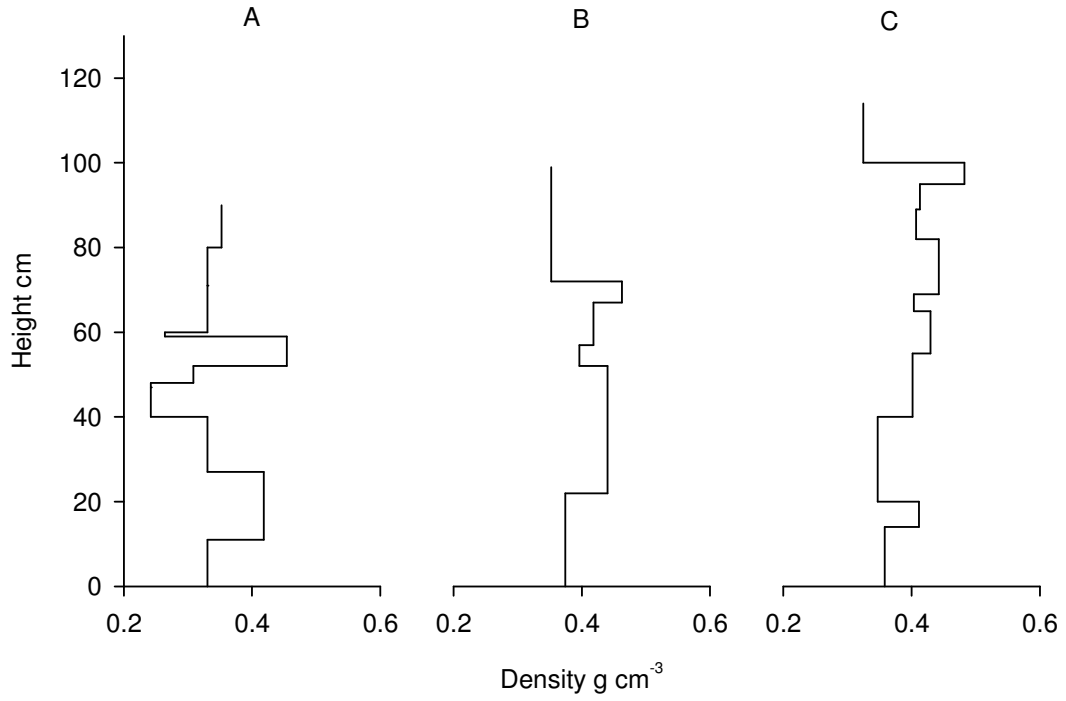

Figure 64: Density profiles along a ~3 m section in the trench excavated in spring 2006, intervals between sections are approximately 1 m; height is above the end-of-summer 2005 surface.

To investigate short scale variability further, the density profiles from the snowpits and the shallow cores for autumn 2004 are presented in Figure 65. Cores are retrieved as close as possible to the face of the snowpit that has been logged (Figure 21), typically less than 0.5 m. Figure 65 further clarifies that even over very short spatial scales, the density profiles show high variability, demonstrating that snowpack stratification is locally highly variable and that spatially-consistent ice layers are rarely present, even at length scales as short as 1 m.

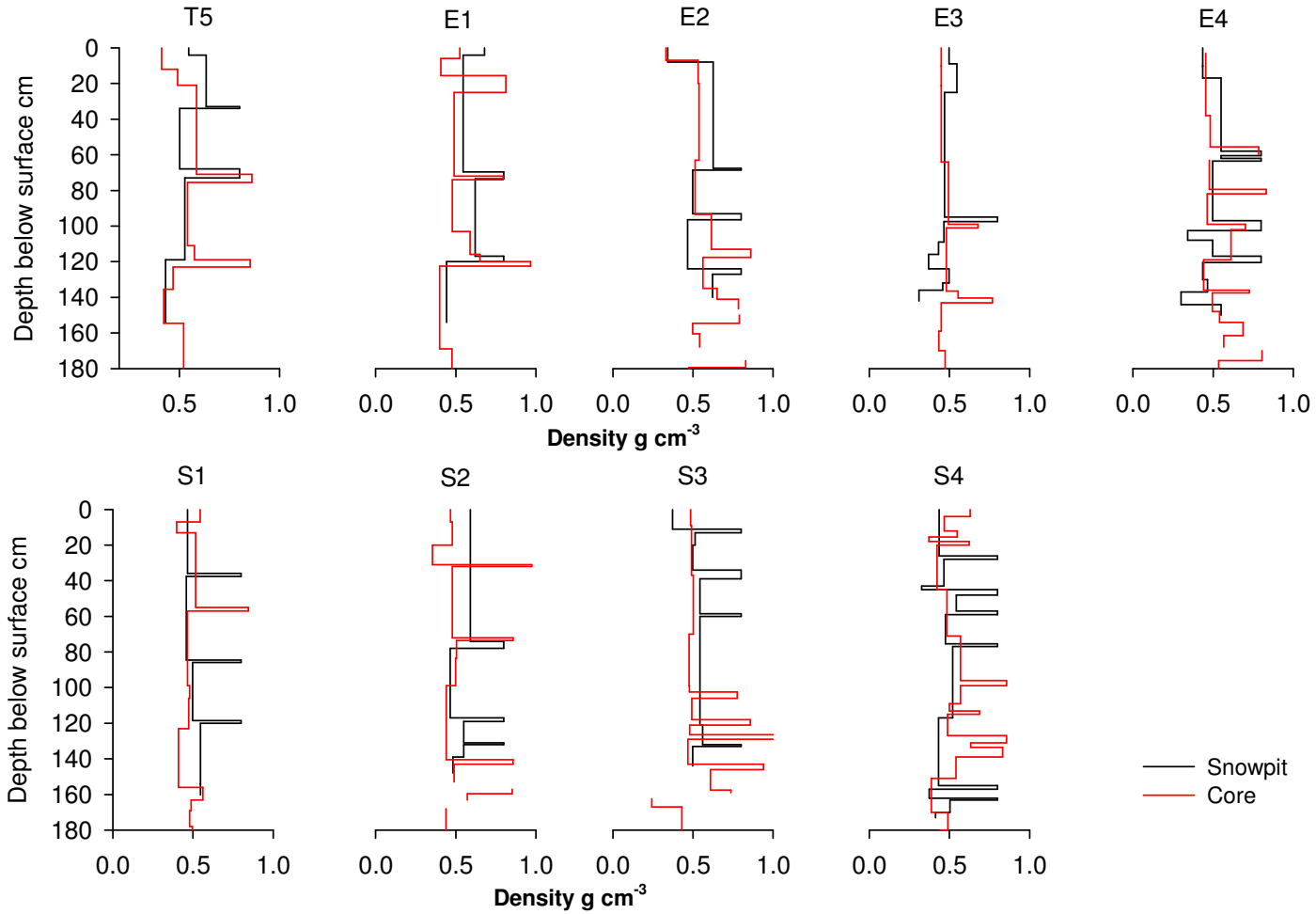

Figure 65: Density profile from snowpits and shallow cores within 1 km² of T5 in autumn 2004.

5.3.2.2 Spatial variability of stratigraphy

In an effort to further resolve the length scale variation in snowpack stratigraphy, sketches of the stratigraphic continuity are shown in Figure 67 and Figure 68 for both sides of the three 'pits' in the 7 m trench (Figure 27, Figure 57 and Figure 58). These profiles extend from the spring 2006 surface, down through the end-of-summer 2005 surface, approximately half way into the 2004 - 2005 accumulation. Sketches (Figure 67 and Figure 68) are used to record the presence of fossilized windcrusts, ice features, the hardness of the winter snowpack (measured as hard, medium or soft), and the presence of large icy crystals (autumn hoar). Figure 66 is a picture of one of the dividing walls between the 'pits' in the trench, showing the typical stratigraphy in the winter 2005 snowpack, where fossilised wind crusts, and softer, less dense layers, that are more translucent than the surrounding snowpack.

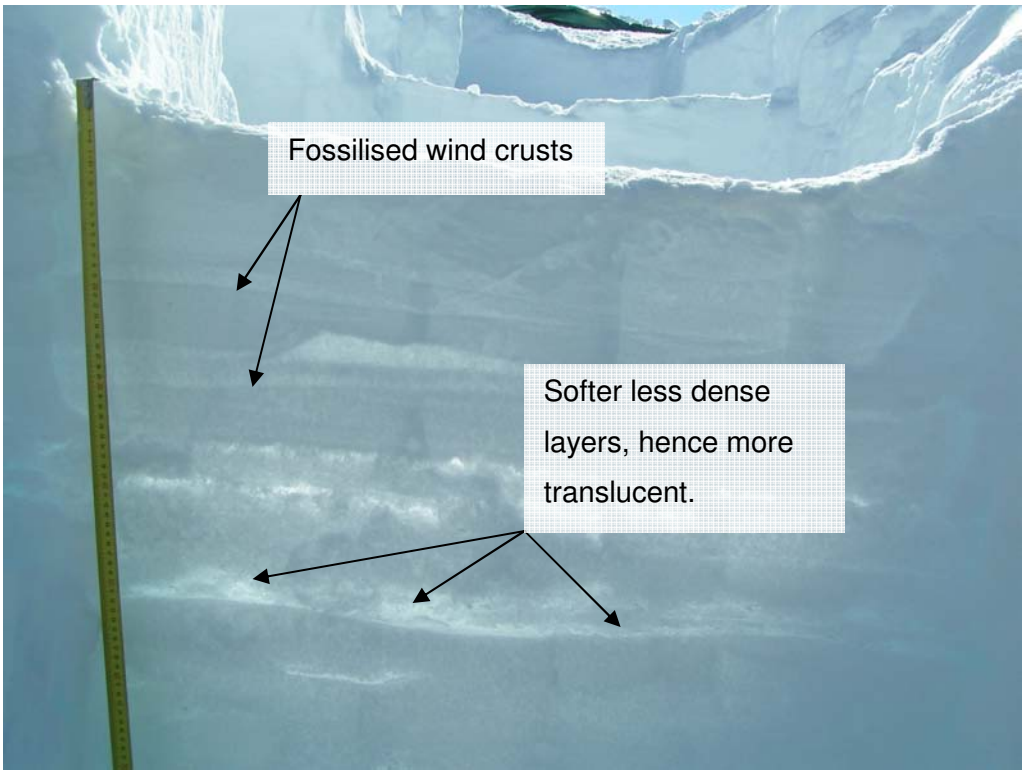

Figure 66: Dividing wall between 'pits' in 7 m trench showing typical stratigraphy.

The end-of-summer 2005 surface is apparent in both transects as the first icy layer, and for separating snow from firn. A layer of large crystals are also detailed in all sketches, above each end-of-summer 2005 icy layer, representing the autumn hoar. In the winter snowpack, windcrusts are sketched. Continuity along many of these is apparent, although their form is complex, making it hard to discernibly trace one continuously, even along a short 3 m transect. In the 2005 snowpack (below the end-of-summer 2005 icy layer), continuous features are less apparent. Ice features are present, and show signs of linear continuity, but are broken, and contain noise from other ice features, such as pipes, as seen in the bottom part of the sketch of A2 (Figure 68).

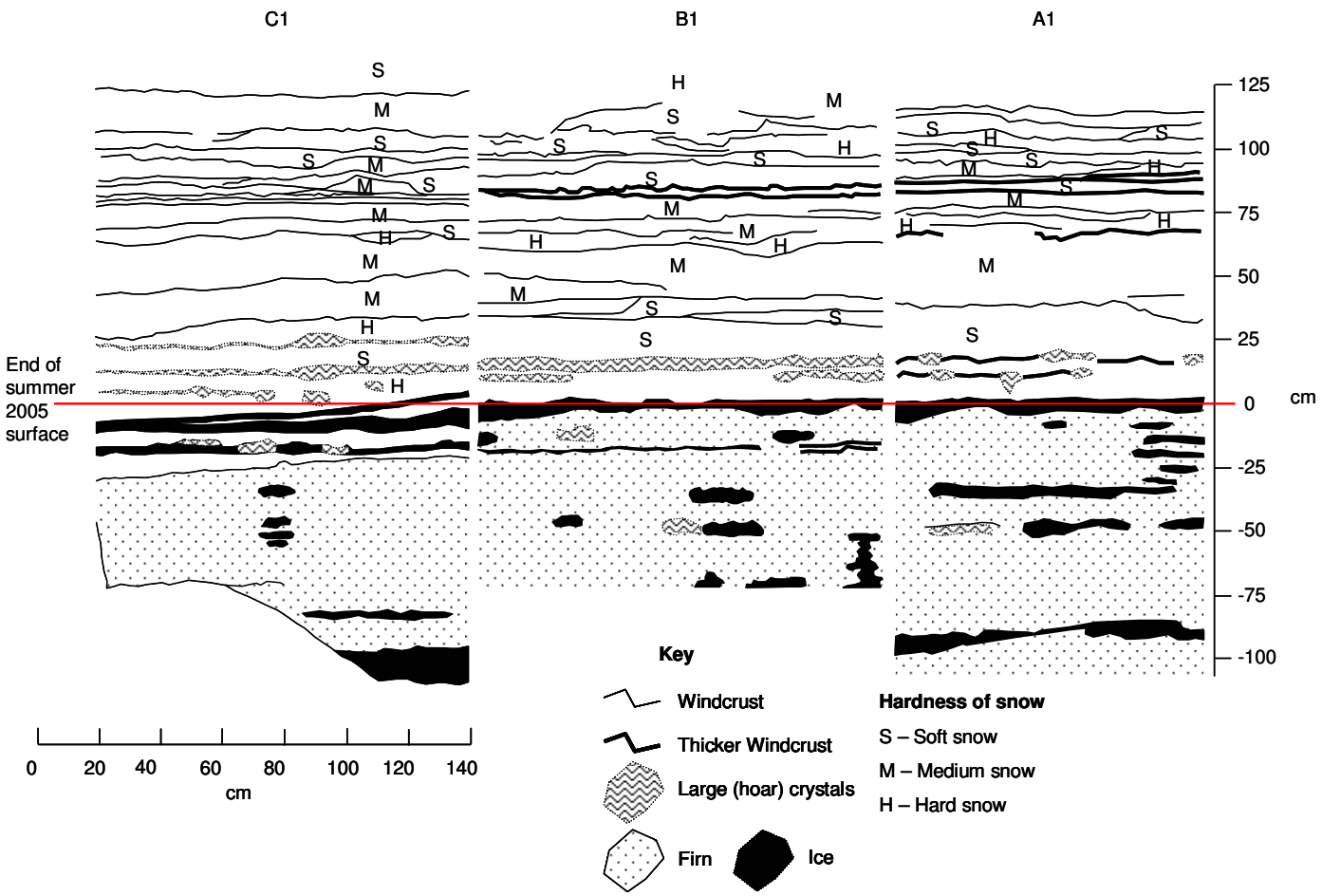

Figure 67: Sketch of the stratigraphy over a 3 m section from the side of the trench, closest to the E1 – E4 transect. The depth of the trench starts from the spring 2006 surface, extending into the 2004 - 2005 snowpack.

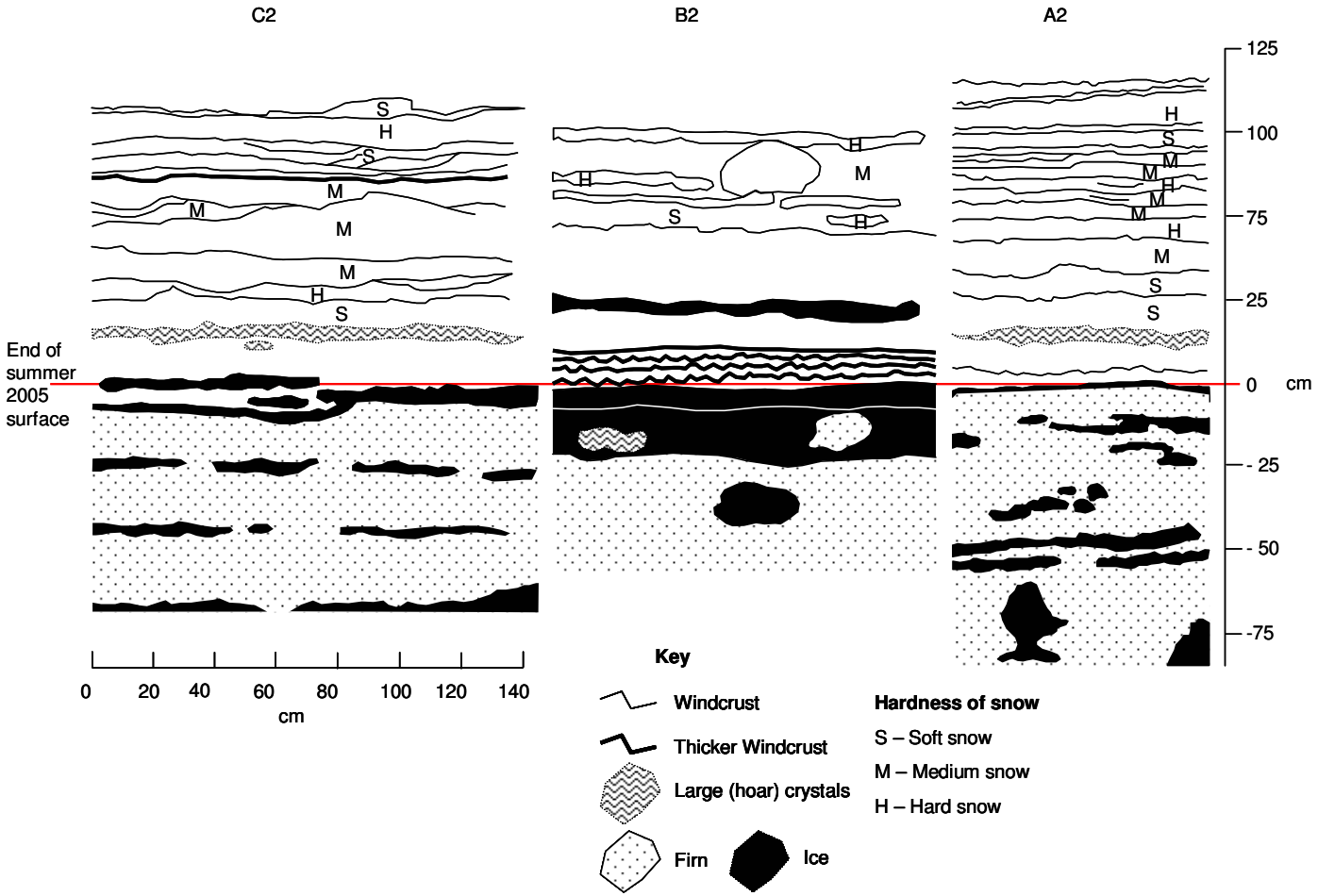

Figure 68: Sketch of detailed stratigraphy in ~3 m trench, on side furthest from EGIG line, parallel to and approximately 1 m away (opposite, in plan view) from that detailed in Figure 67

5.3.2.3 Continuity of windcrusts and ice features

Fossilised windcrusts were present in the winter 2005 snowpack along the length of the ~7m trench (Figure 27); typical examples of these can be seen in Figure 69 and Figure 70; Figure 71 shows sketches of windcrusts for 6 m of the 2005 – 2006 winter snowpack on the south east side of the trench (Figure 27). Continuous layers are detailed but it is clear that there are many breaks and irregularities along each section further confirming the observations in Figure 67 and Figure 68.

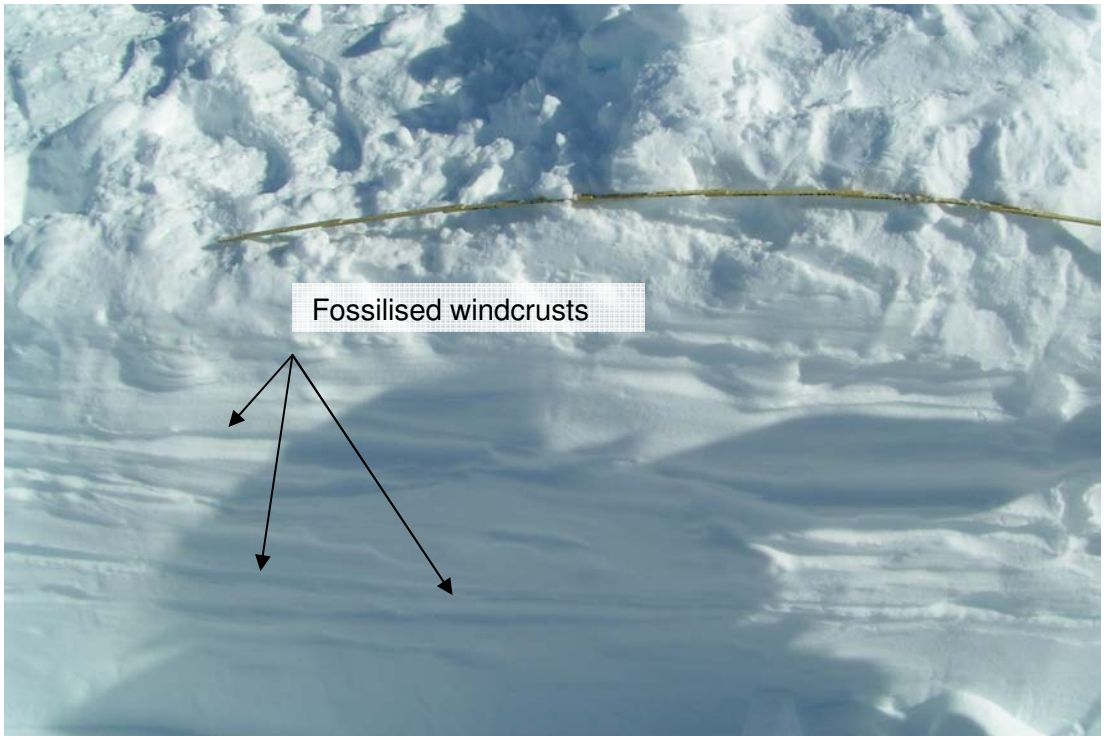

Figure 69: Fossilised windcrusts in the winter 2005 snowpack in one section of the 7 m trench.

Figure 70: The 7 m trench, the continuity of some of the fossilised windcrusts is apparent.

The avalanche probe recorded the depths of 'hard layers' which in the spring picked out fossilised windcrusts, and in the autumn ice layers, along a 100 m transect from T5 to S3, distinguishing any spatial continuity apparent in layer hardness over this length scale. In spring 2004 measurements were taken at 5 m intervals (Figure 72), and in autumn 2004 and spring 2006 at 1 m intervals. In spring 2004 there are 2 layers which appear consistently between ~80 and 100 cm depth. However in spring 2006 and autumn 2004 where measurements are made at 1 m intervals, the results are far noisier. Some layers seem roughly continuous around 30 cm and 80 cm depth in autumn 2004, and 30 cm, 60 cm and 120 cm in spring 2006. However, it is impossible, without excavation, to confirm whether these layers are indeed continuous, and if the results from spring 2006 and autumn 2004 are plotted again at 5 m resolution, by plotting every fifth measurement (Figure 73), the presence of continuous layers becomes even more questionable. Overall, the findings from the trench excavations (Figure 67 and Figure 68) and avalanche probe transects confirm the snowpit stratigraphy results indicating that ice layers/windcrusts typically exist in short (<5 m) scales in the vicinity of T5.

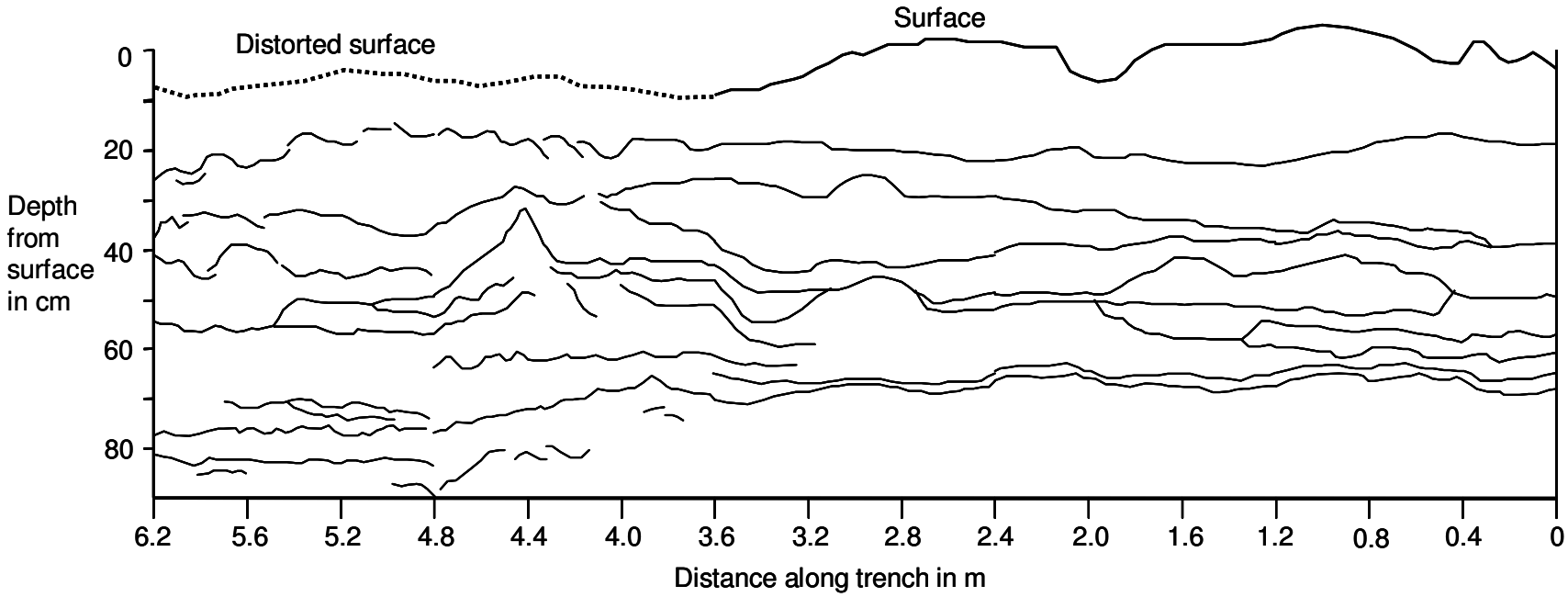

Figure 71: Sketch of windcrusts in 2004 – 2005 winter snowpack along 6.2 m. The trench is parallel to E1 to E4 transect, 0 m is closest to T5 and distances extend towards E3.

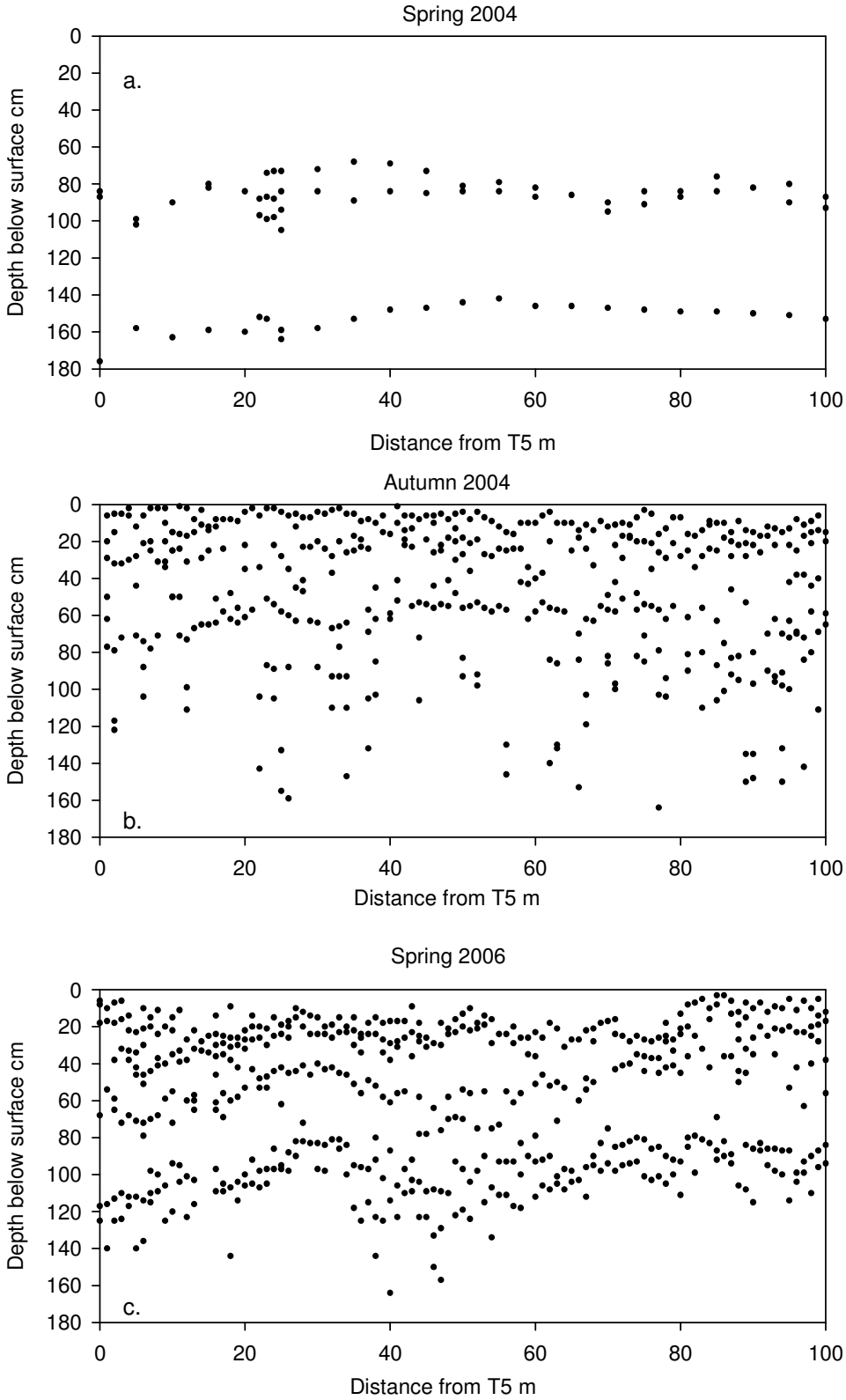

Figure 72: Avalanche probe measurements to depths of 'harder' layers along a 100 m transect from T5 to S3 in spring 2004 (a), at 5 m intervals and in autumn 2004 (b) and spring 2006(c) at 1 m intervals.

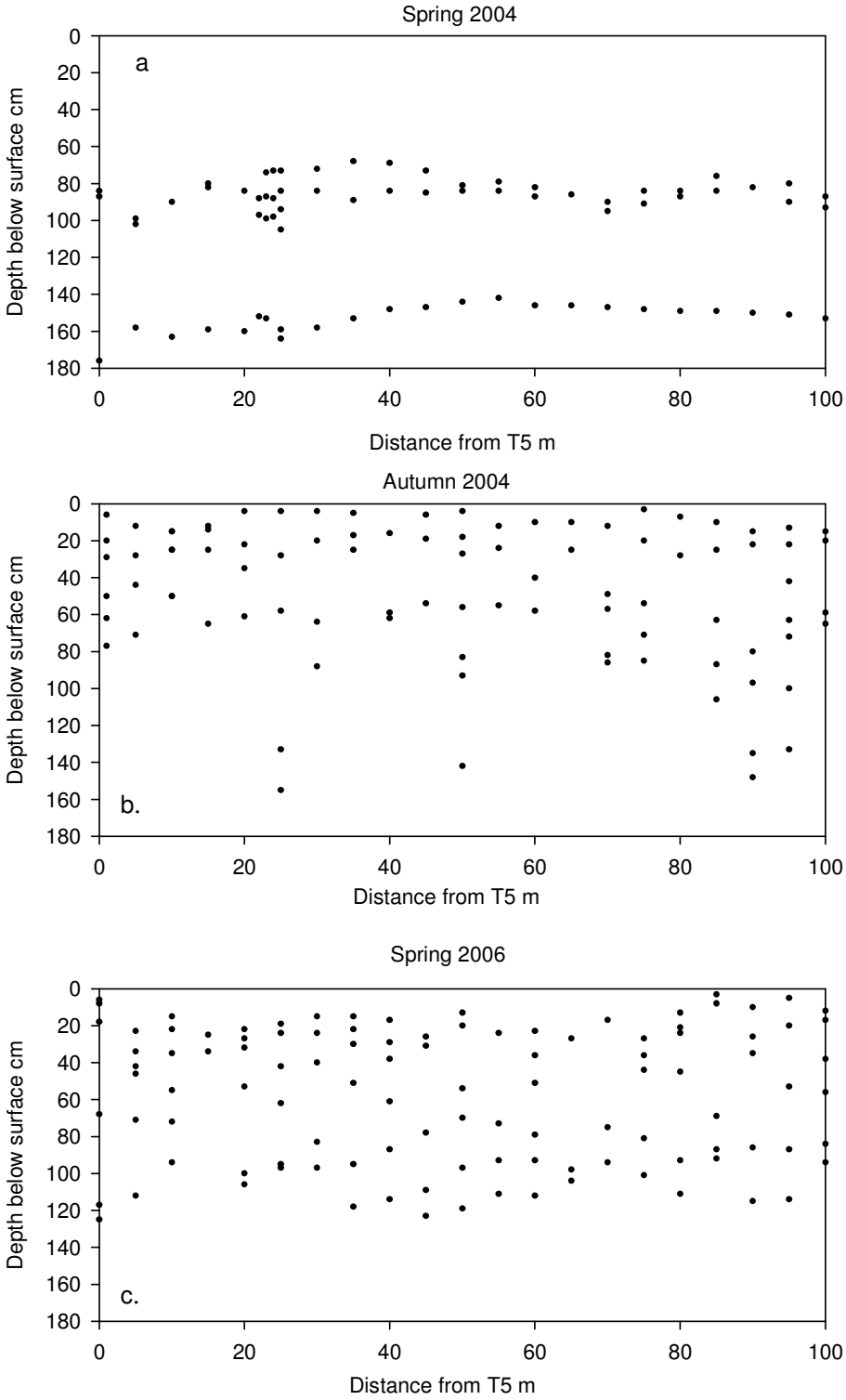

Figure 73: Avalanche probe measurements between T5 and S1 in spring 2004(a) and 2006 (c) and autumn 2004 (b) at 5 m intervals.

5.3.3 Ice formation within the annual snowpack

5.3.3.1 Percentage of snowpack that forms as ice

The occurrence of melt, percolation and refreezing ensures that a proportion of the snowpack in the percolation zone is composed of ice features. The percentage of the annual snowpack that is composed of ice will reflect the extent of summer melt and the snowpack temperature and thickness at the end of the winter (Braithwaite & others, 1994; Bøggild & others, 2005). The 17 m core retrieved from E3 in spring 2003 has been divided into years according to its stable isotope concentration (Figure 52), and the w.e. accumulation for each year calculated (Figure 54). The percentage of the annual accumulation that occurs as ice within a given year is plotted in Figure 74. This includes ice pipes and lenses, and gives an average of 7% of the accumulation as ice; the coefficient of variation is 87%, indicating very high inter-annual variability.

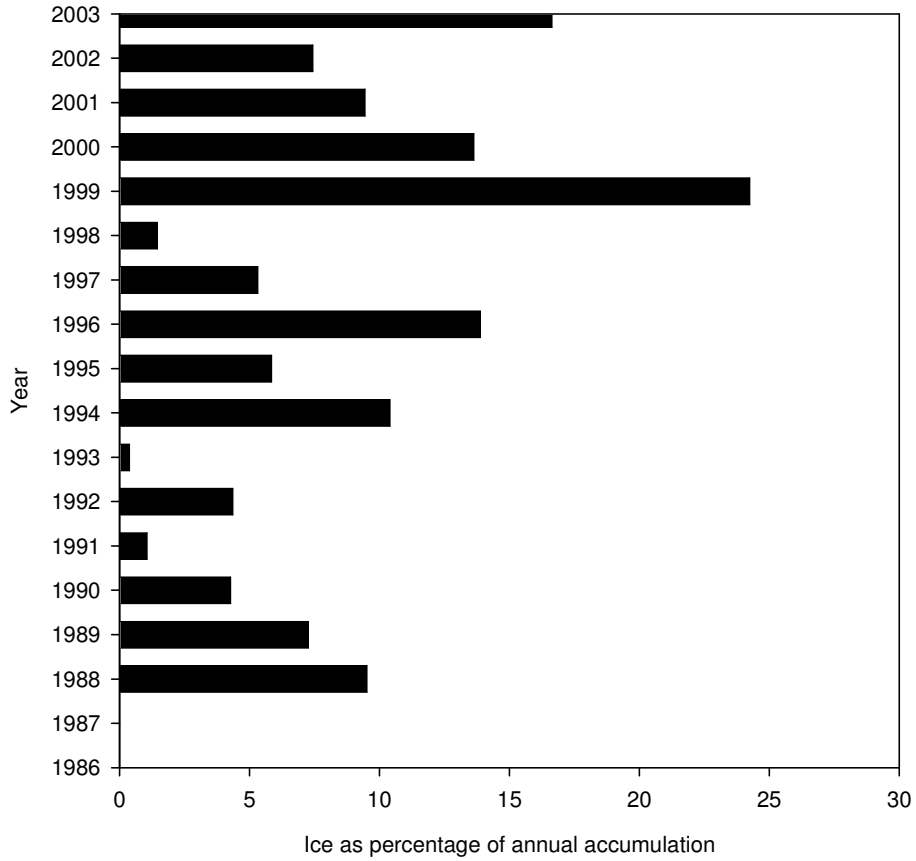

Figure 74: Ice as a percentage of the annual accumulation (w.e.) from 2003 to 1986 as determined from the 17 m core retrieved at E3.

5.3.3.2 The distribution of ice within the snowpack

The precise position of ice features within the snowpack is important because of their potential role as reflecting horizons from radar waveforms (Scott & others, 2006b). At the nine autumn snow pits excavated in the vicinity of T05 in autumn 2004, the total number of ice layers of thickness ≥1cm in each pit varies between one and six (mean = 3.1), while the combined ice thickness in each pit varies between 2.0 and 9.2 cm w.e. (mean = 6.1 cm, s.d. 2.6 cm) . This accounts for between 3.0 and 10.9% (mean = 7.5%) of the total annual accumulation. The distribution of ice layers in the autumn snowpack at the nine T05 sites does not reveal any clear depth of

preferential formation, with layers being well distributed throughout the snowpack (Figure 75).

Similar values are obtained from T06, where two ice layers totalled 6.4 cm w.e., representing 9.0% of the annual accumulation. In contrast, T04 is characterised by a substantially greater proportion of ice, yielding five ice layers (totalling 15.6 cm w.e.) which accounted for 23.9% of the annual accumulation (Figure 76).

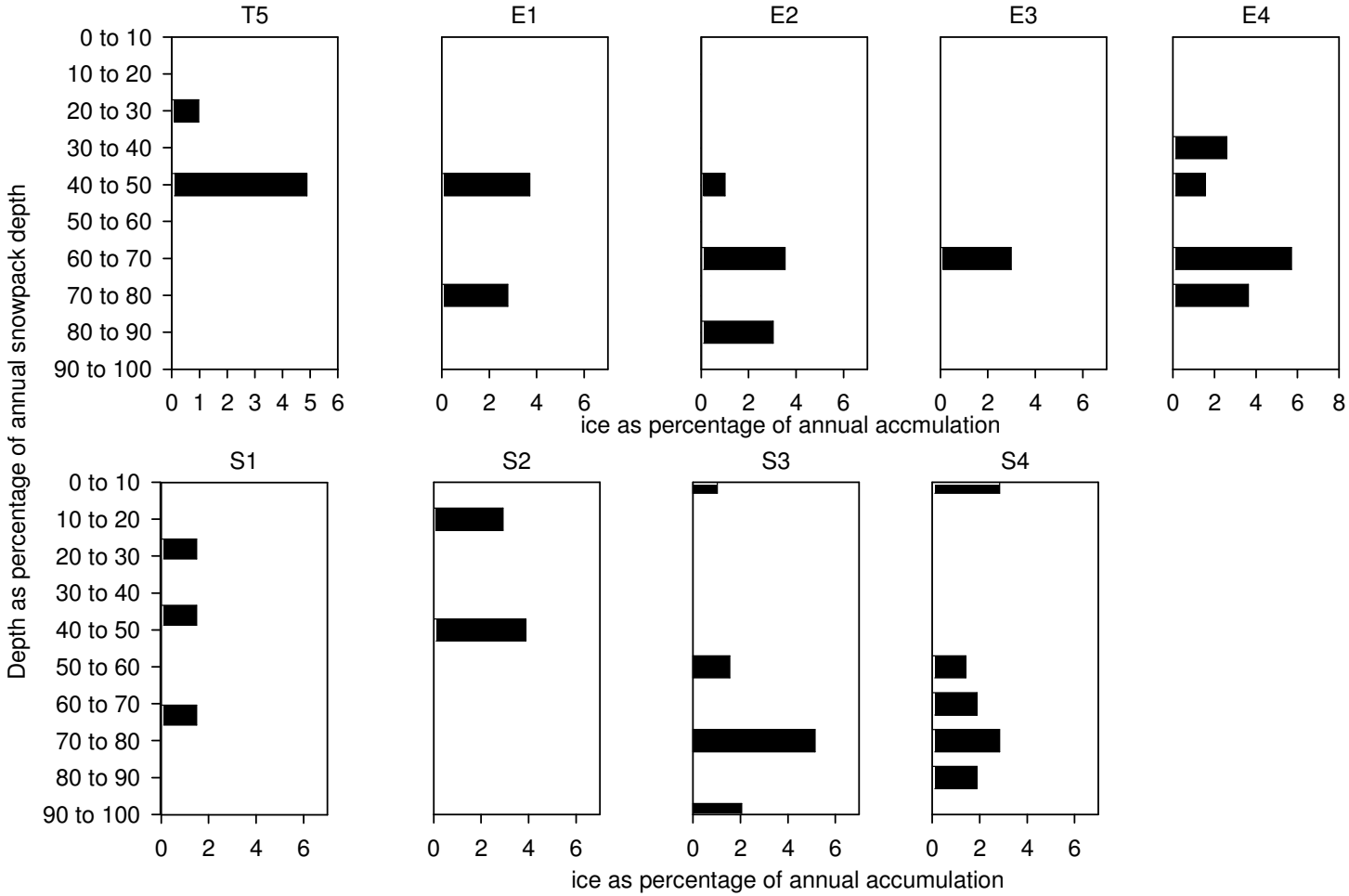

Figure 75: Location of ice layers in autumn 2004 snowpits.

The location of ice layers within the snowpack can be compared between T4, T5 and T6 in the 2003 – 2004 snowpack from the snowpits dug in autumn 2004, and also in the 2004 – 2005 snowpack from cores retrieved in spring 2006. In the 2003 – 2004 snowpack it is apparent there is more ice present at T4 (24%), than T5 (3 – 11%) and T6 (9%). At T04 and T06, ice formation is concentrated at the base of the snowpack, with 75% of the ice present in the lowermost 10% of the snowpack at T06 and 82% of the ice present in the lowermost 30% at T04 (Figure 76). However, it is clear from the variability in ice distribution at the nine T05 sites (Figure 75), that results from single pits at T04 and T06 may not be representative of those general areas. In the 2004 – 2005 snowpack, more ice is again present at T4 (18%) than T5 (7%) and T6 (8%). At T5 and T6 the ice is located in the top 30% of the snowpack whereas at T4 46% of the ice present is in the top 30%, and the remaining 54% located between 60 and 90% of the snowpack depth (Figure 77).

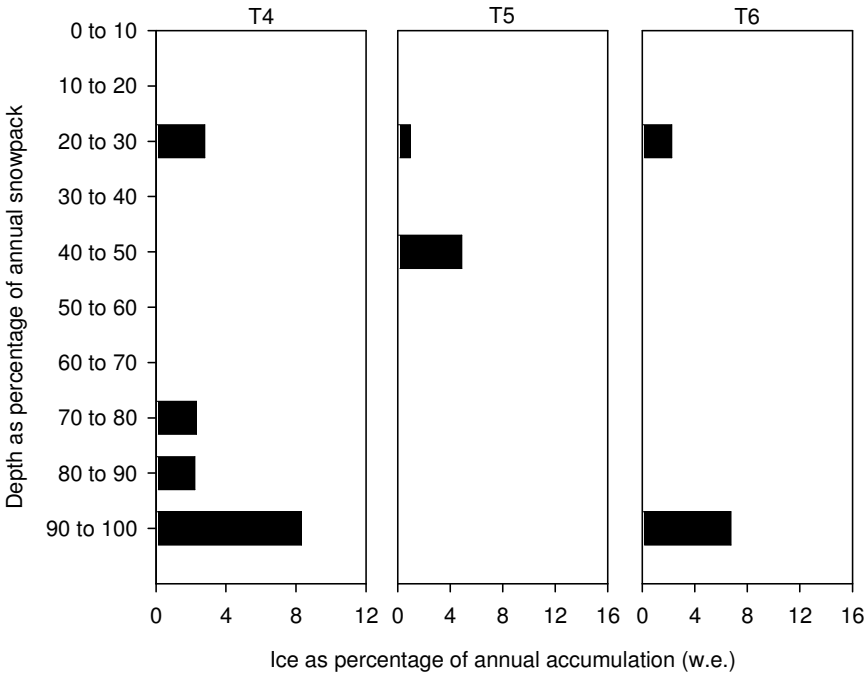

Figure 76: The location of ice layers expressed as a percentage of the 2003 - 2004 accumulation within the snowpacks at T4, T5 and T6, as derived from the snowpits.

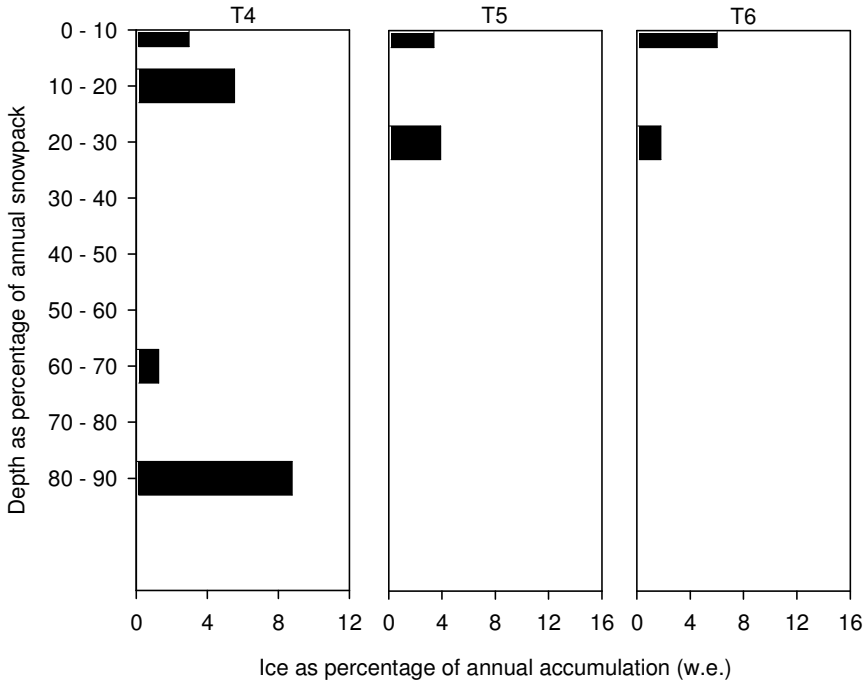

Figure 77: The location of ice layers expressed as a percentage of the 2004 - 2005 accumulation within the snowpacks at T4, T5 and T6, as derived from the shallow cores.

Thus, the available data do not suggest any obvious trend in the location of ice layer formation along the 20 km transect studied in the post melt and refreezing snowpack.

In spring 2006 shallow cores were retrieved from the end-of-summer 2005 surface at the base of the snowpit. As noted earlier, there are no accumulation records for T1 to T3 and T7 from 2004 to 2005; hence it is not possible to identify the end-of-summer 2004 layer within the cores. The depths (below the end-of-summer 2005 surface) to each ice layer within the cores have been plotted against the ice present as a percentage of the accumulation over the 2 m core (Figure 78). This gives a broad indication of the amount of ice forming at each location, and the distribution of ice within the snowpack.

With the exception of T2, all locations between T1 and T4 have considerably more ice present (mean 16%, s.d. 7) than between T5 and T7 (mean 4%, s.d. 1). However there is no statistically significant change in w.e. present as ice associated with change in elevation, even though it makes intrinsic sense that the higher percentages of ice are found in the cores obtained at the lower elevations.

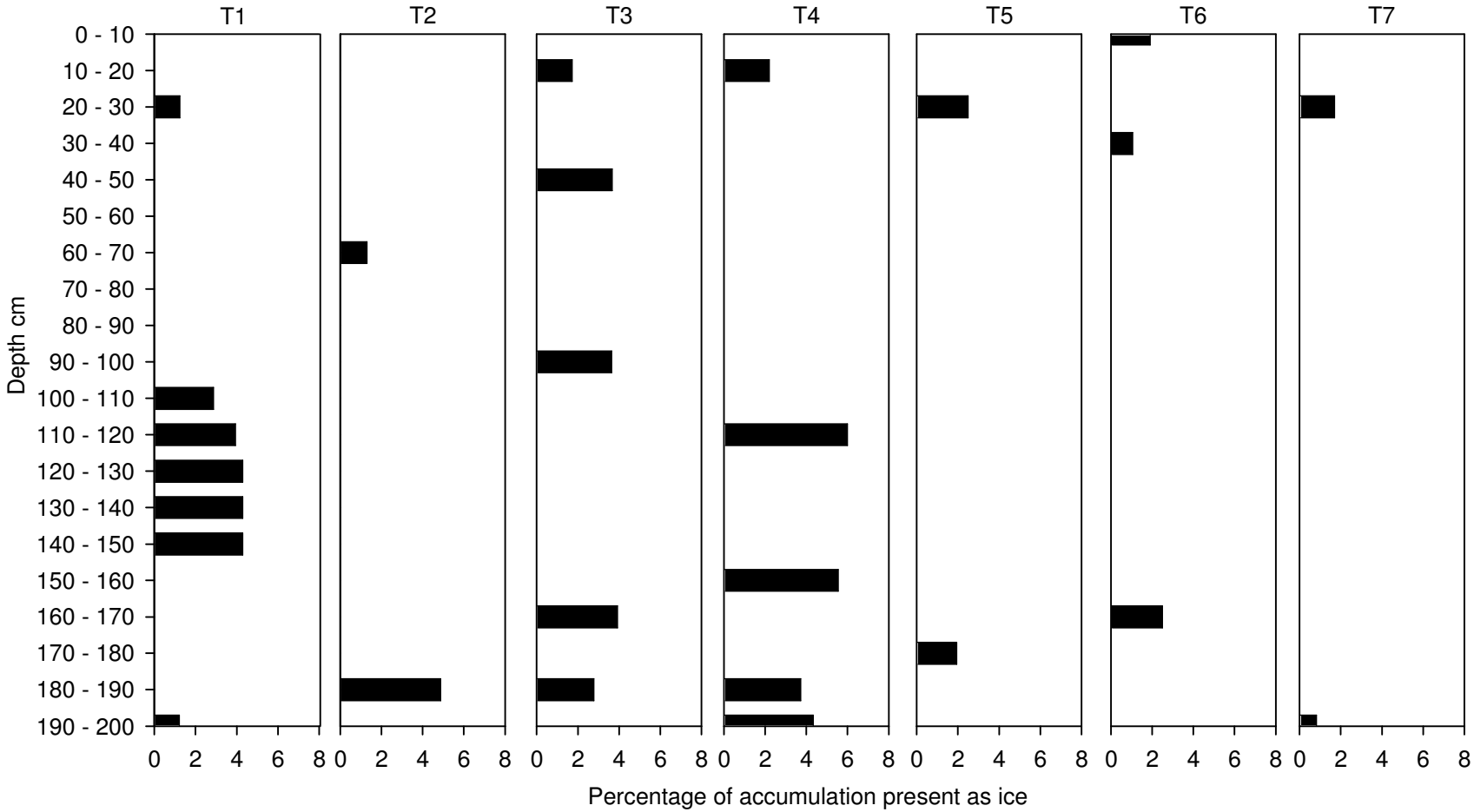

Figure 78: Location of ice layers within 2 m cores retrieved below the end-of-summer 2005 surface. Ice is as a percentage of the total accumulation over the 2 m core.

5.3.3.3 Grain size variations at ice-firn boundaries

The locations of the 34 ice layers from all nine autumn 2004 snowpits are not correlated with any particular stratigraphic boundary: 26% of layers are located on (downwards) fine-to-coarse snow grain transitions, 18% on (downwards) coarse-to-fine grain transitions, and the remaining 56% occur where there is no apparent change in grain size. However, transitions where there is no apparent change in grain size probably results from thin wind-crusts which will not be visually obvious in the metamorphosed autumn snowpack.

5.4 Discussion

Snowpack investigations in 2004 at nine sites within 1 km^2 of T05 in the percolation zone of the Greenland Ice Sheet demonstrate that, while there was a 7.6 cm (5.3%) increase in average snowpack thickness between spring and autumn (Figure 59), there was a substantial (26.2%) increase in mean snowpack density over the same period (Figure 60). These density increases result primarily from surface melting, meltwater percolation and subsequent refreezing at depth within the surface snow pack. The fact that densities increased substantially without any decrease in snow depth results from additional mass inputs as summer precipitation in the form of snow or rain. In addition, snow compaction during warmer summer temperatures also contributes to increased densities.

The consequence of the melt, percolation and refreezing processes is a complex end-of-summer snowpack containing numerous individual ice layers or lenses located at different depths (Figure 75, Figure 76, Figure 77 and Figure 78). These ice inclusions are rarely spatially continuous, even at short length scales of <1 m (Figure 67), contrasting with the findings of Pfeffer and Humphrey (1996) at the Tassersiaq ice

cap, West Greenland where the overall pattern of stratigraphy was easily traceable from one pit to another. The difference between that study and this likely reflects the complex stratigraphically-controlled snowpack permeability (Wankiewicz, 1979) at T05 resulting from the presence of sastrugi and buried wind crusts in this zone of persistent katabatics (Steffen & Box, 2001). These wind crusts, which are often observable in the snow pits as 1-2 mm thick ice layers (Figure 69, Figure 70 and Figure 71) act as hydraulic barriers to the downward percolation of meltwater. This effect is consistent with almost one in five (18%) of the ice layers measured in snowpits being associated with coarse-to-fine grain boundaries, and 56% of layers being disassociated with any visible transition, while ice layers in Pfeffer and Humphrey's (1996) study were overwhelmingly associated with (downward) fine-to-coarse grain boundaries.

Sketches of windcrusts in the spring 2006 snowpack over ~6 m show there is limited linear continuity present, although this is noisy (Figure 71) – this corresponds to findings of harder layers with the avalanche probe, where in spring and autumn 2004 and spring 2006 some linear features appear to be present in the 1 - 5 m scale (Figure 72), although, when the autumn 2004 and spring measurements are plotted at 5 m resolution the clarity of the layers diminishes (Figure 73). These features may be due to the presence of spatially continuous ice features, however continuity over this scale is not apparent in the snowpit and core density profiles (Figure 60, Figure 63, Figure 64 and Figure 65) and so the continuous 'hard' features are more likely to represent less spatially diverse changes in snowpack hardness (Pfeffer & others, 1991) .

Dunse and others (2008) found continuous internal reflecting horizons (IRHs) between T5 and E4, and T5 and S4 using ground penetrating radar at 500 and 800 MHz in spring 2004. As IRHs are often associated with ice-layer clusters, (Dunse & others, 2008) have interpreted the IRHs as icy end-of-summer surfaces. However, our results indicate the complexity of the location of icy features within the

snowpack, and associated density changes, means the interpretation of these horizons may be ambiguous.

While the ice layers identified in our study are rarely spatially continuous, their presence (and the overall increase in near surface density they create) will result in very different radar echo returns between spring and autumn with a resultant affect on radar 'estimates' of elevation (Jezek & others, 1994; Scott & others, 2006a). This impact will have a seasonal pattern because the end-of-summer layers are progressively buried during the winter by the lower density winter snowpack. Work is currently ongoing to determine precisely how these seasonal changes will influence elevation estimates derived from radar altimeters. The considerable change in snowpack density between seasons (Figure 60 and Figure 61) also ensures that, even if surface elevation changes only slightly (Figure 59), the actual mass change may be considerable (Figure 62). Thus, in areas such as the percolation zone, where the snowpack shows substantial seasonal changes in density, mass balance estimates cannot be simply based on measured changes in surface elevation. Figure 74 demonstrates that the percentage of accumulation stored as ice each year, as a result of melt and refreezing, can vary greatly, with a coefficient of variation of 87% (varying between 0% in 1986 and 1987 to 24% in 1999); thus the seasonal densification of the snowpack due to the inclusion of ice features can vary greatly further complicating estimates of mass balance based purely on changes in elevation.

While these results suggest the regular presence of ice layers in the autumn snowpack they do not replicate those of Pfeffer and Humphrey (1998) who found an increase in the incidence of internal ice layers at colder sites located higher in the percolation zone. Instead, the results presented tentatively suggest a decrease in ice volume as you move higher in the percolation zone from T1 to T7 (Figure 78). However, a more extensive transect covering a greater altitudinal range is required to clarify the distribution and concentration of ice layers more effectively.

The inter-annual variability in accumulation needs to be quantified and accounted for, if potential changes in mass balance as a consequence of climatic change are to be correctly interpreted. At T5, the average annual accumulation between end-of-summer 2003 and end-of-summer 2004 was 79.6 cm w.e., with 31.6% of this volume accumulated in summer 2004. This mean accumulation is 22-115% higher than measurements in the vicinity of T05 from 27 of the years between 1950 and 1988 and 52% higher than the mean accumulation rate of 52.2 cm w.e. during these 27 years (Figure 79) (Benson, 1962; Stober, 1986; Seckel, 1977; Anklin & othes, 1994). When these results are combined with the accumulation records derived from the 17 m core (Figure 54), the average annual accumulation is 53 cm w.e., with a coefficient of variation of 20% (Figure 79).

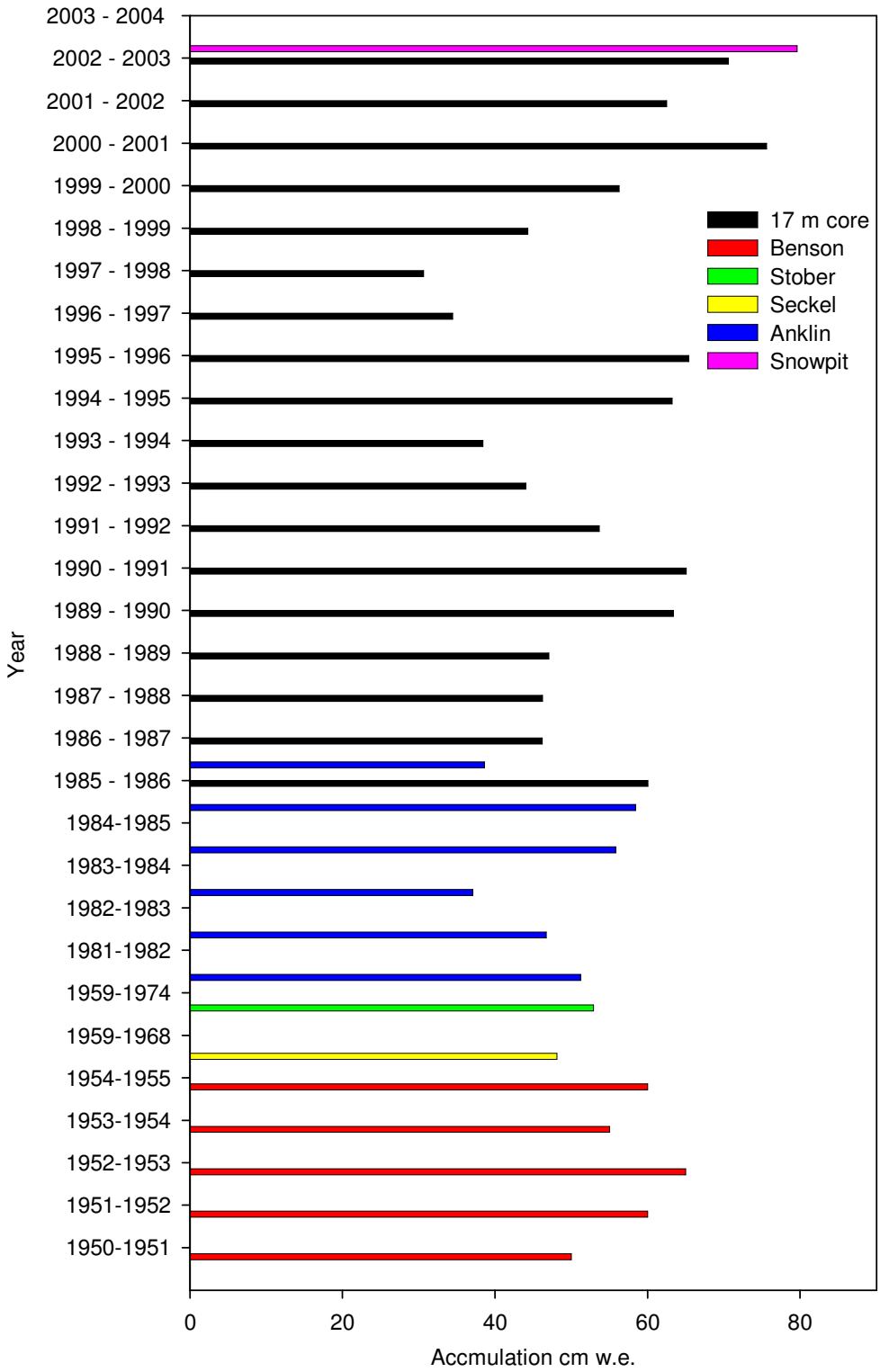

Figure 79: Previous accumulation rates (cm w.e.) measured at T5: annual 1950-55 (Benson, 1962); average 1959-74(Stober, 1986); average 1959-68 (Seckel, 1977); annual 1982-88 (Anklin, 1994) 1985-1003 derived from the 17 m core and 2003-2004 from autumn snowpit measurements.

More recently, automated snow depth measurements have been made within 3 km of T06 at Crawford Point (69° 52′ 47″ N 49° 59′ 12″ W, Figure 2), a Greenland Climate network (GC-Net) Automatic Weather Station (AWS), at an elevation of 2022 m (Steffen & others, 1996; Steffen & Box, 2001). These data reveal that average annual accumulated snow/firn depth in eight of the years between 1995 and 2004 is 1.08 m and that the inter-annual variability in this rate is high (Figure 80), characterised by a coefficient of variation of 38%. The annual (2003-2004) accumulated snow depth of 1.41 m measured at T06 in the present study is considerably higher than the 1.08 m accumulation over the same time period at Crawford Point. Thus, both the high inter-annual variability in accumulation measured at Crawford Point, in the 17 m core, and from previous measurements and the spatial difference in accumulation between Crawford Point and T06 in 2003-2004 emphasises that any single annual measurement of accumulation is inadequate for investigating rates of long-term change on the basis of comparisons with data from earlier years. Additional measurements of snow accumulation in the vicinity of T05 in 2004 using airborne radar and laser altimetry indicate that snow depth distribution is bi-modal with accumulation on low gradient plateaus (such as T05) averaging 0.2 m deeper than on more steeply-sloping terrain (Helm & others, 2007). Thus, a longer time series as obtained from the 17 m core (Figure 52) is essential to obtain data that can effectively characterise inter-annual variability in accumulation rates.

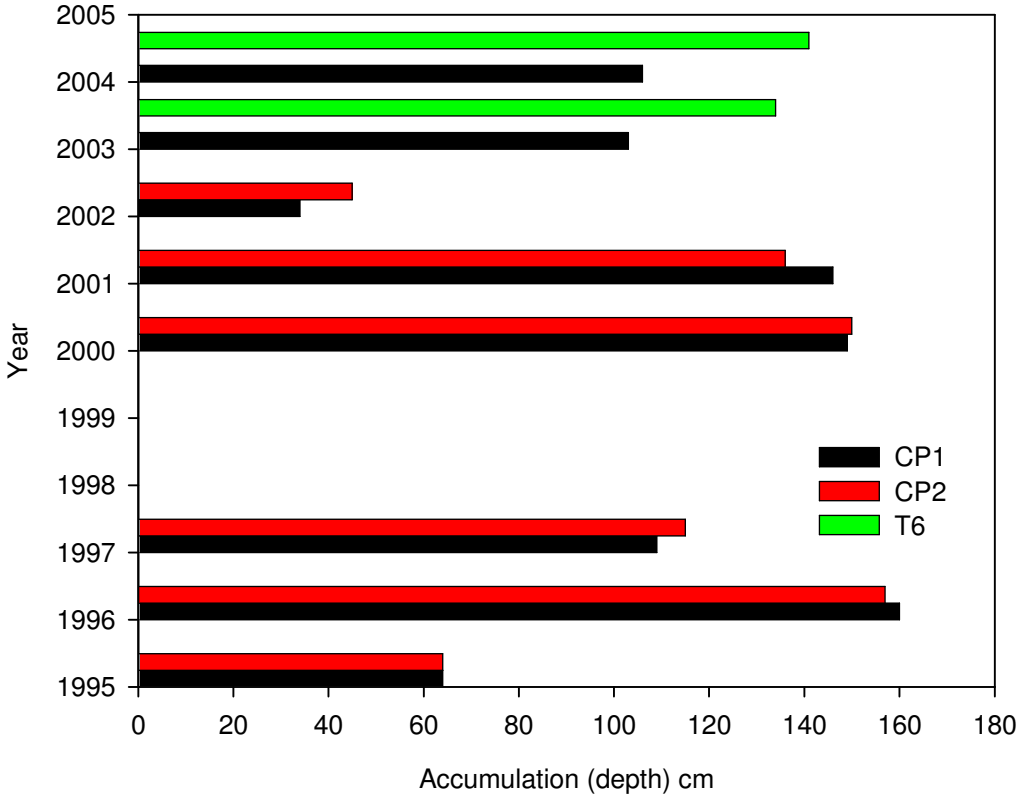

Figure 80: Annual snow height measurements made from Crawford Point AWS, compared to our measurement at T6.

5.5 Conclusions

The conclusions are drawn from measurements of snowpack structure, made before and after summer melting in 2004, with additional measurements made in spring 2006, carried out in the percolation zone of the Greenland Ice Sheet. These were made along two 1 km-long transects from T05.

Results show that a small increase in snowpack depth of 5.3% was observed between spring and autumn 2004 within the percolation zone. However, mean snowpack densities increased significantly, by 26.2%, and included the creation of

numerous ice layers (Figure 76). Densification results from several processes, including: warming of the snowpack before the onset of melt; additional summer mass inputs in the form of solid and liquid precipitation; surface melting; meltwater percolation; subsequent refreezing at depth within the snowpack, and snow compaction during warmer summer temperatures.

The considerable change in snowpack density between seasons (Figure 60) indicates that significant changes in mass can occur in this zone with only very limited changes in surface elevation. For example, at T05 the 4.5% increase in snow depth reflected a 31.6% increase in net accumulation. Thus, in areas such as the percolation zone, where the snowpack shows substantial seasonal changes in density, mass balance estimates should not be based solely on observed changes in surface elevation.

Density/depth profiles from nine sites within 1 km^2 around T05 reveal that the snowpack in this region has a highly variable density stratigraphy, and that this stratigraphy changes over short temporal and spatial scales.

Ice layers are rarely spatially continuous at length scales >~1 m (e.g. Figure 63 and Figure 67) and this complexity may be partly responsible for prohibiting clear identification of annual layers in deeper core and n-probe derived depth-density profiles. Ice layers and lenses formed within the near-surface snow pack contribute markedly to the overall increase in near surface density and these will result in very different radar echo returns between spring and autumn. Unless this seasonal affect is accounted for it may contribute to ambiguous radar measurements of surface elevation (Jezek & others, 1994; Scott & others, 2006a).

The percentage of the annual accumulation that is accounted for by ice layers varies between 1 and 25% annually between 1986 and 2003, as measured in the 17 m core retrieved at E3 in spring 2004 (Figure 74). This variability in snowpack melt and

refreezing, combined with high inter-annual variability in accumulation (Benson, 1962; Seckel, 1977; Stober, 1986; Anklin, & others, 1994) all ensure that there are significant complications in using elevation change as an accurate indication of change in mass balance.

The depth of discontinuous ice layers in the autumn snowpack shows no systematic relationship with boundaries defined by grain-size change, as described by Pfeffer and Humphrey (1996). Instead, the precise depths of ice inclusions in this area of the Greenland Ice Sheet may often be controlled by the formation and burial of sastrugi and wind crusts that are prevalent within the spring snowpack in this region. Also, there were no discernible increases in internal ice layers at higher colder sites in the percolation zone, as reported by Pfeffer and Humphrey (1998).

Chapter 6 – Snowpack and firn densification gradients at long (>10 km) length scales in the percolation zone of the Greenland Ice Sheet

6.1 Introduction

Densification of the snowpack associated with seasonality in spring and autumn 2004 across a 1 km^2 area, was presented in Chapter 5. These results revealed a clear densification in the snowpack between the pre melt, spring and post melt, autumn snowpack. Whilst the changes observed are significant with reference to mass balance investigations from estimates of ice-sheet elevation from satellite radar platforms, the data were only representative of short (1 m – 1 km) length scales. In this Chapter, results are presented from a longer transect across the percolation zone in order to investigate densification processes at length scales >10 km. More specifically, in spring 2006, density measurements were made at seven sites along a 57 km transect of the EGIG line spanning an elevation range of 1680 m to 2050 m. By looking at the average density in both the winter 2005 – 2006 snowpack, and the 2004 – 2005 snowpack that has undergone a summer melt and refreezing cycle, it is possible to investigate spatial changes in pre and post melt snowpack densities. These could be compared to post melt snowpack densities in the 2002 – 2003 and 2003 – 2004 snowpack, as measured at T4 and T6 (Figure **15**), in spring and autumn 2004.

It is important to quantify the change in snowpack density associated with seasonality and in particular to determine the densification gradients associated with changes in elevation (and thus temperature). Results presented in Chapter 5 reveal the substantial variability in post melt snowpit densities observed at nine sites within 1 km^2 of T5 in 2004 (between 0.47 and 0.57 g cm^{-3}); no obvious spatial patterns are apparent at this resolution. At longer length scales snowpack densities

are known to decrease with increasing elevation with progression from the ELA to the dry snow zone in the interior (Benson, 1962). Identifying the relationship between the change in density and elevation (and thus temperature) could make it possible to interpolate seasonal densification values between elevations across the whole of the percolation zone. If this could be tied to temperature or a surrogate indicator, such as positive degree days (PDDs), there is potential to use measurements from AWS to calibrate mass balances as derived from elevation changes measured by satellite radar altimetry.

The importance of understanding rates of firn densification to enable accurate estimates of mass balance measurements derived from satellite platforms using surface elevation changes is increasingly being recognised (Arthern and Wingham, 1998; Reeh & others, 2005; Zwally & others, 2005; Thomas & others, 2008). As a result firn densification models, that include parameterisation of melt and refreezing processes are now being developed (Li & others, 2007). However, it is essential that these models are calibrated using field measurements to reduce model error. With surface temperatures across the Greenland Ice Sheet increasing and forecast to continue to do so (Christensen & others, 2007), it is also important to develop an understanding of how these changes in density may change with global warming.

6.2 Methods

6.2.1 Density measurements from T1 to T7

Density measurements were collected at sites T1 to T7 (Figure **15**) in spring 2006, spanning 57 km across the percolation zone, over an elevation range of 370 m (1680m to 2050 m). Snowpits were dug to the end-of-summer 2005 surface (Figure

81) and logged, as detailed in Chapter 3. Shallow firn cores of ~2 m were retrieved from the bottom of the snowpit (Figure 81) extending into the firn below the end of summer 2005 surface. The average winter pre-melt (2005-2006) snowpack density is derived from the snowpit data (referred to as '2006 pit' data), and post melt densities for the one year old firn from the 2004-2005 accumulation at each site for the end-of-summer 2005 snowpack are derived from the firn cores (Figure 81) retrieved from the bottom of each snowpit (referred to as '2005' data).

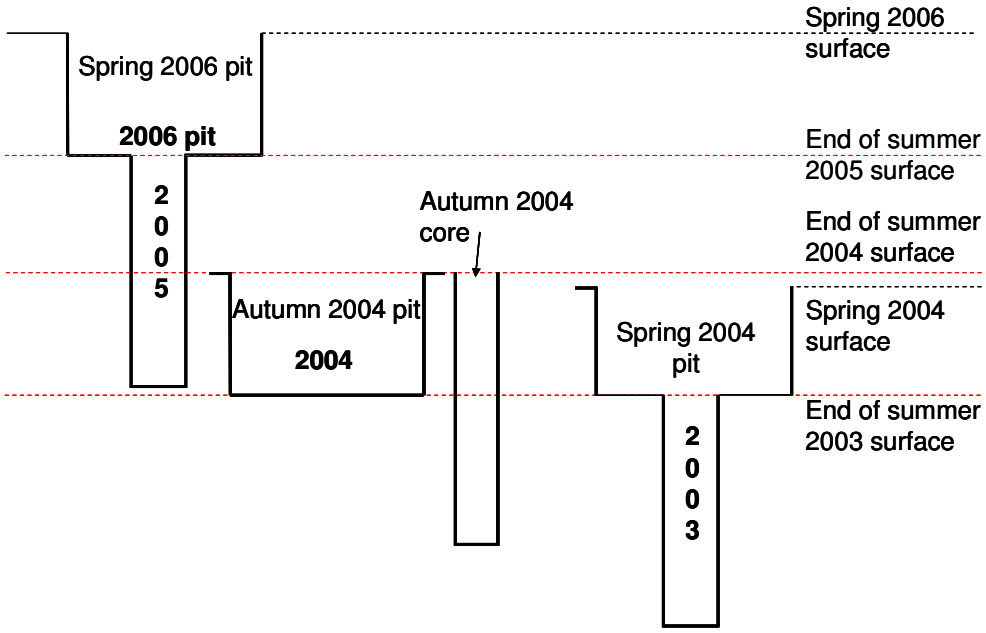

Figure 81: Diagram showing the location of where measurements for 2003, 2004 and 2005 accumulations were retrieved from.

In the absence of accumulation records for 2004 to 2005 at sites T1 to T3 and T7, it is not possible to identify exactly the end-of-summer 2004 surface layer in the shallow cores retrieved. The core lengths of ~2 m would almost certainly exceed one year's accumulation, based on previous measurements (Benson, 1962; Seckel, 1977; Stober, 1986; Anklin & others, 1994). Consequently, it is not possible to precisely isolate the 2004 – 2005 accumulation that has been affected by one summer's melt and refreezing. The average density for the full length of the (~2 m) core has therefore been used since the 'average' values are not found to vary significantly with depth down core (Table 11), indicating the length of core chosen is arbitrary.

6.2.2 Density measurements from T4, T5 and T6 in 2003, 2004 and 2005

Due to the emplacement of accumulation stakes at T4, T5 and T6 in spring 2004 it is possible to identify the end-of-summer 2005 surface in cores retrieved in spring 2006. Using the isotope record from the 17 m core (retrieved from E3), it is possible to estimate the depth to the end-of-summer 2002 surface. The end-of-summer 2003 surface is located in the snowpits dug in spring 2004. Figure 81 summarises where each set of results has been taken from, in relation to each other. Full details on the retrieval of each set of data are given in the following sections.

2003 data

Cores retrieved in spring 2004, from the bottom of the snowpits (the end-of-summer 2003 surface) are used to find the average density for the one year old firn from the 2002 – 2003 accumulation year (referred to as '2003') data. In order to initially identify an approximate depth for the end-of-summer 2002 layer in the cores, the accumulation from end-of-summer 2002 to end-of-summer 2003 is derived from the isotope record in the long core retrieved at E3 in spring 2004 (Figure 52). This depth (1.42 m) provides an indication of the end-of-summer 2002 to end-of-summer 2003 snowpack depth at T4, T5 and T6. The stratigraphic descriptions from the shallow cores are then used to identify the end-of-summer 2002 surface by looking in detail at the stratigraphy in the core around 1.42 m depth. For example at T6 there is a layer of 'coarse firn' overlaying a layer of 'firm firn' between 124 to 134.8 cm depth – although this is slightly shallower than indicated by the isotope record, the description indicates that this layer of 'coarse firn' is the autumn 2002 hoar overlying the 'firm firn' end-of-summer 2002 surface. Where descriptions of stratigraphy do not clearly identify the autumn hoar, the closest stratigraphic layer to 142.5 cm depth is used. For example, at T4, there is a layer of firn from 129 to 142.5 cm depth; – in this case the end-of-summer 2002 surface is placed at 142.5 cm

depth. This method, whilst slightly subjective, does enable the identification of the end-of-summer 2002 surface in the cores retrieved in spring 2004 at T4, T5 and T6. These can then be used to provide average densities for the 2002 – 2003 accumulation and is referred to as '2003'.

2004 data

The end-of-summer 2003 surface was located in the snowpack at T4, T5 and T6 in snowpits dug in spring 2004 (Figure 81), and the total accumulation found from snowpit depth and density measurements made in autumn 2004. Therefore the snowpits dug in autumn 2004 at T4, T5 and T6 give the average density for 2003 – 2004 post melt and refreezing accumulation, and will be referred to as '2004'

2005 data

It is possible to identify the annual accumulation at T4, T5 and T6 for 2004 – 2005. Accumulation stakes were emplaced at T4, T6 and all nine sites within 1 km^2 of T5 in spring 2004, and measurements from the surface to the top of the exposed pole were taken at the start and end of spring 2004, autumn 2004 and spring 2006 field seasons. In spring 2006 the depth from the surface to the end-of-summer 2005 layer was found from the snowpits, which combined with the accumulation stake measurements was used to find the depth of the 2004 – 2005 accumulation. The depth of accumulation at each of these sites was then used with the cores retrieved in spring 2006, from the end-of-summer 2003 surface (Figure 81), to prescribe the appropriate firn core length representing the 2004-2005 accumulation. Stratigraphy was also used to confirm the end-of-summer 2004 surface layer. For example, the end-of-summer 2004 layer could in places be recognised where large

unconsolidated crystals overlay an icy layer depicting the autumn hoar on top of the previous year's summer surface; this was especially obvious at T6. Thus, the cores retrieved in spring 2006 provide the average post melt density over 2 m for T1, T2, T3 and T7; this would include the 2004 – 2005 accumulation and extend part way into 2003 – 2004 accumulation. These shall be referred to as '2005' results.

6.3 Results

6.3.1 Densities along the T1 to T7 transect

The average '2006 pit' snowpack density across the transect is 0.40 g cm^{-3}, s.d. 0.018. This is consistent with the average snowpack density from nine sites within 1 km^2 of T5 in spring 2004, of 0.42 g cm^{-3}, s.d. 0.02 (Figure **16**). The mean '2005' firn density from cores retrieved at all seven locations is 0.55 g cm^{-3}, s.d. 0.06.

The average density at each location was found by dividing the total accumulation w.e. by the total depth. In the '2006 pit' data, this was the pit depth, and in '2005' one year old firn data, this was the depth to the bottom of the nearest stratigraphic layer, closest to a depth of 2 m. In order to demonstrate the relative invariance in mean snow density with depth in shallow cores, Table 11 shows the cumulative snowpack density with depth through the core. For each stratigraphic layer within each core/pit, the average density to that layer was calculated by dividing the total accumulation w.e. at that depth by the depth. For example, Table 11 shows the depth to each core section (top and bottom) at T6 in spring 2004, the density as measured in the field and the cumulative accumulation w.e.

Depth to stratigraphic layer (cm)		Density of Stratigraphic layer	Cumulative accumulation	Cumulative average density
Top	Bottom	g cm^{-3}	cm w.e.	g cm^{-3}
0	12.5	0.15	1.85	0.15
12.5	16	0.86	4.87	0.30
16	35	0.45	13.42	0.38
35	53.5	0.40	20.75	0.39
53.5	76	0.44	30.73	0.40
76	89.5	0.14	32.68	0.37
89.5	91.5	0.90	34.48	0.38
76	89.5	0.48	41.01	0.46
89.5	103	0.42	46.70	0.45
103	115.5	0.42	51.98	0.45
115.5	124	0.38	55.18	0.44
124	134.8	0.55	61.15	0.45
134.8	140	0.55	64.02	0.46
140	142	0.55	65.13	0.46
142	152	0.55	70.66	0.46
152	164.5	0.48	76.64	0.47
164.5	182.5	0.46	84.90	0.47
182.5	206.5	0.46	95.91	0.46
206.5	218.5	0.32	99.75	0.46
218.5	221	0.86	101.91	0.46
221	239.5	0.32	107.83	0.45

Table 11: Table showing the depth to the top and bottom of each stratigraphic section retrieved at T6 in spring 2004, the density of each stratigraphic layer, the accumulation as a w.e., and the cumulative average density accumulation (g cm^{-3}).

Using the average densities for each stratigraphic layer in the cores and pits, the '2006 pit' and '2005' core data have been compared using the 't-test' (Table 12). At all sites, the core and snowpack densities are found to be significantly different to one another. These difference in average densities are also very clearly demonstrated by a frequency distribution of '2006 pit' and '2005' densities at T1 (Figure 82).

	Average densities				
	Pit	Core	T	DF	P
T1	0.41	0.57	28.12	20	0.01
T2	0.41	0.56	31.58	20	0.01
T3	0.38	0.59	104.62	29	0.01
T4	0.42	0.59	46.88	26	0.01
T5	0.42	0.54	53.72	43	0.01
T6	0.38	0.46	24.93	25	0.01
T7	0.41	0.47	11.09	25	0.01

Table 12: Table showing the average snowpack densities for '2006 pit', and '2005' at sites T1 to T7, t value, degrees of freedom ($(n_1+n_2)-2$) and significance.

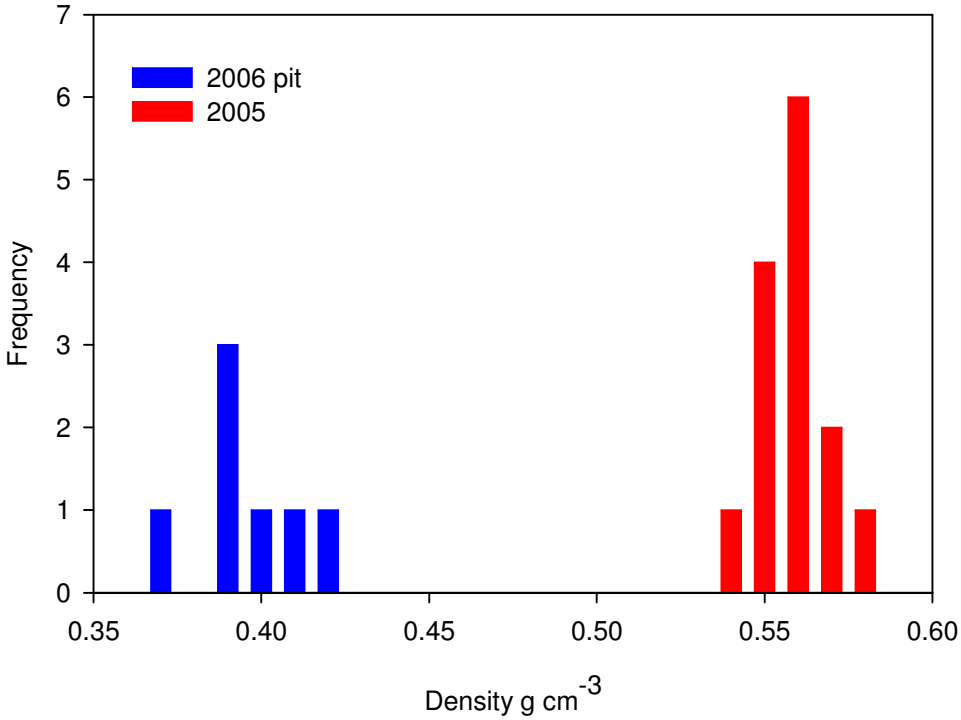

Figure 82: The frequency of average densities for each stratigraphically distinct layer at T1 in '2006 pit' (prior to melt) and '2005' (post melt) data.

When the densities are plotted against the elevation (Figure 83), there is a significant negative trend in the 2005 core densities whereby density decreases by 0.032 g cm^{-3} per 100 m increase in elevation (32 kg m^{-3} per 100 m elevation) where p=0.03. There is a small but insignificant (p = 0.69) negative trend of 0.0024 g cm^{-3} per 100 m increase in elevation (2.4 kg m^{-3} per 100 m) in the 2006 pit densities. The difference in gradient between the two lines is significant (p=0.025).

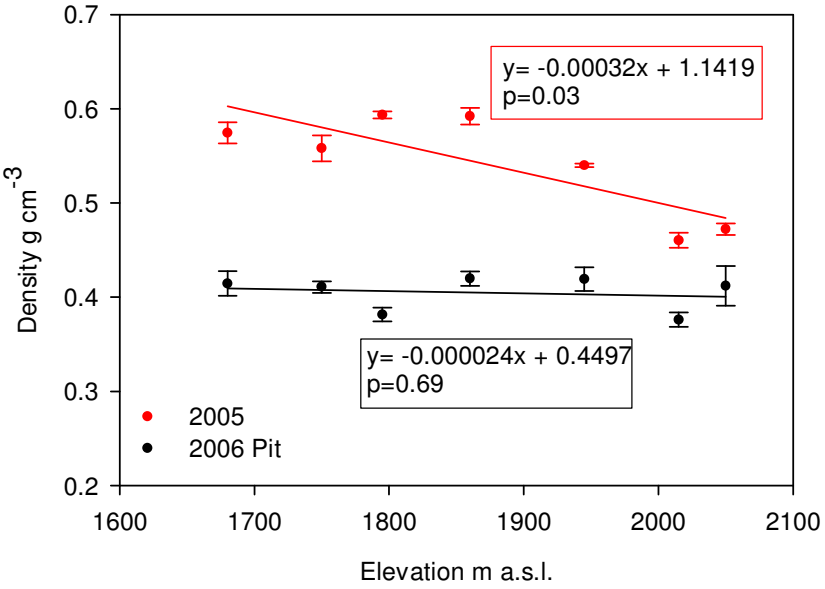

Figure 83: Graph showing average densities in the '2006 pits', and '2005' at T1 to T7.

The accumulation for the 2005-2006 winter snowpack shows a general decrease with increasing elevation (Figure 84) for both snowpack depth (a decrease of 9 cm per 100 m increase in elevation), and accumulation w.e. (4 cm w.e. decrease per 100 m increase in elevation). However, neither of these trends are significant (p>0.1).

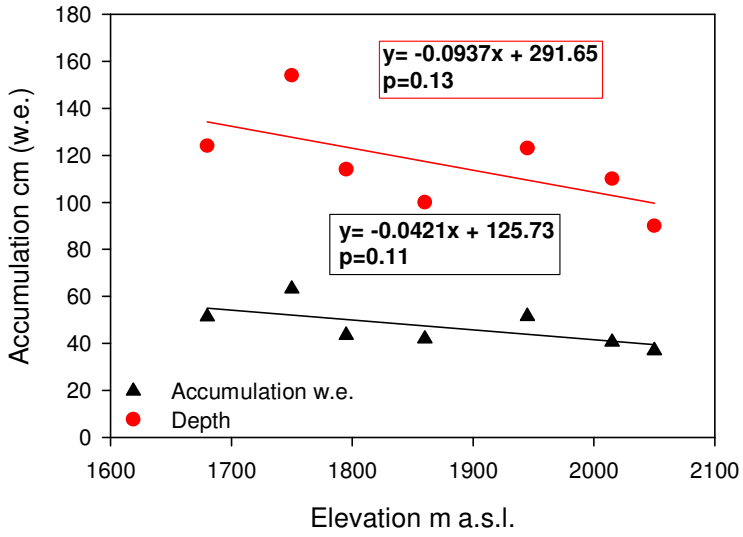

Figure 84: 2005 – 2006 winter accumulation from T1 – T7 as a snowpack depth and accumulation w.e.

6.3.2 Change in density between T4 and T6 in 2003, 2004 and 2005

With the density data collected at T4, T5 and T6, it is possible to obtain firn densities following summer melt and refreezing processes for the years 2003 (end-of-summers 2002 – 2003), 2004 (end-of-summers 2003 – 2004) and 2005 (end-of-summers 2004 – 2005). Three years of data enable inter-annual comparisons in the densification gradient along a ~20 km transect spanning an elevation range of 155 m between 1860 and 2015 m a.s.l. (Figure 85).

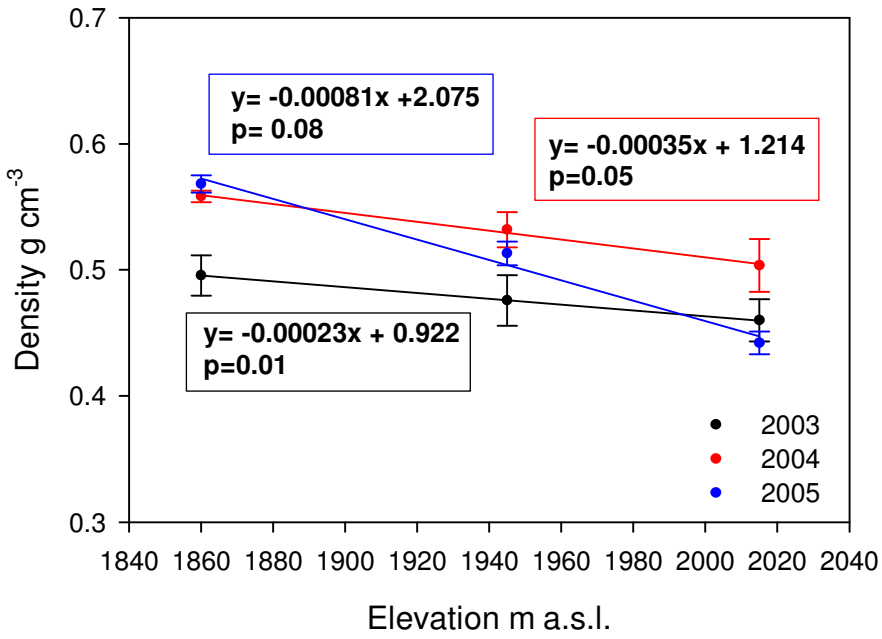

Figure 85: Average firn densities at T4. T5 and T6, for 2003, 2004 and 2005; the gradients of density with elevation for 2004 and 2005 are significant, and significantly different from each other.

As expected, the average densities show a negative correlation with increased elevation. This gradient is significant above the 95% level for the 2003 (p=0.007) and 2004 (p= 0.05) data. In 2005 the gradient is steepest although it is only significant at the 90% level (p=0.08). The shallowest gradient is present in 2003, where density decreases by 0.023 g cm^{-3} per 100 m increase in elevation (23 kg m^{-3} per 100 m). In 2004 density decreases by 0.035 g cm^{-3} per 100 m increase in elevation (35 kg m^{-3} per

100 m), and in 2005 by 0.08 g cm^{-3} per 100 m (81 kg m^{-3} per 100 m). The differences between all the gradients are significant at the 95% level.

6.4 Discussion

In Chapter 5 density results from nine sites within 1 km^2 of T5 clearly show that there is little variation in snowpack density prior to summer melt. The 2005 – 2006 winter snowpack densities, measured between T1 and T7 (Figure 83), replicate these results, demonstrating there is little variation in densities, and suggesting that at the scales observed, distance into the ice sheet, and elevation have minimal effect on the winter snowpack.

Accumulation is expected to decrease with increasing elevation due to continentality (Benn & Evans, 1998) and the '2006 pit' results show, as expected, a slight decrease of 4.2 cm w.e. per 100 m increase in elevation (Figure 84). This result, however, is not statistically significant. The complexities associated with accumulation include local topography (Helm & others, 2007) and circulation patterns (Hanna & others, 2001) and it is likely that a longer transect would be needed to reveal a significant decrease in accumulation with elevation change.

The post melt densities demonstrate that there is a gradient associated with density and elevation. From T1 to T7 in the 2005 data, average densities are seen to decrease at 0.032 g cm^{-3} per 100 m elevation (32 kg m^{-3} per 100 m). This is expected since the more melt a snowpack experiences, the more dense it will become on re-freezing, as higher sites are colder, they experience less melt. The decrease in post melt density with increasing elevation will have an impact on the change in elevation expected due to seasonal densification. Assuming a constant seasonal densification along this transect will result in errors in interpreting elevation changes as changes in mass.

The results from T5 in spring and autumn 2004 and from T1 to T7 in spring 2006 provide two key parameters regarding the seasonal densification of the snowpack in the percolation zone in this part of the Greenland Ice Sheet:

1. The processes of summer melt, percolation and refreezing result in the increase in density of the snowpack between spring and autumn, by 0.11 g cm^{-3} at T5 in 2004.
2. The post melt density decreases with increasing elevation, by 0.032 g cm^{-3} per 100 m (32 kg m^{-3} per 100 m) between T1 and T7.

With regards to accumulation and snowpack depth, the following results are established:

1. There is no significant change in snowpack depth with elevation from T1 to T7.
2. There is no significant change in accumulation with elevation from T1 to T7.

These simple results can be used to investigate theoretically the sensitivity of mass balance measurements as derived from surface elevation changes along the EGIG line between T1 and T7. For example, a theoretical 1 m snowpack with an average spring 2004 density of 0.42 g cm^{-3} has an accumulation of 42 cm w.e. (Figure 86). It is possible to apply these pre melt parameters to each location from T1 to T7 since there is no significant change in snowpack depth or accumulation from T1 to T7. Therefore each theoretical snowack at every location from T1 to T7 can be prescribed with the same spring snowpack properties as T5; that is, 1 m deep, a density of 0.42 g cm^{-3} and an accumulation of 42 cm w.e. (Figure 86).

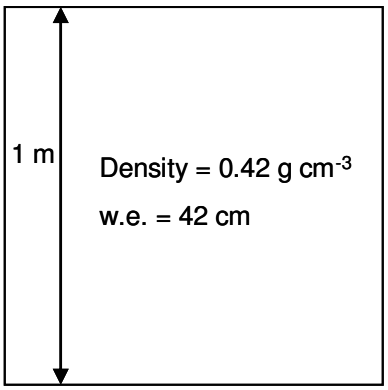

Figure 86: Theoretical snowpack

If it is assumed for simplicity that there is no mass loss or gain to this snowpack over the summer (i.e. the w.e. remains constant), and the only change to the snowpack is in the change in density and associated change in volume, it is possible using a prescribed densification gradient to calculate the post melt densities, and associated change in elevations.

At T5 in 2004, the snowpack increased in density by 0.11 g cm^{-3} from spring to autumn to a post melt density of 0.53 g cm^{-3}. If this same seasonal densification is applied to the theoretical 1 m snowpack, the resultant theoretical autumn snowpack, will be 79.3 cm deep, 20.7 cm lower than in the spring (Figure 87).

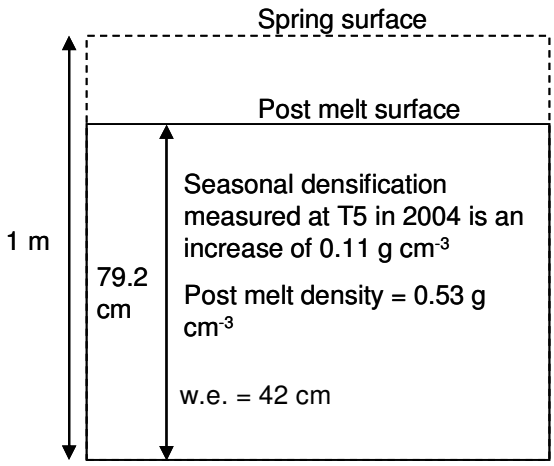

Figure 87: Theoretical post melt snowpack when seasonal densification measured at T5 in 2004 is applied.

Since the densification gradient between T1 and T7 is known (Figure 83), it can be used in conjunction with the T5 densification 'baseline' data to calculate the post melt densities in each theoretical autumn snowpack along the transect (from T1 to T7), and from this the associated elevation changes. The results of applying the densification gradient between T1 and T7 (0.032 g cm^{-3} per 100 m, 32 kg m^{-3} per 100m) along the transect to obtain post melt densities and elevations of the theoretical snowpacks are shown in Figure 88, and the values are given in Table 13.

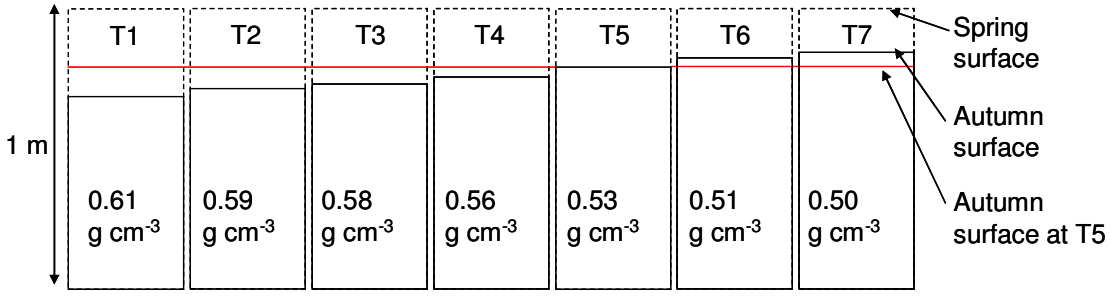

Figure 88: Post melt densities of 1 m theoretical snowpack when the densification gradient relating density with elevation is applied along the transect between T1 and T7.

	Elevation	Snowpack depth	Difference from T5 snowpack depth
	m a.s.l.	cm	cm
T1	1680	68.3	-10.9
T2	1750	70.9	-8.3
T3	1795	72.7	-6.6
T4	1860	75.4	-3.9
T5	1945	79.2	0.0
T6	2015	82.7	3.5
T7	2050	84.6	5.4

Table 13: Depths of the 1 m theoretical snowpack between T1 and T7 post melt and resulting difference in depth between each site and T5.

It is clear that these small changes in density can have significant impacts on annual snowpack height changes. If elevation changes are being interpreted as changes in mass, it is important that not only seasonal densification is accounted for, but also the gradient of post melt density with elevation.

Table 13 shows the difference in elevation of each post melt snowpack, from the T5 post melt snowpack. Clearly, if only seasonal densification is accounted for using a single point (e.g. the snowpack is expected to increase in density as at T5 from 0.42 g cm^{-3} to 0.53 g cm^{-3}) and the densification gradient is not accounted for, elevation changes that are greater (e.g. at T1, where the end-of-summer snowpack is 10.9 cm thinner than at T5) or less (e.g. at T7, 5.4 cm thicker) than expected will occur. Failing to take the seasonal densification gradient into account is of greatest concern because it will vary between years (Figure 85). As a result, elevation changes which occur due to densification at different elevations may be misinterpreted as changes in mass.

Braithwaite and others (1994) showed that snowpack density depends on both accumulation and melt. Both of these processes vary inter-annually, as seen in the 17 m core retrieved at E3, (Figure 54), and the temperature record from Crawford Pont AWS (Steffen & others, 1996). It is important to consider how variations in accumulation and melt might affect the anticipated densification of the snowpack, and how this may vary with elevation.

To investigate how variation in accumulation may impact on changes in elevation due to densification (based on the previous model); two further hypothetical snowpacks are set up, one 0.5 m deep and the other 1.5 m deep. The same spring density (0.42 g cm^{-3}) is applied to both snowpacks, and so their respective accumulations are 21 and 63 cm w.e.. Again, it is assumed there is no mass loss or accumulation over the summer period, so their accumulations remain constant. The seasonal densification at T5 is taken to be 0.11 g cm^{-3}, and the gradient of 0.032 g cm^{-3} per 100 m increase in elevation (32 kg m^{-3} per 100 m) is applied along the transect. The new elevation at each location is then calculated, and the difference between this and the elevation at T5 is found. Figure 89 presents the differences in snowpack depth for each location (T1 to T7) from the snowpack depth at T5 for the 0.5 m, 1 m and 1.5 m theoretical snowpacks. The greater the annual accumulation,

the greater the absolute discrepancy in elevation change associated with densification of the snowpack between each location and that expected at T5.

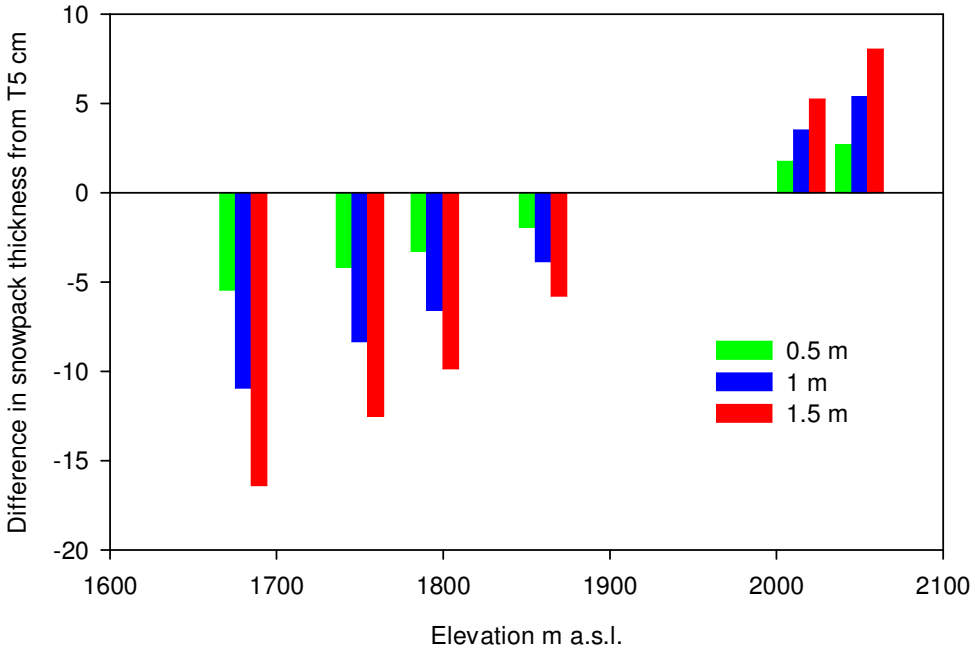

Figure 89: Graph showing the difference between the snowpack thickness calculated due to seasonal densification at T5, and the snowpack thickness at each location (T1 to T7) when a densification gradient relating density to elevation is applied. Results are shown for three hypothetical snowpacks, with initial depths of 0.5 m, 1 m and 1.5 m.

To investigate how different melt rates may effect the densification of the snowpack, and associated elevation change, it is possible to compare the gradient of density with elevation, with a temperature lapse rate, to find the relationship between density and temperature. Using the densification gradient of -0.032 g cm^{-3} per 100 m (-32 kg m^{-3} per 100 m) (Figure 83), and average lapse rate for Greenland of 1 °C every 142 m (Hanna & others, 2005); the average post melt snowpack density increases by 0.0426 g cm^{-3} °C^{-1}. Projected warming in the Arctic is expected to be between 2 °C and 4 °C by 2040 (ACIA, 2005) which would correspond to an increase in average post melt snowpack density of 0.085– 0.170 g cm^{-3}. For a theoretical 1 m thick snowpack with the pre melt spring density of 0.42 g cm^{-3}, a 2 °C increase in average temperature would result in an increase in post melt density at T5 from 0.53 to 0.62 g cm^{-3}. This density approximates that calculated for T1 post melt

(0.61 g cm^{-3}) assuming current melt conditions and an initial theoretical 1 m spring snowpack (Figure 88). These calculations clearly demonstrate how increasing temperatures will result in enhanced seasonal densification at a site and will result in the inland migration of the upper limit of the percolation zone. The potential post melt snowpack depths between T1 and T7 for a theoretical 1 m spring snowpack, assuming current temperatures and 2 °C and 4 °C warming are shown in Figure 90 and Table 14. Pfeffer & others (1991) calculated that a snowpack density of 0.83 g cm^{-3} was required for pore closure and runoff. The density at T1 under 4 °C warming is 0.79 g cm^{-3} (Table 14), indicating the advancement of the runoff limit inland with warming.

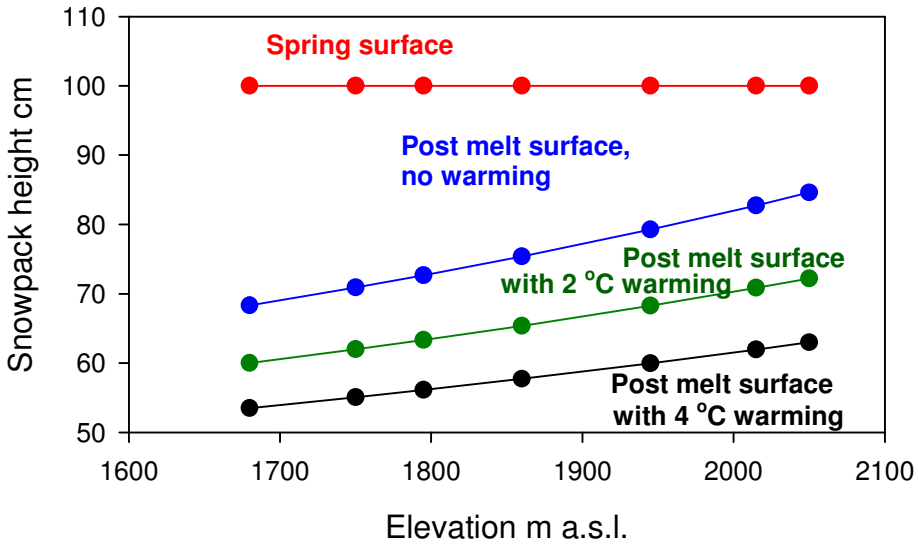

Figure 90: Effect of projected warming on seasonal densification, and resultant surface lowering at sites T1 to T7 in a theoretical snowpack, with 1 m depth in spring, and constant w.e. of 42 cm.

The changes in snowpack thickness due to densification are significant under both warming scenarios, emphasising the importance of accounting for seasonal densification when deriving mass balances from elevation changes. These findings are especially important given recent warming observed over Greenland (Hanna & others, 2008) and the projected warming over the next century (Trenberth & others, 2007).

	Elevation m a.s.l	2 ℃ warming Density g cm^{-3}	Snowpack thickness change cm	4 ℃ warming Density g cm^{-3}	Snowpack thickness change cm
T1	1680	0.70	-40.00	0.79	-46.51
T2	1750	0.68	-38.02	0.76	-44.94
T3	1795	0.66	-36.67	0.75	-43.88
T4	1860	0.64	-34.62	0.73	-42.28
T5	1945	0.62	-31.73	0.70	-40.03
T6	2015	0.59	-29.15	0.68	-38.05
T7	2050	0.85	-27.79	0.67	-37.01

Table 14: Post melt densities for a hypothetical 1 m snowpack where temperatures have warmed by 2 °C and 4°C. The elevation change due to densification is also shown.

In all of the above scenarios, estimates of snowpack elevation change have been based on a linear densification gradient derived from a single melt-season across a 57 km transect. This is clearly an over-simplification of reality. Densification gradients may not be linear and they will typically vary on an inter-annual basis as a result of different seasonal accumulation and melt rates. The post melt densities at T4, T5 and T6 in the 2003, 2004 and 2005 snowpacks demonstrate that the densification gradient can vary substantially between years (Figure 85).

As before, it is possible to calculate the potential elevation difference between T5, and T4 and T6, where different gradients of change in density with elevation are applied. This is done by again using a theoretical 1 m snowpack, w.e. 42 cm, and no mass loss or gain over the summer. At T5 the post melt density is 0.53 g cm^{-3}, the densities at T4 and T6 are calculated used the gradients for the 2003, 2004 and 2005 snowpacks. The difference in elevation at T4 and T6 to T5 for each of the three gradients are presented in Table 15.

	Density g cm^{-3}			Elevation difference from T5 cm		
	2003	2004	2005	2003	2004	2005
T4	0.550	0.560	0.599	-2.819	-4.212	-9.111
T5	0.530	0.530	0.530	0.000	0.000	0.000
T6	0.514	0.506	0.473	2.483	3.841	9.493

Table 15: Post melt densities at T4, T5 and T6 calculated for the 1 m theoretical snowpack, with the densification gradients measured in the 2003, 2004 and 2005 snowpacks. The differences in elevation for T4 and T6 to T5 are shown.

Changes in snowpack density, and the differences in elevation between T4 and T6 with T5 are significant (between 2.9 cm and 10 cm), if a 1 cm elevation change can be interpreted as a 1 km^3 change in volume (Thomas & others, 2008), it is essential that densification gradients, and annual fluctuations are accounted for.

Since snowpack density is determined by accumulation and melt, it is likely that the gradient of densification with elevation will also vary as a result of variation in accumulation and melt. The PDDs for 2003, 2004 and 2005 are calculated by integrating all positive temperatures recorded at Crawford Point (Steffen & others, 1996) by time. The accumulation and average density at T6 (the closest measurement location to Crawford Point), are presented alongside the PDDs and density gradients for 2003, 2004 and 2005 in Table 16.

	PDD	T6 Density g cm^{-3}	Snowpack depth (T6) m	Gradient of densification g cm^{-3} per 100 m	kg m^{-3} per 100 m
2003	15	0.46	1.35	-0.023	-23
2004	78	0.5	1.41	-0.035	-35
2005	5	0.44	1.23	-0.081	-81

Table 16: Table of PDDs, average snowpack density and depth at T6 in 2003, 2004 and 2005, and the gradient of densification between T4 and T6 in 2003, 2004 and 2005.

From Table 16 it can be seen that the density of the snowpack at T6 is higher when the PDD are higher, as is the case in 2004. This would be expected, since positive degree days are the positive temperatures integrated with respect to time, therefore, a higher number of PDDs reflects higher temperatures, longer periods of positive

temperatures, or both. This would result in more melt, and this would be reflected in the larger density of the snowpack. This pattern is reflected in the average densities, and number of positive degree days in 2003 (second highest density, and second highest number of PDDs) and 2005 (lowest density and fewest PDDs). The accumulation (as a snowdepth) follows the same pattern, so in years with the most PDDs, the accumulations are greatest (e.g. 2004) and in years of fewest PDDs the accumulation is lowest (as in 2005).

Since melt (i.e. PDDs) and accumulation determine snowpack density (Braithwaite & others, 1994), it is possible that these factors will also determine the gradient of densification with elevation. The gradients for 2003 and 2004 are statistically significant (α=0.05), whereas the gradient for 2005 is not (p=0.08). From these data, the year with the steepest gradient (2004) corresponds to the year with the most PDD's and highest accumulation, and the year with the shallowest gradient (2003) corresponds to the year with the fewest PDDs and lowest accumulation.
Due to the limited number of data points, it is not possible to run a multiple regression on these data to determine the relationship, or the significance of the relationship.

It is also important to consider the spatial variability of snowpack density over small spatial scales (as shown in Chapter 5). In autumn 2004, post melt and refreezing snowpack density measurements were taken from snowpits at nine locations (T5, E1-E4, S1-S4) within 1 km^2 ((Parry & others, 2007) and Chapter 5). Table 17 shows the variability seen between snowpits with density varying between 0.60 g cm^{-3} at E2 and 0.47 g cm^{-3} at E3. In 2004, the average densities at T4 and T6 were 0.56 g cm^{-3} and 0.50 g cm^{-3} respectively, values which fall within the range seen at T5. This demonstrates that average snowpack densities vary greatly over short length scales. This emphasises the importance of reducing errors by taking multiple measurements at one site.

Location	Average density g cm^{-3}
T5	0.53
E1	0.56
E2	0.60
E3	0.47
E4	0.51
S1	0.50
S2	0.56
S3	0.54
S4	0.49

Table 17: Table showing average snowpit densities following summer melt and refreezing at nine locations within the 1 km^2 grid at T5 in autumn 2004.

6.5 Conclusions

In the winter snowpack, prior to summer melt, average densities are not seen to vary with elevation, when measured along a 57 km transect from T1 to T7, spanning 370 m elevation, from 1680 m a.s.l. to 2050 m a.s.l. (Figure 83). It would be expected that the accumulation, and so snowpack depth, would decrease with elevation, due to the increasing distance inland (Benn & Evans, 1998), and a gradient of -9 cm (snowpack depth) per 100 m elevation and -4 cm w.e. per 100 m elevation are calculated, although they are not statistically significant (Figure 84).

The post melt densities from T1 to T7, as measured in 2 m cores, retrieved from the end-of-summer 2005 surface (Figure 81), are seen to decrease with increasing elevation (-0.032 g cm^{-3} per 100 m, or 32 kg m^{-3} per 100 m). This gradient is found to have a significant effect on the change in snowpack thickness with seasonal densification, demonstrating the importance of accounting for the elevation, when determining the elevation change that occurs as a result of densification, rather than a change in mass.

The gradient of densification with elevation is measured between T4 and T6 (155 m elevation range) for the 2003, 2004 and 2005 post melt snowpacks. The densification

gradient is seen to vary significantly between these years. Failure to account for this change in gradient can result in errors between the predicted change in snowpack depth due to seasonal densification, and the actual change when the gradient and annual change in gradient are accounted for. These errors have theoretically been calculated to be as high as 10 cm, which could be misinterpreted as a 150 km^3 mass loss, so demonstrating the importance in accounting for densification gradients, and the annual changes in the gradient.

By combining the gradient of density with elevation, and a temperature lapse rate, it is possible to find the potential increase in snowpack density with increases in temperature. With warming in the Arctic projected to be 2 to 4 °C, as expected, the post melt densities are projected to increase at all locations. This results in the inland migration of snowpack densities that are measured under present climatic conditions, for example the expected density at T3 under current condition is 0.58 g cm^{-3}, with 2 °C warming, this density would be seen at T7, 255 m higher. This would also lead to the inland migration of the runoff limit, where snowpack densities at higher elevations will reach the pore close off limit, resulting in higher runoff from the ice sheet.

The variability in post melt snowpack density is high, as found in autumn 2004 at nine sites within 1 km^2 of T5; the variability of the densities overlaps the average densities found at T4 and T6 in the same year. It is therefore essential to take many samples at each site to account for the variability, and to find the density change with elevation from this.

Chapter 7: Conclusions

7.1 Introduction

This thesis is intimately linked with the European Space Agency's CryoSat programme, a satellite bourne radar altimeter developed with the intention of providing estimates of ice sheet elevation down to near centimetre resolution (Wingham & others, 2001). It is clear that, as with any new instrument, effective calibration is required in order to determine the accurate values of the parameters being measured. As a result, the CryoSat Calibration-Validation Experiment (CryoVex) was conceived, of which this work is a key part. The loss of CryoSat on launch in October 2005 ensured that the material presented in this thesis could not directly contribute to the calibration of the satellite. Nevertheless, the data collected and presented still have considerable significance for characterising those aspects of the snowpack and firn that could impact on the accuracy and calculation of errors of elevation estimates from previous and current radar satellite missions such as ERS-1 and ERS-2 and for the future CryoSat 2, due to launch in 2009. The data are also valuable in enhancing our understanding of the poorly characterised glaciological processes that operate in the percolation zone of an ice sheet where complex seasonal variations in the snowpack facies occur across a spatially extensive region.

7.2 Thesis Objectives

The overall aim of this thesis was to investigate processes operating in the percolation zone of the Greenland Ice Sheet that could impact the accuracy to which the CryoSat radar altimeter measures surface elevation change. More specifically,

this thesis aimed to investigate the effects that the seasonal processes of summer melt, percolation and refreezing have on the snowpack and firn in the percolation zone of the Greenland Ice Sheet. These objectives were defined in the introduction as follows:

1. To measure inter-annual variability in accumulation.
2. To investigate the reliability of using long cores to measure inter-annual accumulation in the percolation zone of the Greenland Ice Sheet.
3. To develop an understanding of spatial and temporal changes in snowpack properties, including ice layer concentration and location, and firn grain size, at small length scales (1 m to 1 km) and longer length scales (>10 km).
4. To quantify seasonal changes in density and accumulation of the snowpack.
5. To determine densification gradients across longer scale (>10 km) transects of the percolation zone.
6. To determine inter-annual variation of densification gradients across a >10 km transect of the percolation zone.

These objectives were achieved by undertaking the following research:

7.2.1 Measuring inter-annual variability in accumulation.

- Snowpack height measurements from Crawford Point AWS were used alongside density measurements from T6 (the closest field site) to derive annual accumulations for the years 1996 to 2003.
- Identification of annual layers from seasonal fluctuations in isotopic concentrations in the 17 m core retrieved from E3 enabled accumulations from 1986 to 2003 to be calculated.

7.2.2 To investigate the reliability of using long cores to measure inter-annual accumulation in the percolation zone of the Greenland Ice Sheet.

- Comparisons between snowpit stratigraphic descriptions, and those made from shallow firn cores were made to see if the end-of-summer/autumn hoar couplet could be identified in the core record.
- Concentrations of Cl^-, SO_4^{2-}, NO_3^-, Na^+, K^+, Mg^{2+} and Ca^{2+} were measured from samples collected from distinctive stratigraphic layers in spring and autumn 2004 snowpits, and along the length of the core at 10 cm resolution in spring 2006 snowpits and analysed for seasonal changes in the ion concentrations.
- A 17 m core was retrieved from E3 (located 100 m from T5), and analysed for stratigraphy, including the distribution of ice features. At 10 cm resolution, the core was analysed for; density; ionic concentrations of Cl^-, SO_4^{2-}, NO_3^-, Na^+, K^+, Mg^{2+} and Ca^{2+} ; isotopic concentrations of ^{18}O and ^{2}H with a more detailed isotopic re-analysis at 2.5 cm resolution for a 2 m section of the core.
- The longer time series of density measurements derived from the n-probe profiles (down to depths of between 4 and 9 m), and directly measured at 10 cm resolution in the 17 m core, enabled investigation into the possibility of using density changes to identify the 'end-of-summer surface/autumn hoar couplet', and thereby providing a temporal constraint on the data.

7.2.3 To develop an understanding of spatial and temporal changes in snowpack properties, including ice layer concentration and location, and firn grain size, at small length scales (1 m to 1 km) and longer length scales (>10 km).

- Descriptions of snowpack facies in spring and autumn 2004 and spring 2006 were recorded, and compared. Additionally, in the autumn 2004 snowpits, and all shallow cores collected in spring 2006, the volume of ice present in the snowpack as lenses, layers, pipes and blobs was quantified.
- In the autumn 2004 snowpits, the location of all ice features in relation to snowpack depth, and the grain size of the adjacent stratigraphic layers were recorded.
- Snowpack density, accumulation and snow depth data were obtained from nine sites in spring 2004 and spring 2006 to investigate inter-annual variations in spring snowpack characteristics.

7.2.4 To quantify seasonal changes in density and accumulation of the snowpack.

- Density, accumulation and snow depth data from nine snowpits within 1 km^2 of T5 on the EGIG line in the percolation zone of the Greenland Ice Sheet were collected in spring and autumn 2004, thus enabling a direct comparison of the snowpack density, accumulation and thickness prior to and following the summer 2004 processes of melt, percolation and refreezing.
- Longer time series of snowpack and firn density data were collected using the n-probe at eleven sites within 1 km^2 of T5 in spring 2004 and at six of the sites in autumn 2004. These data provided information on the seasonal densification of the snowpack.

7.2.5 To determine densification gradients across a longer scale (>10 km) transects of the percolation zone.

- In spring 2006 snowpits were dug through the 2005 – 2006 winter snowpack to the end-of-summer 2005 surface, and shallow firn cores were retrieved from the end-of-summer 2005 surface, over a 370 m elevation range, along a 57 km transect across the percolation zone, at seven sites from T1 (1680m a.s.l.) to T7 (2050 m a.s.l.). From these data a post melt densification gradient can be obtained by comparing the average densities from the one year old shallow firn cores with elevation at each site.

7.2.6 To determine inter-annual variation of densification gradients across >10 km scale transects of the percolation zone.

- Snowpits and shallow cores were used to obtain density, accumulation, snowpack depth and facies at three sites along a ~20 km transect centred on T5 in spring 2004 and 2006 and autumn 2004. The combination of data enabled the gradient of seasonal densification with elevation to be calculated and compared for the 2003, 2004 and 2005 melt seasons.
- Temperature measurements from the PARCA AWS at Crawford Point (2000 m a.s.l. and 2 km from T6) were used to aid interpretation of the observed compared seasonal changes in snowpack densities.

7.3 Conclusions

7.3.1 Measuring inter-annual variability in accumulation.

- In Chapter 4 the annual accumulations from 1986 to 2003 are found from the 17 m core. The mean annual accumulation between 1986 and 2003 was 53.7 cm w.e., with high inter-annual variability (s.d.= 12.9 cm w.e.). The year with the lowest accumulation was 2003, with 30.6 cm w.e., and the highest accumulation was in 2001, 75.6 cm w.e.. These values are significantly different to those obtained from measurements of snowpack height (from Crawford Point AWS), and the average autumn 2004 density at T6. There are however many errors associated with determining the mass balance from the AWS measurements, including, gaps in measurements and additionally the distance the AWS is from E3 (where the core was retrieved from).
- There is a high inter-annual variability in accumulation measured in data sets collected since 1950 (Benson, 1962; Seckel, 1977; Stober, 1986; Anklin,& others, 1994), showing annual accumulation to be 53 cm w.e. on average, with variations of 20 – 38%.

7.3.2 To investigate the reliability of using long cores to measure inter-annual accumulation in the percolation zone of the Greenland Ice Sheet.

- Results in Chapter 4 demonstrate that the seasonal fluctuations in ^{18}O and ^{2}H are preserved in the snowpack, and the summer maxima (Dansgaard, 1964) were successfully used to identify annual layers in a 17 m core retrieved from a site with 10% melt in summer 2004.

- Visual descriptions of stratigraphy within the 17 m core are not sufficient alone to identify the end-of-summer surface/autumn hoar couplet. In addition measurements of crystal type and the hardness of the layer are also required and still often leave ambiguity in interpretation.
- Direct measurements of density from the 17 m core reveal large fluctuation with depth, between 0.36 and 0.90 g cm^{-3}. These fluctuations are smoothed out in the profile derived from n-probe measurements. Identification of an end-of-summer surface/autumn hoar density couplet is not apparent in direct density measurements, but can be seen in places in those derived from the n-probe. Unfortunately, while this couplet is at times very obvious, it is not possible to use this technique to identify annual layers unambiguously, as it is highly subjective. Thus, the density structure of firn cores cannot be used to resolve annual layers in this part of the percolation zone.

7.3.3 To develop an understanding of spatial and temporal changes in snowpack properties, including ice layer concentration and location, and firn grain size, at small length scales (1 m to 1 km) and longer length scales (>10 km).

- Chapter 5 presents results of density/depth profiles from nine sites within 1 km^2 around T05 revealing that the snowpack in this region has a highly variable density stratigraphy, and that these stratigraphy changes occur over short temporal and spatial scales.
- Ice layers are rarely spatially continuous at length scales >~1 m, and this complexity may be partly responsible for prohibiting clear identification of annual layers in deeper core and neutron probe depth density profiles. Ice layers and lenses formed within the near-surface snow pack contribute markedly to the overall increase in near surface density and these will result in very different radar echo returns between spring and autumn. Unless this

seasonal effect is accounted for it may contribute to ambiguous radar 'estimates' of surface elevation Jezek & others, 1994; Scott & others, 2006a).

- The percentage of the annual accumulation that is present as ice features varies between 0% (1986 and 1987) and 24% (1999), as measured between 1986 and 2003 in the 17 m core retrieved from E3.
- The location of ice layers within the snowpack, as measured at nine locations in the autumn 2004 snowpits within 1 km^2 of T5, and from 2 m cores retrieved from the end-of-summer 2005 surface at seven sites along a 57 km transect, over 370 m elevation range from T1 to T7, show no systematic relationship with boundaries defined by grain-size. In addition and in contrast to the results of Pfeffer and Humphrey (1998) there was no increase in the number of internal ice layers at higher colder sites along the transect from T1 to T7.

7.3.4 To quantify seasonal changes in density and accumulation of the snowpack.

- Results in Chapter 5 show that small increases in snowpack depth were observed between spring and autumn 2004 within the percolation zone, the average for the nine sites within 1 km^2 of T5 is an increase of 5.3%. However, mean snowpack densities increased significantly over this period (on average by 26.2%). The considerable change in snowpack density between seasons indicates that significant changes in mass can occur in this zone with only very limited changes in surface elevation. For example, at T05 the 4.5% increase in snow depth reflected a 31.6% increase in net accumulation. Thus, in areas such as the percolation zone, where the snowpack shows substantial seasonal changes in density, mass balance estimates should not be based solely on observed changes in surface elevation.

7.3.5 To determine densification gradients across a longer scale (>10 km) transects of the percolation zone.

- In the winter snowpack, prior to summer melt, average densities are not seen to vary with elevation, when measured along a 57 km transect from T1 to T7, spanning 370 m elevation, from 1680 m a.s.l. to 2050 m a.s.l. (Chapter 6).
- The post melt densities in the one year old firn from T1 to T7 are seen to decrease with increasing elevation (-0.032 g cm^{-3} per 100 m, or 32 kg m^{-3} per 100 m). This gradient is found to have a significant effect on the change in snowpack depth with seasonal densification, which could potentially lead to errors where snowpack depth may be up to 11 cm lower than would be expected if the gradient is not accounted for. This could potentially be misinterpreted as a significant mass loss if 1 cm elevation change represent 15 km^3 volume change (Hanna & others, 2008).

7.3.6 To determine inter-annual variation of densification gradients across a 57 km transect of the percolation zone.

- In Chapter 6 the gradient of decrease in density with elevation is seen to significantly vary inter-annually when measured over a 155 m elevation range (T4 to T6) in 2003, 2004 and 2005 post melt snowpacks. Failure to account for this change in gradient can result in substantial errors between the predicted change in snowpack depth due to seasonal densification, and the actual change when the gradient and annual change in gradient are accounted for. These errors have theoretically been calculated to be as high as 10 cm, which could be misinterpreted as a 150 km^3 mass loss, so demonstrating the importance in accounting for densification gradients, and the annual changes in the gradient.

7.4 Limitations

The primary limitation to the work presented in this thesis is spatial; measurement locations were limited to 1 km^2 in spring and autumn 2004, and a 57 km transect in spring 2006. The area of the Greenland Ice Sheet is 1.7×10^6 km^2, with the percolation zone covering 44 to 79% (Wang & others, 2007). Of course, it is not possible to undertake fieldwork at high resolution over an area of this scale; however, the validity of the conclusions from this thesis would be greatly improved by repetition of snowpack density measurements in spring and autumn at different latitudes, and also on the east coast of the ice sheet. From this a fuller understanding of large scale spatial variability in seasonal densification could be developed, which is important when accounting for this effect on mass balance measurements derived from elevation change.

Additionally, the density measurements from T1 to T7 in spring 2006 did not cover the entire extent of the percolation zone; a more thorough understanding of the change in seasonal densification with elevation could be ascertained from a transect extending from the ELA to the dry snow zone.

Accumulation results from previous expeditions (Benson, 1962; Seckel, 1977; Stober, 1986; Anklin & others, 1994), and derived from the 17 m core retrieved at E3 show there is high inter-annual variability. Additionally, the 17 m core demonstrates the percentage of the snowpack that occurs as ice also varies highly between years. The seasonal densification results presented in this thesis only span one year; in order to account for the effect of inter-annual variations in accumulation and melt, this would need to be investigated over a series of years.

Since there are no density measurements for the 2003 – 2004 and 2004 – 2005 snowpacks prior to melt, it is not possible to measure the seasonal densification at T1 – T7, only the post melt densities. Repeated measurements at these sites in spring and autumn would enable the change in density with elevation to be measured.

High variability in average snowpack densities was measured at nine sites within 1 km^2 of T5, where some autumn snowpit results exceeded the average post melt densities at lower elevations (e.g. T1). This high variability at short scales needs to be investigated at each location along the transect, and accounted for when gradients of seasonal densification with elevation are calculated.

The inter-annual comparison of changes in post melt snowpack density is limited to three locations. The post melt density with elevation gradients calculated are significant, and significantly different from each other; however, more measurements from an extended transect would make these conclusions more robust, and extend the area investigated.

The isotope concentrations measured in the 17 m core at E3 demonstrate that it is possible to identify annual layers by locating the summer maxima (Dansgaard, 1964), and using density measurements, to derive annual accumulations. As the core is a point measurement, annual accumulations derived from it are subject to errors from redistribution of mass by the wind and the short scale variability of ice features. To improve the accuracy of annual accumulations derived from cores, many cores would be retrieved from the same area, to smooth out the noise.

7.5 Future work

At the outset of this investigation, the primary aim was to provide data for the calibration of mass balance measurements made by CryoSat. Following the unsuccessful launch the data has been used as a basis for an investigation into the consequences of melt water percolation and refreezing in the percolation zone of the Greenland Ice Sheet. The conclusions of this thesis provide a basis for further fieldwork, to constrain and develop understanding of the implications of mass balance measurements derived from elevation changes.

For validation of CryoSat 2 interpretations of elevation changes as changes in mass balance, it is important that the change in seasonal densification and the change in densification with elevation are fully accounted for. Repeated snowpack density measurements prior to and post melt along a transect spanning the entire percolation zone, combined with a series of meteorological weather stations would enable the spatial component of seasonal densification to be fully explored, and related to temperature, and temperature gradients. Due to the high short scale variability found at T5, it is important repeated measurements are taken at each location, so errors can be derived, and trends measured more accurately.

Since the CryoSat 2 mission is only planned for three years, it is important that any measurements made are placed in context of inter-annual variability. The isotope concentrations from the 17 m core show that seasonal fluctuations can be used to identify annual layers at T5, and so this technique is proven to be an effective way of measuring previous annual accumulations. In 2004 10% of the snowpack at E3 (where the 17 m core was retrieved from) was found to undergo melt. It is important to ascertain the maximum melt extent in a snowpack, before the seasonal fluctuations in the isotope record are lost. This can be done by retrieving cores at lower, warmer elevations in the percolation zone; thus providing a spatial limitation to the effectiveness of this technique.

So as to avoid underestimation of annual mass balances it is important that the possibility of melt water percolating through more than one years' snowpack is further investigated and quantified. Repeated visits in spring and autumn, and use of dye tracing would make this more accurate. Repeated measurements spanning the percolation zone would mean the spatial extent of the varying depth of percolation could also be investigated.

Appendix 1: Investigations of meltwater refreezing and density variations in the snowpack and firn within the percolation zone of the Greenland ice sheet

Victoria Parry, Peter Nienow, Douglas Mair, Julian Scott, Bryn Hubbard, Konrad Steffen and Duncan Wingham

Annals of Glaciology 46
p. 61-68
Published 2007

Appendix 2: Importance of seasonal and annual layers in controlling backscatter to radar altimeters across the percolation zone of an ice sheet

Julian Scott, Peter Nienow, Douglas Mair, Victoria Parry, Elizabeth Morris and Duncan Wingham

Geophysical Research Letters 33
L24502, DOI: 10.1029/2006GL027974
Published 2006

Appendix 3: A ground-based radar backscatter investigation in the percolation zone of the Greenland ice sheet

Julian Scott, Doug Mair, Pete Nienow, Victoria Parry, Elizabeth Morris

Remote Sensing of the Environment
104
361-373
Published in 2006

Appendix 4: Characteristics and small-scale variability of GPR signals and their relation to snow accumulation in Greenland's percolation zone

Thorben Dunse, Olaf Eisen, Veit Helm, Wolfgang Rack, Daniel Steinhage, Victoria Parry

Journal of Glaciology
54 (185)
333-342
Published in 2008

Appendix 5: Winter accumulation in the percolation zone of Greenland measured by airborne radar altimeter

Veith Helm, Wolfgang Rack, Robert Cullen, Peter Nienow, Doug Mair, Victoria Parry, Duncan Wingham

Geophysical Research Letters 34
L06501, DOI: 10.1029/2006GL029185
Published 2007

Appendix 6: Summary of data collected

Spring 2004

- Stratigraphic descriptions; temperature measurements; and density, hardness and grain size measurements from stratigraphic layers in snowpits at T4, T6, T5, E1, E2, E3, E4, S1, S2, S3, S4.
- Density measurements and basic stratigraphic description of cores retrieved from the bottom of snowpits at T4, T6, T5, E1, E2, E3, E4, S1, S2, S3 and S4.
- N-probe profiles from T5, E1, E2, E3, E4, S1, S2, S3 and S4.
- 17 m core retrieved from bottom of snowpit at E3
- Avalanche probe measurements to 'hard' layers at 5 m intervals from T5 to E3.
- Samples for ionic analysis collected from each stratigraphic layer in snowpits T4, T6, T5, E1, E2, E3, E4, S1, S2, S3 and S4.

Autumn 2004

- Stratigraphic descriptions; temperature measurements; and density, hardness and grain size measurements from stratigraphic layers in snowpits at T4, T6, T5, E1, E2, E3, E4, S1, S2, S3, S4.
- Density measurements and basic stratigraphic description of cores retrieved from the surface at T4, T6, T5, E1, E2, E3, E4, S1, S2, S3 and S4.
- N-probe profiles from T5, S1, S2, S3, S4, E1 and E2.
- Avalanche probe measurements to 'hard' layers at 1 m intervals from T5 to E3.
- Samples for ionic analysis collected from each stratigraphic layer in snowpits T4, T6, T5, E1, E2, E3, E4, S1, S2, S3 and S4.

Spring 2006

- Stratigraphic descriptions; temperature measurements; and density, hardness and grain size measurements from stratigraphic layers in snowpits at T1, T2, T3, T4, T5, T6, T7, E1, E2, E3, E4, S1, S2, S3, S4.
- Stratigraphic sketches of two parallel 3 m sections of a ~2 m deep trench.
- Density measurement at 1 m intervals along a 3 m section of one side of the trench.
- Sketches of windcrusts in top 90 cm along 6 m of the trench.
- Density measurements and basic stratigraphic description of cores retrieved from the bottom of snowpits at T1, T2, T3, T4, T5, T6, T7, E1, E2, E3, E4, S1, S2, S3, S4.
- Avalanche probe measurements to 'hard' layers at 1 m intervals from T5 to E3.
- Samples for ionic analysis collected at 10 cm resolution in snowpits T5, E1, E2, E4, S1 and S2.

Appendix 7: Snowpit and core stratigraphic descriptions

Spring 2004 snowpit

E1 Height cm Top	Bottom	Hardness	Grain size mm	Description
147	146	Fist	1	Needles/ capped ends
146	143	Pencil	<0.5	Rounded irregular
143	139	Finger	<0.5	Rounded irregular
139	89	Finger	<0.5	Rounded irregular
89	80	Pencil	0.5 - 1	Rounded irregular
80	75	Pencil	0.5 - 1	Rounded irregular
75	74	Knife	0.5 - 1	Rounded irregular
74	69	Finger	0.5 - 1	Rounded irregular
69	41	Pencil	1	Rounded irregular
41	18	Finger	1 - 2.0	Rounded irregular and faceted
18	5	Finger	1 - 2.0	Rounded irregular and faceted
5	0	Fist	1 - 2.0	Rounded irregular and faceted

E2 Height cm Top	Bottom	Hardness	Grain size mm	Description
145	141.5	Finger	<0.5	Rounded irregular
141.5	77	Finger	0.5	Rounded irregular
77	53	Pencil	0.5	Rounded irregular
53	53	Knife		
53	28	Pencil	<1	Rounded irregular
28	8	Finger	1	Faceted
8	0	Fist	2	Faceted

E3 Height cm Top	Bottom	Hardness	Grain size mm	Description
136	109	Finger	0.5	Rounded irregular
109	104	Pencil	0.5	Rounded irregular
104	89	Finger	0.5	Rounded irregular
89	55	Hard Pencil	1	Rounded irregular
55	31	Pencil	1.0 - 2.0	Irregular faceted
31	24	Finger	1.0 - 2.0	Irregular faceted
24	8	Pencil	2	Irregular faceted
8	0	Finger	1.0 - 2.0	Irregular faceted

Spring 2004 snowpit

E4 Height cm Top	Bottom	Hardness	Grain size mm	Description
143	139	Fist	<2	Stellar/Needles
139	136	Finger	<0.5	Rounded irregular
136	112	Soft finger	<1	Rounded irregular
112	83	Finger	<0.5	Rounded irregular
83	75	Hard Pencil	<0.5	Rounded irregular
75	48	Pencil	<1	Rounded irregular
48	38	Finger	1.0 - 2.0	Faceted
38	9	Finger	1.0 - 2.0	Faceted
9	0	Finger	1.0 - 2.0	Faceted

S1 Height cm Top	Bottom	Hardness	Grain size mm	Description
147.5	147	Fist	1	Needles/ capped columns
147	142	Finger	<0.5	Rounded irregular
142	139	Finger	<0.5	Rounded irregular
139	85	Finger	<0.5	Rounded irregular
85	39	Pencil	0.5 - 1.0	Rounded irregular
39	19	Finger	1.0 - 2.0	Rounded irregular and faceted
19	8	Pencil	1.0 - 2.0	Rounded irregular and faceted
8	0	Fist	2	Faceted

S2 Height cm Top	Bottom	Hardness	Grain size mm	Description
138	132	Finger	<0.5	Rounded irregular
132	131.5	Pencil	<0.5	Rounded irregular
131.5	120	Fist	<0.5	Rounded irregular
120	100	Fist	<0.5	Rounded irregular
100	91	Fist	<0.5	Rounded irregular
91	82	Fist	<0.5	Rounded irregular
82	82	Pencil		
82	77	Fist	0.5	Rounded irregular
77	76	Soft fist	0.5	Rounded irregular
76	67	Finger	0.5	Rounded irregular
67	60	Finger	<0.5	Rounded irregular
60	50	Pencil	<0.5	Rounded irregular
50	40	Fist	0.5	Rounded irregular
40	36	Fist	1	Irregular
36	35	Pencil		
35	32	Fist	1	Irregular
32	31.5	Pencil		
31.5	5	Fist	1	Irregular
5	0	Very soft fist	1 to 2	Faceted

Spring 2004 snowpit

S3 Height cm Top	Bottom	Hardness	Grain size mm	Description
144	140	Finger	<0.5	Rounded irregular
140	129	Fist	0.5	Rounded irregular
129	125	Finger	0.5	Rounded irregular
125	119	Finger	0.5 - 1.0	Rounded irregular
119	90	Pencil	0.5 - 1.0	Rounded irregular
90	62	Pencil	1	Rounded irregular
62	55	Finger	1.0 - 2.0	Irregular
55	50	Fist	1.0 - 2.0	Irregular/ sub-faceted
50	39	Pencil	1.0 - 2.0	Irregular
39	13	Finger	1.0 - 2.0	Irregular/ sub-faceted
13	8	Pencil	1.0 - 2.0	Irregular faceted
8	0	Finger	2	Irregular faceted

S4 Height cm Top	Bottom	Hardness	Grain size mm	Description
142	131	Fist	1.0 - 2.0	Needles/ Stellar
131	124	Finger	<0.5	Rounded irregular
124	117	Knife	0.5	Rounded irregular
117	91	Finger	0.5	Rounded irregular
91	57	Pencil	0.5 - 1	Rounded irregular
57	45	Finger	1.0 - 2.0	Faceted irregular
45	42	Pencil	1	Faceted irregular
42	9	Hard finger	2	Faceted irregular
9	0	Soft finger	1.0 - 2.0	Faceted irregular

T4 Height cm Top	Bottom	Hardness	Grain size mm	Description
112	107	Fist	1.0 - 2.0	Needles/ Stellar fragments
107	102	Pencil	<0.5	Irregular rounded
102	72	Finger	<1.0	Irregular rounded
72	43	Knife	0.5 - 1.0	Irregular rounded
43	38	Pencil	1.0 - 2.0	Irregular faceted
38	8	Pencil	1.0 - 2.0	Irregular lightly faceted
8	0	Fist	1.0 - 2.0	Irregular faceted

Spring 2004 snowpit

T5 Height cm Top	Bottom	Hardness	Grain size mm	Description
146	139.5	Finger	<0.5	Rounded irregular
139.5	134	Fist	<0.5	Rounded irregular
134	87.5	Finger	<0.5	Rounded irregular
87.5	78.5	Finger	0.5	Rounded irregular
78.5	38	Pencil	1	Rounded irregular
38	18	Finger	1	Faceted - Sugary texture
18	8	Pencil	1 to 2	Faceted - Sugary texture
8	0	Fist	1 to 2	Faceted - Sugary texture

T6 Height cm Top	Bottom	Hardness	Grain size mm	Description
130	124	Fist	<0.5	Rounded irregular
124	71	Finger	<1	Rounded irregular
71	57	Pencil	0.5	Rounded irregular
57	47	Hard finger	<1	Faceted
47	28	Finger	1.0 - 2.0	Faceted
28	3	Fist	1.0 -3.0	Faceted
3	0	Very soft fist	2.0 - 4.0	Faceted

Autumn 2004 snowpit

E1 Height cm Top	Bottom	Hardness	Grain size mm	Description
154	150	Knife	<1	Rounded irregular
150	84.5	Knife	1 to 2	Irregular faceted
84.5	80.5	Ice		
80.5	37	Pencil	1 to 2	Rounded irregular
37	34	Ice		
34	0	Finger	1 to 3	Irregular Facetted

E2 Height cm Top	Bottom	Hardness	Grain size mm	Description
140	132	Fist, fresh snow	0.5-1	Broken Stellar
132	72.5	Pencil	1.0-2.0	Facetted irregular
72.5	71.5	Ice		
71.5	47	Pencil	0.5-1	irregular rounded facetted
47	43.5	Ice		
43.5	16	Pencil	1.0-2.0	rounded irregular
16	13	Ice		
13	0	Finger	1.0-2.0	factted irregular

Autumn 2004 snowpit

E3 Height cm Top	Bottom	Hardness	Grain size mm	Description
142	133	Pencil	1	Rounded irregular
133	117	Knife	2.0-3.0	Facetted irregular
117	47	Pencil	2.0-3.0	facetteded irregular
47	44.5	Ice		
44.5	33	Finger	1.0-2.0	Rounded irregular
33	26	Fist	2.0-3.0	Facetted irregular
26	18	Pencil	1.0-2.0	Facetted irregular
18	10	Finger	1.0-2.0	Rounded irregular
10	6	Pencil	1.0-2.0	Facetted irregular
6	0	Fist	1.0-2.0	irregular

E4 Height cm Top	Bottom	Hardness	Grain size mm	Description
150	140	Pencil	2.0-3.0	irreguler
140	133	Finger	2.0-3.0	Irregular
133	92	Knife	2.0-3.0	Irregular
92	89.5	Ice		
89.5	88	Knife	1.0-2.0	Irregular
88	86.5	Ice		
86.5	53	Pencil	1.0-2.0	Irregular
53	47.5	Ice		
47.5	42	Pencil	2.0-3.0	Irregular
42	33	Finger	1.0-2.0	Irregular
33	29.5	Ice		
29.5	20	Finger	1.0-2.0	Irregular
20	13	Pencil	1.2-2.0	Irregular
13	6	Finger	2.0-3.0	Facetted irregular
6	0	Knife	2.0-3.0	Facetted irregular

S1 Height cm Top	Bottom	Hardness	Grain size mm	Description
160.3	153.8	Pencil	<1	Rounded irregular
153.8	120	Knife		
120	118.5	Knife		
118.5	86	Pencil	1 to 2	
86	84.5	Ice		
84.5	37.5	Pencil	1 to 2	
37.5	36	Ice		
36	0	Finger	1 to 3	Irregular faceted

Autumn 2004 snowpit

S2 Height cm Top	Bottom	Hardness	Grain size mm	Description
148	139	Pencil	<1	Rounded irregular
139	132	Knife	<4	Refrozen facetted
132	131	Ice		
131	119	Knife		Refrozen facetted
119	117	Ice		
117	78	Pencil	<2	Refrozen, cemented
78	74	Ice		
74	0	Finger	1.0 - 2.0	Irregular faceted

S3 Height cm Top	Bottom	Hardness	Grain size mm	Description
150	144	Fist	0.5 - 1.0	Rounded irregular
144	133	Knife	1.0 - 3.0	Rounded irregular
133	132	Ice		
132	121	Finger	1.0 - 2.0	Rounded irregular
121	60	Hard Pencil	1.0 - 4.0	Faceted irregular
60	58.5	Ice		
58.5	39	Finger	1.0 - 2.0	Irregular faceted
39	34	Ice		
34	20	Finger	1.0 - 2.0	Rounded irregular
20	13	Pencil	1.0 - 2.0	Faceted irregular
13	11	Ice		
11	0	Fist	1.0 - 3.0	Faceted irregular

S4 Height cm Top	Bottom	Hardness	Grain size mm	Description
173	170	Pencil	<1	Rounded irregular
170	163	Knife	<3	Refrozen crystals
163	162	Ice		
162	157	Finger	1.0-2.0	irregular facetted
157	155	Ice		
155	117	Finger	1.0-2.0	irregular facetted
117	77	Pencil	1	Rounded irregular
77	75.5	Ice		
75.5	59	Fist	1.0-3.0	irregular facetted
59	57	Ice		
57	48	Finger	1.0-2.0	irregular facetted
48	45	Ice		
45	43	Fist	3.0-4.0	irregular facetted
43	28	Pencil	1.0-2.0	irregular facetted
28	26	Ice		
26	0	Fist	1.0-3.0	irregular facetted

Autumn 2004 snowpit

T4 Height cm Top	Bottom	Description
117	115	Squashed snow
115	76	Firn
76	72.5	Ice
72.5	44	Firn
44	38	Firn
38	35	Ice
35	21	Firn
21	18	Ice
18	13	Firn
13	4	Mainly ice
4	1	Firn
1	0	Mainly ice

T5 Height cm Top	Bottom	Hardness	Grain Size mm	Description
154	150	Knife	<1	Rounded irregular
150	121	Knife	1 to 3	Irregular Facetted
121	120	Ice	0	0
120	86	Pencil	1 to 2	Irregular Facetted
86	81	Ice	0	0
81	35	Pencil	1 to 2	Irregular Rounded
35	0	Finger	1 to 3	Irregular facetted

T6 Height cm Top	Bottom	Hardness	Grain size mm	Description
141	125	Knife	1.0 - 3.0	Facetted
125	114	Finger	0 - 2.0	Facetted
114	112	Ice		
112	70	Pencil	1.0 - 2.0	Facetted
70	53	Hard Pencil	1	Facetted
53	36	Knife	1	Irregular
36	11	Finger	1.0 - 3.0	Facetted
11	5	Ice		
5	0	Fist	2.0 - 4.0	Facetted

Spring 2006 snowpit

E1 Height cm Top	Bottom	Hardness	Grain size mm	Description
124	112	Fist	<0.5	Irreg
112	69	Pencil	<0.5	rd irreg
69	61	Fist	<1.0	rd irreg
61	45	finger	<1.0	rd irreg
45	36	Knife	<0.5	rd irreg
36	22	Finger	1	Facetted irreg
22	0	Fist	1.0-2.0	Facetted irreg

E2 Height cm Top	Bottom	Hardness	Grain size mm	Description
95	88	Finger/Pencil	<0.5	rd irreg
88	82	Finger	<1	rd irreg + original snow ?
82	70	Knife	<1	rd irreg
70	60	Finger	<2	Facetted irreg
60	54	Pencil	<1	rd irreg
54	36	Finger	<1	rd irreg
36	16	Finger	<2	Facetted irreg
16	9	Pencil	<2	Facetted irreg
9	0	Fist	1 to 4	Facetted

E3 Height cm Top	Bottom	Hardness	Grain size mm	Description
120	93	Finger	<0.5	rd irreg
93	62	Finger	<1.0	rd irreg
62	60	Pencil	<0.5	rd irreg
60	54	Finger	<1.0	facetted irreg
54	49	Pencil	<0.5	rd irreg
49	39	Finger	<2.0	facetted irreg
39	18	Pencil	<1.0	rd irreg
18	0	Fist	<3.0	facetted

E4 Height cm Top	Bottom	Hardness	Grain size mm	Description
115	102	Fist	<0.5	Irreg Fragment
102	86	Pencil	<0.5	rd irreg
86	82	Fist	<1.0	rd irreg
82	73	Finger	<1.0	rd irreg
73	63	Pencil	<1.0	rd irreg
63	56	Pencil	<1.0	rd irreg
56	51	Knife	<0.5	rd irreg
51	34	Pencil	<1.0	rd irreg
34	17	Finger	<2.0	Rirreg facetted
17	0	Fist	2.0-4.0	facetted

Spring 2006 snowpit

S1 Height cm Top	Bottom	Hardness	Grain size mm	Description
125	106.5	Fist	<0.1	Blown fragment, angular irreg
106.5	76	Knife	<0.5	irreg
76	72	Finger	1.0-2.0	rd irreg
72	67	Knife	0.5-1.0	rd irreg
67	47	Finger	1	rd irreg
47	40	Pencil	1	Facetted rounded
40	30	Finger	1.0-1.5	Facetted rounded
30	20	Finger	1.0-2.0	Facetted rounded
20	0	Fist	2	Facetted

S2 Height cm Top	Bottom	Hardness	Grain size mm	Description
105	102	Fist	0.5	irregular
102	85	Pencil	0.5	irregular
85	54	Knife	0.1 - 1	facetted irregular
54	38	Pencil	1	facetted irregular
38	32	Knife	0.5	rounded irregular
32	14	Pencil	1.0 - 2.0	facetted irregular
14	0	Finger	1.0 - 3.0	facetted irregular

S3 Height cm Top	Bottom	Hardness	Grain size mm	Description
93	80	finger	<0.5	rounded irregular
80	59	knife	<0.5	rounded irregular
59	52	finger	0.5 - 1	irregular
52	34	pencil	1	irregular
34	32	knife	<0.5	rounded irregular
32	25	finger	1.0-2.0	irregular
25	20	fist	2	facetted irregular
20	7	fist	1.0-2.0	facetted irregular
7	0	knife	2.0-4.0	facetted irregular

S4 Height cm Top	Bottom	Hardness	Grain size mm	Description
97.5	73.5	Finger	<0.5	rd irreg
73.5	56	Knife	<0.5	rd irreg
56	42	Pencil	0.5-1	irreg
42	34	Knife	0.5-1	irreg facet
34	19	finger	1.0-2.0	facet irreg
19	0	Finger	1.0-2.5	racet irreg

Spring 2006 snowpit

T1 Height cm Top	Bottom	Hardness	Grain size mm	Description
124	86	Fist	<1.0	rd irreg
86	79	Knife	<0.5	rd irreg
79	65	Pencil	<1.0	rd irreg
65	59	Knife/finger	<4.0	facetted
59	40	Finger	<2.0	facetted
40	17	Pencil	<2.0	facetted
17	0	Fist	3.0-6.0	facetted

T2 Height cm Top	Bottom	Hardness	Grain size mm	Description
154	139	Fist	<0.5	rd irreg
139	116	Finger	<1.0	rd irreg
116	112	Pencil	<1.0	rd irreg
112	104	Finger	<1.0	rd irreg
104	101	Pencil	<0.5	rd irreg
101	79	Pencil	<0.5	rd irreg
79	71	Knife	<0.5	rd irreg
71	68	Knife	<2.0	facetted, v icy
68	58	Finger	<2.0	facetted
58	41	Pencil	<1.0	rd irreg
41	31	Pencil	<2.0	facetted
31	0	Fist	3.0-6.0	facetted

T3 Height cm Top	Bottom	Hardness	Grain size mm	Description
114	100	Finger	<0.5	rd irreg
100	87	Fist	<1	rd irreg
87	83	Knife	<0.5	rd irreg
83	75	Finger	<1	rd irreg
75	73	Pencil	<0.5	rd irreg
73	65	Finger	<2	Facetted irreg
63	53	Finger	<1	rd irreg
53	33	Pencil	<1	rd irreg
33	12	Knife	<1	rd irreg
12	0	Fist	2 to 3	Facetted

T4 Height cm Top	Bottom	Hardness	Grain size mm	Description
100	90	Pencil	<0.5	rd irreg
90	80	Finger	<1.0	rd irreg
80	63	Knife	<0.5	rd irreg
63	47	Finger	<1.0	facetted irreg
47	29	Pencil	<0.5	rd irreg
29	14	Fist	1.0-2.0	facetted
14	10	Pencil	<2.0	facetted
10	0	Fist	2.0-4.0	facetted

Spring 2006 snowpit

T5 Height cm Top	Bottom	Hardness	Grain size mm	Description
123	118	Finger	<0.5	rd irreg
118	100	Pencil	<0.5	rd irreg
100	94	Knife	<0.5	rd irreg
94	78	Pencil	<1	rd irreg
78	47	Finger	<1	rd irreg
47	43	Knife	<0.5	rd irreg
43	29	Finger	1 to 2	Facetted irreg
29	0	Fist	1 to 2	Facetted irreg

T6 Height cm Top	Bottom	Hardness	Grain size mm	Description
110	92	Fist	<0.5	rounded long flakes
92	70	Finger	<0.5	rd irreg
70	59	Pencil	<0.5	rd irreg
59	39	Finger	<2.0	irreg facetted
39	35	Pencil	<1.0	rd irreg
35	23	Finger	<2.0	facetted
23	14	Fist	<2.0	facetted
14	12	Pencil	1	facetted
12	0	Fist	<3.0	facetted

T7 Height cm Top	Bottom	Hardness	Grain size mm	Description
90	79	Fist	<1	rd irreg
79	62	Finger	<1	rd irreg
62	55	Pencil	<0.5	rd irreg
55	17	Finger	<1	rd irreg
17	13	Knife	<1	rd irreg
13	2	Finger	<3	Facetted
2	0	Fist	<4	Facetted

Spring 2004 core

E1 Depth cm			E2 Depth cm			E3 Depth cm			E4 Depth cm		
Top	Bottom	Description	Top	Bottom	Description	Top	Bottom	Description	Top	Bottom	Description
0	2	Ice and firn	0	2		0	5	Crumbly firn	0	2	Firn
2	7.5	Firn	2	3.7	Ice	5	7	Ice	2	2.8	Ice
7.5	9	Ice	3.7	7.5		7	16.5	Crumbly firn	2.8	5	Firn
9	10.5	Disintegrated	7.5	9.5	Ice	16.5	18.2	Ice	5	6	Ice
10.5	12	Ice	9.5	14		18.2	39.5	Firn	6	13	Crumbly firn/ ice layers
12	15	Crumbly firn	14	15.5	Ice layers	39.5	51	Firn	13	15	Ice and firn
15	17	Ice	15.5	19		51	66.5	Firn	15	18.3	Firn
17	31.5	Crumbly firn	19	19.5	Ice layers	66.5	68	Ice	18.3	20	Ice and firn
31.5	39.5	Firn	19.5	23.7		68	83	Firn	20	33	Crumbly firn
39.5	40.3	Ice	23.7	24.7	Ice layers	83	85	Ice	33	36	Ice
40.3	53.5	Firn	24.7	26.8		85	95.5	Firn	36	43.5	Firn
53.5	55.5	Ice	26.8	27.4	Ice	95.5	102.5	Firn	43.5	44.5	Ice
55.5	62.5	Firn	27.4	44.3		102.5	106.5	very crumbly firn	44.5	46.7	Firn
62.5	68.5	Firn	44.3	46	Ice	106.5	125	firn	46.7	48.3	Ice
68.5	70.2	Ice	46	64		125	126	Ice	48.3	55	Firn
70.2	80.5	Firn	64	69.5		126	150.5	Firn	55	58.5	Ice
80.5	86.5	Crumbly firn	69.5	71	Ice layer 1/2 way across	150.5	173.5	Firn	58.5	69	Firn and ice pipe
86.5	90.5	Firn	71	100		173.5	176	Ice and firn	69	72	Ice
90.5	92.5	Ice	100	121.5		176	180	Firn	72	92.5	Firn
92.5	100.5	Crumbly firn	121.5	136	large crystals, like refrozen	180	182	Ice	92.5	117	Crumbly firn
100.5	135	Firn and ice inclusions	136	150.5	hoar, gradually getting	182	185	Firn	117	122.3	Firn
135	138.5	Ice	150.5	174	smaller no clear divide.	185	188.5	Ice	122.3	123.2	Ice lens
138.5	148.5	Firn	174	175	Ice layer				123.2	152.5	Firn
148.5	150	Ice Blob	175	188.5					152.5	177.5	Firn and lots of ice
150	171	Firn	188.5	195.5	Ice layer				177.5	181.5	Ice
171	180.5	Ice							181.5	195.5	half ice/firn, from ice to firn
180.5	188.5	Firn							195.5	205.5	ice & clear firn
									205.5	207.5	Ice and firn
									207.5	216.5	Firn

Spring 2004 core

S1 Depth cm			S2 Depth cm			S3 Depth cm			S4 Depth cm		
Top	Bottom	Description	Top	Bottom	Description	Top	Bottom	Description	Top	Bottom	Description
0	8	Firn	0	1.5	Ice	0	2.5	Firn	0	15	Crumbly firn
8	11	Very crumbly ice	1.5	7.7		2.5	4	Ice	15	37.5	Crumbly firn
11	14.5	Firn and ice	7.7	10.4	very clear ice	4	7	Crumbly firn	37.5	81	Firn
14.5	16.7	Crumbly Firn	10.4	13.5		7	8	Ice	81	82	Ice
16.7	18.5	Ice	13.5	14.5	Ice	8	12	Firn	82	90.5	Firn
18.5	45		14.5	17.3		12	15.5	Ice and firn	90.5	92.5	Ice and firn
45	58		17.3	18.5	Ice	15.5	23.5	Crumbly firn	92.5	98.5	Firn
58.5	59.7	Firn with 1/2 ice lens	18.5	21.3		23.5	42.5	Firn	98.5	108	Crumbly firn
59.7	88.5	Firn	21.3	22.6	very clear ice	42.5	65	Firn	108	113	Firn
88.5	90		22.6	26		65	74	Firn	113	114	Ice
90	100	crumbly firn	26	28.5	Crumbled	74	83	Firn	114	122.5	Fine
100	107.5	Crumbly firn	28.5	59		83	84	Ice	122.5	123.5	Ice
107.5	112		59	59.5		84	96.5	Firn	123.5	158.5	Firn
112	114.5	Ice	59.5	93.2		96.5	97.5	Ice	158.5	170.5	Ice
114.5	121.5	Very crumbly	59	74.7		97.5	104	Very crumbly firn	170.5	180.5	Firn
121.5	145.5	Firn	74.7	76.7	very clear ice	104	118.5	Firn	180.5	183	Ice lens and firn
145.5	148	Ice and firn	76.7	79.7		118.5	119.5	Ice	183	200	Firn
148	177	Firn	79.7	81.4	Ice	119.5	132.5	Firn			
177	191	firn	81.4	97.2		132.5	134.5	Ice			
191	200	Ice	97.2	97.4	Ice lens	134.5	155.5	Firn			
			97.4	105.2	Ice lens	155.5	162.5	Firn			
			105.2	106.2	Ice lens	162.5	164.8	Ice and firn			
			106.2	109.7	Ice lens	164.8	167.5	Firn			
			109.7	111.4	Ice	167.5	172.5	Ice			
			111.4	116.7		172.5	199.5	Ice			
			116.7	140.4							
			140.4	144.7	Multiple ice layers						
			144.7	148.7							

Spring 2004 core

T4 Depth cm			T5 Depth cm			T6 Depth cm		
Top	Bottom	Description	Top	Bottom	Description	Top	Bottom	Description
0	4	Firn	0	1.3	Icy	0	12.5	Very icy firn
4	5	Ice and firn - disintigrated	1.3	15	Crumbly firn	12.5	16	Ice
5	12.5	Firn	15	16.5	Ice	16	35	Firn
12.5	30	Very crumbly firn	16.5	71	Firn	35	53.5	Firn
30	51	Firn	71	80	Firn, very crumbly	53.5	76	Firn
51	53.5	Ice	80	105.5	Firn, very crumbly	76	89.5	Firn
53.5	76.5	Firn	105.5	115	Crumbly firn	89.5	91.5	Ice
76.5	88	Crumbly firn	115	124	Firn	76	89.5	
88	90	Ice	124	125.5	Ice	89.5	103	Pure firn
90	99	Very crumbly firn	125.5	134	Firn	103	115.5	Firn
99	125.5	Firn	134	138.3	Firn with ice inclusions	115.5	124	Firn
125.5	129	Ice	138.3	146	Firn with ice Pipe	124	134.8	Coarse firn
129	142.5	Firn	146	149.5	Dense ice	134.8	140	Firmer firn
142.5	150	Ice	149.5	160.5	Firn	140	142	Ice
150	165	Firn	160.5	162.5	Firn with ice inclusions	142	152	Firn
165	170.5	Firn and ice	162.5	184.5	Firn with multiple ice inclusions	152	164.5	Firn
170.5	183.5	Firn	184.5	194.5	Ice	164.5	182.5	Firn
183.5	188	Ice	194.5	207.5	Firn and ice inclusions	182.5	206.5	Firn
188	193	Firn				206.5	218.5	Firn
						218.5	221	Ice
						221	239.5	Firn

Appendix 8: Spring and autumn density profiles derived from n-probe measurements

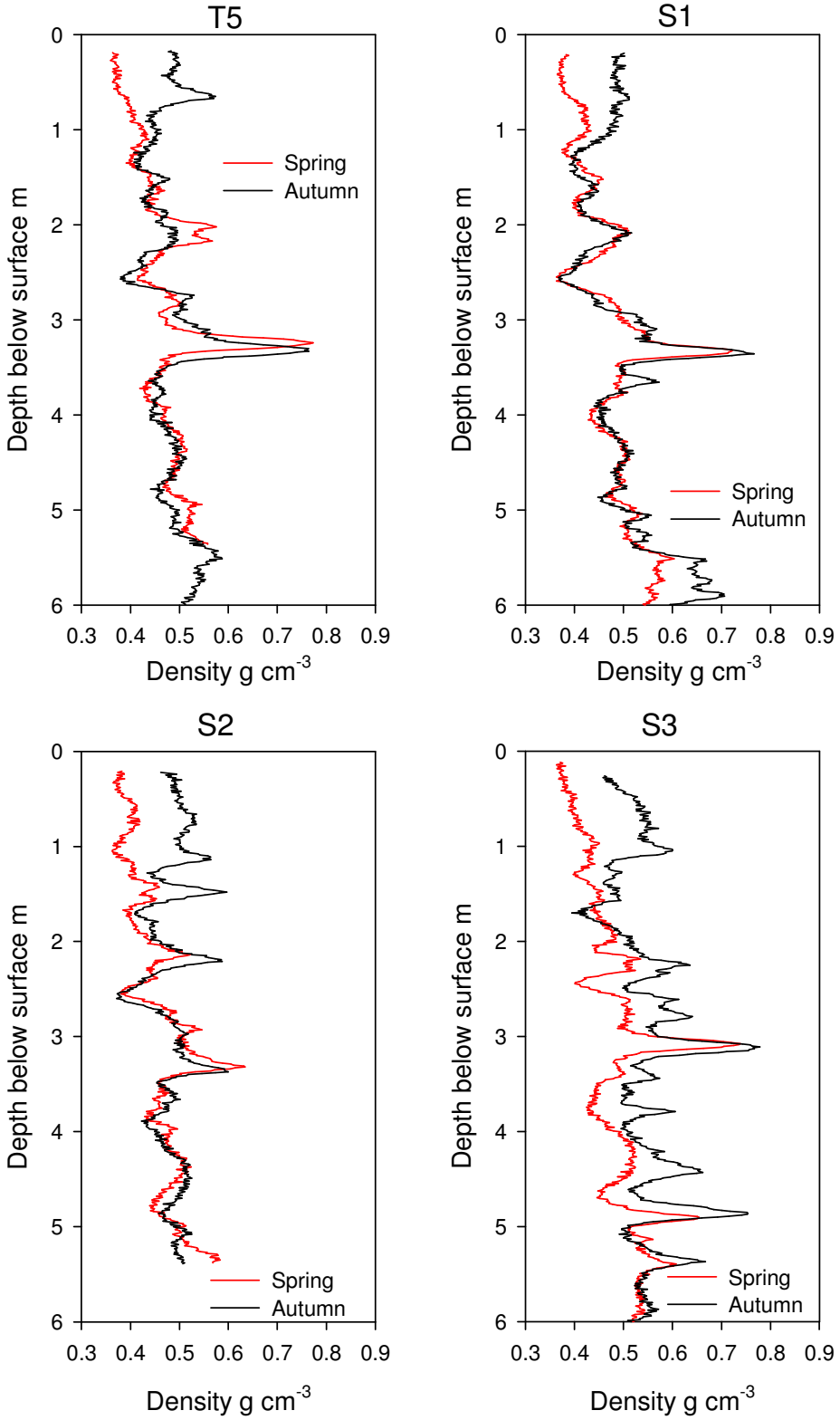

Spring and autumn density profiles derived from n-probe measurements

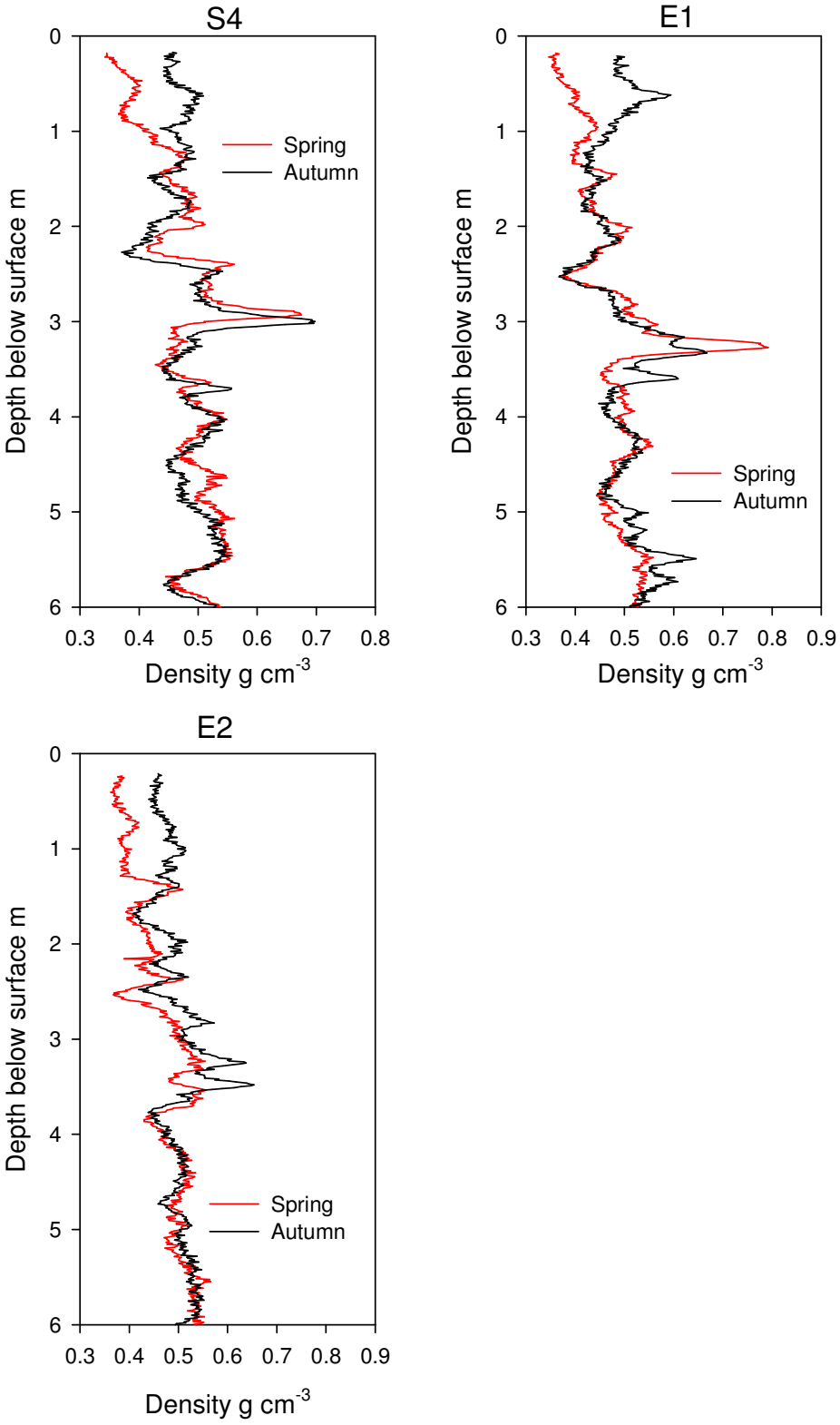

References

Abdalati, W. & Steffen, K. (2001) Greenland Ice Sheet melt extent: 1979-1999. *Journal of Geophysical Research-Atmospheres*, **106**, 33983-33988.

ACIA (2005) *Arctic Climate Impact Assessment* Cambridge University Press, New York, pp1042

Alley, R. (1988) Concerning the deposition and diagenesis of strata in polar firn. *Journal of Glaciology*, **34**, 283-290.

Alley, R., Saltxman, E., & Cufffey, K. (1990) *Geophysical Research Letters*, **17**, 2393.

Alley, R., Shuman, A., Meese, D., Gow, A., Taylor, K., Cuffey, M., Fitzpatrick, J., Grootes, P., Zielinski, G., Ram, M., & Elder, B. (1997) Visual-stratigraphic dating of the GISP2 ice core: Basis, reproducibility, and application. *Journal of Geophysical Research*, **102**, 26,367-26,381.

Alley, R., Spencer, M.K., & Anandakrishnan, S. (2007) Ice-sheet mass balance: assessment, attribution and prognosis. *Annals of Glaciology*, **46**, 1-7.

Andersen, K., Svensson, A., Johnsen, S.J., Rasmussen, S.O., Bigler, M., Rothlisberger, R., Ruth, U., Siggaard-Andersen, M., Steffensen, J.P., Dahl-Jensen, D., Vinther, B.M., & Clausen, H.B. (2006) The Greenland Ice Core Chronology 2005, 15-42 ka. Part 1: constructing the time scale. *Quaternary Science Reviews*, **25**, 3246-3257.

Anklin, M., Bales, R., Moseley-Thompson, E. & Steffen, K. (1998) Annual accumulation at two sites in northwest Greenland during recent centuries. *Journal of Geophysical Research*, **103**, 28775-28783

Anklin, M., Stauffer, B., Geis, K. & Wagenbach, D. (1994) Pattern of annual snow accumulation along a West Greenland flow line: no significant change observed during recent decades. *Tellus*, **46**, 294-303

Arthern, R.J. & Wingham, D.J. (1998) The natural fluctuations of firn densification and their effect on the geodetic determination of ice sheet mass balance. *Climatic Change*, **40**, 605-624.

Arthern, M., Wingham, D., Ridout, A. (2001) Controls on ERS altimeter measurements over ice sheets: Footprint-scale topography, backscatter fluctuations, and the dependence of microwave penetration depth on satellite orientation. *Journal of Geophysical Research*, ***106,*** *33,471-33,484*

Bales, R. & Wolff, E. (1995) Interpreting natural climate signals in ice cores. *EOS*, **76**, 482-483.

Bales, R., McConnell, J.R., Mosley-Thompson, E., & Csatho, B. (2001a) Accumulation over the Greenland Ice Sheet from historical and recent records. *Journal of Geophysical Research-Atmospheres*, **106**, 33813-33825.

Bales, R., McConnell, J.R., Mosley-Thompson, E. & Lamorey, G. (2001b) Accumulation map for the Greenland Ice Sheet: 1971-1990. *Geophysical Research Letters*, **28**, 2967-2970.

Bamber, J. & Payne, T., eds. (2004) *Mass balance of the cryosphere: observations and modelling of contemporary and future changes*, University of Cambridge, Cambridge, UK pp 641.

Benn, D. & Evans, D. (1998) *Glaciers and Glaciation*, Hodder Arnold, London 760pp.

Benson, C. (1962). Stratigraphic studies in the snow and firn of the Greenland Ice Sheet. In: *SIPRE Research Report*, Vol. 70, Cold Regions Research and Engineering Laboratory, Hanover, N. H., 93pp.

Bindschadler, R., Zwally, J., Major, J., & Brenner, A. (1989). *Surface topography of the Greenland Ice Sheet from satellite radar altimetry*. National Aeronautics and Space Administration, Washington D.C.

Bøggild, C.E., Forsberg, R., & Reeh, N. (2005) Meltwater retention in a transect across the Greenland ice sheet. *Annals of Glaciology*, **40**, 169-173.

Box, J.E. (2001) Surface water exchanges on the Greenland Ice Sheet derived from automated Weather Stations data, PhD Thesis, Department of Geography, Cooperative Institute for Research in Environmental Sciences, University of Colorado, Boulder, 190pp.

Box, J.E. (2005) Greenland ice sheet surface mass-balance variability: 1991-2003. *Annals of Glaciology*, **42**, 90-94.

Box, J.E., Bromwich, D.H., & Bai, L.S. (2004) Greenland Ice Sheet surface mass balance 1991-2000: Application of Polar MM5 mesoscale model and in situ data. *Journal of Geophysical Research-Atmospheres*, **109**, D16105, DOI: 10.1029/2003JD004451.

Braithwaite, R.J. (1994) Thoughts on monitoring the effects of Climate-Change on the surface elevation of the Greenland Ice-Sheet. *Global and Planetary Change*, **9**, 251-261.

Braithwaite, R.J., Laternser, M., & Pfeffer, W.T. (1994) Variations of near-surface firn density in the lower accumulation area of the Greenland Ice-Sheet, Pakitsoq, west Greenland. *Journal of Glaciology*, **40**, 477-485.

Braithwaite, R.J. & Ølesen, O. (1989) Calculation of Glacier ablation from air temperature, west Greenland. *In: Glacier Fluctuations and Climatic Change* Ed. Oerlemans J. pp 219-233, Kluwer, Dordrecht.

Brown, G. (1977) Average impulse response of a rough surface and its implications. *IEEE Trans. Ant. Prop*, **25**, 67-74

Brooks, R., Campbell, W., Ramseier, R., Stanley, H., & Zwally, J. (1978) Ice sheet topography by satellite altimetry. *Nature*, **274**, 539-543.

Campbell, F.M.A., Nienow, P.W., & Purves, R.S. (2006) Role of the supraglacial snowpack in mediating meltwater delivery to the glacier system as inferred from dye tracer investigations. *Hydrological Processes*, **20**, 969-985.

Chen, J., Wilson, C., & Tapley, B. (2006) Satellite gravity measurements confirm accelerated melting of Greenland Ice Sheet. *Science*, **313**, 1958-1960.

Christensen, J.H., Hewitson, B., Busuioc, A., Chen, A., Gao, X., Held, I., Jones, R., Kolli, R.K., Kwon, W.-T., Laprise, R., Rueda, V.M., Mearns, L., Menendez, C.G., Raisnen, J., Rinke, A., Sarr, A., & Whetton, P. (2007). Regional Climate Projections. In: *Climate Change 2007: The Physical Science Basis. Contribution of Working Group I to the Fourth Assessment Report of the Intergovernmental Panel on Climate Change* (eds Solomon, S., Qin, D., Manning, M., Chen, Z., Marquis, M., Averyt, K.B., Tignor, M. & Miller, H.L.), pp. 902-903. Cambridge University Press, Cambridge, UK and New York, NY, USA.

Clark, I. & Fritz, P. (1997) *Environmental isotopes in hydrogeology*, Lewis Publishers, New York, 328pp.

Colbeck, S.E., Akitaya, R., Armstrong, H., Grubler, H., Lafeuille, K., Lied, K., McClung, D. & Morris, E. (1990) The international classification for seasonal snow on the ground. In: *Working group on Snow Classification* (ed. International Commission on Snow and Ice). Association of Scientific Hydrology, Wallingford, Oxon, 23pp.

Comiso, J.C. & Parkinson, C.L. (2004) Satellite-observed changes in the Arctic. *Physics Today*, **57**, 38-44.

Dansgaard, W. (1964) Stable isotopes in precipitation. *Tellus*, **16**, 436-468.

Dansgaard, W., Johnsen, S.J., Clausen, H.B., Dahl-Jensen, D., Gundestrup, N.S., Hammer, C.U., Hvidberg, C.S., Steffensen, J.P., Sveinbjornsdottir, A.E., Jouzel, J., & Bond, G. (1993) Evidence for general instability of past climate from a 250-kyr ice-core record. *Nature*, **264**, 218-220.

Davies, T.D., Vincent, C.E., & Brimblecombe, P. (1982) Preferential elution of strong acids from a Norwegian ice cap. *Nature*, **300**, 161-163.

Davis, C. & Moore, R. (1993) A combine surface and volume scattering model for ice-sheet radar altimetery. *Journal of Glaciology*, **39**, 675-686.

Davis, C. & Zwally, J. (1993) Geographic and seasonal variations in the surface properties of the ice sheets by satellite-radar altimetry. *Journal of Glaciology*, **39**, 687-697

Dibb, J.E., Whitlow, S.I., & Arsenault, M. (2007) Seasonal variations in the soluble ion content of snow at Summit Greenland: Constraints from three years of daily surface snow samples. *Atmospheric Environment*, **41**, 5007-5019.

Donelly, T., Waldron, S., Tait, A., Dougans, J., & Bearhop, S. (2001) Hydrogen isotope analysis of natural abundance and deuterium-enriched waters by reduction over chromium on-line to a dynamic dual inlet isotope-ratio mass spectrometer. *Rapid Communications in Mass Spectrometry*, **15**, 1297-1303.

Douglas, B.C., Cheney, R.E., Miller, L., Agreen, R.W., Carter, W.E., & Robertson, D.S. (1990) Greenland Ice-Sheet - Is it growing or shrinking? *Science*, **248**, 288-288.

Drinkwater, M.R., Francis, R., Ratier, G., & Wingham, D.J. (2004) The European Space Agency's earth explorer mission CryoSat: measuring variability in the cryosphere. *Annals of Glaciology*, **39**, 313-320.

Dunse, T., Eisen, O., Helm, V., Rack, W., Steinhage, D., & Parry, V. (2008) Characteristics and small-scale variability of GPR signals and their relation to snow accumulation in Greenland's percolation zone. *Journal Glaciology*, **54**, 333-342.

Epstein, S. & Mayeda, T.K. (1953) Variations of the $^{18}O/^{16}O$ ratio in natural waters. *Geochimica et Cosmochimica Acta*, **4**, 213.

ESA (2007) Cryosat - 2 - Scientific Objectives. European Space Agency, http://www.esa.int/esaLP/ESAW3J1VMOC LPcryosat 0.html, Date accessed: 28th March 2008

Fahnestock, M., Bindschadler, R., Kwok, R., & Jezek, J. (1993) Greenland Ice Sheet surface properties and ice dynamics from ERS-1 SAR imagery. *Science*, **262**, 1530-1534.

Fichefet, T., Poncin, C., Goosse, H., Huybrechts, P., Janssens, I., & Le Treut, H. (2003) Implications of changes in freshwater flux from the Greenland ice sheet for the climate of the 21st century. *Geophysical Research Letters*, **30**, 1911, DOI:10.1029/2003GL017826.

Fischer, H. & Wagenbach, D. (1996) Large-scale spatial trends in recent firn chemistry along an east-west transect through central Greenland. *Atmospheric Environment*, **30**, 3227-3238.

Fischer, H., Wagenbach, D., Laternser, M., & Haeberli, W. (1995) Glacio-meterological and isotopic studies along the EGIG line, central Greenland. *Journal of Glaciology*, **41**, 515-527

Hall, D.K., Williams, R.S., Luthcke, S.B., & Digirolamo, N.E. (2008) Greenland Ice Sheet surface temperature, melt and mass loss: 2000-06. *Journal of Glaciology*, **53**, 81-93.

Hanna, E., Huybrechts, P., Janssens, I., Cappelen, J., Steffen, K., & Stephens, A. (2005) Runoff and mass balance of the Greenland ice sheet: 1958-2003. *Journal of Geophysical Research-Atmospheres*, **110**, D13108, DOI: 10.1029/2004JD005641.

Hanna, E., Huybrechts, P., Steffen, K., Cappelen, J., Huff, R., Shuman, C., Irvine-Fynn, T., Wise, S., & Griffiths, M. (2008) Increased runoff from melt from the Greenland Ice Sheet: A response to global warming. *Journal of Climate*, **21**, 331-341.

Hanna, E., McConnell, J., Das, S., Cappelen, J., & Stephens, A. (2006) Observed and modelled Greenland Ice Sheet snow accumulation, 1958-2003, and links with regional climate forcing. *Journal of Climate*, **19**, 344-358.

Hanna, E., Valdes, P., McConnell, J. (2001) Patterns and variations of snow accumulation over Greenland, 1979-98, from ECMWF analyses, and their verification. *Journal of Climate*, **14**, 3521-3535

Hawley, R., Morris, E., Cullen, R., Nixdorf, U., Shepherd, A., & Wingham, D. (2006) ASIRAS airborne radar resolved internal annual layers in the dry-snow zone of Greenland. *Geophysical Research Letters*, **33**, L04502, DOI:10.1029/2005GL025147.

Hawley, R. & Morris, E.M. (2006) Borehole optical stratigraphy and neutron-scattering density measurements at Summit, Greenland. *Journal of Glaciology*, **52**, 491-496.

Heidam, N. (1984) The components of the arctic aerosol. *Atmospheric Environment*, **18**, 329-343.

Heinemann, G. & Klein, T. (2002) Modelling and observations of the katabatic flow dynamics over Greenland. *Tellus*, **54**, 542-554.

Helm, V., Rack, W., Cullen, R., Nienow, P., Mair, D., Parry, V., & Wingham, D.J. (2007) Winter accumulation in the percolation zone of Greenland measured by airborne radar altimeter. *Geophysical Research Letters*, **34**, L06501, DOI: 10.1029/2006GL029185

Houghton, J., Meira Filho, L., Callander, B., Harris, N., Kattenberg, A., & Maskell, K. (1996). *Climate Change 1995: The Science of Climate Change*, Cambridge University Press, Cambridge, UK, 572pp.

IPCC (2007). IPCC, 2007: Summary for Policymakers. In: *The Physical Science Basis. Contribution of Working Group I to the Fourth Assessment Report of the Intergovernmental Panel on Climate Change* (eds Solomon, S., Qin, D., Manning, M., Chen, Z., Marquis, M., Averyt, K.B., Tignor, M. & Miller, H.L.), Cambridge University Press, Cambridge, UK and New York, NY, USA, pp. 2-4.

Isaksson, E., Pohjola, V., Jauhiainen, T., Moore, J., Pinglot, J.M., Vaikmae, R., Van de Wal, R.S.W., Hagen, J.O., Ivask, J., Karlof, L., Martma, T., Meijer, H.A.J., Mulvaney, R., Thomassen, M., & Van den Broeke, M. (2001) A new ice-core record from Lomonosovfonna, Svalbard: viewing the 1920-97 data in relation to present climate and environmental conditions. *Journal of Glaciology*, **47**, 335-345.

Jezek, K.C. & Gogineni, S. (1992) Microwave remote sensing of the Greenland ice sheet. *IEEE Geoscience Remote Sensing Society Newsletter*, **85**, 6-10.

Jezek, K.C., Gogineni, P., & Shanableh, M. (1994) Radar measurements of melt zones on the Greenland Ice-Sheet. *Geophysical Research Letters*, **21**, 33-36.

Joughin, I., Das, S.B., King, M.A., Smith, B.E., Howat, I.M., & Moon, T. (2008) Seasonal speedup along the western flank of the Greenland Ice Sheet. *Science*, **320**, 781-783.

Krabill, W. & Martin, C. (1987) Aircraft positioning using Global Positioning System carrier phase data. *Journal Institute of Navigation*, **34**, 1-21.

Krabill, W., Thomas, R., Martin, C., Swift, R., & Frederick, E. (1995) Accuracy of airborne laser altimetry over the Greenland Ice Sheet. *International Journal of Remote Sensing*, **16**, 1211-1222.

Krabill, W., Abdalati, W., Frederick, E., Manizade, S., Martin, C., Sonntag, J., Swift, R., Thomas, R., Wright, W., & Yungel, J. (2000) Greenland ice sheet: High-elevation balance and peripheral thinning. *Science*, **289**, 428-430.

Krabill, W., Hanna, E., Huybrechts, P., Abdalati, W., Cappelen, J., Csatho, B., Frederick, E., Manizade, S., Martin, C., Sonntag, J., Swift, R., Thomas, R., & Yungel, J. (2004) Greenland Ice Sheet: Increased coastal thinning. *Geophysical Research Letters*, **31**, L24402, DOI:10.1029/2004GL021533.

LaChapelle, E. (1969) *Field guide to snow crystals*, University of Washington Press, Seattle, 101pp.

Legresy, B., Remy, F. (1997) Altimetric observations of surface characteristics of the Antarctic ice sheet *Journal of Glaciology*, **43**, 595-596

Lemke, P., Ren, J., Alley, R.B., Allison, I., Carrasco, J., Flato, G., Fujii, Y., Kaser, G., Mote, P., Thomas, R.H., & Zhang, T., eds. (2007) *Observations: Changes in Snow, Ice and Frozen Ground*. Cambridge University Press, Cambridge, UK and New York, NY, USA.

Li, J., Zwally, H.J., & Comiso, J.C. (2007) Ice-sheet elevation changes caused by variations of the firn compaction rate induced by satellite-observed temperature variations (1982-2003). *Annals of Glaciology*, **46**, 8-13.

Liljequist, G. (1970) *Klimatologi*. Generalstabens Litografiska Anstalt, Stockholm.
Luthcke, S.B., Zwally, H.J., Abdalati, W., Rowlands, D.D., Ray, R.D., Nerem, R.S., Lemoine, F.G., McCarthy, J.J., & Chinn, D.S. (2006) Recent Greenland ice mass loss by drainage system from satellite gravity observations. *Science*, **314**, 1286-1289.
McConnell, J.R., Mosely-Thompson, E., Bromwich, D., Bales, R., & Kyne, J. (2000a) Interannual variations of snow accumulation on the Greenland Ice Sheet (1985-1996): newobservations versus model predictions. *Journal of Geophysical Research*, **105**, 4039-4046.
McConnell, J.R., Arthern, R.J., Mosley-Thompson, E., Davis, C.H., Bales, R.C., Thomas, R., Burkhart, J.F., & Kyne, J.D. (2000b) Changes in Greenland ice sheet elevation attributed primarily to snow accumulation variability. *Nature*, **406**, 877-879.
McConnell, J.R., Lamorey, G., Hanna, E., Mosley-Thompson, E., Bales, R.C., Belle-Oudry, D., & Kyne, J.D. (2001) Annual net snow accumulation over southern Greenland from 1975 to 1998. *Journal of Geophysical Research-Atmospheres*, **106**, 33827-33837.
McGoogan, J., Miller, L., Brown, G., & Hayne, G. (1974) The S-193 radar altimeter experiment. *Proceedings IEEE*, **62**, 793-803.
Meese, D., Gow, A., Grootes, P., Mayewski, P., Ram, M., Suiver, M., Taylor, K., Waddington, E., & Zielinski, G. (1994) The accumulation record from the GISP2 Core as an indicator of climate change throughout the Holocene. *Science*, **266**, 1680-1682.
Morris, E.M. & Cooper, J.D. (2003) Instruments and methods - Density measurements in ice boreholes using neutron scattering. *Journal of Glaciology*, **49**, 599-604.
Morris, E.M. & Thomas, A.G. (1985) Preferential discharge of pollutants during snowmelt in Scotland. *Journal of Glaciology*, **31**, 190-193.
Mosley-Thompson, E., McConnell, J.R., Bales, R.C., Lin, P.N., Steffen, K., Thompson, L.G., Edwards, R., & Bathke, D. (2001) Local to regional-scale variability of annual net accumulation on the Greenland ice sheet from PARCA cores. *Journal of Geophysical Research-Atmospheres*, **106**, 33839-33851.
Mote, T.L. (2007) Greenland surface melt trends 1973-2007: Evidence of a large increase in 2007. *Geophysical Research Letters*, **34**, L22507, DOI: 10.1029/2007GL031976.
Nghiem, S.V., Steffen, K., Neumann, G., & Huff, R. (2007) Snow accumulation and snowmelt monitoring in Greenland and Antarctica. *Dynamic Planet: Monitoring and Understanding a Dynamic Planet with Geodetic and Oceanographic Tools*, **130**, 31-38.
NICL (2008a) National Ice Core Laboratory. Ice core sites - Greenland, University of New Hampshire, http://nicl-smo.unh.edu/icecoresites/greenland.html, Date accessed: 16th July 2008.
NICL (2008b) National Ice Core Laboratory. Ice core sites – Greenland, University of New Hampshire, http://bprc.osu.edu/Icecore/Icegif/greenLand.gif, Date accesses: 16th July, 2008.

Østrem, G. & Brugman, M. (1991). *Glacier mass-balance measurements*. Environment Canada, Saskatchewan, Canada, 224pp.

Parry, V., Nienow, P., Mair, D., Scott, J., Hubbard, B., Steffen, K., & Wingham, D. (2007) Investigations of meltwater refreezing and density variations in the snowpack and firn within the percolation zone of the Greenland ice sheet. *Annals of Glaciology*, **46**, 61-68.

Paterson, W. (1994) *The Physics of Glaciers*, 3rd edn. Butterworth-Heineman, Oxford, 481pp.

Pfeffer, W.T. & Humphrey, N.F. (1996) Determination of timing and location of water movement and ice-layer formation by temperature measurements in sub-freezing snow. *Journal of Glaciology*, **42**, 292-304.

Pfeffer, W.T. & Humphrey, N.F. (1998) Formation of ice layers by infiltration and refreezing of meltwater. *Annals of Glaciology*, **26**, 83-91.

Pfeffer, W.T., Illangasekare, T.H., & Meier, M.F. (1990) Analysis and modelling of melt-water refreezing in dry snow. *Journal of Glaciology*, **36**, 238-246.

Pfeffer, W.T., Meier, M.F., & Illangasekare, T.H. (1991) Retention of Greenland runoff by refreezing - implications for projected future sea-level change. *Journal of Geophysical Research-Oceans*, **96**, 22117-22124.

Pielmeier, C. & Schneebeli, M. (2002) Snow stratigraphy measured by snow hardness and compared to surface section images. In: *International Snow Science Workshop*, Penticton, B.C., Canada.

Pohjola, V.A., Martma, T.A., Meijer, H.A.J., Moore, J.C., Isaksson, E., Vaikmae, R., & Van de Wal, R.S.W. (2002a) Reconstruction of three centuries of annual accumulation rates based on the record of stable isotopes of water from Lomonosovfonna, Svalbard. *Annals of Glaciology*, **35**, 57-62.

Pohjola, V., Moore, J., Isaksson, E., Jauhiainen, T., Van de Wal, R., Martmas, T., Meijer, H. & Vaikmae, R. (2002b) Effect of periodic melting on geochemical and isotopic signals in an ice core from Lomonosovfonna, Svalbard. *Journal of Geophysical Research – Atmospheres* **107,** 4036, DOI: 10.1029/2000JD000149

Rahmstorf, S. & Ganopolski, A. (1999) Long-term global warming scenarios computed with an efficient coupled climate model. *Climatic Change*, **43**, 353-367.

Ramillien, G., Lombard, A., Cazenave, A., Ivins, E.R., Llubes, M., Remy, F., & Biancale, R. (2006) Interannual variations of the mass balance of the Antarctica and Greenland ice sheets from GRACE. *Global and Planetary Change*, **53**, 198-208.

Rasmussen, S.O., Andersen, K.K., Siggaard-Andersen, M.L., & Clausen, H.B. (2002) Extracting the annual signal from Greenland ice-core chemistry and isotopic records. *Annals of Glaciology*, **35**, 131-135.

Reeh, N. (2004) Land ice (glaciers and ice sheets) in the climate system. In: *Workshop at the Norweigen Polar Institute*, Norsk Polarinstitutt, Tromso, Norway, pp. 43-45.

Reeh, N., Fisher, D.A., Koerner, R.M., & Clausen, H.B. (2005) An empirical firn-densification model comprising ice lenses. *Annals of Glaciology*, **42**, 101-106.

Ridley, J.K. & Partington, K. (1988) A model of satellite radar altimeter return from ice sheets. *International Journal of Remote Sensing*, **9**, 601-624.

Rignot, E., Braaten, D., Gogineni, S.P., Krabill, W.B., & McConnell, J.R. (2004) Rapid ice discharge from southeast Greenland glaciers. *Geophysical Research Letters*, **31**, L10401, DOI:10.1029/2004GL019474.

Rignot, E. & Kanagaratnam, P. (2006) Changes in the velocity structure of the Greenland Ice Sheet. *Science*, **311**, 986-990.

Rignot, E. & Thomas, R.H. (2002) Mass balance of polar ice sheets. *Science*, **297**, 1502-1506.

Robin, G. (1966) Mapping the Antarctic ice sheet by satellite altimetry. *Journal of Glaciology*, **28**, 179-185.

Scott, J.B.T., Mair, D., Nienow, P., Parry, V., & Morris, E. (2006a) A ground-based radar backscatter investigation in the percolation zone of the Greenland Ice Sheet. *Remote Sensing of Environment*, **104**, 361-373.

Scott, J.B.T., Nienow, P., Mair, D., Parry, V., Morris, E., & Wingham, D.J. (2006b) Importance of seasonal and annual layers in controlling backscatter to radar altimeters across the percolation zone of an ice sheet. *Geophysical Research Letters*, **33**, L24502, DOI:10.1029/2006GL027974.

Seckel, S. (1977) Hohenanderungen im gronlandischen Inlandeis zwischen 1959 und 1968. *Medd. Gronl*, **187**, 192-200.

Sharp, M., Skidmore, M., & Nienow, P. (2002) Seasonal and spatial variations in the chemistry of a high arctic supraglaical snow cover. *Journal of Glaciology*, **48**, 149-158.

Shepherd, A. & Wingham, D. (2007) Recent sea-level contributions of the Antarctic and Greenland ice sheets. *Science*, **315**, 1529-1532.

Sinniah, K. & Piers, K. (2001) Ion Chromatography: analysis of ions in pond waters. *Journal of Chemical Education*, **78**, 358-632.

Souchez, R. & Lorrain, R. (1991) *Ice Composition and Glacier Dynamics*, Springer-Verlag, New York, 207pp.

Steffen, K. & Box, J. (2001) Surface climatology of the Greenland Ice Sheet: Greenland Climate Network 1995-1999. *Journal of Geophysical Research-Atmospheres*, **106**, 33951-33964.

Steffen, K., Box, J.E., & Abdalati, W. (1996) Greenland Climate Network: GC-Net, in Colbeck, S. C. (ed.) *CRREL 96-27 Special Report on Glaciers, Ice Sheets and Volcanoes*, pp. 98-103.

Steffen, K. & Huff, R. (2008) Greenland melt extent, 2005, CIRES, http://cires.colorado.edu/science/groups/steffen/greenland/melt2005, Date accessed: 16th July 2008.

Steffen, K., Nghiem, S.V., Huff, R., & Neumann, G. (2004) The melt anomaly of 2002 on the Greenland Ice Sheet from active and passive microwave satellite observations. *Geophysical Research Letters*, **31**, L20402, DOI:10.1029/2004GL020444.

Steffensen, J. (1988) Analysis of the seasonal variation in dust, Cl-, NO3- and SO24- in two central Greenland firn cores. *Annals of Glaciology*, **10**, 171-177.

Stober, M. (1986) Die deutschen geodatischen arbeiten in Rahmen der internationalen glaziologischen Gronland Expeditions (EGIGE 1959-1974). *Deut. Geod. Komm. Publ*, **B281**.

Svensson, A., Nielsen, S.W., Kipfstuhl, S., Johnsen, S.J., Steffensen, J.P., Bigler, M., Ruth, U., & Rothlisberger, R. (2005) Visual stratigraphy of the North Greenland Ice Core Project (NorthGRIP) ice core during the last glacial period. *Journal of Geophysical Research-Atmospheres*, **110**, D02108, DOI: 10.1029/2004JD005134

Thomas, R.H. (2001) Program for arctic regional climate assessment (PARCA): Goals, key findings, and future directions. *Journal of Geophysical Research-Atmospheres*, **106**, 33691-33705.

Thomas, R., Csatho, B., Davis, C., Kim, C., Krabill, W., Manizade, S., McConnell, J., & Sonntag, J. (2001) Mass balance of higher elevation parts of the Greenland Ice Sheet. *Journal of Geophysical Research-Atmospheres*, **106**, 33707-33716.

Thomas, R., Davis, C., Frederick, E., Krabil, W., Li, Y., Manizade, S., & Martin, C. (2008) A comparison of Greenland ice-sheet volume changes derived from altimetry measurements. *Journal of Glaciology*, **54**, 203-212.

Thomas, R., Frederick, E., Krabill, W., Li, Y., Manizade, S., & Martin, C. (2006) Progressive increase in ice loss from Greenland. *Geophysical Research Letters*, **33**, L10503, DOI: 10.1029/2006GL026075.

Trenberth, K.E., Jones, P.D., Ambenje, P., Bojariu, R., Easterling, D., Tank, A.K., Parker, D., Rahimzadeh, F., Renwick, J.A., Rusticucci, M., Soden, B., & Zhai, P. (2007). *Observations: Surface and Atmospheric Climate Change. In Climate Change 2007: The Physical Science Basis. Contribution of Working Group I to the Fourth Assessment Report of the Intergovernmental Panel on Climate Change* (eds Solomon, S., Qin, D., Manning, M., Chen, Z., Marquis, M., Averyt, K.B., Tignor, M. & Miller, H.L.), Cambridge University Press, Cambridge, UK, New York, NY, USA, 237pp.

Trigt, R.V. (2002) Laser spectrometry for stable isotope analysis of water: biomedical and paleoclimatological applications, University of Groningen, http://irs.ub.rug.nl/ppn/235247219, Date accessed 25th July 2008.

Urey, H.C. (1947) The thermodynamic properties of isotopic substances. *Journal of Chemical Society*, **May 1947**, 562-581.

Van der Veen, C. & Bolzan, J. (1999) Interannual variability in net accumulation on the Greenland Ice Sheet: Observation and implications for mass balance measurements. *Journal of Geophysical Research*, **104**, 2009-2014.

Van der Veen, C.J. (1993) Interpretation of short-term ice-sheet elevation changes inferred from satellite altimetry. *Climatic Change*, **23**, 383-405.

Velicogna, I. & Wahr, J. (2005) Greenland mass balance from GRACE. *Geophysical Research Letters*, **32**, L18505, DOI:10.1029/2005GL023955.

Velicogna, I. & Wahr, J. (2006a) Acceleration of Greenland ice mass loss in spring 2004. *Nature*, **443**, 329-331.

Velicogna, I. & Wahr, J. (2006b) Measurements of time-variable gravity show mass loss in Antarctica. *Science*, **311**, 1754-1756.

Wadham, J., Bottrell, S., Tranter, M., & Raiswell, R. (2004) Stable isotope evidence for microbial sulphate reduction at the bed of a polythermal high Arctic glacier. *Earth and Planetary Science Letters*, **219**, 341-355.

Wang, L., Sharp, M., Rivard, B., & Steffen, K. (2007) Melt season duration and ice layer formation on the Greenland Ice Sheet, 2000-2004. *Journal of Geophysical Research-Earth Surface*, **112**, F04013, DOI:10.1029/2007JF000760.

Wankiewicz, A., ed. (1979) *A review of water movement in snow*. U.S. Army Corps of Engineers. Cold Regions Research and Engineering Laboratory, Hanover, New Hampshire, pp. 222-252.

Warrick, R., Provost, C., Meier, M., Oerlemans, J., & Woodworth, P. (1996). Changes in sea level. In: *Climate Change 1995: The Science of Climate Change* (ed J. Houghton), Cambridge University Press, New York, pp. 359-405.

Williams, D. (1964). *Accuracy of field snow surveys in western United States including Alaska*. Soil Conservation Service. U.S. Department of Agriculture, Mimeo.

Wingham, D., Forsberg, R., Laxon, S., Lemke, P., Miller, H., Raney, K., Sandven, S., Vincent, P., & Rebhan, H. (2001). *CryoSat calibration and validation concept*. Centre Polar Observation and Modelling, University College London, London, 91pp.

Wingham, D.J. (1995) Elevation change of the Greenland Ice-Sheet and its measurement with satellite radar altimetry. *Philosophical Transactions of the Royal Society of London Series A - Mathematical Physical and Engineering Sciences*, **352**, 335-346.

Wingham, D.J., Ridout, A.J., Scharroo, R., Arthern, R.J., & Shum, C.K. (1998) Antarctic elevation change from 1992 to 1996. *Science*, **282**, 456-458.

Work, R., Stockwell, H., Freeman, T., & Beaumont, R. (1965). *Accuracy of field snow surveys, Western United States, including Alaska*. Cold Regions Research and Engineering Laboratory, U.S Army Corps of Engineers, Hanover, New Hampshire.

Zwally, H.J., Abdalati, W., Herring, T., Larson, K., Saba, J., & Steffen, K. (2002) Surface melt-induced acceleration of Greenland ice-sheet flow. *Science*, **297**, 218-222.

Zwally, H.J., Brenner, A.C., Major, J.A., Bindschadler, R.A., & Marsh, J.G. (1989) Growth of Greenland Ice Sheet - Measurement. *Science*, **246**, 1587 - 1589.

Zwally, H.J., Giovinetto, M.B., Li, J., Cornejo, H.G., Beckley, M.A., Brenner, A.C., Saba, J.L., & Yi, D.H. (2005) Mass changes of the Greenland and Antarctic ice sheets and shelves and contributions to sea-level rise: 1992-2002. *Journal of Glaciology*, **51**, 509-527.

Zwally, H.J. & Li, J. (2002) Seasonal and interannual variations of firn densification and ice-sheet surface elevation at the Greenland summit. *Journal of Glaciology*, **48**, 199-207.

Zwally, J., Bindschadler, R., Brenner, A., Martin, T., & Thomas, R. (1983) Surface elevation contours of the Greenland and Antarctic ice sheets. *Journal of Geophysical Research*, **88**, 1589-1596.